

| | | | |
|--|---|--|---|
|  | <p align="center">NASA Engineering and Safety Center Technical Assessment Report</p> | <p align="center">Document #: NESC-RP- 06-065</p> | <p align="center">Version: 1.0</p> |
| <p>Title: Fracture Mechanics Based Methods Development for COPVs with Metallic Liners</p> | | <p align="center">Page #: 1 of 164</p> | |

**Fracture Mechanics Based Methods Development for
Composite Overwrapped Pressure Vessels (COPV) with
Metallic Liners**

July 8, 2010

| | | | |
|--|---|-----------------------|------------|
|  | NASA Engineering and Safety Center Technical Assessment Report | Document #: | Version: |
| | | NESC-RP-06-065 | 1.0 |
| Title: Fracture Mechanics Based Methods Development for COPVs with Metallic Liners | | Page #: 2 of 164 | |

Report Approval and Revision History

Approval and Document Revision History

NOTE: This document was approved at the July 8, 2010, NRB. This document was submitted to the NESC Director on August 9, 2010, for configuration control.

| | | |
|-------------------|-----------------------------------|---------|
| Approved Version: | <i>Original Signature on File</i> | 8/11/10 |
| 1.0 | NESC Director | Date |

| Version | Description of Revision | Office of Primary Responsibility | Effective Date |
|---------|-------------------------|---|----------------|
| 1.0 | Initial Release | Dr. Robert S. Piascik, NASA Technical Fellow for Materials | 7/08/10 |

| | | | |
|--|---|-----------------------|------------|
|  | NASA Engineering and Safety Center Technical Assessment Report | Document #: | Version: |
| | | NESC-RP-06-065 | 1.0 |
| Title: | | Page #: | |
| Fracture Mechanics Based Methods Development for COPVs with Metallic Liners | | 3 of 164 | |

Table of Contents

Volume I: Technical Assessment Report

| | | |
|------------|--|-----------|
| 1.0 | Notification and Authorization | 7 |
| 2.0 | Signature Page | 8 |
| 3.0 | Team List | 9 |
| 3.1 | Acknowledgements | 9 |
| 4.0 | Executive Summary | 10 |
| 5.0 | Introduction | 11 |
| 5.1 | Background and Problem Description | 12 |
| 5.2 | Approach..... | 13 |
| 6.0 | Data and Test Analysis | 14 |
| 6.1 | Laser Notch Process..... | 15 |
| 6.2 | Tensile Tests | 19 |
| 6.3 | Baseline FCG Rate Tests | 20 |
| 6.4 | Uniaxial Coupon FCG Tests..... | 21 |
| 6.4.1 | Uniaxial Test Procedure..... | 22 |
| 6.4.2 | Uniaxial Fatigue Precracking..... | 23 |
| 6.4.3 | Uniaxial Guide Plates for R = -1 FCG Tests | 24 |
| 6.4.4 | Uniaxial FCG Loading..... | 26 |
| 6.4.5 | Uniaxial FCG Test Results | 31 |
| 6.5 | Pressurized COPV Tests | 37 |
| 6.5.1 | COPV Test Procedure..... | 38 |
| 6.5.2 | Liner Precracking – Laser Notch versus Manufacturing Surface Defects | 41 |
| 6.5.3 | NDE Eddy Current Detection of Cracks..... | 47 |
| 6.5.4 | Composite Wrapping and Finite Element Analyses | 49 |
| 6.5.5 | COPV FCG Testing | 49 |
| 6.6 | FEAs of COPVs..... | 52 |
| 6.7 | FCG Rate Calculations | 55 |
| 6.8 | NASGRO FCG Predictions | 67 |
| 6.9 | Eddy Current NDE..... | 76 |
| 6.9.1 | Location of ID Cracks in Bare Liners..... | 77 |
| 6.9.2 | Location of OD Cracks in Wrapped COPVs | 79 |
| 6.9.3 | Location of ID Cracks in Wrapped COPVs..... | 81 |
| 6.9.4 | Location of ID Cracks in Tested COPVs..... | 83 |
| 7.0 | Findings, Conclusions, and NESC Recommendations | 85 |
| 7.2 | Observations | 86 |
| 7.1 | Findings | 87 |
| 7.3 | NESC Recommendations..... | 88 |
| 8.0 | Alternate Viewpoints | 88 |

| | | | |
|--|---|-----------------------|------------|
|  | NASA Engineering and Safety Center Technical Assessment Report | Document #: | Version: |
| | | NESC-RP-06-065 | 1.0 |
| Title: | | Page #: | |
| Fracture Mechanics Based Methods Development for COPVs with Metallic Liners | | 4 of 164 | |

| | | |
|-------------|---------------------------------|-----------|
| 9.0 | Other Deliverables | 88 |
| 10.0 | Lessons Learned..... | 89 |
| 11.0 | Definition of Terms..... | 89 |
| 12.0 | Acronyms List | 90 |
| 13.0 | References..... | 91 |

List of Figures

| | | |
|----------------|--|----|
| Figure 5.1-1. | Schematic of crack shapes used in the uniaxial and COPV FCG rate tests | 14 |
| Figure 6.1-1. | Laser notch test setup..... | 16 |
| Figure 6.1-2. | Cross section of a laser notch..... | 17 |
| Figure 6.1-3. | SEM photograph of a fatigue surface revealing the laser notch and the laser produced recast region..... | 18 |
| Figure 6.1-4. | Number of fatigue cycles required to obtain visually apparent (with a 20x optical microscope) fatigue crack growth from a laser notch..... | 19 |
| Figure 6.2-1. | Stress-strain behavior of the material used in the uniaxial coupon tests that were conducted according to ASTM Standard E8 [ref. 3]. | 20 |
| Figure 6.3-1. | Linear elastic FCG rate results from the M(T) tests that were conducted according to ASTM Standard E647 [ref. 4]..... | 21 |
| Figure 6.4-1. | Dogbone coupon for uniaxial FCG testing | 23 |
| Figure 6.4-2. | Schematic of saw cuts relative to the position of the fatigue crack | 23 |
| Figure 6.4-3. | Photograph of guide plates with edge-mounted extensometers..... | 24 |
| Figure 6.4-4. | Example of end buckling in a 0.032-inch thick dogbone coupon..... | 25 |
| Figure 6.4-5. | Guide plates, discontinuous stiffeners, and dogbone coupon | 26 |
| Figure 6.4-6. | Typical stress-strain curve for a uniaxial fatigue test | 27 |
| Figure 6.4-7. | SEM photograph (50x) of a typical fracture surface (UNI-090-35-01) with the four regions identified. The dash lines highlight the recast region that is more apparent in Figure 6.4-8..... | 29 |
| Figure 6.4-8. | SEM photograph (100x) of a fracture surface (UNI-090-35-01) showing the maximum depth location..... | 30 |
| Figure 6.4-9. | SEM photograph (1000x) of fracture surface (UNI-090-35-01) showing fatigue striations..... | 31 |
| Figure 6.4-10. | Stress-strain curve from the cyclic fatigue tests of coupons UNI-090-40-06 and UNI-090-40-07 | 37 |
| Figure 6.5-1. | Hydrostatic testing system | 38 |
| Figure 6.5-2. | Schematic of the liner used in the pressurized COPV tests | 40 |
| Figure 6.5-3. | Schematic of the laser notch locations for the liners | 40 |
| Figure 6.5-4. | Procedure used to extract the fatigue crack that initiated from a manufacturing defect on the liner ID..... | 42 |
| Figure 6.5-5. | SEM photograph of a fatigue crack that nucleated from a liner manufacturing defect that leaked during precracking. The dashed lines highlight the crack front boundaries..... | 42 |
| Figure 6.5-6. | Higher magnification SEM photographs of the fatigue crack shown in Figure 6.5-5. | 43 |
| Figure 6.5-7. | Procedure used to view the smaller fatigue cracks that nucleated from manufacturing defects on the liner ID..... | 44 |



**NASA Engineering and Safety Center
Technical Assessment Report**

Document #:
**NESC-RP-
06-065**

Version:
1.0

Title:

**Fracture Mechanics Based Methods Development for
COPVs with Metallic Liners**

Page #:
5 of 164

Figure 6.5-8. Optical photograph of two small cracks that were parallel to the liner crack that leaked during precracking 45

Figure 6.5-9. Procedure used to view the edge of the small fatigue cracks that nucleated from manufacturing liner defects..... 46

Figure 6.5-10. SEM photographs of fatigue cracks that initiated from manufacturing defects..... 46

Figure 6.5-11. The results of the eddy current scan of a bare liner 18119 and the fracture surface corresponding to the location of the eddy current indications. The color indicates the relative intensity of the signal. 48

Figure 6.6-1. Predicted and measured hoop strain for a COPV subjected to an autofrettage and one MDP cycle 55

Figure 6.7-1. Definition of the average crack length for K calculations 58

Figure 6.7-2. Average FCG rate as a function of the maximum K for all COPV tests 59

Figure 6.7-3. Average FCG rate for the COPV ID cracks in the depth direction with and without the approximation for the influence of the crack face pressure. 60

Figure 6.7-4. Regression power law fits to the FCG rate measurements in the depth direction for the OD and ID cracks in the COPV tests..... 62

Figure 6.7-5. Regression power law fits to the FCG rate measurements in the surface direction for the OD and ID cracks in the COPV tests..... 63

Figure 6.7-6. Semi-elliptical crack front assumptions for two fatigue cracks in COPVs..... 64

Figure 6.7-7. FCG rate data collected for the COPV and uniaxial tests with the results from the cracks fronts shown in Figure 6.7-6 identified..... 65

Figure 6.7-8. Crack lengths and depths of the ID and OD cracks that nucleated from manufacturing defects and inspection limits..... 66

Figure 6.7-9. Comparison of the FCG rates from the fully reversed, fully plastic uniaxial tests and the results from the COPV tests. Plotted are da/dN and dc/dN for crack depth and half surface dimensions, respectively. 67

Figure 6.8-1. NASGRO® material model 13AB1 input parameters..... 68

Figure 6.8-2. NASGRO® material model 13AB1 for 6061-T62 aluminum fit to data for four stress ratios 69

Figure 6.8-3. NASGRO® material model M6AB13AB1 for 6061-T62 aluminum for $R = -0.7$ and the measurements from the COPV tests 71

Figure 6.9-1. Photograph of the eddy current inspection system 77

Figure 6.9-2. Eddy current scan of bare liner COPV 18115 after 10,000 precrack cycles..... 78

Figure 6.9-3. Crack ID01 of COPV 18115..... 79

Figure 6.9-4. The four co-linear cracks that coalesced into crack ID02 of COPV 18115..... 79

Figure 6.9-5. High frequency eddy current scan of wrapped COPV 18115..... 80

Figure 6.9-6. High frequency eddy current scan of wrapped COPV 18118 prior to fatigue testing 81

Figure 6.9-7. Low frequency eddy current scan of crack ID01 in the wrapped and un-wrapped COPV 18115 prior to fatigue testing..... 82

Figure 6.9-8. Low frequency eddy current scan of crack ID02 in the wrapped and un-wrapped COPV 18115 prior to fatigue testing..... 82

Figure 6.9-9. Five crack locations on the ID surface of COPV 18118 determined by post-test eddy current inspection of the ID surface..... 83

Figure 6.9-10. Location of the five ID cracks in COPV 18118 that were identified in the post-test eddy current inspection of the ID surface..... 84

| | | | |
|--|---|-----------------------|------------|
|  | NASA Engineering and Safety Center Technical Assessment Report | Document #: | Version: |
| | | NESC-RP-06-065 | 1.0 |
| Title: | | Page #: | |
| Fracture Mechanics Based Methods Development for COPVs with Metallic Liners | | 6 of 164 | |

Figure 6.9-11. Photograph (50x) of the fracture surface of cracks ID01a and ID01b of COPV 18118... 84

List of Tables

| | |
|--|----|
| Table 6.2-1. Results from the 6061-T62 Tensile Tests | 19 |
| Table 6.4-1. Cyclic Strains for the Four Loading Conditions used in the Uniaxial Tests..... | 28 |
| Table 6.4-2. Uniaxial FCG Tests conducted on the 0.125-inch Thick Coupons | 32 |
| Table 6.4-3. Uniaxial FCG Tests conducted on the Lot 1 0.09-inch Thick Coupons | 33 |
| Table 6.4-4. Uniaxial FCG Tests Conducted on the Lot 2 0.09-inch Thick Coupons | 34 |
| Table 6.4-5. Uniaxial FCG Tests Conducted on the 0.05-inch Thick Coupons..... | 35 |
| Table 6.4-6. Uniaxial FCG Tests Conducted on the 0.032-inch Thick Coupons..... | 36 |
| Table 6.5-1. Summary of COPV Tests | 51 |
| Table 6.5-2. Dimensions of the COPV ID Cracks | 52 |
| Table 6.6-1. FEA Material Properties | 53 |
| Table 6.6-2. FEA Results | 54 |
| Table 6.8-1. Percent Error for the NASGRO® Predictions (13AB1 material model) for the Tests with OD Cracks | 72 |
| Table 6.8-2. Percent Error for the NASGRO® Predictions for the Tests with ID Cracks..... | 73 |
| Table 6.8-3. Percent Error for the NASGRO® Predictions (no threshold material model) for the Tests with OD Cracks | 75 |
| Table 6.8-4. Percent Error for the NASGRO® Predictions (no threshold material model) for the Tests with ID Cracks..... | 76 |

Volume II: Appendices

| | |
|--|-----|
| Appendix A. LEFM Fatigue Crack Growth Rate Data | 93 |
| Appendix B. Fracture Surfaces from the Uniaxial Tests..... | 101 |
| Appendix C. Fracture Surfaces from the COPV Tests..... | 117 |
| Appendix D. Calculated Stress Intensity Factor Values for the Elastic Uniaxial and COPV Tests..... | 164 |

| | | | |
|--|---|---|------------------------|
|  | NASA Engineering and Safety Center Technical Assessment Report | Document #: NESC-RP- 06-065 | Version: 1.0 |
| Title: Fracture Mechanics Based Methods Development for COPVs with Metallic Liners | | Page #: 7 of 164 | |

Volume I: Technical Assessment Report

1.0 Notification and Authorization

Dr. Ivatury S. Raju, the NASA Technical Fellows for Structures, and Dr. Robert S. Piascik, the NASA Technical Fellows for Materials requested independent joint Technical Discipline Team (TDT) assessment to generate the elastic/plastic crack growth data needed for required safety and reliability analyses of aluminum-lined composite overwrapped pressure vessels (COPVs) used for NASA spacecraft.

A NASA Engineering and Safety Center (NESC) out-of-board activity was approved by the NESC Director, Mr. Ralph R. Roe, on October 31, 2006. This investigation was authorized by the NESC Director at the NESC Review Board (NRB) on July 31, 2006. The assessment plan was approved by the NRB on March 8, 2007.

This assessment will be conducted under the jurisdiction of the NASA Composite Pressure Vessel Working Group (CPV WG). Dr. Piascik was selected to lead this assessment. Mr. Joseph Lewis, of the Jet Propulsion Laboratory (JPL) and a CPV WG team member, provided the technical direction for the assessment.

The investigation is being performed at the request of the NESC Director, who will be the primary stakeholder with interest from the NASA Headquarters (Office of Safety and Mission Assurance), the Exploration Systems Missions Directorate (Constellation Program (CxP), Crew Exploration Vehicle (CEV), International Space Station (ISS), and the Science Missions Directorate Office (Mars Science Laboratory (MSL) Project, Earth Science Missions, and Solar System Exploration missions).

| | | | |
|--|---|--------------------------------------|------------------------|
|  | NASA Engineering and Safety Center Technical Assessment Report | Document #: NESC-RP-06-065 | Version: 1.0 |
| Title: Fracture Mechanics Based Methods Development for COPVs with Metallic Liners | | | Page #: 8 of 164 |

2.0 Signature Page

Submitted by:

| | | | |
|-----------------------|------|---------------------|------|
| Dr. Robert S. Piascik | Date | Dr. Ivatury S. Raju | Date |
|-----------------------|------|---------------------|------|

Significant Contributors:

| | | | |
|----------------------|------|---------------------|------|
| Dr. David S. Dawicke | Date | Mr. Joseph C. Lewis | Date |
|----------------------|------|---------------------|------|

Signatories declare the findings and observations compiled in the report are factually based from data extracted from Program/Project documents, contractor reports, and open literature, and/or generated from independently conducted tests, analysis, and inspections.

| | | | |
|--|---|-----------------------|---------------------|
|  | NASA Engineering and Safety Center Technical Assessment Report | Document #: | Version: |
| | | NESC-RP-06-065 | 1.0 |
| Title: Fracture Mechanics Based Methods Development for COPVs with Metallic Liners | | | Page #: 9 of 164 |

3.0 Team List

| Name | Discipline | Organization |
|-------------------------------|---------------------------------|-------------------------------------|
| Core Team | | |
| Robert Piascik | NESC Lead | LaRC |
| Ivatury Raju | NESC Deputy Lead | LaRC |
| Joseph Lewis | Fracture Mechanics Lead | JPL |
| David Dawicke | Fracture Mechanics | AS&M |
| Russell Wincheski | NDE | LaRC |
| Phil Allen | Fracture Mechanics | MSFC |
| Roy Savage | MTSO Program Analyst | LaRC |
| Consultants | | |
| James Chang | Fracture Mechanics | The Aerospace Corporation |
| Bradley Forsyth | Test and Experiment Design | Wendell Hull Associates |
| Nathanael Greene | Composite Structure & Test | WSTF |
| Mark Leifeste | Composite Materials & Processes | WSTF |
| James Newman | Fracture Mechanics | Mississippi State University |
| Walt Reuter | Fracture Mechanics | Idaho National Laboratory (retired) |
| Regor Saulsberry | NDE | WSTF |
| Tommy Yoder | Composite Mechanical Damage | WSTF |
| Administrative Support | | |
| Tina Dunn-Pittman | Project Coordinator | LaRC/ATK |
| Linda Burgess | Planning and Control Analyst | LaRC/ATK |
| Erin Moran | Technical Writer | LaRC/ATK |

3.1 Acknowledgements

A number of other individuals provided specialized technical assistance to the assessment team, including: Professor Mool Gupta of the University of Virginia who performed the laser notches; Jim Harris and Jim Shih of Carleton Technologies, Inc., who performed the analysis, design, and wrapping of the composite overwrap; William Johnston of Lockheed Martin Space Operations who provided technical assistance for the design and implementation of the test systems, data acquisition systems, and guide plates; Chris Wright and Tracy Bridges of NASA Langley Research Center (LaRC) who conducted the uniaxial and hydrostatic tests, respectively; Jim Baughman of Lockheed Martin Space Operations who performed the scanning electron

| | | | |
|--|---|--------------------------------------|------------------------|
|  | NASA Engineering and Safety Center Technical Assessment Report | Document #: NESC-RP-06-065 | Version: 1.0 |
| Title: Fracture Mechanics Based Methods Development for COPVs with Metallic Liners | | Page #: 10 of 164 | |

microscope (SEM) examinations; and Harold Claytor of Lockheed Martin Space Operations who performed the destructive crack extraction of the COPVs.

4.0 Executive Summary

Composite overwrapped pressure vessels (COPVs) are used in human and robotic space missions to contain high pressure fluids. COPVs consist of a thin inner metallic liner that must remain intact to ensure safe, leak-free operation and a composite overwrap for strength. The American National Standards Institute (ANSI)/American Institute of Aeronautics and Astronautics, Inc. (AIAA)-S081 [ref. 1, 2] safety and reliability standards for COPV fracture control requirements stipulate that the composite overwrap and metallic liner must be designed for both damage tolerance life (safe-life) and leak before burst (LBB) considerations. Safe-life means that the largest crack contained in the liner or composite overwrap that can be missed by a nondestructive examination (NDE) will not grow to failure in four expected service lifetimes. LBB means that a crack in a liner that is growing at the maximum design pressure (MDP), by any growth mechanism, will grow through the liner and leak the pressurized media without fracture occurring.

COPVs can be designed to have either elastically or plastically responding liners. The first loading cycle of a COPV is an autofrettage cycle that exceeds MDP and plastically deforms the liner, conforming it to the composite overwrap inner surface. COPVs with elastically responding liners will not experience plastic deformation after the initial autofrettage cycle. COPVs with plastically responding liners will experience tensile and compressive plastic deformation for pressurization cycles that follow the autofrettage cycle. Test and/or analytical methods exist for qualification of COPVs for both safe-life and LBB in elastically responding COPVs and for LBB in plastically responding COPVs. However, no accepted analytical or coupon test methods exist for safe-life qualification of plastically responding liners, leaving full-scale COPV testing as the only approved method.

The objective of this study was to develop and validate a new test method to provide a first-of-kind methodology to predict the safe-life behavior of COPVs containing plastically responding metallic liners. Aluminum alloy 6061-T62, a common COPV liner material, was selected for this study. Features of the test method developed herein included: (1) laser induced notches (artificial crack starters) in the outside (OD) surface of thin cylindrical COPV liners (Note: manufacturing induced surface flaws that nucleated fatigue cracks were also observed and used in this study), (2) coupon test methods for simulating COPV liner cyclic tensile/compressive loading, (3) unique fractographic-based measurements for determining the fatigue crack growth (FCG) rates of small surface cracks, and (4) special eddy current inspection method for detecting small surface cracks.

| | | | |
|--|---|--------------------------------------|------------------------|
|  | NASA Engineering and Safety Center Technical Assessment Report | Document #: NESC-RP-06-065 | Version: 1.0 |
| Title: Fracture Mechanics Based Methods Development for COPVs with Metallic Liners | | Page #: 11 of 164 | |

The results of this study are summarized below:

1. A new test procedure for the characterization of small (depths ranging from 0.001 to 0.03 inches) surface fatigue cracks contained in both thin uniaxial test coupon and metallic COPV liners was developed. This test procedure uniquely characterized the growth of small fatigue cracks subjected to strains that replicated the hoop strains due to the autofrettage, proof, and MDP cycling of both plastically and elastically responding COPVs. The test procedure was validated for elastically responding COPVs by demonstrating correlation between the behavior of the surface cracks in the uniaxial test coupons and artificial and manufacturing surface cracks in the COPV liners.
2. The new test procedure was used to successfully test uniaxial coupons subjected to fully reversed, fully plastic conditions that simulated the hoop strains in the liner of a plastically responding COPV. The resulting FCG rate measurements were at least an order of magnitude faster than similar tests conducted under elastic conditions. However, the COPVs used in the study were incapable of achieving plastically responding behavior; therefore correlation with the uniaxial coupons could not be demonstrated. Additional testing of COPVs with plastically responding liners will be required to fully demonstrate correlation between coupon tests and plastically responding COPVs for safe-life qualification.
3. The existence of unexpected manufacturing induced flaws in the inside (ID) and OD liner surfaces presented difficulties that were overcome by the development of a special eddy current inspection method capable of detecting fatigue cracks nucleating from these flaws. The assessment scope was expanded to include an investigation into the feasibility of detecting cracks in the liner that nucleated from manufacturing defects and laser notches from an examination of the composite OD.

Three recommendations for future work directed to the Composite Pressure Vessel (CPV) Working Group were generated by the results of this study:

1. Additional COPV tests should be conducted using liners that are 0.05 to 0.03 inches thick to provide crack growth rate data for plastically responding liners.
2. Additional investigations should be performed to characterize the detectability of cracks by size, shape, and location.
3. The data generated in this study should be used to evaluate existing elastic plastic fracture mechanics (EPFM) techniques and guide the development of new EPFM tools.

| | | | |
|--|---|--------------------------------------|------------------------|
|  | NASA Engineering and Safety Center Technical Assessment Report | Document #: NESC-RP-06-065 | Version: 1.0 |
| Title: Fracture Mechanics Based Methods Development for COPVs with Metallic Liners | | Page #: 12 of 164 | |

5.0 Introduction

COPVs are used in human and robotic space missions to contain high pressure fluids. A COPV consists of a thin inner metallic liner that must remain intact to ensure safe operation and a composite overwrap for strength. The inability to predict a minimum safe operating life for COPVs would create safety and programmatic risks that include loss of life, facilities, spacecraft, and mission, and/or launch delays. The COPV fracture control requirements stipulate that the composite overwrap and metallic liner must be designed for both damage tolerance life (safe-life) and LBB considerations. Safe-life means that the largest crack that can be missed by a NDE will not grow to failure in four expected surface life times. LBB means that a crack in a liner that is growing at MDP, by any growth mechanism, will grow through the liner and leak the pressurized media without fracture occurring.

COPVs can be designed to have either elastically or plastically responding liners. The first loading cycle of a COPV is an autofrettage cycle that exceeds MDP and plastically deforms the liner, conforming it to the composite overwrap inner surface. COPVs with elastically responding liners will not experience plastic deformation after the initial autofrettage cycle. COPVs with plastically responding liners will experience tensile and compressive plastic deformation for the pressurization cycles that follow the autofrettage cycle. Test and/or analytical methods exist for qualification of COPVs for both safe-life and LBB in elastically responding COPVs and for LBB in plastically responding COPVs. However, no accepted analytical or coupon test qualification methods exist for plastically responding liners, leaving full-scale COPV testing as the only approved qualification method.

This report describes an investigation for the development and verification of a coupon test method for safe-life qualifications of plastically-responding liners. The test method would require demonstration that the FCG rate of small surface fatigue cracks in uniaxial coupons exhibit similitude with the FCG rate of similar sized cracks in COPVs with plastically responding liners. Here, a small surface fatigue crack is defined as a fatigue crack that nucleated at the ID or OD surface and has not yet penetrated the liner wall thickness.

5.1 Background and Problem Description

A COPV is a container that consists of a thin metallic liner, usually made of an aluminum, titanium, or nickel-based alloy that is wrapped with a composite material, typically an epoxy matrix resin with carbon, Kevlar®, or glass fibers. The metallic liner is used as a containment barrier for the pressurized fluid and the composite overwrap provides strength. The metallic liners are inspected prior to wrapping using NDE techniques to find surface flaws on the ID and

| | | | |
|--|---|--------------------------------------|------------------------|
|  | NASA Engineering and Safety Center Technical Assessment Report | Document #: NESC-RP-06-065 | Version: 1.0 |
| Title: Fracture Mechanics Based Methods Development for COPVs with Metallic Liners | | Page #: 13 of 164 | |

OD surfaces. In aerospace applications, the operational life of a COPV will include an autofrettage pressurization cycle that permanently deforms the liner and conforms it against the composite overwrap inner surface, followed by a number of cycles at lower pressures for leak testing, system integration testing, and finally launch pressurization. COPV liners can be designed to be either elastically-responding or plastically-responding depending on the liner strain at the proof pressure after the (autofrettage) first cycle. Plastically responding liners are thinner, resulting in a weight savings.

The ANSI/AIAA-S081 [ref. 1, 2] safety and reliability standards for COPVs have fracture control qualification requirements for both damage tolerance life (safe-life) and LBB considerations. Safe-life means that the largest crack that can be missed by a NDE with a 90 percent probability with a 95 percent confidence level will not grow to liner fracture or leakage in four service lifetimes. LBB means that a crack in a liner that is growing at MDP, by any growth mechanism, will grow through the liner thickness and leak the pressurized media without fracture occurring. For elastically responding liners, qualification requirements can be verified by test or analysis, and both safe-life and LBB analysis methods exist for elastically responding liners. Linear elastic fracture mechanics (LEFM) analytical approaches are accepted methods for such qualification. However, for plastically responding liners no accepted analysis methods exist, thus expensive testing of full-scale COPVs is required.

The objective of this study is to address the requirements of the ANSI/AIAA-S081 safety and reliability standards for COPVs with plastically responding liners. Test methods were developed to perform the following:

- Simulation of the hoop strain history of a plastically responding COPV liner in a uniaxial coupon test
- Nucleation of small surface fatigue cracks in the OD surface of metallic COPV liners
- Measurement of the FCG rate of non-observable small cracks.

5.2 Approach

The liner material selected for this assessment was 6061-T62 aluminum. Four different thicknesses of 6061-T62 aluminum sheet (0.125 inch, 0.09 inch, 0.05 inch, and 0.032 inch thick) were used for the uniaxial coupons. The liners were 0.09 inches thick. Tensile tests were performed on each sheet of material used in the uniaxial coupons using standard methods [ref. 3], but no tensile tests were conducted on the liner material. The manufacturer of the liner has proprietary tensile data that was used in the finite element analysis (FEA) of the wrapped liners.

Fatigue cracks were initiated in both the uniaxial coupons and liners by first creating small “notches” with a laser machining process, then cycling (precracking) at a maximum stress that



**NASA Engineering and Safety Center
Technical Assessment Report**

Document #:
**NESC-RP-
06-065**

Version:
1.0

Title:

**Fracture Mechanics Based Methods Development for
COPVs with Metallic Liners**

Page #:
14 of 164

was about 80 percent of the material yield stress and a stress ratio (R) = 0.1 for uniaxial coupons and $R = 0$ for the liners. The liners were notched and precracked prior to the composite wrapping. Two different sizes/aspect ratio fatigue cracks were used in this investigation: small semi-circular (surface crack length ($2c$) = 0.04 inch, ratio of crack depth to half surface crack length (a/c) = 1) and long shallow ($2c = 0.1$ inch, $a/c = 0.2$), as illustrated in Figure 5.1.1. The aspect ratios selected were the limits specified in the safe-life and LBB requirements of the COPV standard [ref. 1]. The coupons and liners with small semi-circular notches were precracked until the surface crack measurement reached a value of $2c = 0.04$ inch. The coupons and liners with the long shallow notches were precracked until a fatigue crack was visible at both ends of the notch. Typically, the ends of the post-precracking fatigue cracks were 0.001 to 0.003 inches from the end of the long shallow notches. Eddy current NDE inspections were performed on liners during the fatigue process to detect cracks initiating from manufacturing defects on the ID and OD of the liners.

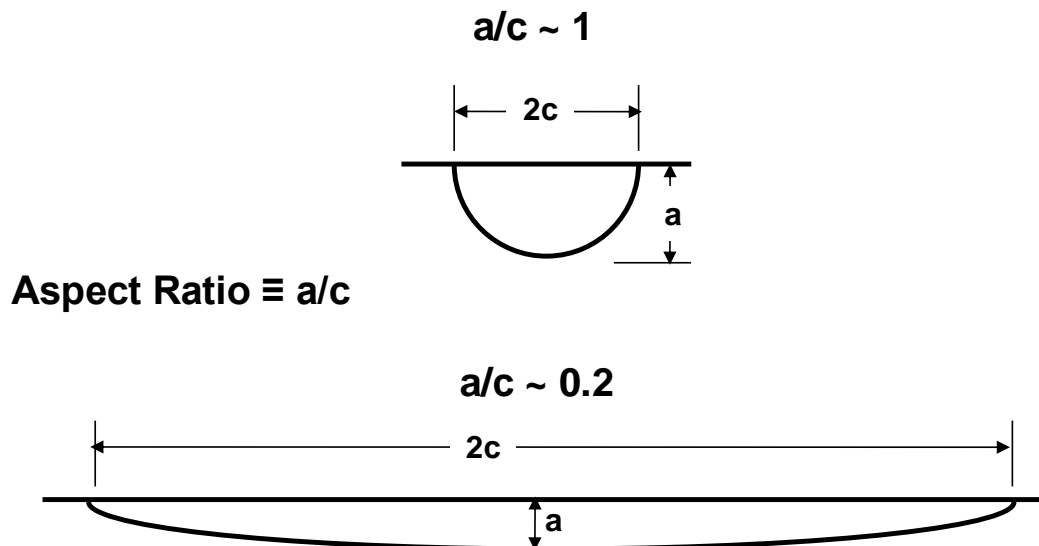


Figure 5.1-1. Schematic of crack shapes used in the uniaxial and COPV FCG rate tests

6.0 Data and Test Analysis

The precracked uniaxial coupons were tested under displacement control to specified strains. The coupons were machined into a “dogbone” shape that had a width (W) = 2 inches in the crack region and $W = 3$ inches in the grip region. Guide plates were utilized to permit the thin sheet coupons to be yielded in compression. The strains were measured from extensometers placed on the edges of the coupon.

| | | | |
|--|---|--------------------------------------|------------------------|
|  | NASA Engineering and Safety Center Technical Assessment Report | Document #: NESC-RP-06-065 | Version: 1.0 |
| Title: Fracture Mechanics Based Methods Development for COPVs with Metallic Liners | | Page #: 15 of 164 | |

The cracked liners were sent to Carleton Technologies, Inc. for the composite overwrap. This vendor designed the wrapping pattern and performed a FEA of the wrapped liner. The cracked COPVs were pressurized to the autofrettage pressure and cycled to the MDP. NDE inspections were performed on the COPVs before and after the pressurization cycles.

The FCG rates were calculated from the post-test examination of the fatigue surfaces. Typically, the part-through cracks in the coupons and COPVs did not break through to the back surface, so the fatigue surfaces needed to be separated for examination. Saw cuts, co-linear with the cracks, were made from the edges of the coupons to within 0.05 inches of the crack tips and the coupon was loaded monotonically until the crack grew to failure. SEM examination of the fatigue surfaces revealed regions of distinct surface morphology that identified: the laser notch, the growth due to the precracking, the growth due to the subsequent autofrettage and MDP fatigue cycles, and the region of ductile fracture due to the final loading. The FCG due to the autofrettage cycle was small and not distinguishable from that of the MDP fatigue cycles. The FCG rates from the elastic uniaxial coupon tests and the elastic multi-axial COPV tests were measured from the fracture surfaces and correlated with the maximum stress intensity factor (K_{max}) parameter. The subsequent sections provide details of the test methods developed and the measurements obtained.

6.1 Laser Notch Process

The size of the desired part-through cracks (0.04 inch long by 0.02 inch deep) and the limitations on the pressurization rate (0.1 Hz) of the hydrostatic testing system for fatigue cycling the COPVs required a highly controllable technique that creates very small, sharp notches. A Yb-fiber laser, with a beam capable of being focused to smaller than 0.002 inches was used to fabricate the notches. The aluminum coupons and liners were mounted on a computer controlled three-axis precision motion stage, as shown in Figure 6.1-1. The following parts were integrated in the laser micromachining process: a Yb-fiber laser module and the remote control system, a laser beam focusing lens, the specimen mounting fixture, a 3-axis motion stage with motion control module, and a compressed air cooling pipeline. The Yb-fiber laser is capable of providing optical power of 20 Watt (W) at a repetition rate of 20 kHz with laser pulse width of 50 nsec. The laser wavelength was 1064 nm.



Title:

**Fracture Mechanics Based Methods Development for
COPVs with Metallic Liners**

Page #:
16 of 164

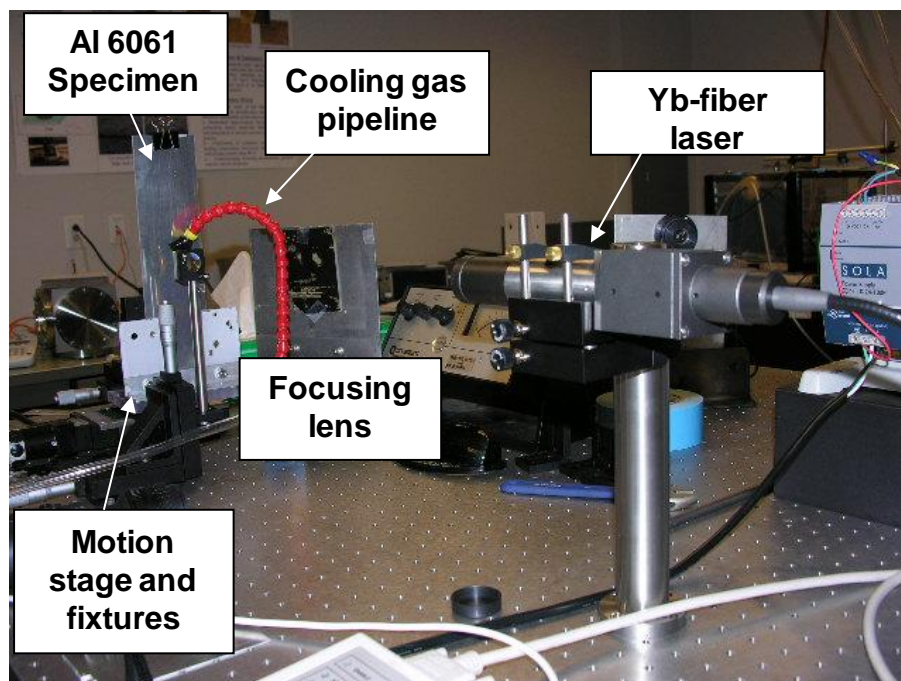


Figure 6.1-1. Laser notch test setup

The Yb-fiber laser delivers a high power 1.06 μm wavelength laser beam to the specimen via a flexible metal-sheathed single mode fiber cable. A repetition rate of 20 kHz and a pulse width of 50 ns were used in the micromachining process. A high laser energy density is required for micromachining because aluminum is highly reflective to the laser wavelength and a laser power of 16 W was employed. The laser beam was directed through a 50 mm focal length, plano-convex lens, and focused onto the specimen surface. A cooling gas pipeline was used to direct compressed air onto the specimen surface and remove the debris. The specimen was mounted on the 3-axis motion stage and moved in the direction perpendicular to the incident laser beam with a speed of 0.2 inch/s. Two metal blocks were used to shield the laser beam so that only the desired portion of the specimen was exposed to incident laser (micro notch length control). The specimen was translated a larger distance than the desired micromachined length to minimize the effect of extra laser exposure time during the initial acceleration and deceleration of the sample stage. Trial tests were conducted and the specimen was cross-sectioned to expose the micronotch in the depth direction. The depth of the micronotch was controlled by the laser processing time. By controlling the distance between the metal plates and the laser scanning time, the length and depth of the notch were then processed to the desired values.

The characteristics of the laser notches were evaluated by examination of the fatigue surfaces and cross sections of the notches. The cross sections were performed by cutting the aluminum



NASA Engineering and Safety Center Technical Assessment Report

Document #:
**NESC-RP-
06-065**

Version:
1.0

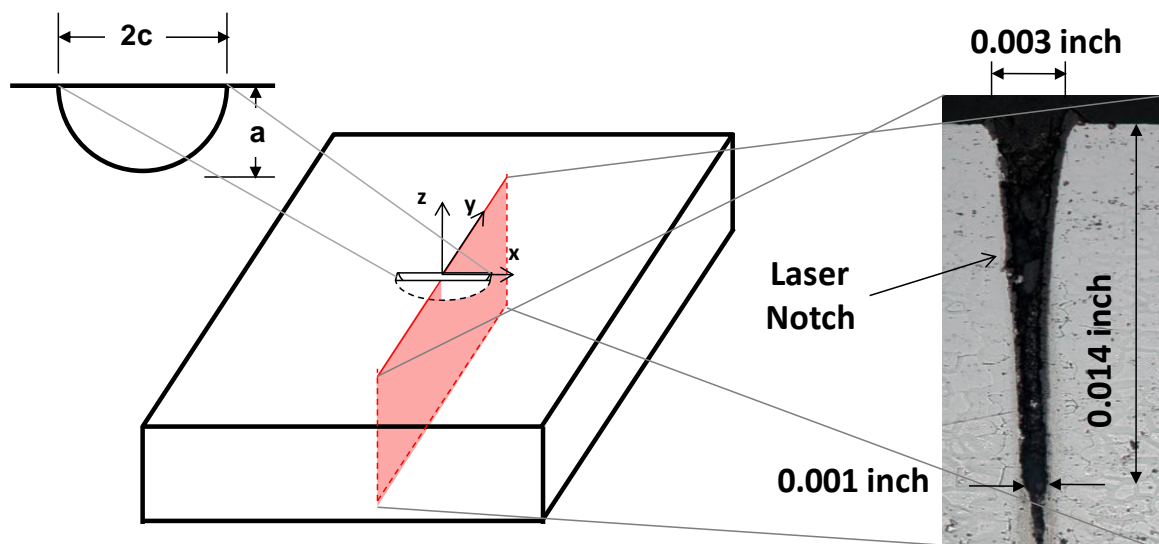
Title:

Fracture Mechanics Based Methods Development for COPVs with Metallic Liners

Page #:
17 of 164

sheet perpendicular to the direction of the notch and polishing the exposed surface, as shown in Figure 6.1-2 for a laser notch that was precracked. The root of this laser notch was about 0.001 inch. Beyond the end of the laser notch was a recast region that resulted from material melted by the laser that was not ejected from the notch, as shown in Figure 6.1-3. The recast region could potentially influence the measured FCG rates, so all notches were precracked beyond the recast region.

The resulting laser notches tended to be more rectangular shaped than semi-circular, as seen in Figure 6.1-3. However, the resulting fatigue cracks quickly grew to a semi-elliptical shape during precracking, but with a deeper aspect ratio than the original notch. The two desired crack shapes, shown in Figure 5.1-1, were obtained by changing the distance between the metal blocks that shield the laser and the processing time. The small semi-circular crack fronts ($a/c \sim 1$) were obtained by positioning the metal blocks 0.02 inches apart and laser processing time was selected to produce a notch depth of about 0.02 inches. The long shallow crack fronts ($a/c \sim 0.2$) were obtained by positioning the metal blocks 0.10 inches apart and reducing the laser processing time to produce a notch depth of about 0.01 inches.



(a) Schematic of cross section

(b) Photograph of cross section

Figure 6.1-2. Cross section of a laser notch



Title:

Fracture Mechanics Based Methods Development for
COPVs with Metallic Liners

Page #:
18 of 164

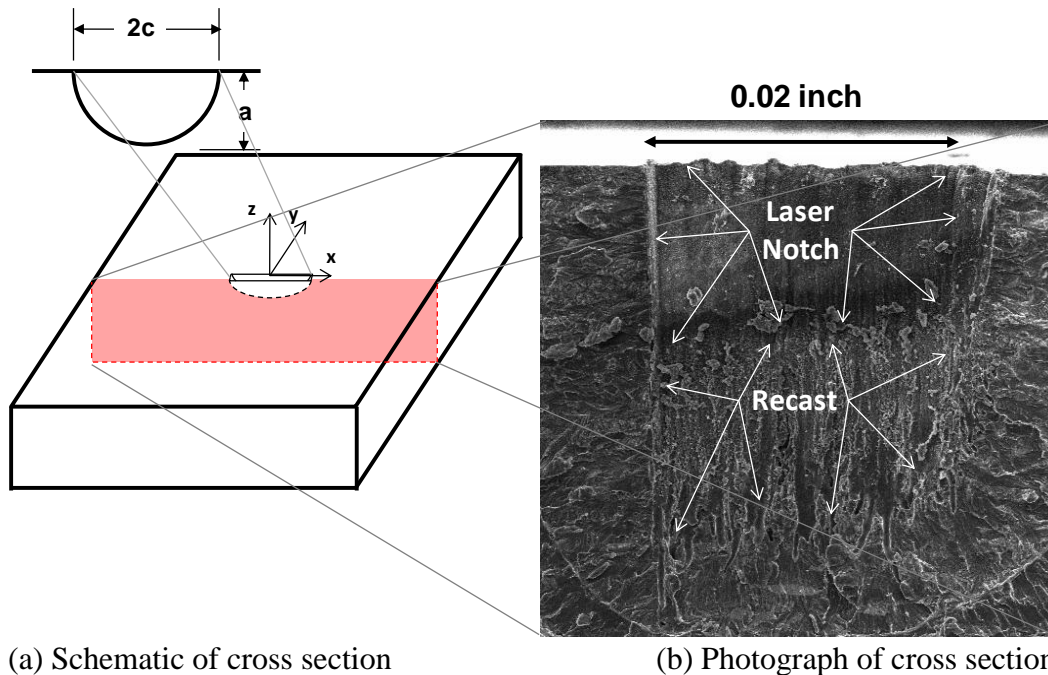


Figure 6.1-3. SEM photograph of a fatigue surface revealing the laser notch and the laser produced recast region

Fatigue cracks behave differently than notches, even notches as sharp as those generated using the laser notching process, and thus cyclic loading (precracking) was required to nucleate true fatigue cracks. The loading frequency of the hydrostatic testing system was about 0.1 Hz, so crack nucleation in less than 5,000 cycles was desired to minimize the time required to precrack to less than a day. A series of tests were conducted to determine the stress level that nucleated a crack in the appropriate number of cycles. The fatigue crack nucleation was examined by fatigue cycling 0.05 inch thick coupons of 6061-T62 aluminum with small laser notches. The coupons were 3 inches wide and had a laser notch with $2c = 0.02$ inches and $a/c \sim 1$. The coupons were fatigue cycled at $R = 0.1$ with peak stresses that ranged between 50 percent and just over 100 percent of the net section material yield stress to develop a relationship between peak cyclic stress and cycles to initiation. Crack nucleation was defined as when cracks observable with a 20x magnification optical microscope (~ 0.001 inches) were present on both ends of the notch. The number of cycles required to initiate an observable fatigue crack decreased as the peak stress increased, but remained a significant value (400 to 1,200 cycles) at peak stresses just above the yield stress, as shown in Figure 6.1-4. This indicated that the notches did not behave like fatigue cracks even at strain levels that approached that of the autofrettage cycle. The number of cycles required to initiate an observable fatigue crack at a peak stress that was 80 percent of the material yield stress was about 3,000 cycles, and this stress level was selected for all precrack loading.



Title:

**Fracture Mechanics Based Methods Development for
COPVs with Metallic Liners**

Page #:
19 of 164

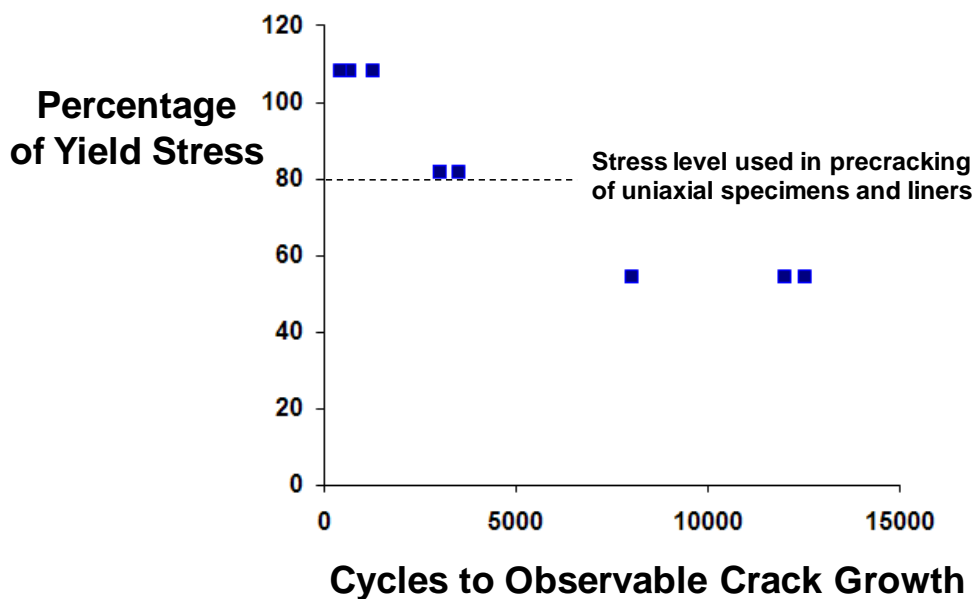


Figure 6.1-4. Number of fatigue cycles required to obtain visually apparent (with a 20x optical microscope) fatigue crack growth from a laser notch

6.2 Tensile Tests

The uniaxial tests were conducted on 0.125 inch, 0.09 inch, 0.05 inch, and 0.032 inch thick sheets of 6061-T62 aluminum to characterize the material behavior. All of the 0.125 inch, 0.05 inch, and 0.032 inch thick coupons were obtained from individual sheets, and the 0.09 inch thick coupons were obtained from two different sheets (lot 1 and lot 2). Tensile tests, using ASTM Standard E8 [ref. 3], were conducted on coupons manufactured from each of the sheets, as summarized in Table 6.2-1. (Note the variability in yield stress (S_o), particularly between lot 1 and lot 2 of the 0.09 inch thick material.) Multiple tests were conducted for each sheet of material and the results reported in terms of engineering stress-strain as shown in Figure 6.2-1. No tests were conducted on the liner material, but the manufacturer provided a yield stress value of 41.5 ksi.

Table 6.2-1. Results from the 6061-T62 Tensile Tests

| | 0.032 inch | 0.050 inch | 0.09 inch Lot 1 | 0.09 inch Lot 2 | 0.125 inch |
|-----------------|------------|------------|-----------------|-----------------|------------|
| E (ksi) | 10042 | 10020 | 9986 | 9708 | 9888 |
| S_o (ksi) | 43.4 | 37.5 | 39.55 | 45.47 | 46.63 |
| S_{ult} (ksi) | 48.3 | 45.7 | 47.25 | 48.86 | 50.41 |
| max strain | 0.146 | 0.142 | 0.150 | 0.105 | 0.129 |



Title:

Fracture Mechanics Based Methods Development for
COPVs with Metallic Liners

Page #:
20 of 164

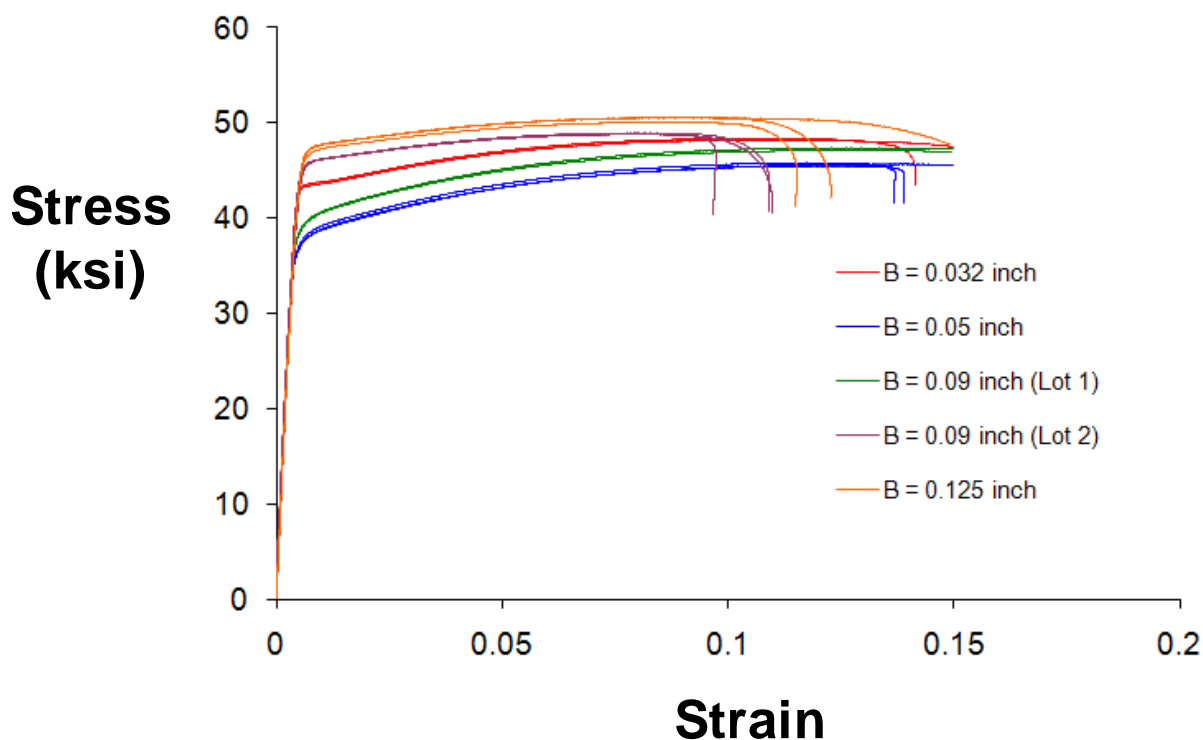


Figure 6.2-1. Stress-strain behavior of the material used in the uniaxial coupon tests that were conducted according to ASTM Standard E8 [ref. 3].

6.3 Baseline FCG Rate Tests

FCG rate tests were conducted under LFM conditions on the 0.09 inch thick 6061-T62 lot 2 aluminum to obtain the baseline FCG rate behavior. The tests and FCG rate measurements were made per ASTM E647 [ref. 4]. The tests were conducted on 3 inch wide middle crack tension (M(T)) coupons subjected to fully reversed loading ($R = -1$) and maximum stresses of 12 percent, 16 percent, and 24 percent of the material yield stress, 5.6 ksi, 7.4 ksi, and 11.1 ksi, respectively. The stress levels were selected to provide coverage of the power law crack growth region. The crack growth rate (calculated with a 3-point average) was plotted as a function of K_{max} , as shown in Figure 6.3-1. K_{max} was used rather than ΔK due to the negative stress ratios. A power law fit to the center portion of the data is also shown in Figure 6.3-1 and Equation 1. The data from the three tests are provided in Appendix A.



Title:

Fracture Mechanics Based Methods Development for
COPVs with Metallic Liners

Page #:
21 of 164

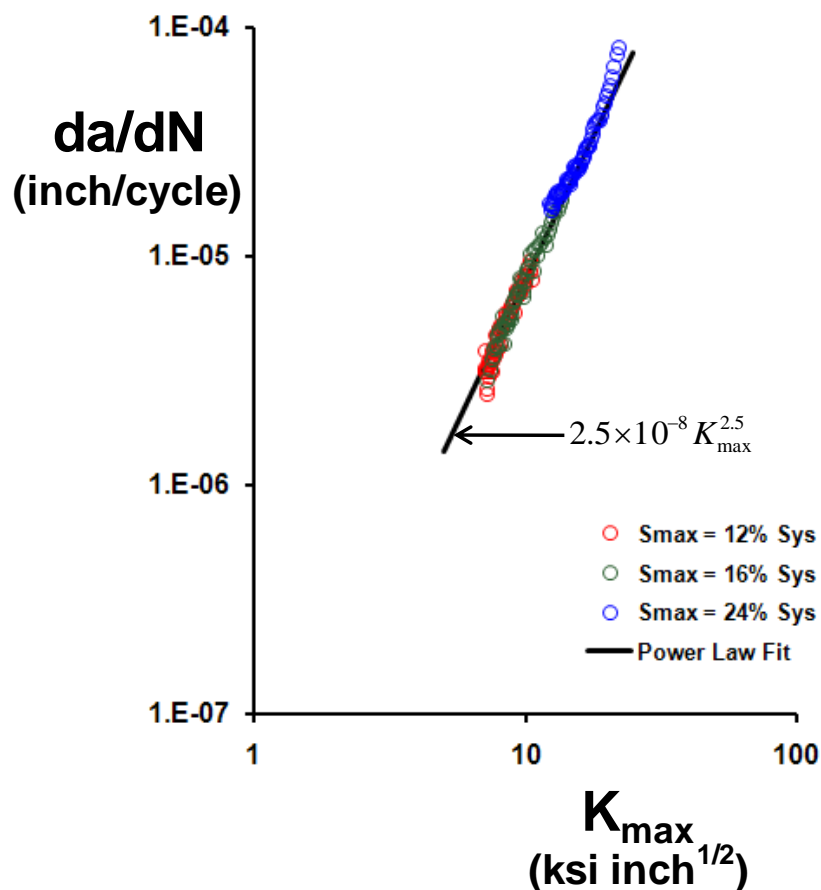


Figure 6.3-1. Linear elastic FCG rate results from the $M(T)$ tests that were conducted according to ASTM Standard E647 [ref. 4].

6.4 Uniaxial Coupon FCG Tests

Tests were conducted on coupons with small surface cracks to generate FCG rate data for comparison with the results from the multi-axial results of the COPV tests. The uniaxial tests were conducted on 0.125 inch, 0.09 inch, 0.05 inch, and 0.032 inch thick coupons. COPV liners will experience tensile yielding during the autofrettage loading and plastically responding liners will experience tensile and compressive yielding during the subsequent MDP cycles. Thin sheet uniaxial coupons will deform out-of-plane (buckle) under high compressive loads, so a guide plate system was necessary to restrain the out-of-plane displacements. The test coupons were originally 3 inches wide, but buckling was observed in the gap between the guide plates and the grips during the initial tests. The 3-inch wide coupons were machined into 2-inch wide dogbone

| | | | |
|--|---|--------------------------------------|------------------------|
|  | NASA Engineering and Safety Center Technical Assessment Report | Document #: NESC-RP-06-065 | Version: 1.0 |
| Title: Fracture Mechanics Based Methods Development for COPVs with Metallic Liners | | Page #: 22 of 164 | |

specimens, as shown in Figure 6.4-1, with enough of the original 3 inch wide section remaining to span the gap between the grips and guide plates.

6.4.1 Uniaxial Test Procedure

The procedure for conducting the uniaxial tests is outlined below:

1. Laser notches were placed in the center of a 3-inch wide, 12-inch long uniaxial specimen. Two sizes of laser notches were used:
 - a. Laser notches with $2c = 0.02$ inches and a depth that was targeted for $a = 0.01$ inches. These notches were intended to produce semi-circular fatigue cracks with $2c = 0.04$ inches and $a/c = 1$.
 - b. Laser notches with $2c = 0.10$ inches and a depth that was targeted for $a = 0.01$ inches. These notches were intended to produce long, shallow fatigue cracks with $a/c = 0.2$.
2. The notched uniaxial coupons were precracked at a peak stress equal to 80 percent of the material yield stress and $R = 0.1$. The semi-circular notches were cycled until $2c = 0.040$ inches was measured. The long, shallow notches were cycled until observable fatigue cracks (~ 0.001 inches) were visible at both notch tips.
3. The cracked uniaxial coupons were machined into a 2-inch wide dogbone coupon, as shown in Figure 6.4-1.
4. Guide plates were installed and extensometers were placed on the edges of the coupon to measure strain.
5. A displacement ramp of 0.005 inches/min was applied to specific maximum and minimum cyclic strains.
6. Surface crack growth was measured with a 20x optical scope through a 0.3-inch diameter hole in the guide plates, when the crack was not obscured by the guide plates.
7. The coupon was removed from the test machine and saw cuts were made from the edge of the coupon to within 0.05 inches of the crack tips, as shown in Figure 6.4-2.
8. The coupon was returned to the test machine and monotonically loaded until failure to expose the fatigue crack surfaces on the two broken sections of the coupon.
9. The fatigue crack surfaces were characterized for length, depth, and fatigue striations.



Title:

Fracture Mechanics Based Methods Development for
COPVs with Metallic Liners

Page #:
23 of 164

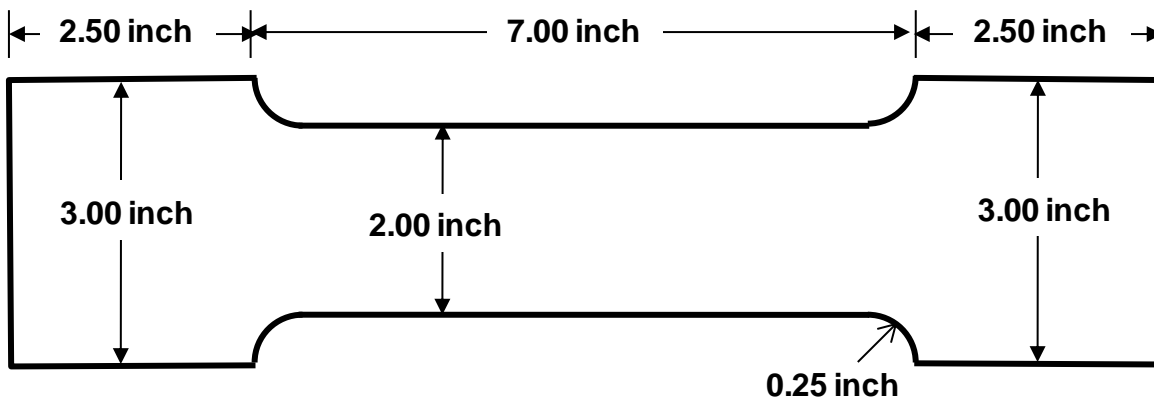


Figure 6.4-1. Dogbone coupon for uniaxial FCG testing

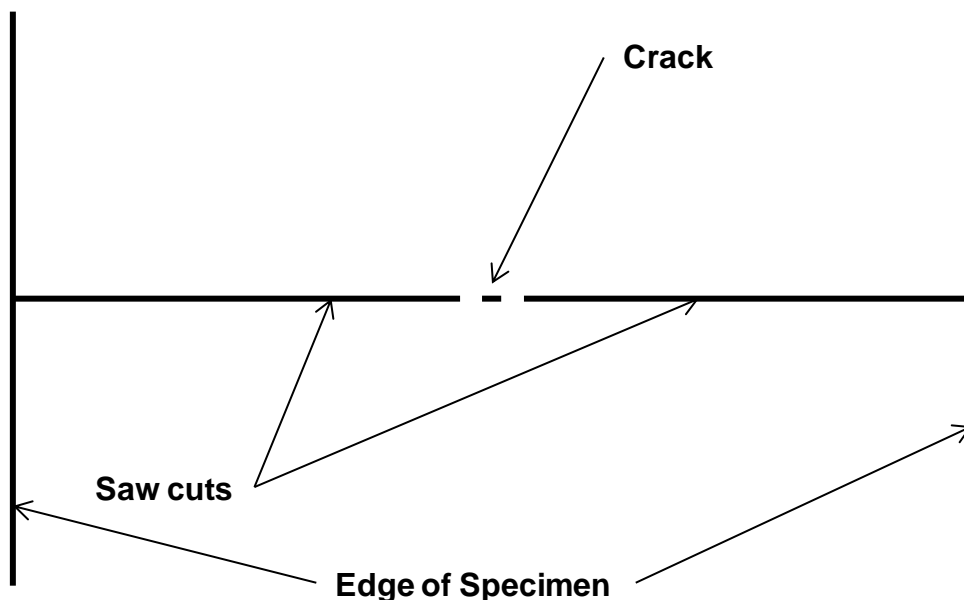


Figure 6.4-2. Schematic of saw cuts relative to the position of the fatigue crack

6.4.2 Uniaxial Fatigue Precracking

The 3-inch wide sheets with the laser notches were precracked until fatigue cracks nucleated at the notches. The precracking was conducted at $R = 0.1$ and a maximum stress that was about 80 percent of the material yield. Guide plates were not necessary because the stress ratio was positive. A frequency of 10 Hz was used during the precracking. The small laser notches that were intended to be semi-circular shaped (target size: 0.02 inches long by 0.01 inches deep) were cycled until the surface tip-to-tip measurement of $2c = 0.04$ inches was achieved. The number of

| | | | |
|--|---|--------------------------------------|------------------------|
|  | NASA Engineering and Safety Center Technical Assessment Report | Document #: NESC-RP-06-065 | Version: 1.0 |
| Title: Fracture Mechanics Based Methods Development for COPVs with Metallic Liners | | | Page #: 24 of 164 |

cycles required to initiate and grow a crack to the desired length was between 20,000 and 30,000. The long-shallow notches (target size: 0.10 inches long by 0.01 inches deep) were cycled until fatigue cracks (~0.001 inches) were observed at both notch ends. The K for a long-shallow crack is greater at the depth than at the surface, so substantial crack depth growth could occur before surface crack growth was visible. The number of cycles required to initiate and grow a crack to the desired length was between 1,500 and 5,000.

6.4.3 Uniaxial Guide Plates for $R = -1$ FCG Tests

Guide plates were necessary to prevent buckling of the thin sheet uniaxial coupons during the high negative loads required for compressive yield. The guide plates consisted of two 0.375 inch aluminum thick plates that sandwiched the coupon, as shown in Figure 6.4-3. The inner surface of the guide plates had a thin sheet of Teflon® tape to allow slippage between the guides and the coupon to minimize load transfer through the guides. The guide plates were hourglass shaped, with the center section about 1.95 inches wide. This was about 0.05 inches less than the width of the dogbone test section to allow extensometer contact. The length of the guide plates was sized to allow the gap between the guide plates and grips to be less than 0.01 inches at the minimum load. A larger gap would permit end buckling in the thinner coupons, as shown in Figure 6.4-4.

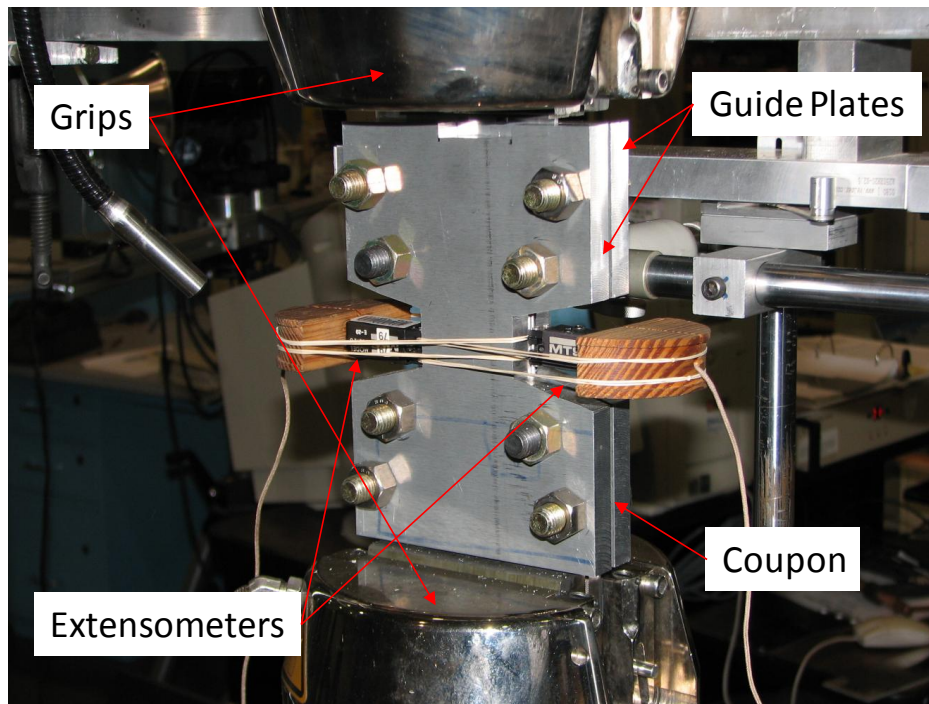


Figure 6.4-3. Photograph of guide plates with edge-mounted extensometers



NASA Engineering and Safety Center Technical Assessment Report

Document #:
**NESC-RP-
06-065**

Version:
1.0

Title:

Fracture Mechanics Based Methods Development for COPVs with Metallic Liners

Page #:
25 of 164

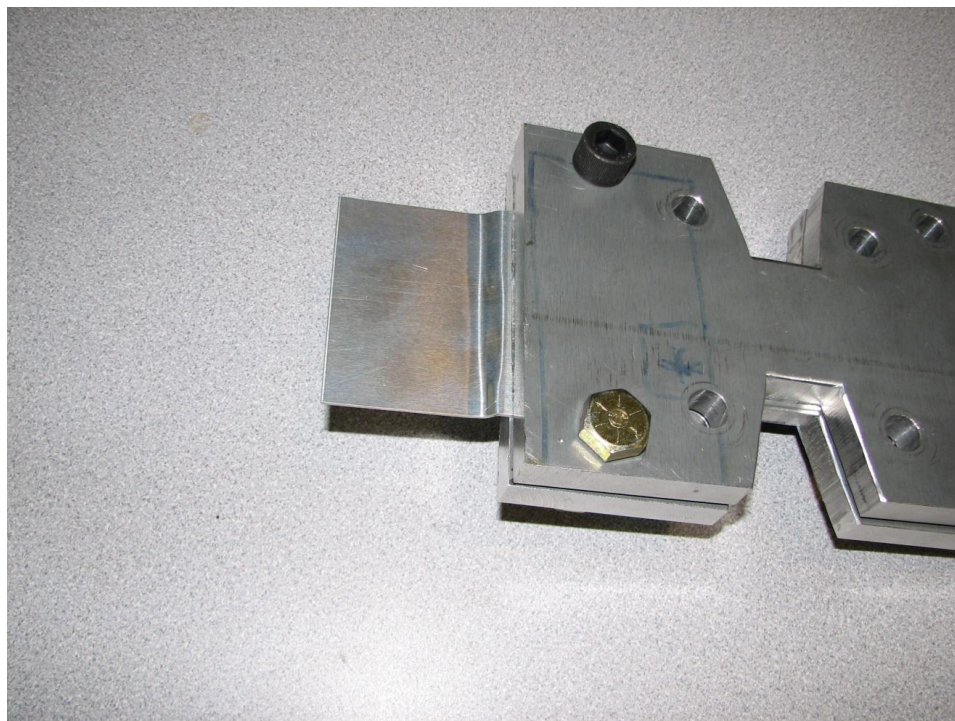


Figure 6.4-4. Example of end buckling in a 0.032-inch thick dogbone coupon

The 0.032-inch thick uniaxial coupons buckled between the guide plates and the grips with the smallest possible gap, so an additional restraint was developed for the thinnest coupons. The 0.375-inch thick guide plates were augmented with two 0.09-inch thick, discontinuous, sheets that were placed between the guide plates and the coupons, as shown in Figure 6.4-5. The 0.09-inch thick sheets were machined with the identical dimensions as the coupon except for the test region that was 0.05 inches narrower than the coupon to allow extensometer contact. The 0.09-inch thick sheets were discontinuous to prevent load transfer around the coupon, but provided sufficient stiffness in the gap between the guide plates and grips to prevent end buckling.

| | | | |
|--|---|--|--------------------------------|
|  | <p align="center">NASA Engineering and Safety Center Technical Assessment Report</p> | <p>Document #: NESC-RP-06-065</p> | <p>Version: 1.0</p> |
| <p>Title: Fracture Mechanics Based Methods Development for COPVs with Metallic Liners</p> | | <p>Page #: 26 of 164</p> | |

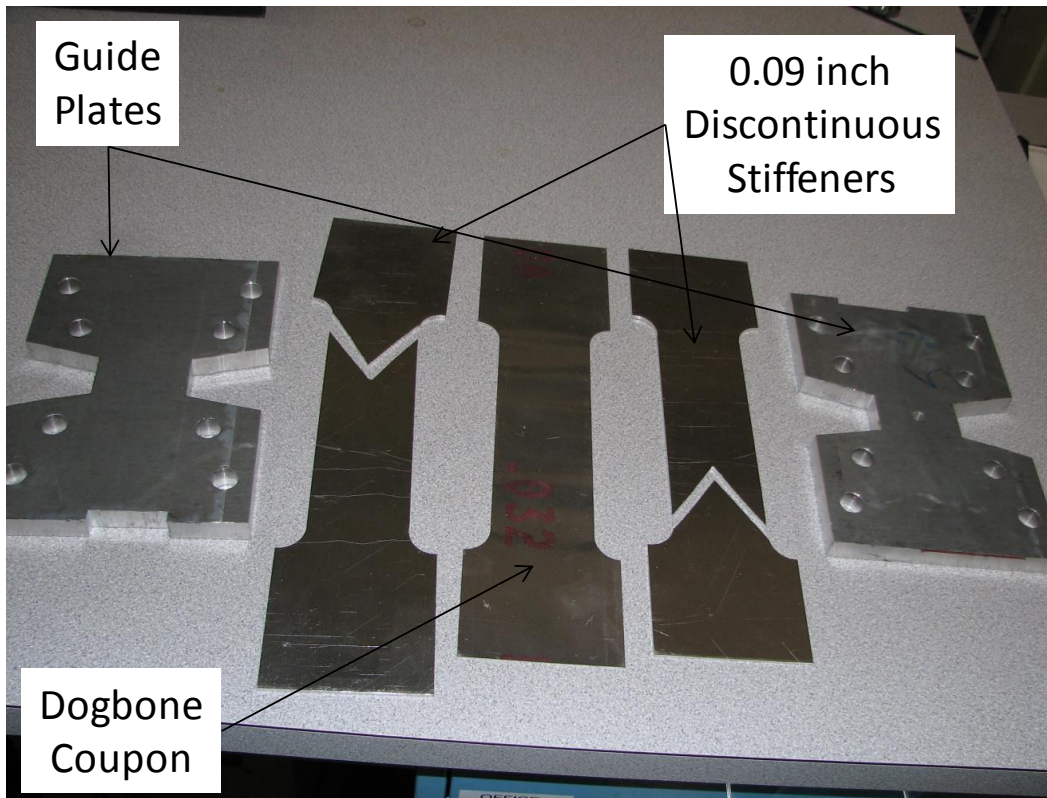


Figure 6.4-5. Guide plates, discontinuous stiffeners, and dogbone coupon

6.4.4 Uniaxial FCG Loading

The 6061-T62 dogbone coupons were laser notched with either small semi-circular or long-shallow notches and were fatigue cycled under displacement control to specific strain limits. The displacement loading ramp rate was 0.005 inches/minute and the strain was obtained from the average of the two edge extensometers. Four different loading conditions were applied: autofrettage, high constant amplitude, low constant amplitude, and COPV simulation. The cyclic strains (typical of COPV operation) for the four loading conditions are provided in Table 6.4-1. The target number of cycles for each test was 200 to represent four repetitions of a 50 cycle service life, but fewer cycles were applied if it appeared from the surface crack measurements that the crack would break through to the back surface. The number of cycles for the elastically responding COPV simulation tests was on the order of 5,000 cycles, because the lower cyclic strain range required more cycles to generate a measureable amount of FCG. The test coupons were loaded monotonically to failure after the desired number of fatigue cycles had been achieved. The first two cycles of a typical stress strain curve for an autofrettage test are shown in Figure 6.4-6. The initial cycle (autofrettage) resulted in significant plastic deformation of the



Title:

**Fracture Mechanics Based Methods Development for
COPVs with Metallic Liners**

Page #:
27 of 164

dogbone coupon. The subsequent unloading to zero strain resulted in compressive yielding. The second (MDP) cycle (loaded to 10,000 $\mu\epsilon$ and unloaded to 0 $\mu\epsilon$) resulted in both tensile and compressive yielding, but to a lesser extent than measured in the autofrettage cycle.

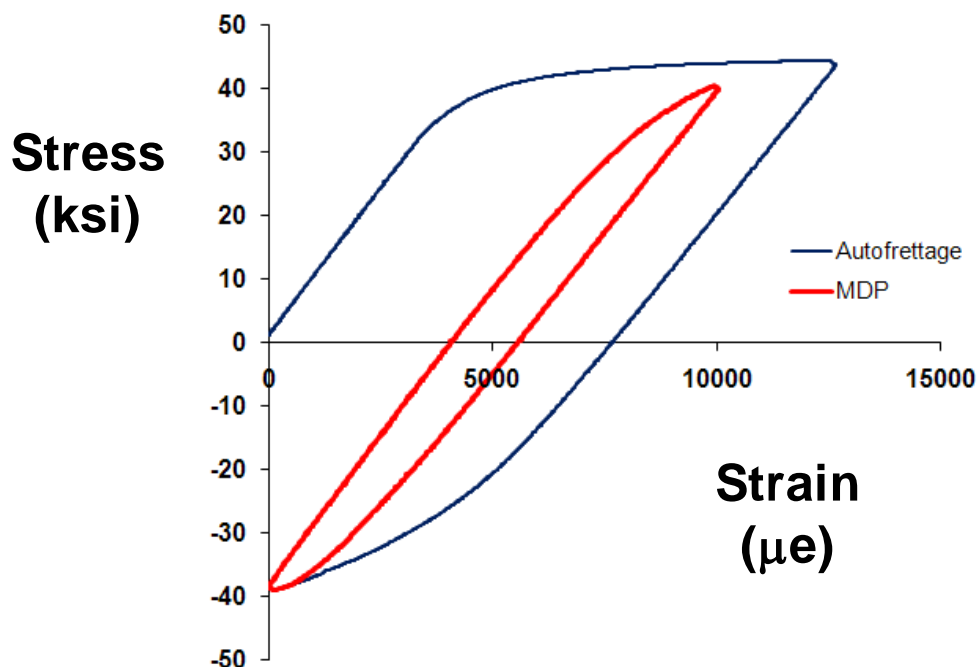


Figure 6.4-6. Typical stress-strain curve for a uniaxial fatigue test



**NASA Engineering and Safety Center
Technical Assessment Report**

Document #:
**NESC-RP-
06-065**

Version:
1.0

Title:

**Fracture Mechanics Based Methods Development for
COPVs with Metallic Liners**

Page #:
28 of 164

Table 6.4-1. Cyclic Strains for the Four Loading Conditions used in the Uniaxial Tests

| | Loading Spectrum Strain ($\mu\epsilon$) | | | |
|--------------------------------------|---|-------------------------|------------------------|-----------------|
| | Autofrettage | High Constant Amplitude | Low Constant Amplitude | COPV Simulation |
| Initial Strain | 0 | 0 | 0 | 0 |
| Max Strain for Cycle 1 | 12,500 | 12,500 | 10,000 | 12,500 |
| Min Strain for Cycle 1 | 0 | 0 | 0 | 5,460 |
| Max Strain for Fatigue Cycles | 10,000 | 12,500 | 10,000 | 10,000 |
| Min Strain for Fatigue Cycles | 0 | 0 | 0 | 5,460 |

Post-test examination of the fracture surfaces revealed distinct differences between the regions created by laser notch, precracking, fatigue cyclic loading, and monotonic loading to failure. A SEM photograph of a typical fracture surface is shown in Figure 6.4-7. The laser notch region was irregular shaped in the depth direction with “fingers” of recast material that extended the effective depth of the notch beyond the desired 0.01 inches, as shown by the dashed line in Figure 6.4-7. This resulted in aspect ratios (a/c) greater than 1 for the semi-circular notches. The “fingers” in the recast region are seen more clearly in SEM photograph shown in Figure 6.4-8. The boundaries between the precrack and the fatigue regions and the fatigue and ductile fracture regions are also well-defined at the magnification shown in Figure 6.4-8, as illustrated by the filled and open triangles, respectively. These boundaries represent the crack front at the end of the precracking and the fatigue loading, respectively. The difference between the two boundaries was the extent of crack growth (Δa) due to the fatigue loading and the FCG rate (da/dN) could be calculated knowing the number of fatigue loading cycles (200 for this test). Crack growth due to the autofrettage cycle was not visible in the SEM photographs and was assumed to be small relative to the damage due to the subsequent 200 cycles. Figure 6.4-9 contains a higher magnification SEM photograph of the fracture surface showing apparent fatigue striations. Fatigue striations are microscopic marks on the crack surface that, under certain loading conditions, have been shown to provide a one-to-one correlation between the crack macroscopically measured crack growth rate and the distance between striation marks [ref. 5]. The FCG rate based on striation spacing width was measured in six locations, as shown in Figure 6.4-9. A comparison was made between the FCG rate calculated from the striation

| | | | |
|--|---|--------------------------------------|------------------------|
|  | NASA Engineering and Safety Center Technical Assessment Report | Document #: NESC-RP-06-065 | Version: 1.0 |
| Title: Fracture Mechanics Based Methods Development for COPVs with Metallic Liners | | | Page #: 29 of 164 |

spacing and overall FCG rate obtained from the distance between the crack fronts in the same region. The average striation FCG rate for the six measurement locations (5.8×10^{-5} inches/cycle) was slightly higher than the overall FCG rate measured from the distance between crack fronts (5.5×10^{-5} inches/cycle).

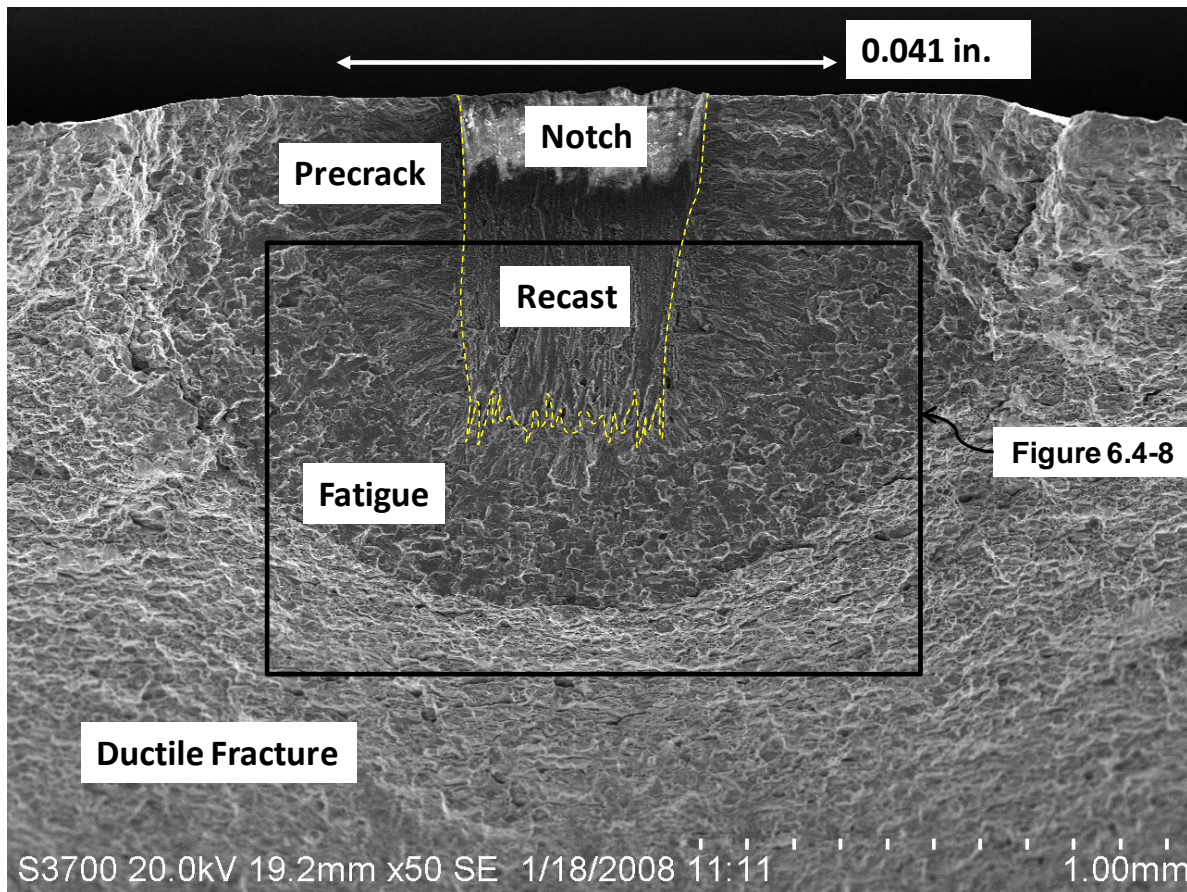


Figure 6.4-7. SEM photograph (50x) of a typical fracture surface (UNI-090-35-01) with the four regions identified. The dash lines highlight the recast region that is more apparent in Figure 6.4-8.



Title:

Fracture Mechanics Based Methods Development for
COPVs with Metallic Liners

Page #:
30 of 164

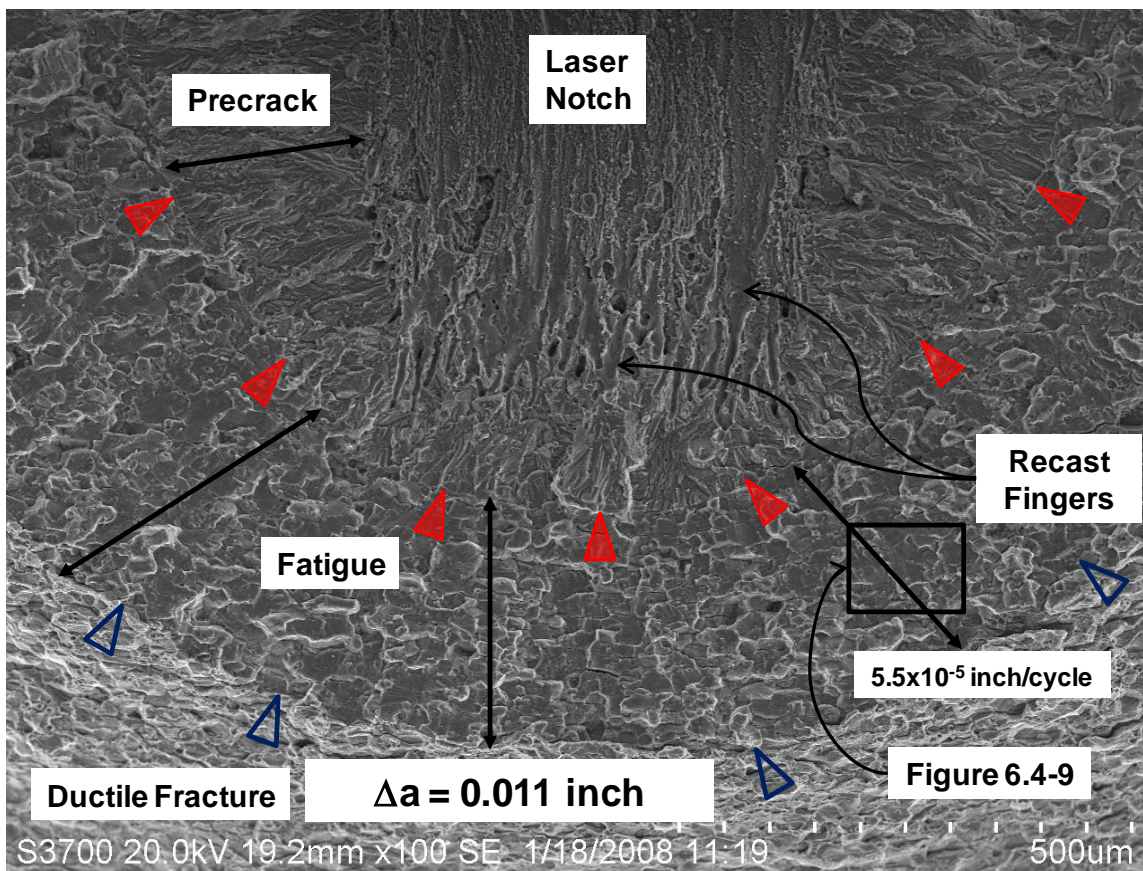


Figure 6.4-8. SEM photograph (100x) of a fracture surface (UNI-090-35-01) showing the maximum depth location

| | | | |
|--|---|--------------------------------------|------------------------|
|  | NASA Engineering and Safety Center Technical Assessment Report | Document #: NESC-RP-06-065 | Version: 1.0 |
| Title: Fracture Mechanics Based Methods Development for COPVs with Metallic Liners | | | Page #: 31 of 164 |

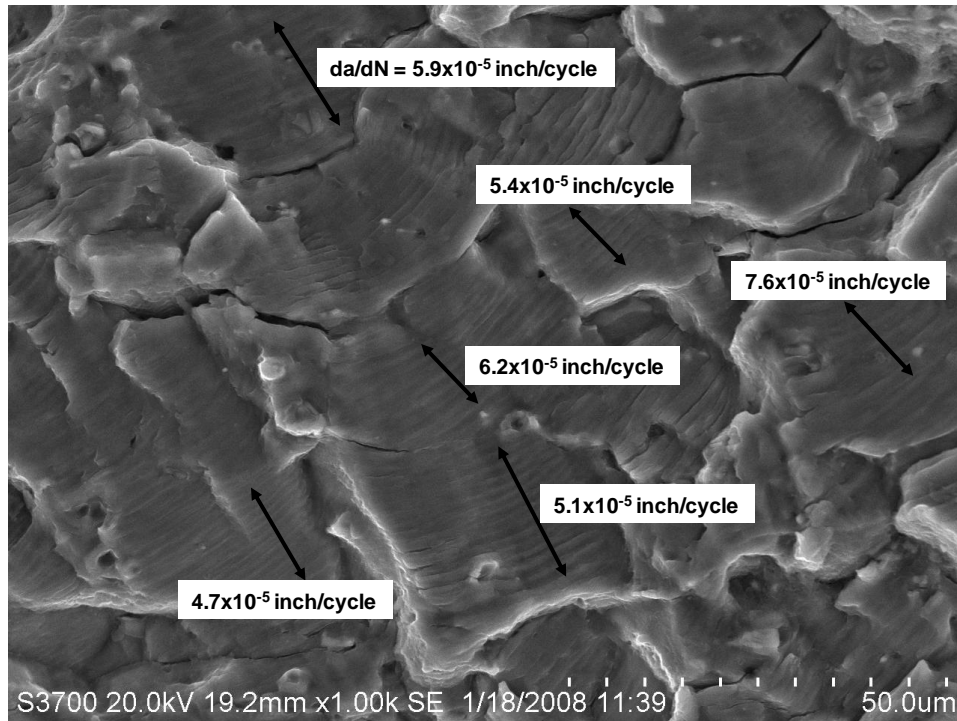


Figure 6.4-9. SEM photograph (1000x) of fracture surface (UNI-090-35-01) showing fatigue striations

6.4.5 Uniaxial FCG Test Results

The uniaxial test conditions and results are listed in Tables 6.4-2 to 6.4-6 and the fracture surfaces are provided in Appendix B. The test conditions include the loading conditions, initial crack lengths, and coupon dimensions. The test results include the final crack length, number of cycles, average crack growth rates, and any optical surface measurements that were made. All of the uniaxial tests, with the exception of UNI-090-40-06 and UNI-090-40-07 (tested to simulate the hoop stress in the elastically responding COPVs), were conducted under fully reversed, fully plastic conditions.



**NASA Engineering and Safety Center
Technical Assessment Report**

Document #:
**NESC-RP-
06-065**

Version:
1.0

Title:

**Fracture Mechanics Based Methods Development for
COPVs with Metallic Liners**

Page #:
32 of 164

Table 6.4-2. Uniaxial FCG Tests conducted on the 0.125-inch Thick Coupons

| Name | UNI-125-35-01 | UNI-125-35-02 | UNI-125-35-03 | | |
|--------------------------------|---------------|---------------|---------------|-------|--------|
| Precrack (% YS) | 80 | 80 | 80 | | |
| 1st Cycle ($\mu\epsilon$) | 12,500 | 12,500 | 10,000 | | |
| Other Cycles ($\mu\epsilon$) | 12,500 | 10,000 | 10,000 | | |
| W (inch) | 1.940 | 2.020 | 1.985 | | |
| B (inch) | 0.125 | 0.125 | 0.125 | | |
| ai (inch) | 0.034 | 0.031 | 0.030 | | |
| af (inch) | 0.041 | 0.039 | 0.049 | | |
| ci (inch) | 0.021 | 0.021 | 0.022 | | |
| cf (inch) | 0.034 | 0.034 | 0.046 | | |
| ai/ci | 1.66 | 1.48 | 1.36 | | |
| af/cf | 1.21 | 1.15 | 1.07 | | |
| N | 100 | 200 | 200 | | |
| da/dN (in/cycle) | 7.00E-05 | 4.00E-05 | 9.50E-05 | | |
| dc/dN (in/cycle) | 1.35E-04 | 6.50E-05 | 1.20E-04 | | |
| Surface Visual Measurements | | 2c | Cycles | 2c | Cycles |
| | | 0.040 | 0 | 0.044 | 0 |
| | | 0.046 | 50 | 0.051 | 50 |
| | | 0.055 | 100 | 0.062 | 100 |
| | | 0.062 | 150 | 0.075 | 150 |
| | | 0.067 | 200 | 0.092 | 200 |
| | | | | | |
| | | | | | |



**NASA Engineering and Safety Center
Technical Assessment Report**

Document #:
**NESC-RP-
06-065**

Version:
1.0

Title:

**Fracture Mechanics Based Methods Development for
COPVs with Metallic Liners**

Page #:
33 of 164

Table 6.4-3. Uniaxial FCG Tests conducted on the Lot 1 0.09-inch Thick Coupons

| Name | UNI-090-35-1 | UNI-090-35-2 | | UNI-090-35-3 | |
|------------------------------------|--------------|--------------|----------|--------------|----------|
| Precrack (% of YS) | 80 | 80 | 80 | 80 | 80 |
| 1st Cycle ($\mu\epsilon$) | 12,500 | 12,500 | 12,500 | 10,000 | 10,000 |
| Other Cycles ($\mu\epsilon$) | 10,000 | 12,500 | 12,500 | 10,000 | 10,000 |
| W (inch) | 1.960 | 1.970 | 1.970 | 1.980 | 1.980 |
| B (inch) | 0.090 | 0.090 | 0.090 | 0.090 | 0.090 |
| ai (inch) | 0.034 | 0.035 | 0.035 | 0.034 | 0.034 |
| af (inch) | 0.044 | 0.044 | 0.044 | 0.046 | 0.046 |
| ci (inch) | 0.021 | 0.021 | 0.021 | 0.020 | 0.020 |
| cf (inch) | 0.039 | 0.046 | 0.046 | 0.042 | 0.042 |
| ai/ci | 1.66 | 1.67 | 1.67 | 1.70 | 1.70 |
| af/cf | 1.14 | 0.96 | 0.96 | 1.10 | 1.10 |
| N | 200 | 120 | 120 | 200 | 200 |
| da/dN (in/cycle) | 5.00E-05 | 7.50E-05 | 7.50E-05 | 6.00E-05 | 6.00E-05 |
| dc/dN (in/cycle) | 9.00E-05 | 2.08E-04 | 2.08E-04 | 1.10E-04 | 1.10E-04 |
| Surface Visual Measurements | | 2c | Cycles | 2c | Cycles |
| | | 0.040 | 0 | 0.041 | 0 |
| | | 0.047 | 20 | 0.049 | 25 |
| | | 0.054 | 40 | 0.054 | 50 |
| | | 0.060 | 60 | 0.057 | 75 |
| | | 0.068 | 80 | 0.062 | 100 |
| | | 0.077 | 100 | 0.069 | 125 |
| | | 0.092 | 120 | 0.076 | 150 |
| | | | | 0.080 | 175 |
| | | | | 0.085 | 200 |



**NASA Engineering and Safety Center
Technical Assessment Report**

Document #:
**NESC-RP-
06-065**

Version:
1.0

Title:

**Fracture Mechanics Based Methods Development for
COPVs with Metallic Liners**

Page #:
34 of 164

Table 6.4-4. Uniaxial FCG Tests Conducted on the Lot 2 0.09-inch Thick Coupons

| Name | UNI-090-36-01 | | UNI-090-36-02 | | UNI-090-36-04 | | UNI-090-40-06 | | UNI-090-40-07 | |
|--------------------------------|---------------|--------|---------------|--------|---------------|--------|----------------|--------|----------------|--------|
| Precrack (% of YS) | 80 | | 80 | | 80 | | 80 | | 80 | |
| 1st Cycle ($\mu\epsilon$) | 0 to 12500 | | 0 to 12500 | | 0 to 12500 | | 0 to 12500 | | 0 to 12500 | |
| Other Cycles ($\mu\epsilon$) | 0 to 10000 | | 0 to 10000 | | 0 to 10000 | | 5,460 to 10000 | | 5,460 to 10000 | |
| W (inch) | 2.025 | | 2.000 | | 2.000 | | 2.000 | | 2.000 | |
| B (inch) | 0.090 | | 0.090 | | 0.090 | | 0.090 | | 0.090 | |
| ai (inch) | 0.012 | | 0.020 | | 0.020 | | 0.022 | | 0.011 | |
| af (inch) | 0.019 | | 0.044 | | 0.058 | | 0.028 | | 0.030 | |
| ci (inch) | 0.050 | | 0.052 | | 0.053 | | 0.020 | | 0.050 | |
| cf (inch) | 0.058 | | 0.070 | | 0.087 | | 0.029 | | 0.057 | |
| ai/ci | 0.24 | | 0.38 | | 0.38 | | 1.13 | | 0.22 | |
| af/cf | 0.33 | | 0.63 | | 0.67 | | 0.98 | | 0.53 | |
| N | 50 | | 150 | | 200 | | 6,000 | | 8,000 | |
| da/dN (in/cycle) | 1.40E-04 | | 1.60E-04 | | 1.90E-04 | | 1.00E-06 | | 2.38E-06 | |
| dc/dN (in/cycle) | 1.50E-04 | | 1.20E-04 | | 1.73E-04 | | 1.50E-06 | | 8.75E-07 | |
| Surface Visual Measurements | 2c | Cycles | 2c | Cycles | 2c | Cycles | 2c | Cycles | 2c | Cycles |
| | 0.100 | 0 | 0.104 | 0 | 0.105 | 0 | | | | |
| | 0.109 | 25 | 0.110 | 25 | 0.110 | 25 | | | | |
| | 0.115 | 50 | 0.117 | 50 | 0.114 | 50 | | | | |
| | | | 0.121 | 75 | 0.121 | 75 | | | | |
| | | | 0.126 | 100 | 0.127 | 100 | | | | |
| | | | 0.129 | 125 | 0.134 | 125 | | | | |
| | | | 0.140 | 150 | 0.142 | 150 | | | | |
| | | | | | 0.157 | 175 | | | | |
| | | | | 0.174 | 200 | | | | | |



**NASA Engineering and Safety Center
Technical Assessment Report**

Document #:
**NESC-RP-
06-065**

Version:
1.0

Title:

**Fracture Mechanics Based Methods Development for
COPVs with Metallic Liners**

Page #:
35 of 164

Table 6.4-5. Uniaxial FCG Tests Conducted on the 0.05-inch Thick Coupons

| Name | UNI-050-35-1 | | UNI-050-35-4 | | UNI-050-35-5 | |
|--------------------------------|--------------|--------|--------------|--------|--------------|--------|
| Precrack (% of YS) | 80 | | 80 | | 80 | |
| 1st Cycle ($\mu\epsilon$) | 12,500 | | 10,000 | | 12,500 | |
| Other Cycles ($\mu\epsilon$) | 10,000 | | 10,000 | | 12,500 | |
| W (inch) | 2.000 | | 1.995 | | 2.000 | |
| B (inch) | 0.050 | | 0.050 | | 0.050 | |
| ai (inch) | 0.026 | | 0.028 | | 0.026 | |
| af (inch) | 0.037 | | 0.043 | | 0.034 | |
| ci (inch) | 0.020 | | 0.021 | | 0.021 | |
| cf (inch) | 0.034 | | 0.042 | | 0.031 | |
| ai/ci | 1.30 | | 1.37 | | 1.27 | |
| af/cf | 1.10 | | 1.02 | | 1.10 | |
| N | 200 | | 100 | | 60 | |
| da/dN (in/cycle) | 5.50E-05 | | 1.50E-04 | | 1.33E-04 | |
| dc/dN (in/cycle) | 6.75E-05 | | 2.15E-04 | | 1.75E-04 | |
| Surface Visual Measurements | 2c | Cycles | 2c | Cycles | 2c | Cycles |
| | 0.040 | 0 | 0.041 | 0 | 0.040 | 0 |
| | 0.046 | 50 | 0.052 | 25 | 0.042 | 10 |
| | 0.055 | 100 | 0.059 | 50 | 0.045 | 20 |
| | 0.062 | 150 | 0.066 | 75 | 0.049 | 30 |
| | 0.068 | 200 | 0.085 | 100 | 0.053 | 40 |
| | | | | | 0.056 | 50 |
| | | | | | 0.062 | 60 |

| | | | |
|---|--|--------------------------------------|------------------------|
|  | NASA Engineering and Safety Center Technical Assessment Report | Document #: NESC-RP-06-065 | Version: 1.0 |
| | Title: Fracture Mechanics Based Methods Development for COPVs with Metallic Liners | | Page #: 36 of 164 |

Table 6.4-6. Uniaxial FCG Tests Conducted on the 0.032-inch Thick Coupons

| Name | UNI-032-36-5 | UNI-032-37-03 |
|--------------------------------|--------------|---------------|
| Precrack (% of YS) | 80 | 80 |
| 1st Cycle ($\mu\epsilon$) | 12,500 | 12,500 |
| Other Cycles ($\mu\epsilon$) | 10,000 | 10,000 |
| W (inch) | 1.995 | 1.973 |
| B (inch) | 0.032 | 0.032 |
| ai (inch) | 0.018 | 0.018 |
| af (inch) | 0.024 | 0.020 |
| ci (inch) | 0.053 | 0.015 |
| cf (inch) | 0.056 | 0.018 |
| ai/ci | 0.34 | 1.20 |
| af/cf | 0.43 | 1.11 |
| N | 10 | 50 |
| da/dN (in/cycle) | 6.00E-04 | 4.00E-05 |
| dc/dN (in/cycle) | 3.00E-04 | 6.00E-05 |

The test coupons were fatigue cycled in displacement control to specified strain limits. The strain was obtained from the average of the two extensometer measurements placed on the edges of the coupon. An elastic-plastic FEA was performed on the pressurized COPVs (see below for details) and the minimum cyclic strain in the crack regions was determined to be 5,460 $\mu\epsilon$. Two uniaxial fatigue tests (UNI-090-40-06 and UNI-090-40-07) were conducted with this minimum cyclic strain to replicate the predicted strain history of the COPVs. The stress-strain curve from these test are shown in Figure 6.4-10 and unlike the stress-strain curve shown in Figure 6.4-6 for a uniaxial test with a minimum strain of 0, the results shown in Figure 6.4-10 show little plasticity after the initial autofrettage cycle. The maximum stress of the cyclic loading of 24 ksi was below the yield stress of the material and $R = -0.7$.



Title:

Fracture Mechanics Based Methods Development for
COPVs with Metallic Liners

Page #:
37 of 164

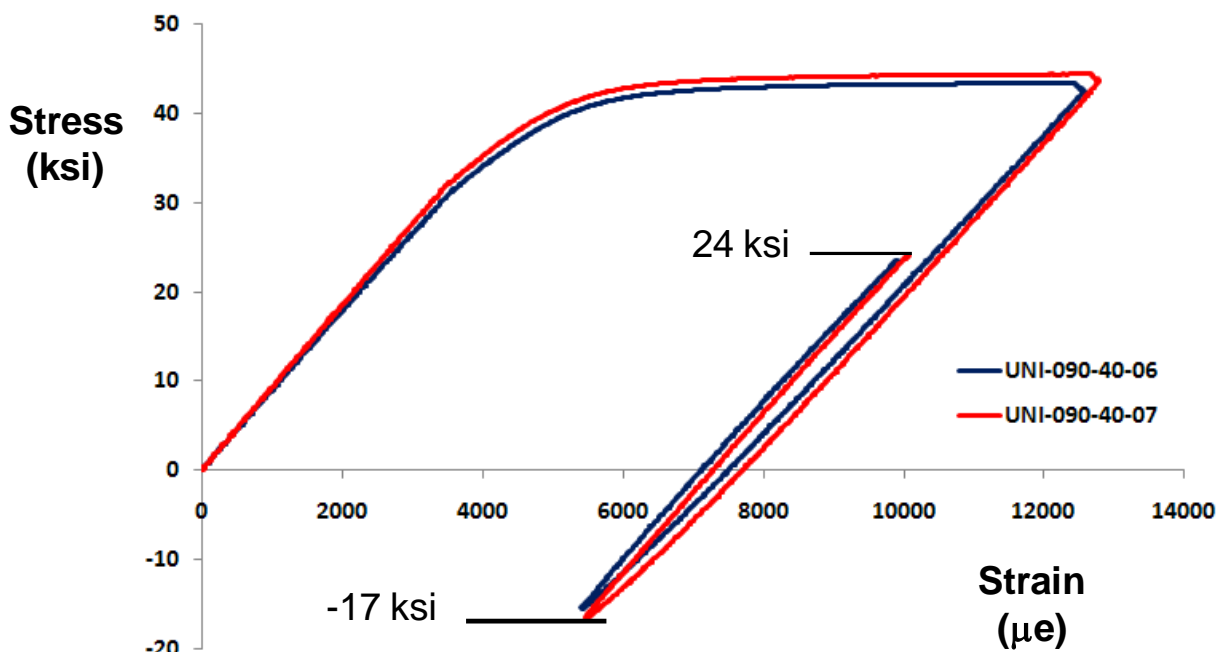


Figure 6.4-10. Stress-strain curve from the cyclic fatigue tests of coupons UNI-090-40-06 and UNI-090-40-07

6.5 Pressurized COPV Tests

FCG tests were conducted on COPVs with liners containing small surface cracks to generate FCG rate data for comparison with the results from uniaxial coupons. The precracking of the liners and the FCG testing of the COPVs were performed using the hydrostatic testing system shown in Figure 6.5-1. The hydrostatic test system was a self-contained unit that used deionized (DI) water to pressurize the liners and COPVs up to 4,000 psid (lbs per square inch difference) at a cyclic rate of 0.1 Hz. The following sub-sections describe the test procedure, precracking and NDE, FEA results, and test results for the multi-axial COPV tests. The liners were made from 6061-T62 aluminum with a yield stress of 41.5 ksi and a thickness of 0.09 inches in the cylindrical section, as shown schematically in Figure 6.5-2. The composite wrapping was T700-24K-50C with a reported 65 percent fiber volume.

| | | | |
|--|---|--|--------------------------------|
|  | <p align="center">NASA Engineering and Safety Center Technical Assessment Report</p> | <p>Document #: NESC-RP-06-065</p> | <p>Version: 1.0</p> |
| <p>Title: Fracture Mechanics Based Methods Development for COPVs with Metallic Liners</p> | | <p>Page #: 38 of 164</p> | |



Figure 6.5-1. Hydrostatic testing system

6.5.1 COPV Test Procedure

The procedure for conducting the pressurized COPV tests is outlined below:

1. The bare liners were polished with 1200 grit abrasive paper to remove machining marks on the exterior surface.
2. Three laser notches were applied to the surface to initiate fatigue cracks. The notches were 120 degrees apart. All of the laser notches were located in the cylindrical region of the liner, with notch #1 about 2 inches from the end of the cylindrical region on the ported end of the liner. Notch #2 was in the center of the cylindrical region. Notch #3 was about 2 inches from the end of the cylindrical region on the unported end of the liner.

| | | | |
|--|---|---|------------------------|
|  | NASA Engineering and Safety Center Technical Assessment Report | Document #: NESC-RP- 06-065 | Version: 1.0 |
| Title: Fracture Mechanics Based Methods Development for COPVs with Metallic Liners | | Page #: 39 of 164 | |

A schematic of the crack locations is provided in Figure 6.5-3. All of the laser notches were nominally the same size for a given liner. Two sizes of laser notches were used:

- a. Laser notches with $2c = 0.02$ inches and a depth that was targeted for $a = 0.01$ inches. These notches were intended to produce semi-circular fatigue cracks with $2c = 0.04$ inches and $a/c = 1$.
 - b. Laser notches with $2c = 0.10$ inches and a depth that was targeted for $a = 0.01$ inches. These notches were intended to produce long, shallow fatigue cracks with $a/c = 0.2$.
3. The notched liners were precracked using a hydrostatic testing machine that had a frequency of about 0.1 Hz. The peak stress was equal to 80 percent of the material yield stress and $R = 0$ (complete depressurization). The semi-circular notches were precracked until $2c = 0.040$ inches was measured for at least one of the laser notches. The long, shallow notches were precracked until observable fatigue cracks (~ 0.001 inches) were visible at both crack tips of all three notches.
 4. The liners with the small semi-circular notches were examined with an eddy current NDE inspection every 2,000 cycles to detect fatigue cracks that developed from manufacturing defects on the liner ID. The precracking was stopped when the NDE inspection detected internal flaws regardless of the size of the cracks at the notches to prevent the internal flaws from growing through the thickness.
 5. The cracked liners were overwrapped with carbon fiber composite.
 6. The wrapped liners (now called COPVs) were pressure loaded to 3,804 psid to produce the autofrettage cycle (12,500 $\mu\epsilon$), depressurized, and then fatigue cycled from zero pressure to 2,460 psid. The test pressures were obtained from FEA, as discussed later.
 7. The COPVs were sectioned and the composite overwrapped removed. The fatigue cracks were located and a sample containing the crack was removed from the liner. Saw cuts, collinear with the direction of crack growth, were made from the edge of the square to within 0.05 inches of the crack tip. The notched square was loaded monotonically to failure to expose the fracture surfaces.



**NASA Engineering and Safety Center
Technical Assessment Report**

Document #:
**NESC-RP-
06-065**

Version:
1.0

Title:

**Fracture Mechanics Based Methods Development for
COPVs with Metallic Liners**

Page #:
40 of 164

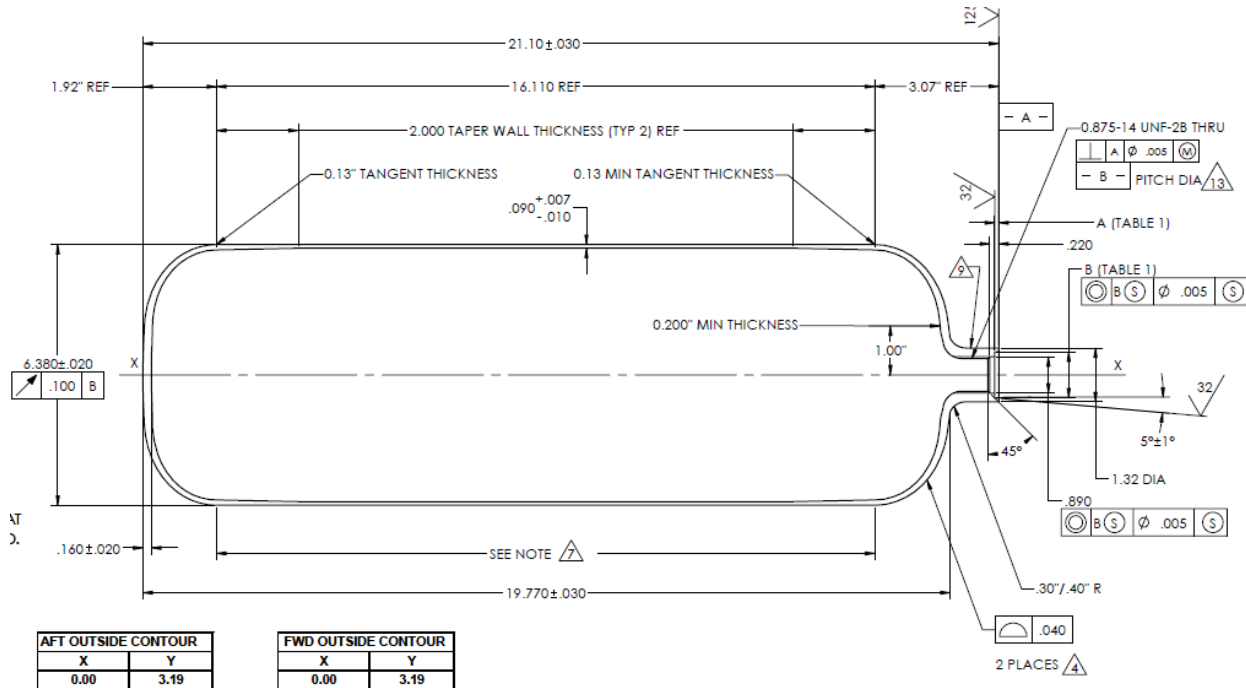


Figure 6.5-2. Schematic of the liner used in the pressurized COPV tests

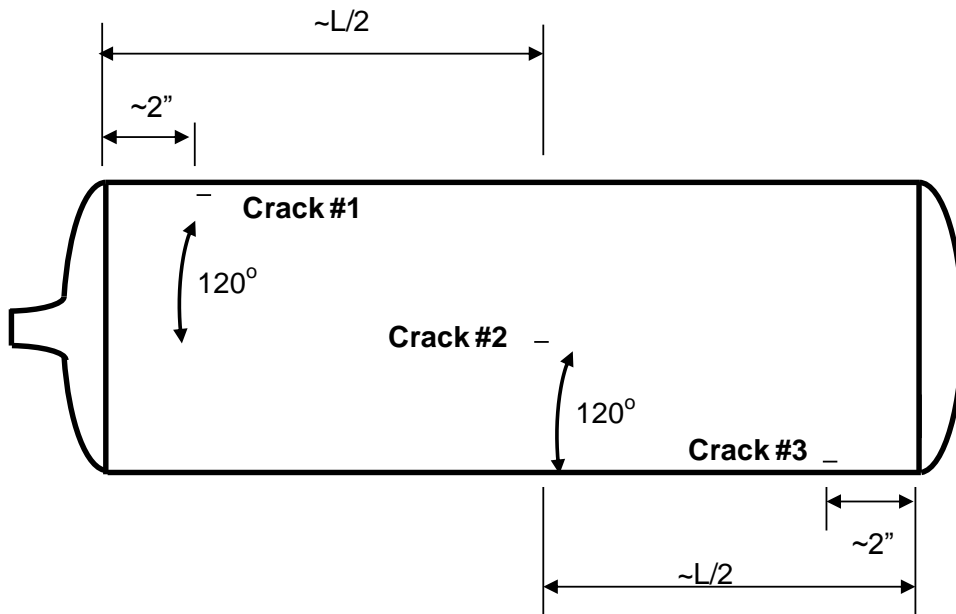


Figure 6.5-3. Schematic of the laser notch locations for the liners

| | | | |
|--|---|--------------------------------------|------------------------|
|  | NASA Engineering and Safety Center Technical Assessment Report | Document #: NESC-RP-06-065 | Version: 1.0 |
| Title: Fracture Mechanics Based Methods Development for COPVs with Metallic Liners | | | Page #: 41 of 164 |

6.5.2 Liner Precracking – Laser Notch versus Manufacturing Surface Defects

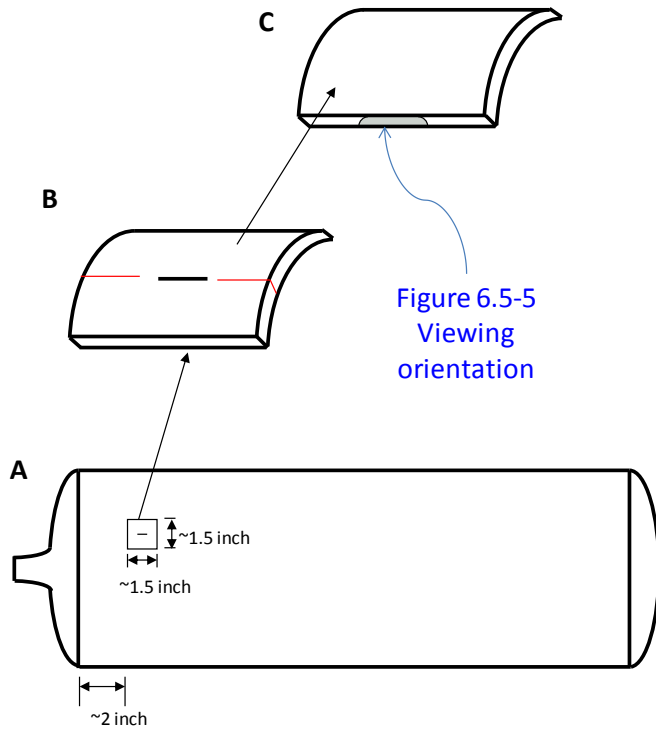
The first notched liner that was precracked developed an exterior crack that nucleated from a manufacturing defect and grew through the thickness and leaked before the cracks that initiated at the laser notches reached the required length. All of the subsequent liners were polished with 1,200 grit abrasive paper to remove machining marks and manufacturing defects. The second notched liner leaked during precracking (after 6,175 cycles at 80 percent of the material yield stress) at a manufacturing defect from the liner ID. In both cases, cracks also nucleated at the laser notches, but had not grown to the required length. The crack in the second notched liner was examined fractographically. The location of the defect and the procedure used to reveal the fracture surface is described in Figure 6.5-4. Examination of the failed surface revealed that a long-shallow (~0.5 inches long by 0.02 inches deep) manufacturing flaw that nucleated a fatigue crack that grew through the thickness and leaked. The outline of the manufacturing defect and the crack front after breaking through the surface are shown as dashed lines in Figure 6.5-5. The manufacturing defect had a flat, featureless appearance that extended along the length of the liner with the crack surfaces perpendicular to the direction of the hoop stress that resulted from the internal pressurization, as shown in Figure 6.5-6a. A sharp interface is visible between the initial defect and the FCG that resulted from the precrack pressure cycles. Likewise, an interface is visible between the fatigue crack region and the ductile tearing region that resulted from the monotonic loading that was performed to separate the crack surfaces. Fatigue striations were visible in the fatigue crack region along the interface with the ductile tearing region, as shown in Figure 6.5-6b.



Title:

Fracture Mechanics Based Methods Development for COPVs with Metallic Liners

Page #:
 42 of 164



- a) A 1.5 inch by 1.5 inch square, containing the crack that grew through the thickness, was removed from the liner
- b) Two saw cuts (red lines) were made in line with the crack tips, but about 0.05 inch from the tips
- c) The remaining ligaments were broken in bending, revealing the surface of the fatigue crack

Figure 6.5-5
 Viewing
 orientation

Figure 6.5-4. Procedure used to extract the fatigue crack that initiated from a manufacturing defect on the liner ID

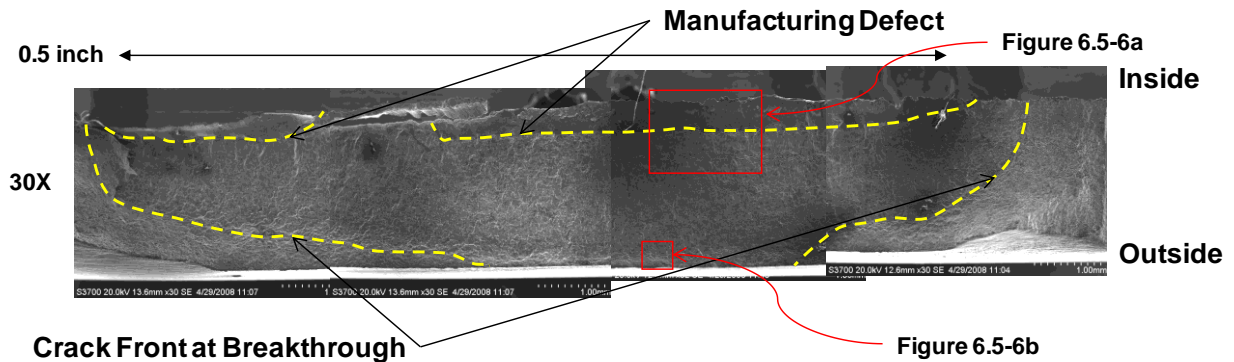
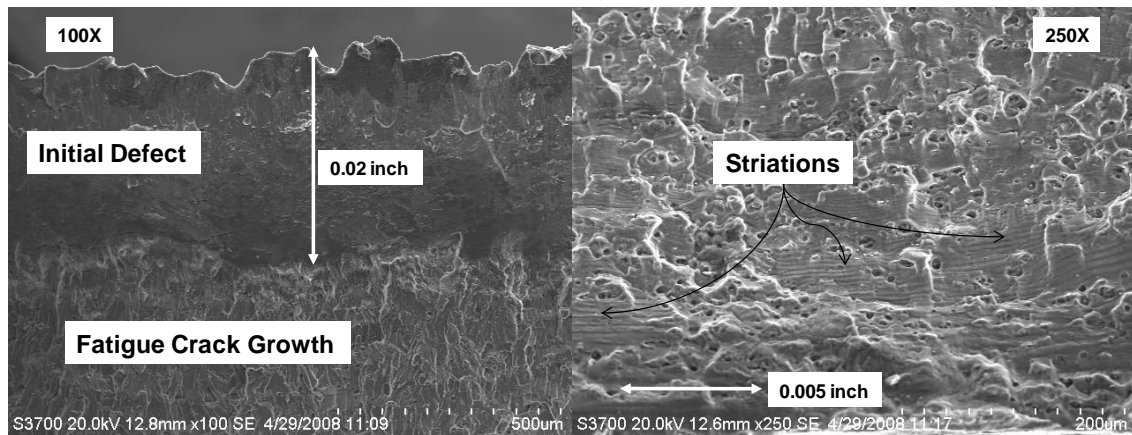


Figure 6.5-5. SEM photograph of a fatigue crack that nucleated from a liner manufacturing defect that leaked during precracking. The dashed lines highlight the crack front boundaries.

| | | | |
|--|---|--------------------------------------|------------------------|
|  | NASA Engineering and Safety Center Technical Assessment Report | Document #: NESC-RP-06-065 | Version: 1.0 |
| Title: Fracture Mechanics Based Methods Development for COPVs with Metallic Liners | | | Page #: 43 of 164 |



a. SEM Photograph of manufacturing flaw b. SEM Photograph of fatigue striations near the leaks site

Figure 6.5-6. Higher magnification SEM photographs of the fatigue crack shown in Figure 6.5-5.

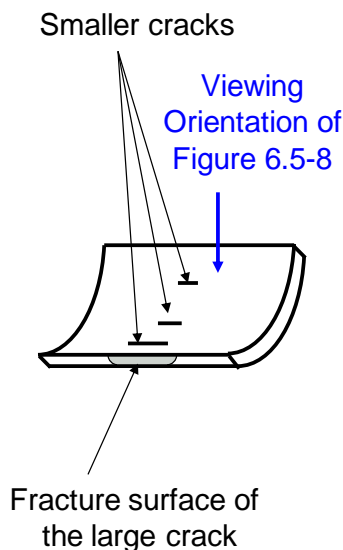
Further examination of the ID surface revealed several smaller cracks that were parallel with the crack that grew through the thickness. These cracks were located after the fracture surfaces of the large crack had been separated, thus the smaller cracks may have been plastically deformed, potentially creating a larger apparent crack opening, due to the separation process. Figure 6.5-7 illustrates the location of the additional cracks and Figure 6.5-8 contains an optical photograph of the ID surface showing the edge of the large crack and two parallel smaller cracks. The segment of liner was cut, as shown in Figure 6.5-9, to reveal the edge of the cracks. The cut segment was polished and examined using a SEM, as shown in Figure 6.5-10. The edge view shows that the internal cracks initiated from sharp, crack-like defects that were 0.02 inches to 0.003 inches deep and growing at about a 45-degree angle to the radial direction. The edges of the internal defects appear to have very smooth crack surfaces that were uncharacteristic of FCG. All of the cracks exhibited a sharp change in trajectory with the fatigue crack turning to grow in a radial direction that would be expected under cyclic hoop stress loading. The crack edges in this portion of the crack exhibited irregular behavior that is characteristic of FCG.



Title:

**Fracture Mechanics Based Methods Development for
COPVs with Metallic Liners**

Page #:
44 of 164



- a) The 1.5 inch by 1.5 inch cutout, described in Figure 6.5-4, was broken into two pieces along the large crack
- b) One fracture surface from the large crack that broke through the thickness was exposed on one edge of the cutout
- c) Additional smaller cracks, parallel to the large crack, were observed on the inside surface
- d) Note that the smaller cracks were exposed to bending stresses during the separation of the fracture surfaces, so the crack opening may be unnaturally large

Figure 6.5-7. Procedure used to view the smaller fatigue cracks that nucleated from manufacturing defects on the liner ID



**NASA Engineering and Safety Center
Technical Assessment Report**

Document #:
**NESC-RP-
06-065**

Version:
1.0

Title:

**Fracture Mechanics Based Methods Development for
COPVs with Metallic Liners**

Page #:
45 of 164

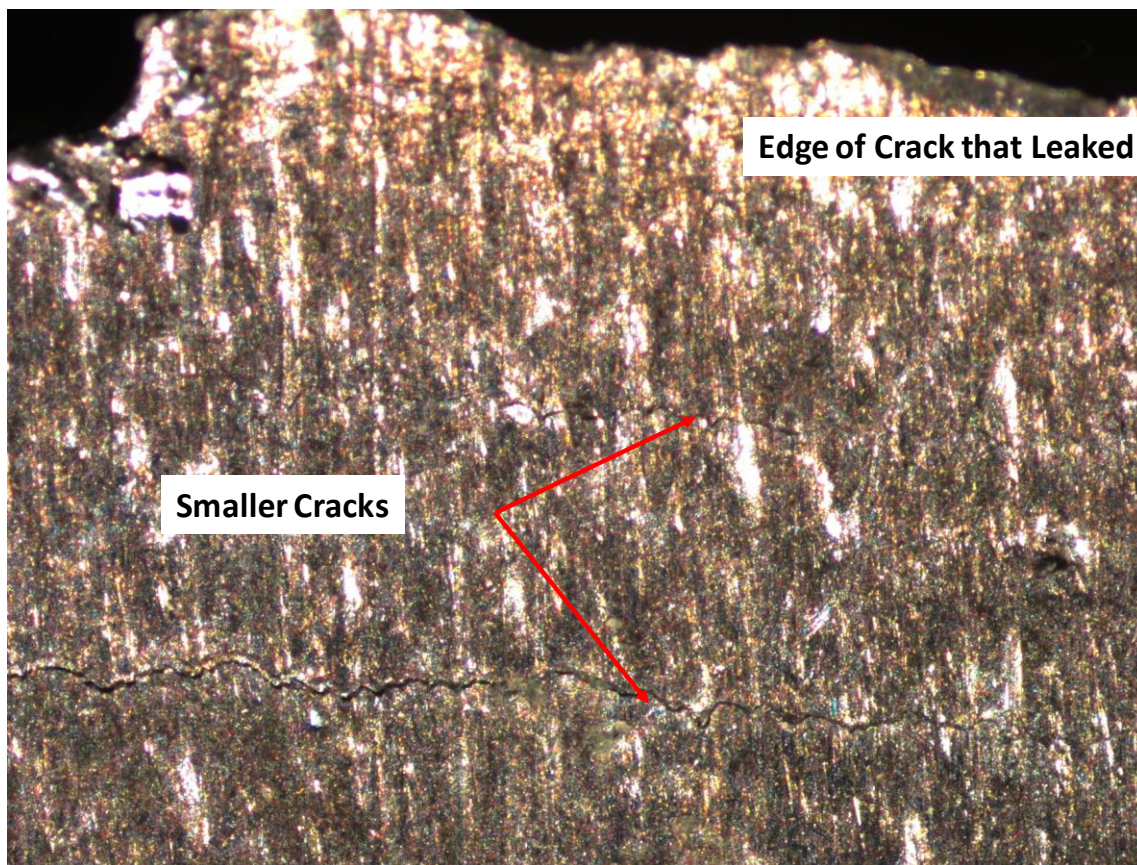


Figure 6.5-8. Optical photograph of two small cracks that were parallel to the liner crack that leaked during precracking

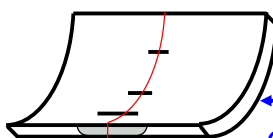


Title:

Fracture Mechanics Based Methods Development for
COPVs with Metallic Liners

Page #:
46 of 164

a) One of the cutout halves was cut in half again along a line that passed through several small cracks (red line)



Viewing
Orientation for
Figure 6.5-10

b) One surface was polished and examined by looking at the edge

c) This view revealed the through-the-thickness shape of the cracks at one point, as shown in Figure 6.5-10

Figure 6.5-9. Procedure used to view the edge of the small fatigue cracks that nucleated from manufacturing liner defects.

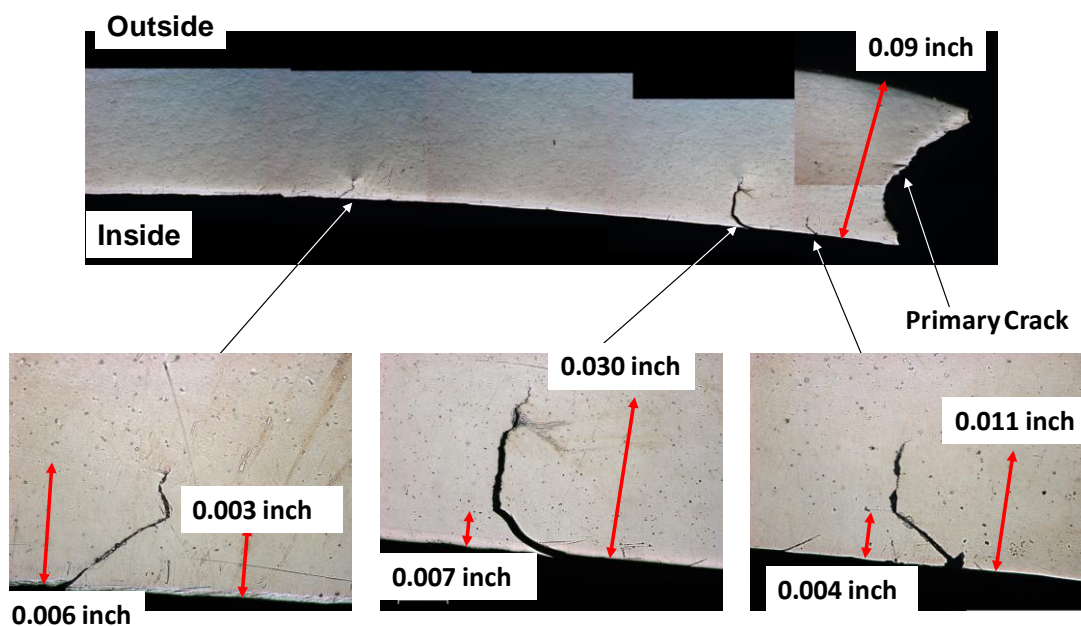


Figure 6.5-10. SEM photographs of fatigue cracks that initiated from manufacturing defects.

| | | | |
|--|---|--------------------------------------|------------------------|
|  | NASA Engineering and Safety Center Technical Assessment Report | Document #: NESC-RP-06-065 | Version: 1.0 |
| Title: Fracture Mechanics Based Methods Development for COPVs with Metallic Liners | | | Page #: 47 of 164 |

6.5.3 NDE Eddy Current Detection of Cracks

The presence of the preexisting, internal defects (manufacturing induced) made the precracking process problematic for the small semi-circular notches. The long, shallow notches nucleated fatigue cracks in about 3,000 to 5000 precracking cycles, but the semi-circular notches required as much as 20,000 cycles. Some preexisting internal defects nucleated and grew through the thickness in 6,000 to 18,000 precracking cycles. Thus, the liners with long, shallow notches were precracked without problems, but the first two liners with small semi-circular notches leaked from cracks growing from interior defects. As a result, the precracking process for the small, semi-circular notches was modified as follows:

1. Precrack the liners for 6,000 cycles.
2. After 6,000 cycles, remove the liners every 2,000 cycles for an eddy current inspection with a probe that was optimized to detect cracks on the ID surface.
3. Stop the precracking when the eddy current inspection detected an internal flaw.

The modified precracking process prevented the internal defects from growing to failure during cycling, but limited $2c \sim 0.03$ inches rather than 0.04 inches in some of the liners. An example NDE scan is shown in Figure 6.5-10 for the same location after 14,000 cycles, 16,000 cycles, 18,000 cycles, and 20,000 cycles. Data was acquired using a commercial version of the Self-Nulling Eddy Current Probe [ref. 6] in driver pickup mode at an operating frequency of 5 kHz. An automated scanning system was created that held the probe normal to the liner surface while it was scanned at a constant velocity of 1.5 inches/second along the liner axial direction. Data was acquired at a rate of 30 Hz while the probe was translated to achieve a grid spacing of 0.05 inch. The liner was then rotated 0.875 degrees and the probe returned to the ported end of the liner before the next scan line of data was acquired. This scanning method enabled the entire cylindrical region of the liner to be scanned in 2-½ hours. C-scan plots of the eddy current data were then constructed from the acquired probe impedance data, with internal defects highlighted in the component of the impedance 90 degrees out of phase with that due to a change in the probe to part spacing. For small flaws the probe diameter was larger than the crack length. The maximum change in probe impedance then occurs when the sensor windings are centered on the flaw with the winding direction at right angles to the indication. A small flaw is thus visualized as two adjacent areas of high impedance relative to the nominally uniform background. While the distance between the two local maximum is a function of the probe diameter, the line connecting the points defines the crack growth direction.

In Figure 6.5-10, the scans at 14,000 and 16,000 cycles did not reveal areas of high localized signals. The scan at 18,000 cycles revealed a possible crack indication, but it was not significantly stronger than the surrounding response. However, by 20,000 cycles the crack had



NASA Engineering and Safety Center Technical Assessment Report

Document #:
**NESC-RP-
06-065**

Version:
1.0

Title:

Fracture Mechanics Based Methods Development for COPVs with Metallic Liners

Page #:
48 of 164

grown sufficiently to produce a very strong, localized signal that had a high likelihood of being an ID crack and the precracking was stopped. Two co-linear fatigue cracks, with a total length that was smaller than the probe diameter, were identified after the liner was wrapped and pressure tested. None of the liners leaked during the precracking process after the NDE inspections were implemented.

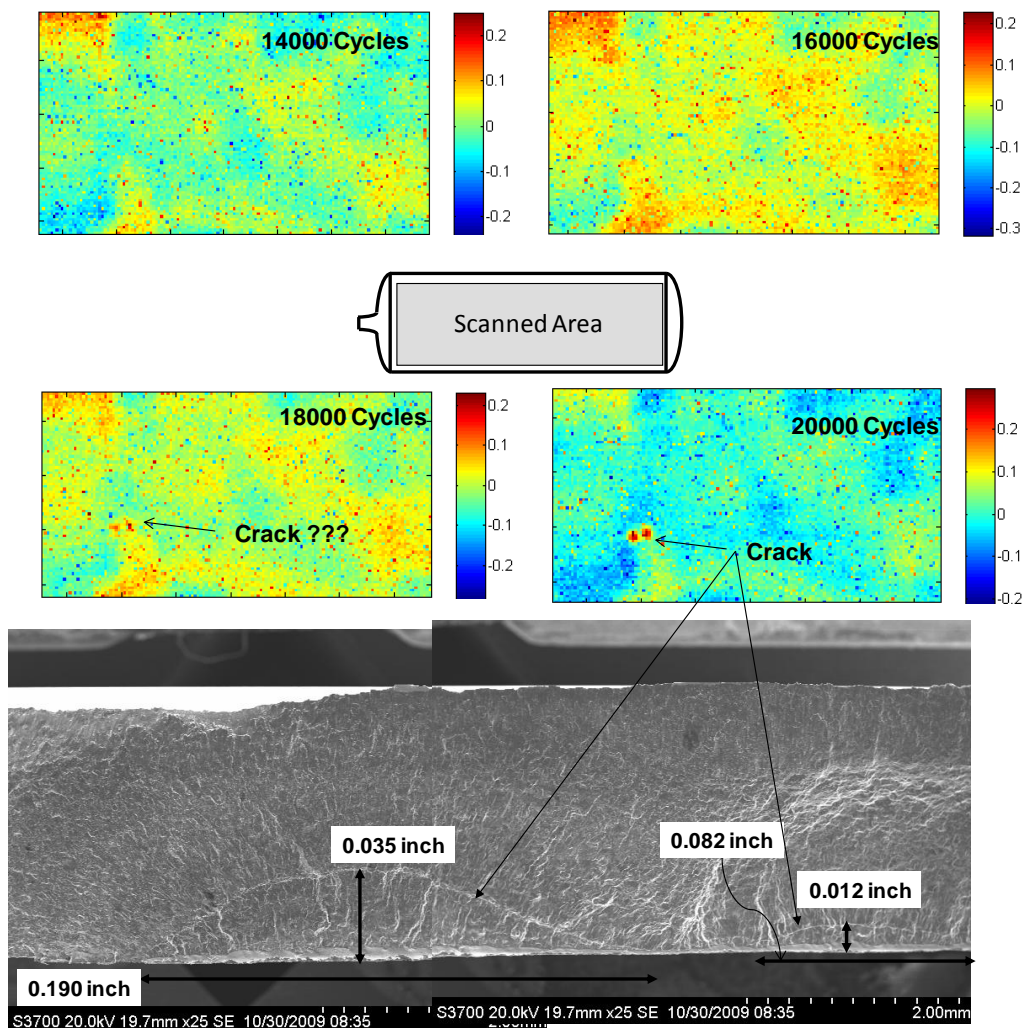


Figure 6.5-11. The results of the eddy current scan of a bare liner 18119 and the fracture surface corresponding to the location of the eddy current indications. The color indicates the relative intensity of the signal.

| | | | |
|--|---|--------------------------------------|------------------------|
|  | NASA Engineering and Safety Center Technical Assessment Report | Document #: NESC-RP-06-065 | Version: 1.0 |
| Title: Fracture Mechanics Based Methods Development for COPVs with Metallic Liners | | Page #: 49 of 164 | |

6.5.4 Composite Wrapping and FEA

The liners with fatigue cracks, both OD cracks that nucleated from the laser notches and ID cracks that initiated from the manufacturing defects, were wrapped with T700-24K-50C carbon fiber tape (reported as 65 percent fiber volume) with an average thickness of 0.027 inch [ref. 7]. An elastic-plastic FEA was conducted to determine the pressure required to obtain a liner strain of 12,500 $\mu\epsilon$ to simulate the autofrettage loading and subsequent loading to 10,000 $\mu\epsilon$ to simulate the MDP. The predicted pressures were 3,804 psid and 2,460 psid for the autofrettage and MDP strains, respectively [ref. 7].

6.5.5 COPV FCG Testing

The COPVs (wrapped, cracked liners) were fatigue cycled using a hydrostatic loading system. The system was capable of loading up to 4,000 psid and a frequency of about 0.1 Hz. The system generated cyclic loads that were within 2 percent of the programmed pressure.

DI water was used as the medium for pressurization. The laser notches used to nucleate the fatigue cracks were placed on the liner OD and would not experience a moist environment during precracking or FCG testing. The unanticipated cracks that nucleated from manufacturing defects on the liner ID would experience a DI water environment that could influence (i.e., accelerate) the measured FCG rate.

The COPVs were initially loaded to 3,804 psid to simulate the autofrettage cycle (hoop strain = 12,500 $\mu\epsilon$), and then completely depressurized. The COPV was then fatigue cycled between zero pressure and 2,460 psid (hoop strain = 10,000 $\mu\epsilon$) for several thousand cycles or until a leak was detected. The system would shut down automatically when a leak was detected. The intent of the fatigue testing was to stop the cycling before the exterior cracks broke through to the ID surface. The COPV liners were elastically responding, unable to achieve tensile and compressive plastic deformation during the cyclic loading after autofrettage. A plastically responding COPV would require a design with a thinner liner or a higher burst pressure than the current design.

The COPVs were examined with an eddy current NDE system after the completion of the fatigue cycles. The complete results of the eddy current measurements are outside the scope of this document. The eddy current measurements identified where the cracks, now hidden by the composite, were located as well as the location of manufacturing ID cracks. The COPVs were cut lengthwise in half, with care taken to avoid any of the identified cracks. After the COPV was sectioned, the composite outer layer was removed, exposing the exterior of the liner. The cracks were located and small squares containing individual cracks (about 1 inch to 2 inch sides) were extracted from the liner. The crack tips were identified using optical microscopes and saw cuts,

| | | | |
|--|---|---|------------------------|
|  | NASA Engineering and Safety Center Technical Assessment Report | Document #: NESC-RP- 06-065 | Version: 1.0 |
| Title: Fracture Mechanics Based Methods Development for COPVs with Metallic Liners | | Page #: 50 of 164 | |

co-linear with the cracks, were made from the edge of the square to within 0.05 inches of the crack tips. The notched squares were then fractured in bending to expose the fracture surfaces. A summary of the tests is provided in Table 6.5-1.

COPV 18119 leaked at a crack that nucleated from a long, shallow manufacturing defect on the liner ID. Close examination of the ID surface around this crack revealed what appeared to be a second crack that was parallel to the crack that leaked. This crack surface was opened in a similar manner described above and revealed 12 small elliptical cracks that had not coalesced into a single crack. The sizes of the 12 ID cracks are summarized in Table 6.5-2. The fracture surfaces of the cracks located in the COPV tests are provided in Appendix C.



NASA Engineering and Safety Center Technical Assessment Report

Document #:
**NESC-RP-
06-065**

Version:
1.0

Title:

Fracture Mechanics Based Methods Development for COPVs with Metallic Liners

Page #:
51 of 164

Table 6.5-1. Summary of COPV Tests

| | | Specimen ID | | | | | |
|-------------------------|------------------------------------|---|--------|--------|--------|--|---|
| | | 18118 | 18117 | 18107 | 18105 | 18103 | 18119 |
| Precrack Cycles | | 4,000 | 2,000 | 4,000 | 4,000 | 19,000 | 20,000 |
| Test Cycles | | 7,184 | 5,000 | 5,000 | 5,000 | 6,000 | 4,179 |
| Crack #1 | 2c_i (inch) | 0.124 | 0.103 | 0.123 | 0.102 | 0.024 | 0.026 |
| | a_i (inch) | 0.0355 | 0.0231 | 0.0330 | 0.0121 | 0.0116 | 0.0135 |
| | a_i/c_i | 0.573 | 0.449 | 0.537 | 0.237 | 0.959 | 1.047 |
| | 2c_f (inch) | 0.238 | 0.160 | 0.183 | 0.117 | 0.038 | 0.037 |
| | a_f (inch) | 0.0775 | 0.0540 | 0.0550 | 0.0234 | 0.0165 | 0.0166 |
| | a_f/c_f | 0.651 | 0.675 | 0.601 | 0.400 | 0.873 | 0.905 |
| | B (inch) | 0.089 | 0.091 | 0.089 | 0.103 | 0.090 | 0.101 |
| Crack #2 | 2c_i (inch) | 0.124 | 0.104 | 0.127 | 0.104 | 0.042 | 0.036 |
| | a_i (inch) | 0.0355 | 0.0221 | 0.0400 | 0.0150 | 0.0207 | 0.0171 |
| | a_i/c_i | 0.573 | 0.425 | 0.630 | 0.288 | 0.998 | 0.950 |
| | 2c_f (inch) | Crack Leaked | 0.160 | 0.215 | 0.123 | 0.062 | 0.053 |
| | a_f (inch) | | 0.0502 | 0.0630 | 0.0280 | 0.0261 | 0.0219 |
| | a_f/c_f | | 0.628 | 0.586 | 0.455 | 0.841 | 0.822 |
| | B (inch) | | 0.087 | 0.089 | 0.090 | 0.092 | 0.090 |
| Crack #3 | 2c_i (inch) | 0.122 | 0.112 | 0.126 | 0.105 | 0.026 | 0.027 |
| | a_i (inch) | 0.0354 | 0.0217 | 0.0380 | 0.0132 | 0.0127 | 0.0128 |
| | a_i/c_i | 0.580 | 0.388 | 0.603 | 0.251 | 0.988 | 0.948 |
| | 2c_f (inch) | 0.233 | 0.141 | 0.206 | 0.117 | 0.037 | 0.038 |
| | a_f (inch) | 0.0673 | 0.0359 | 0.0610 | 0.0228 | 0.0154 | 0.0167 |
| | a_f/c_f | 0.578 | 0.509 | 0.592 | 0.390 | 0.839 | 0.884 |
| | B (inch) | 0.093 | 0.091 | 0.091 | 0.107 | 0.101 | 0.108 |
| Other Cracks | 2c_i (inch) | 0.044 | | | | 0.128 | 0.19 |
| | a_i (inch) | 0.0050 | | | | 0.0092 | 0.035 |
| | a_i/c_i | 0.227 | | | | 0.144 | 0.37 |
| | 2c_f (inch) | 0.049 | | | | 0.159 | Crack Leaked |
| | a_f (inch) | 0.0088 | | | | 0.0225 | |
| | a_f/c_f | 0.363 | | | | 0.283 | |
| Comments | | The 4th crack listed was an ID crack located in the cylindrical section near the ported end | | | | The 4th crack (#1a) listed was an OD crack located near crack #1 | The 4th crack listed was an ID crack that leaked. Additional ID cracks are described in Table 9 |



**NASA Engineering and Safety Center
Technical Assessment Report**

Document #:
**NESC-RP-
06-065**

Version:
1.0

Title:

**Fracture Mechanics Based Methods Development for
COPVs with Metallic Liners**

Page #:
52 of 164

Table 6.5-2. Dimensions of the COPV ID Cracks

| Crack # | COPV | c_i (inch) | a_i/c_i | a_i (inch) | c_f (inch) | a_f/c_f | a_f (inch) |
|---------|-------|--------------|-----------|--------------|--------------|-----------|--------------|
| ID6 | 18118 | 0.022 | 0.227 | 0.0050 | 0.024 | 0.363 | 0.0088 |
| ID1 | 18119 | 0.024 | 0.234 | 0.0056 | 0.028 | 0.321 | 0.0090 |
| ID2 | 18119 | 0.013 | 0.284 | 0.0038 | 0.015 | 0.382 | 0.0058 |
| ID3 | 18119 | 0.020 | 0.453 | 0.0092 | 0.023 | 0.628 | 0.0146 |
| ID4 | 18119 | 0.022 | 0.221 | 0.0048 | 0.023 | 0.358 | 0.0082 |
| ID5 | 18119 | 0.020 | 0.307 | 0.0061 | 0.021 | 0.463 | 0.0097 |
| ID6 | 18119 | 0.014 | 0.450 | 0.0061 | 0.017 | 0.541 | 0.0090 |
| ID7 | 18119 | 0.012 | 0.258 | 0.0030 | 0.013 | 0.322 | 0.0041 |
| ID8 | 18119 | 0.035 | 0.105 | 0.0037 | 0.037 | 0.156 | 0.0057 |
| ID9 | 18119 | 0.021 | 0.228 | 0.0048 | 0.022 | 0.298 | 0.0065 |
| ID10 | 18119 | 0.020 | 0.215 | 0.0043 | 0.021 | 0.277 | 0.0058 |
| ID11 | 18119 | 0.009 | 0.149 | 0.0013 | 0.009 | 0.223 | 0.0020 |
| ID12 | 18119 | 0.006 | 0.435 | 0.0027 | 0.007 | 0.466 | 0.0034 |
| ID1a | 18118 | 0.024 | 0.123 | 0.0029 | 0.024 | 0.246 | 0.0060 |
| ID2 | 18118 | 0.008 | 0.815 | 0.0064 | 0.010 | 0.822 | 0.0081 |
| ID4 | 18118 | 0.009 | 0.604 | 0.0055 | 0.011 | 0.676 | 0.0075 |
| ID5 | 18118 | 0.019 | 0.184 | 0.0035 | 0.021 | 0.333 | 0.0070 |
| ID1b | 18118 | 0.013 | 0.262 | 0.0034 | 0.015 | 0.460 | 0.0069 |

6.6 COPVs FEA

An elastic-plastic FEA was conducted to calculate the pressures necessary to obtain the required hoop strains in the liners [ref. 7]. The liner was modeled with eight node axisymmetric elements. Four elements were used across the thickness of each layer. The boundary conditions for the analysis consisted of a pressure load on the liner ID and an axial load acting on the sidewall section. The material properties of the liner and composite are provided in Table 6.6-1. The results of the FEA are provided in Table 6.6-2. A COPV was instrumented with four strain gages, orientated in the hoop direction, along the center of the COPV and 90 degrees apart around the circumference. The measurements from the four strain gages are averaged and compared against the FEA, as shown in Figure 6.6-1.



**NASA Engineering and Safety Center
Technical Assessment Report**

Document #:
**NESC-RP-
06-065**

Version:
1.0

Title:

**Fracture Mechanics Based Methods Development for
COPVs with Metallic Liners**

Page #:
53 of 164

Table 6.6-1. FEA Material Properties

| Component | Material | Property | Value |
|------------------|---------------------------------------|-----------------|----------------|
| Liner | 6061-T6 Aluminum | Young's Modulus | 10,000,000 psi |
| | | Poisson Ratio | 0.33 |
| | | Tangent Modulus | 75,500 psi |
| | | Yield Strength | 41,500 psi |
| Composite | T700-24K-50C (65% Fiber Volume) | E_x | 19,880,000 psi |
| | | E_y | 2,967,000 psi |
| | | E_z | 2,967,000 psi |
| | | ν_{xy} | 0.326 |
| | | ν_{yz} | 0.514 |
| | | ν_{xz} | 0.326 |
| | | G_{xy} | 1,020,000 psi |
| | | G_{yz} | 980,000 psi |
| | | G_{xz} | 1,020,000 psi |



**NASA Engineering and Safety Center
Technical Assessment Report**

Document #:
**NESC-RP-
06-065**

Version:
1.0

Title:

**Fracture Mechanics Based Methods Development for
COPVs with Metallic Liners**

Page #:
54 of 164

Table 6.6-2. FEA Results

| Pressure (psi) | Liner Hoop Strain (microstrain) | OD Hoop Strain (microstrain) |
|---------------------------|--|---|
| 95 | 182 | 176 |
| 190 | 364 | 353 |
| 1997 | 3815 | 3702 |
| 3804 | 12840 | 1250 |
| 1802 | 9050 | 8783 |
| 0 | 5624 | 5441 |
| 2460 | 10300 | 10000 |
| 3800 | 12830 | 12490 |
| 4000 | 13210 | 12860 |
| 4200 | 14730 | 14340 |
| 4400 | 15660 | 15260 |
| 4600 | 16610 | 16180 |
| 4800 | 17530 | 17090 |
| 5000 | 18470 | 18010 |



Title:

Fracture Mechanics Based Methods Development for
COPVs with Metallic Liners

Page #:
55 of 164

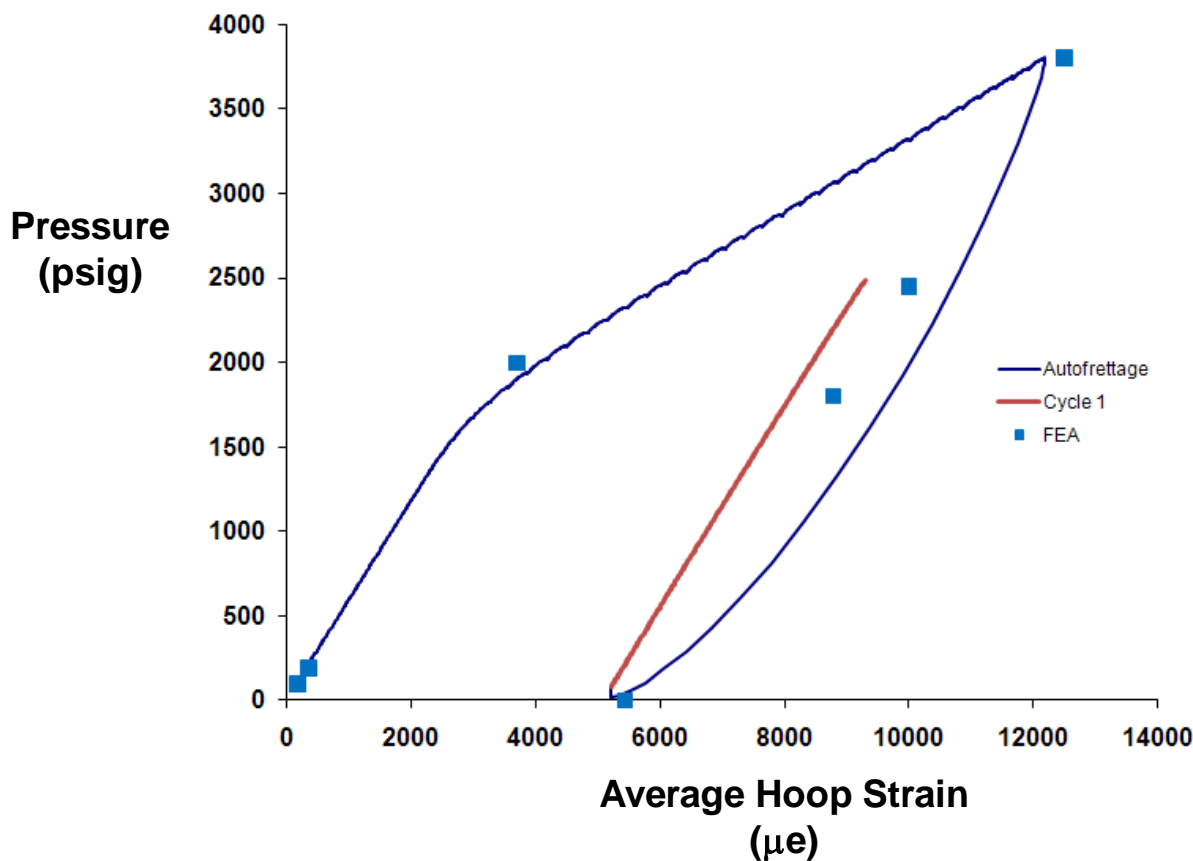


Figure 6.6-1. Predicted and measured hoop strain for a COPV subjected to an autofrettage and one MDP cycle

6.7 FCG Rate Calculations

The average FCG rate (da/dN and dc/dN) was calculated by measuring the difference between the crack length at the end of the fatigue region and the crack length at the end of the precrack region for each of the cracks located in the COPV and uniaxial coupons. The precrack and fatigue regions are identified in Figure 6.4-8. The average da/dN was obtained by measuring the difference at the maximum depth location ($a_f - a_i$) and dividing by the number of fatigue cycles. Likewise, the average dc/dN was obtained by measuring the maximum difference in the surface direction ($c_f - c_i$) and dividing by the number of fatigue cycles. In most cases this maximum difference was at the surface, but in a few cases the maximum difference was slightly below the surface.

| | | | |
|--|---|-----------------------|------------|
|  | NASA Engineering and Safety Center Technical Assessment Report | Document #: | Version: |
| | | NESC-RP-06-065 | 1.0 |
| Title: | | | Page #: |
| Fracture Mechanics Based Methods Development for COPVs with Metallic Liners | | | 56 of 164 |

The LEFM parameter K was used to correlate the FCG rate behavior for all of the tests conducted under elastic conditions. The cyclic stress intensity factor, $\Delta K = K_{\max} - K_{\min}$, is often used to characterize the FCG rate behavior for positive stress ratios ($R > 0$) to highlight the influence of the mean stress. The mean stress for negative stress ratios has less of an influence on the FCG rate behavior because fatigue damage accumulates predominately during the portion of the loading cycle where the crack surfaces are separated. Thus, for negative R the entire ΔK range does not contribute to damage and K_{\max} was used to correlate the FCG rate behavior for all of the tests conducted under elastic conditions. K_{\max} was calculated for the average depth and surface crack length of the fatigue region using the K solution SC04 from NASGRO® [ref. 8]. This K solution was derived for a surface crack on the ID or OD surfaces, but does not account for the influence of a pressurized fluid (σ_p) on the surfaces of the ID cracks. The influence of pressure was estimated from solutions provide by Tada, et al. [ref. 9] and increased K by about 15 percent.

$$K_{depth} = K_{SC04} + \sigma_p \sqrt{\pi a} \quad [1]$$

$$K_{surface} = K_{SC04} + \sigma_p \sqrt{\pi c} \quad [2]$$

The average crack depth and the average aspect ratio were calculated as shown in Figure 6.7-1. The maximum cyclic stress needed for the K calculation was obtained from the measured applied load in the uniaxial tests. However, the maximum cyclic hoop stress in the COPV tests could not be calculated from a direct measurement of a physical quantity. Instead, the maximum hoop stress was estimated from the stresses in the uniaxial coupons at equivalent strains. A maximum stress of 24 ksi and a minimum stress of -17 ksi were used for the two uniaxial tests where the minimum cyclic strain was 5,460 $\mu\epsilon$ and for all COPV tests, see Figure 6.4-10. The pressure of the fluid for the ID cracks in the COPV tests was $\sigma_p = 2.46$ ksi.

The average crack growth rate as a function of the calculated maximum K is shown in Figure 6.7-2 for all of the uniaxial and COPV tests. The green symbols of Figure 6.7-2 represent the results of the baseline $M(T)$ tests and the solid green line is the power law fit to the center portion of this data. The circular symbols represent the average FCG rate at the maximum depth location (da/dN) and the square symbols represent the average FCG rate at the surface (dc/dN). The influence of the approximation of the crack face pressure on K for the depth direction of the COPV ID cracks is illustrated in Figure 6.7-3. The magnitude of K change due to the crack face pressure modification is not large, but does enhance the correlation with the long crack trend line, as shown in Figure 6.7-3.

| | | | |
|--|---|--------------------------------------|------------------------|
|  | NASA Engineering and Safety Center Technical Assessment Report | Document #: NESC-RP-06-065 | Version: 1.0 |
| Title: Fracture Mechanics Based Methods Development for COPVs with Metallic Liners | | | Page #: 57 of 164 |

The dark blue symbols are the results from the uniaxial tests that were conducted with the same elastic cyclic strains as predicted for the hoop strain of the COPV tests and these symbols fall close to the baseline $M(T)$ power law fit. The red symbols are the results from the cracks on the liners OD and the yellow symbols are the results from the cracks on the liner ID in the COPV tests. The ID cracks were typically smaller in the depth direction than the OD cracks, thus had both smaller K_{max} values and lower FCG rates. The COPV FCG rate results for the maximum depth locations (square symbols) were scattered around the power law fit for both the ID and OD cracks, while the COPV FCG rate results for the surface locations (circular symbols) were generally above the power law fit (a faster FCG rate). Appendix D contains the average crack front dimensions, K values, and FCG rates for all of the elastic tests. The test results shown in Figure 6.7-2 are presented with the acknowledgment of the following points:

1. The identification of the crack front location at surface was more difficult than that at the maximum depth location, as seen in the photographs shown in Appendix C, increasing the error in the measurement of the change in crack length. This was especially true for the cracks that initiated from long, shallow manufacturing defects on the ID surface and did not yet developed into elliptical shaped fatigue cracks. While the surface lengths of these cracks may be 0.05 inches or more, the change in surface crack length was often less than 0.005 inches. Thus, small errors in establishing the intersection of the crack fronts and the surface may result in large errors in the amount of crack growth during the fatigue loading.
2. The NASGRO® solution SC04 for a surface crack on the ID or OD of a hollow pressurized cylinder was used to calculate K. This solution assumes an elliptical shape based on the maximum crack depth and total surface crack length, so the calculated K for non-elliptical shaped cracks will have errors. These errors will likely be greater at the surface than the maximum depth because the crack fronts at the maximum depth tend to be closer to an elliptical shape.
3. The small ID surface cracks of COPV 18119 were co-linear and some were located in close proximity, likely increasing K at the surface.
4. The hoop stress for the COPV tests was estimated from the uniaxial tests and does not account for the multi-axial stresses present in the COPV tests.
5. The hoop stress in the COPV tests also have an unknown through-the-thickness gradient that is not accounted for in the K_{max} calculations.
6. The influence of constraint variations along the crack front is not accounted for in the K_{max} calculation.



Title:

**Fracture Mechanics Based Methods Development for
COPVs with Metallic Liners**

Page #:
58 of 164

7. The DI water environment experienced by the ID cracks could influence (i.e., accelerate) the FCR rate.

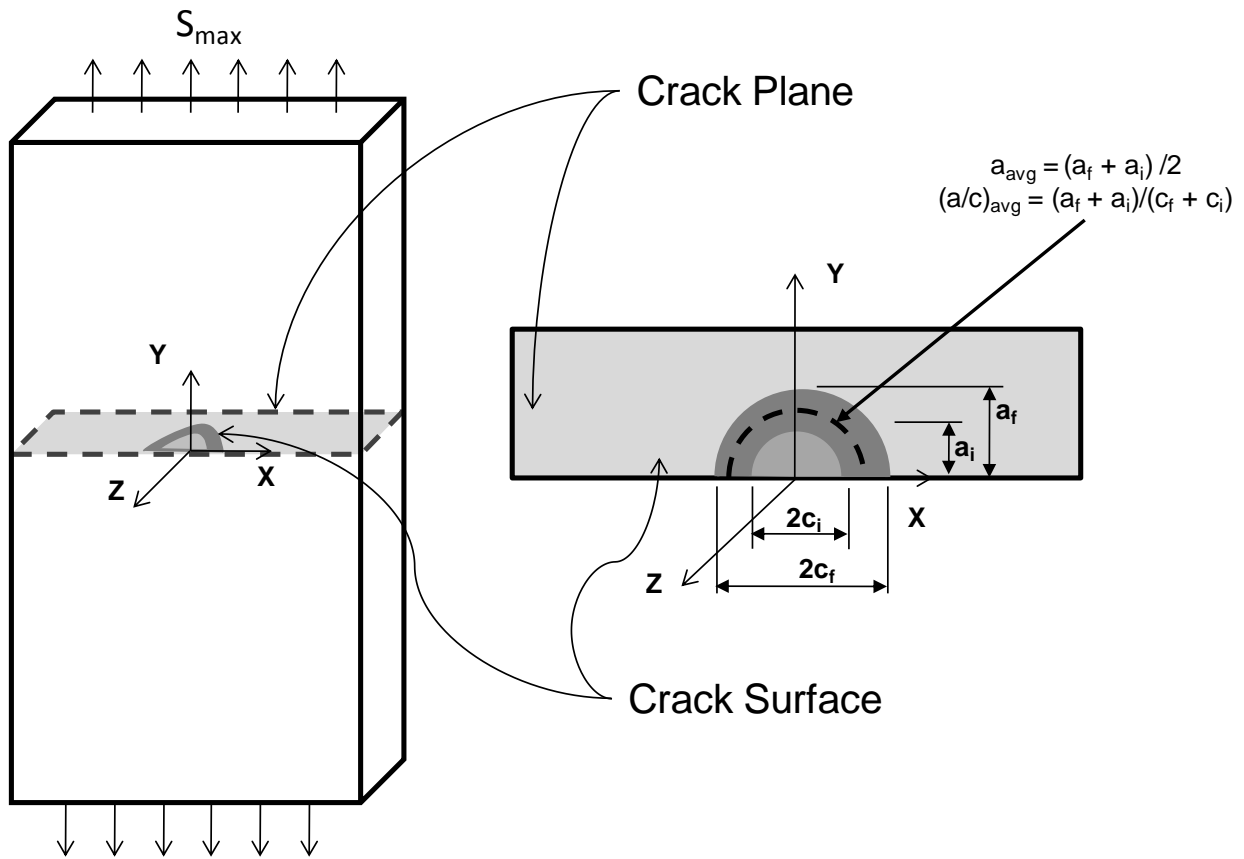


Figure 6.7-1. Definition of the average crack length for K calculations



NASA Engineering and Safety Center Technical Assessment Report

Document #:
**NESC-RP-
06-065**

Version:
1.0

Title:

Fracture Mechanics Based Methods Development for COPVs with Metallic Liners

Page #:
59 of 164

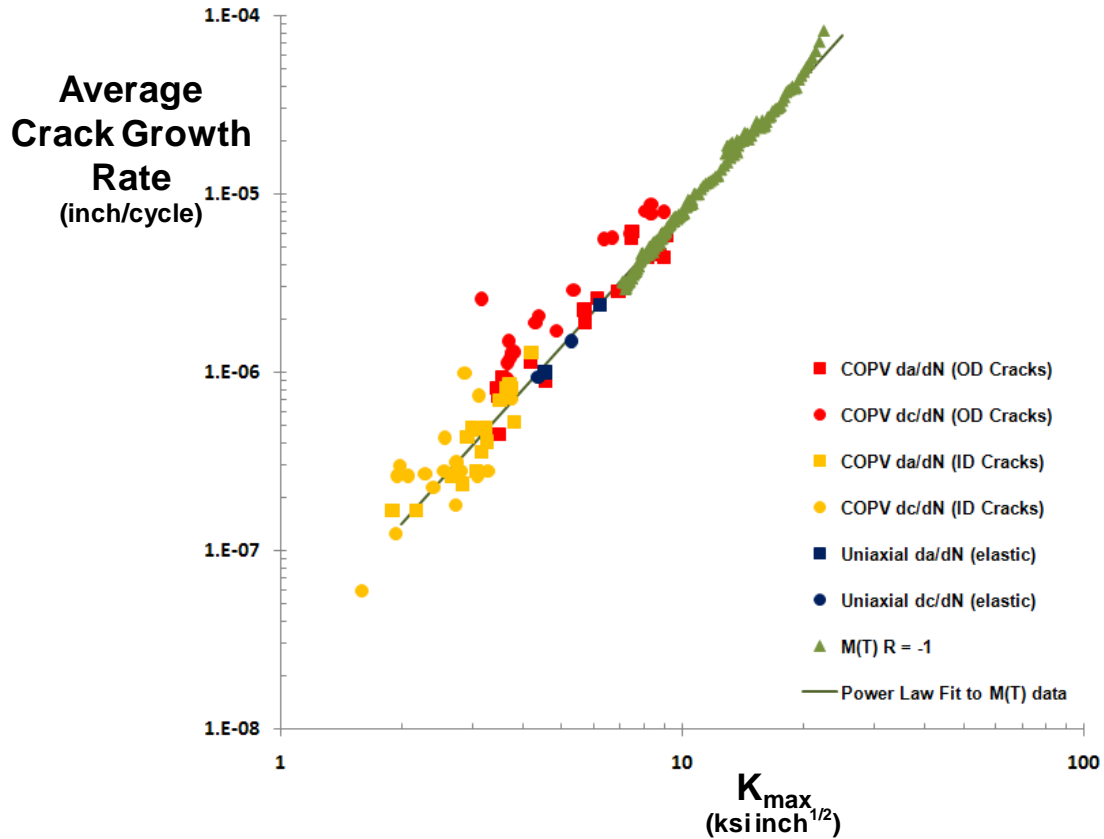


Figure 6.7-2. Average FCG rate as a function of the maximum K for all COPV tests



NASA Engineering and Safety Center Technical Assessment Report

Document #:
**NESC-RP-
06-065**

Version:
1.0

Title:

Fracture Mechanics Based Methods Development for COPVs with Metallic Liners

Page #:
60 of 164

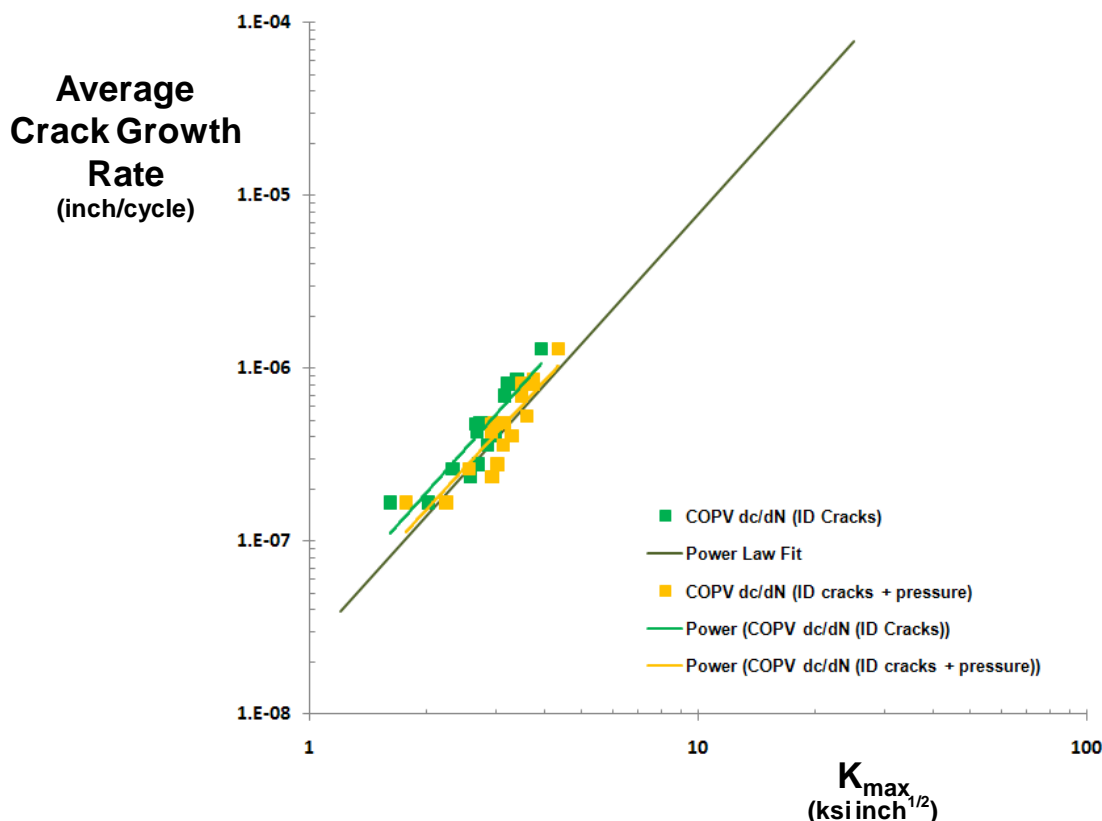


Figure 6.7-3. Average FCG rate for the COPV ID cracks in the depth direction with and without the approximation for the influence of the crack face pressure.

Figure 6.7-4 contains the regression fits for the average FCG rates in the depth (da/dN) direction for the OD and ID cracks in the pressurized COPV tests. The regression fit for the average FCG rate for the OD cracks (red square symbols) for any given K_{max} within the range of the test data, resulted in a FCG rate within -30 to +10 percent of the rate determined from the fit to the power law region of the M(T) data. The regression fit for the average FCG rate for the ID cracks (yellow symbols), for any given K_{max} within the range of the test data, resulted in a FCG rate that was about +10 to -1 percent faster than that determined from the fit to the power law region of the M(T) data. The small differences between the regression fits and the power law relationship indicate that the small surface crack FCG rate in the depth direction correlates with the long crack through-the-thickness M(T) tests. In addition, the surface crack FCG data does not exhibit threshold behavior for K as low as $K_{max} = 1.7 \text{ ksi inch}^{1/2}$.

Figure 6.7-5 contains the regression fits for the FCG rates in the surface (dc/dN) for the OD and ID cracks in the pressurized COPV tests. The regression fit for the FCG rates for the OD cracks

| | | | |
|--|---|--------------------------------------|------------------------|
|  | NASA Engineering and Safety Center Technical Assessment Report | Document #: NESC-RP-06-065 | Version: 1.0 |
| Title: Fracture Mechanics Based Methods Development for COPVs with Metallic Liners | | | Page #: 61 of 164 |

(red circular symbols), for any given K_{max} within the range of the test data, resulted in a FCG rate that was -50 to +150 percent faster than that of the rate determined from the fit to the power law region of the $M(T)$ data. The regression fit for the FCG rate for the ID cracks (yellow circular symbols), for any given K_{max} within the range of the test data, resulted in a FCG rate that was +40 to -10 percent faster than that determined from the fit to the power law region of the $M(T)$ data. The surface FCG rate behavior of the small surface cracks did not correlate with the long crack power law relationship as closely as did the depth FCG rate behavior. The scatter in the surface FCG rate behavior was also about twice that observed in the depth FCG rate behavior. These differences may be due, at least in part, to errors associated with the identification of the intersection of the crack fronts and the surface (i.e., measurement errors) and the crack shape assumptions used in the K calculation.

The cracks that nucleated from manufacturing defects typically had a shape that varied substantially from the semi-elliptical shapes that developed from the laser notches. Figure 6.7-6 contains the photographs of two fracture surfaces and semi-elliptical fits to the crack depth and surface measurements. Figure 6.7-6a contains a photograph of the fracture surface of a crack that nucleated from a laser notch (OD crack #2 from COPV 18103) along with the semi-elliptical crack front shapes defined by the surface and depth crack measurements. The semi-elliptical crack fronts closely follow the crack fronts that developed from the laser notch. Figure 6.7-6b contains a photograph of the fracture surface of a crack that nucleated from a manufacturing defect (ID crack #8 from COPV 18119) along with the semi-elliptical crack front shapes defined by the surface and depth crack measurements. The actual crack front shapes are highlighted by dashed lines and the assumed semi-elliptical crack front shapes are shown as solid lines in Figure 6.7-6a and 6.7-6b. The semi-elliptical crack fronts do not accurately follow the crack front shapes, particularly in the vicinity of where the crack intersects the free surface. The corresponding $da/dN - K_{max}$ (depth) and $dc/dN - K_{max}$ (surface) data points are identified in Figure 6.7-7. Both the $da/dN - K_{max}$ and $dc/dN - K_{max}$ data points from the cracks that nucleated from the laser notch correlated with the power law from the $M(T)$ tests. However, for crack that nucleated from the manufacturing defect, the $da/dN - K_{max}$ data point correlated with the $M(T)$ power law line, but the $dc/dN - K_{max}$ data points were about a factor of 2 above the power law line.



Title:

Fracture Mechanics Based Methods Development for
COPVs with Metallic Liners

Page #:
62 of 164

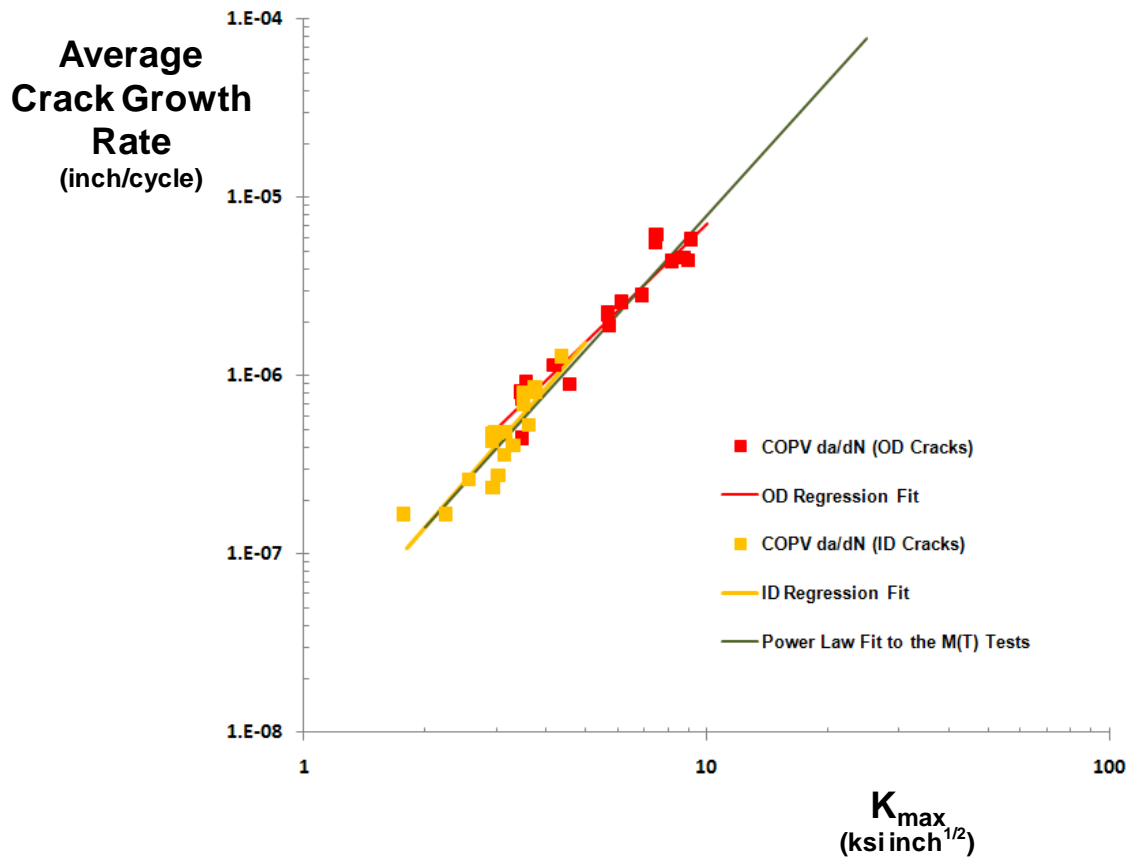


Figure 6.7-4. Regression power law fits to the FCG rate measurements in the depth direction for the OD and ID cracks in the COPV tests



NASA Engineering and Safety Center Technical Assessment Report

Document #:
**NESC-RP-
06-065**

Version:
1.0

Title:

Fracture Mechanics Based Methods Development for COPVs with Metallic Liners

Page #:
63 of 164

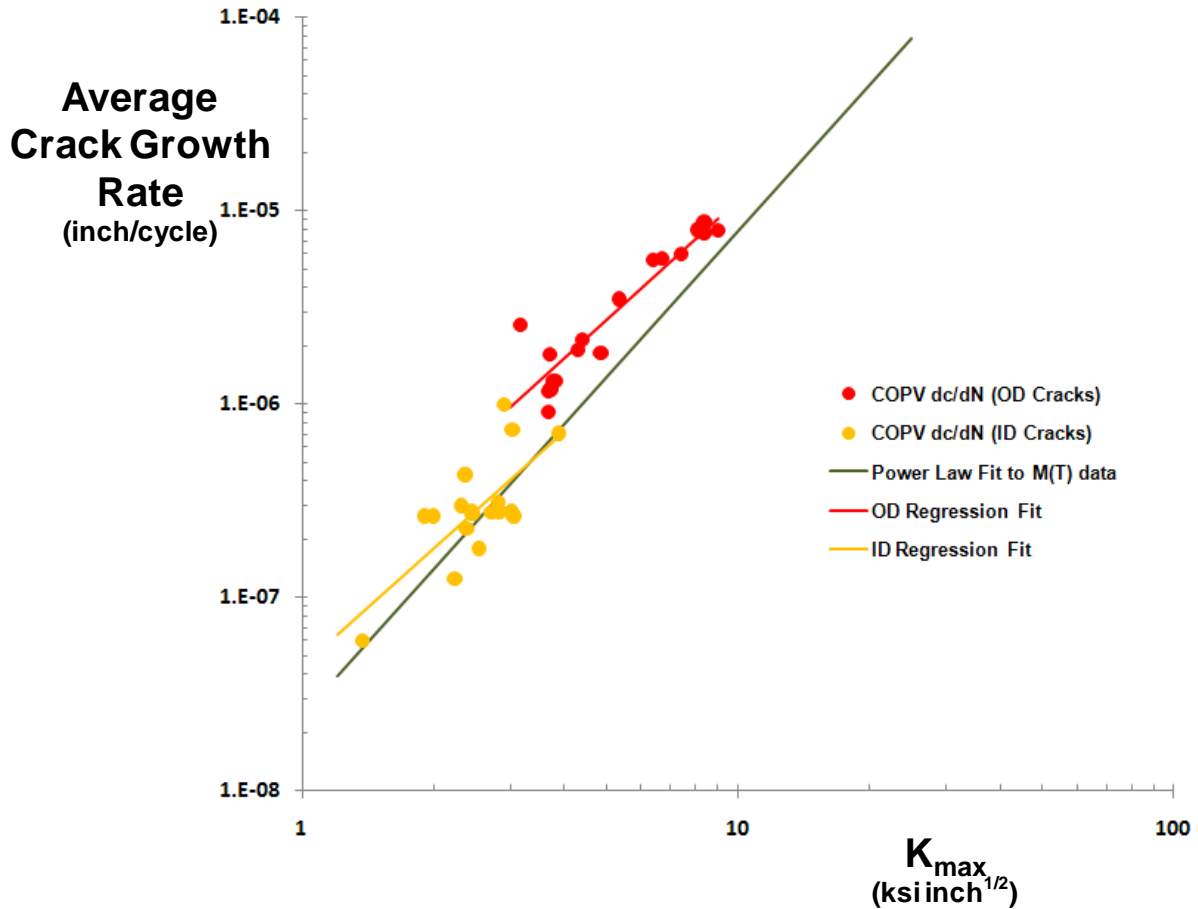


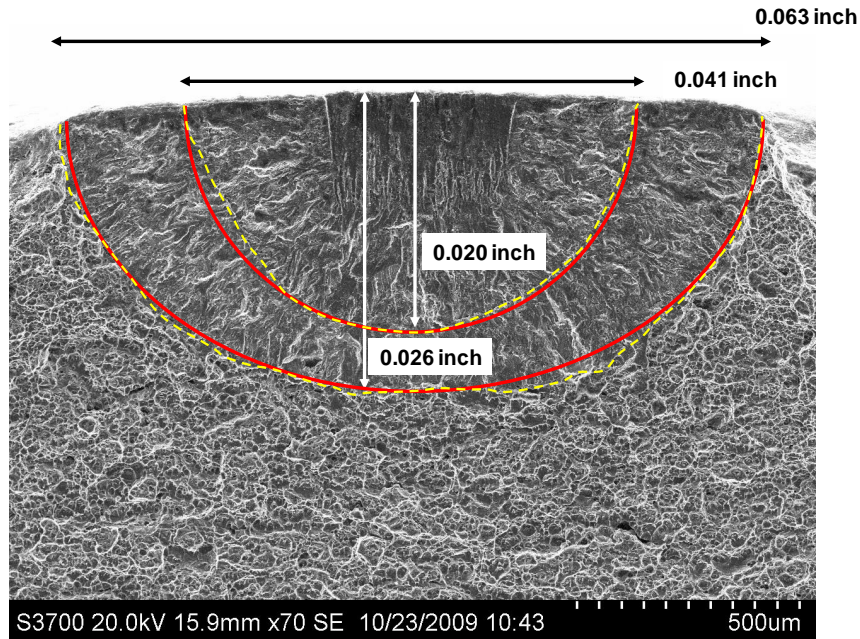
Figure 6.7-5. Regression power law fits to the FCG rate measurements in the surface direction for the OD and ID cracks in the COPV tests



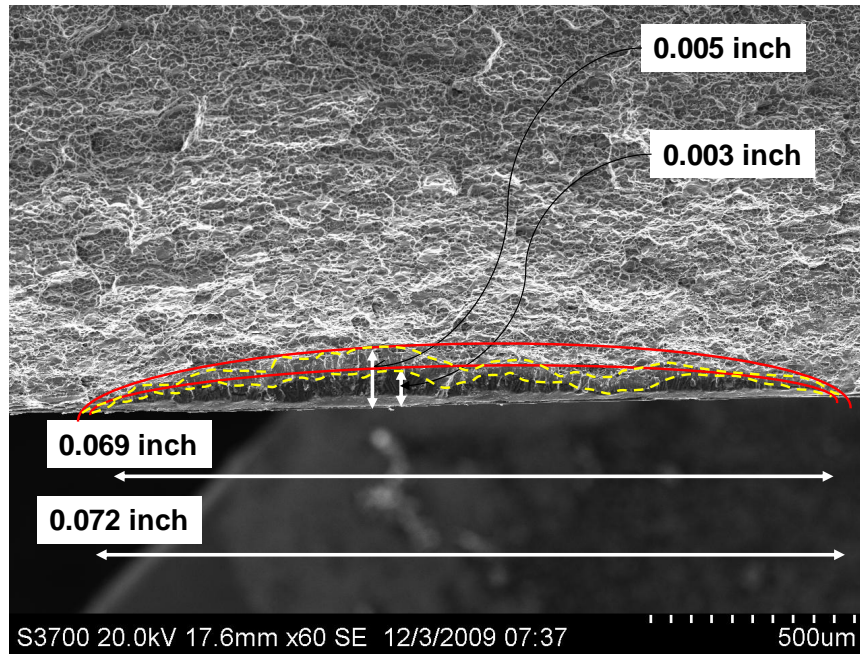
Title:

Fracture Mechanics Based Methods Development for
COPVs with Metallic Liners

Page #:
64 of 164



a. COPV 18103 crack OD02



b. COPV 18119 crack ID08

Figure 6.7-6. Semi-elliptical crack front assumptions for two fatigue cracks in COPVs



Title:

Fracture Mechanics Based Methods Development for
COPVs with Metallic Liners

Page #:
65 of 164

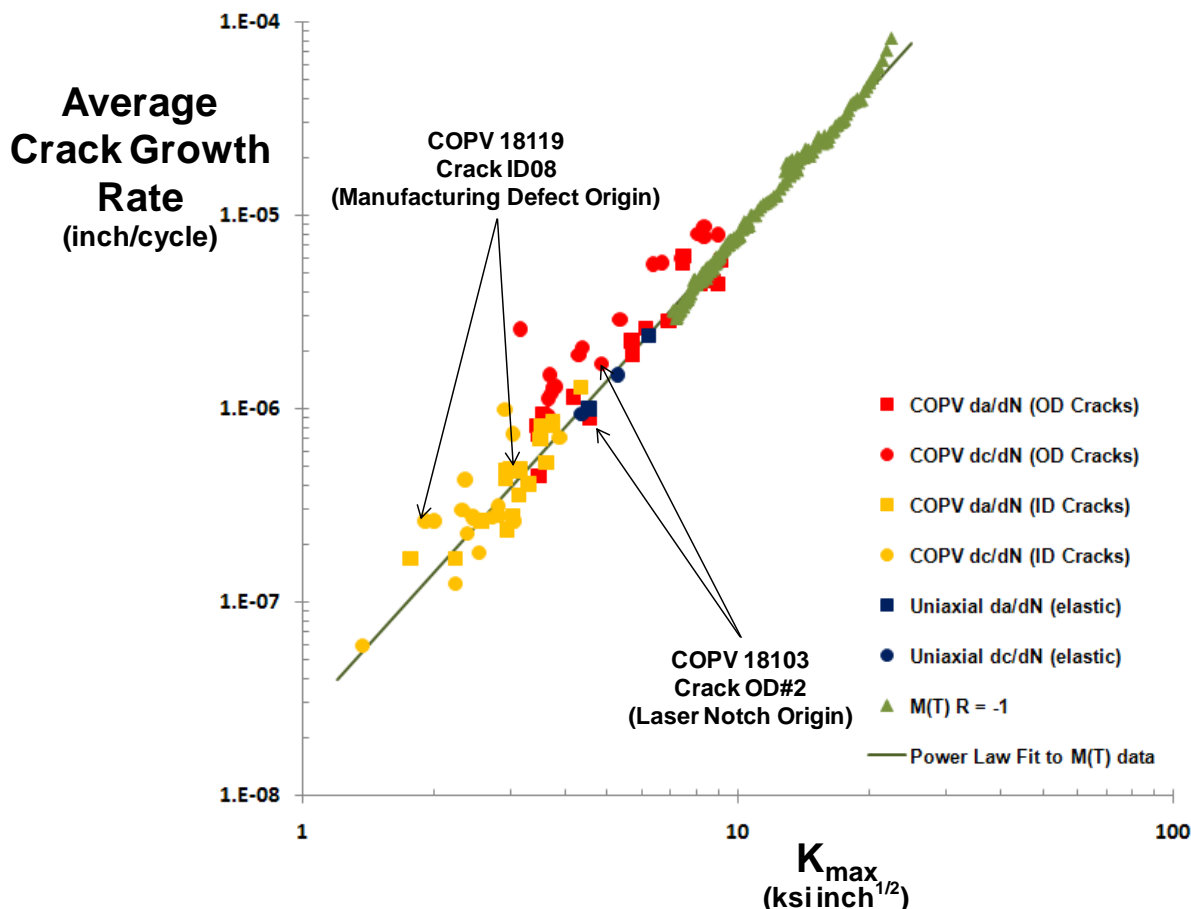


Figure 6.7-7. FCG rate data collected for the COPV and uniaxial tests with the results from the cracks fronts shown in Figure 6.7-6 identified

A total of 30 cracks that nucleated from manufacturing defects were located either using NDE or as a result of leakage. The largest defect, prior to precracking, had a depth of 0.02 inches and $2c \sim 0.5$ inches. The crack depth and surface crack length for each of the cracks that nucleated from manufacturing defects are shown in Figure 6.7-8. NSTS Orbiter Special Penetrant Inspection (SPI) [ref. 10] and Enhanced Penetrant Inspection (EPI) [ref. 11] methods have been proposed for the inspection of COPV liners prior to applying the composite overwrap. The SPI and EPI methods require the detection of 0.025 inch deep and 0.015 inch deep semi-circular ($a/c = 1$) surface cracks, respectively. The detectible limits for other aspect ratios were obtained by assuming the inspection methods could detect semi-elliptically shaped cracks that were equal in area to the detection limit $a/c = 1$ crack [ref. 12]. Four of the manufacturing defects (~ 13 percent

| | | | |
|--|---|--------------------------------------|------------------------|
|  | NASA Engineering and Safety Center Technical Assessment Report | Document #: NESC-RP-06-065 | Version: 1.0 |
| Title: Fracture Mechanics Based Methods Development for COPVs with Metallic Liners | | | Page #: 66 of 164 |

of the total) exceeded the SPI limit and three others (~23 percent of total) also exceeded the EPI limit, as shown in Figure 6.7-8.

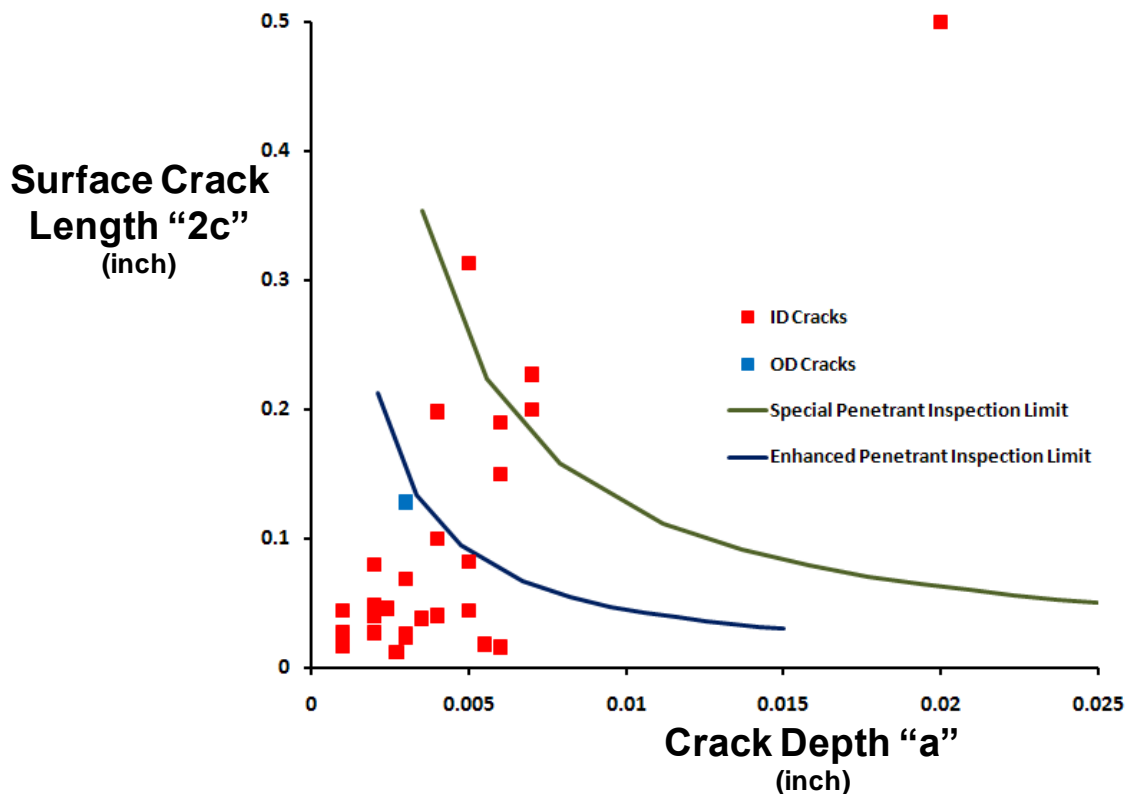


Figure 6.7-8. Crack lengths and depths of the ID and OD cracks that nucleated from manufacturing defects and inspection limits

The uniaxial tests that were conducted under fully reversed ($R = -1$), fully plastic (both tensile and compressive cyclic yielding) conditions violate LEFM assumptions, thus K_{max} was not used to represent the crack tip driving force. A comparison of the measured FCG rates from the elastically responding COPV tests and from the fully reversed, fully plastic uniaxial tests was made on the basis of the crack dimension, as shown in Figure 6.7-9. The crack depth dimension (a) was used for the depth FCG rates (da/dN) and the surface half-crack dimension (c) was used for the surface FCG rates (dc/dN). The uniaxial tests were conducted with a single crack with aspect ratios that were approximately $a/c = 1$ and 0.2 and the thicknesses of 0.032 inch, 0.05 inch, 0.09 inch, and 0.125 inch were included in Figure 6.7-9. The data from the elastically responding COPVs included both the cracks that nucleated from laser notches and from manufacturing defects. The measured crack growth rates from the uniaxial tests, shown as blue



Title:

Fracture Mechanics Based Methods Development for COPVs with Metallic Liners

Page #:
 67 of 164

symbols, were more than an order of magnitude higher than those measured in the COPV tests. Note that the stress in the fully reversed, fully plastic uniaxial tests was about 50 percent greater than the hoop stress the elastically responding COPVs. Given this change in applied stress, LEFM assumptions using the long crack power law would only predict an increase in the FCG rate by about a factor of 3.

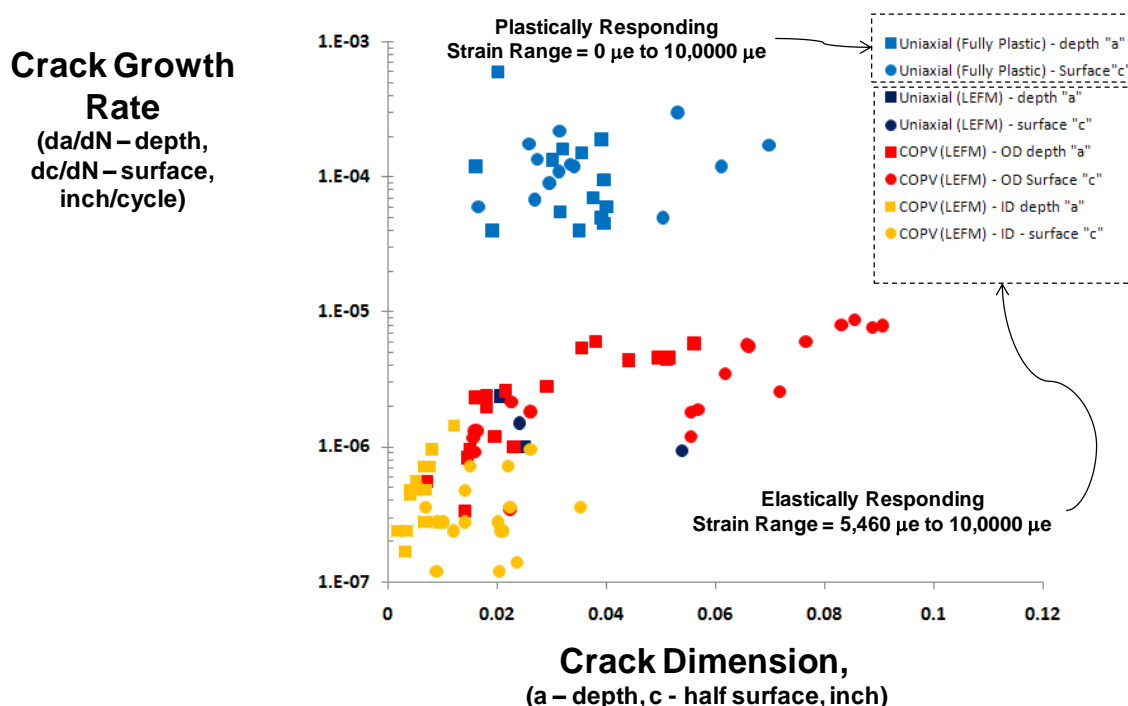


Figure 6.7-9. Comparison of the FCG rates from the fully reversed, fully plastic uniaxial tests and the results from the COPV tests. Plotted are da/dN and dc/dN for crack depth and half surface dimensions, respectively.

6.8 NASGRO® FCG Predictions

The NASGRO® crack growth analysis code [ref. 7] was used to evaluate LEFM techniques for predicting the FCG in the surface and depth directions for the elastically responding COPV and uniaxial tests. The material model M6AB13AB1 from the NASGRO® material behavior database for 6061-T62 aluminum was used to characterize the crack growth rate behavior. The NASGRO® material model M6AB13AB1 is described in Equation 3 and the NASGRO® input parameters are provided in Figure 6.8-1. The parameter “f” is a plasticity induced closure function that is related to R and the ratio of maximum applied stress to flow stress (S_{max}/S_o) and expressed in polynomial form in reference 8. The parameter ΔK_{th} is the threshold stress intensity

| | | | |
|--|---|-----------------------|------------|
|  | NASA Engineering and Safety Center Technical Assessment Report | Document #: | Version: |
| | | NESC-RP-06-065 | 1.0 |
| Title: | | | Page #: |
| Fracture Mechanics Based Methods Development for COPVs with Metallic Liners | | | 68 of 164 |

factor range and is a function of R and the NASGRO® input parameters ΔK_1^* , C_{th} , and C_{th-} . The parameter K_c is a function of the NASGRO® input parameters K_{1e} , K_{1c} , A_k , and yield stress.

$$\frac{da}{dN} = C \left[\left(\frac{1-f}{1-R} \right) \Delta K \right]^n \frac{\left(1 - \frac{\Delta K_{t0}}{\Delta K} \right)^p}{\left(1 - \frac{K_{max}}{K_c} \right)^q} \quad (3)$$

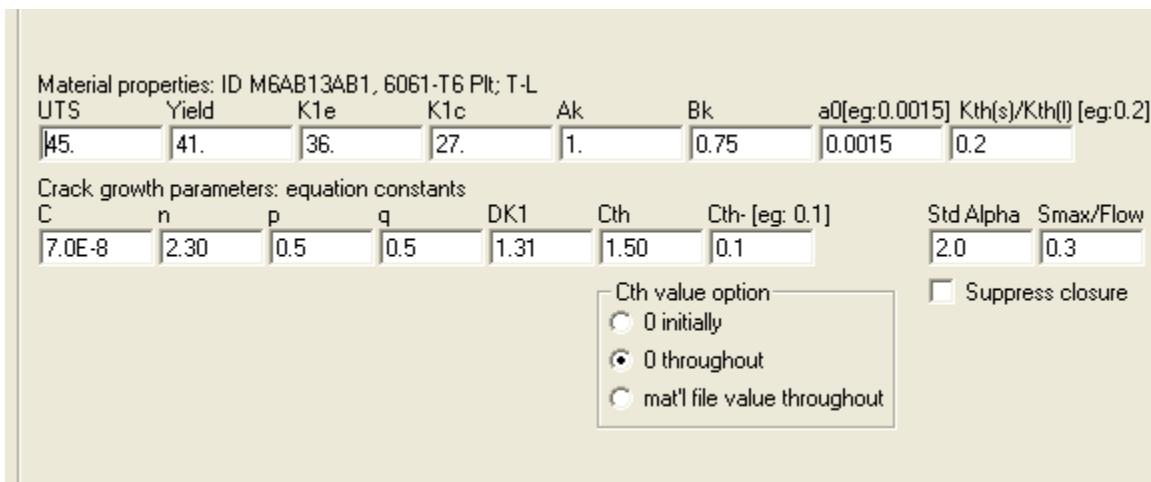


Figure 6.8-1. NASGRO® material model 13AB1 input parameters

The results from the M6AB13AB1 material model are shown in Figure 6.8-2 for the data sets provided by the NASGRO® database ($R = 0.75, 0.5,$ and 0.1) along with the $R = -1$ data obtained from the M(T) tests shown in Figure 6.3-2. Note that the NASGRO® model exhibits a threshold where the FCG rate drops off sharply for the lower K values. However, the data used to generate the model parameters were all above the threshold region.

The individual cracks were modeled assuming a semi-elliptical shape identified by the initial crack depth and surface length. The NASGRO® K SC17 solution for a surface crack in a flat, rectangular plate was used for the uniaxial coupons and the COPV cracks were modeled with the NASGRO® K SC04 solution for cracks in a pressurized hollow cylinder. K for the ID COPV cracks was modified to include the influence of the internal pressure on the crack surfaces, as described by Equations 1 and 2. The SC17 K solution accurately modeled the coupon configuration and loading conditions, but the K solution SC04 used to model the cracks in pressurized liners required the following assumptions:

- a) The crack front shape was an ellipse defined by the maximum depth and surface crack lengths.



Title:

**Fracture Mechanics Based Methods Development for
COPVs with Metallic Liners**

Page #:
69 of 164

- b) The influence of the liner axial stress on K is small.
- c) The hoop strains the wrapped liner at maximum and minimum test pressures were accurately predicted by the elastic-plastic FEA model and the resulting hoop stresses were similar to the stresses calculated for the uniaxial coupons subjected to strains equivalent to the calculated liner hoop strains.
- d) The influence of the through-the-thickness stress gradient in the liner on K is small.

The potential effects of these assumptions have not been characterized.

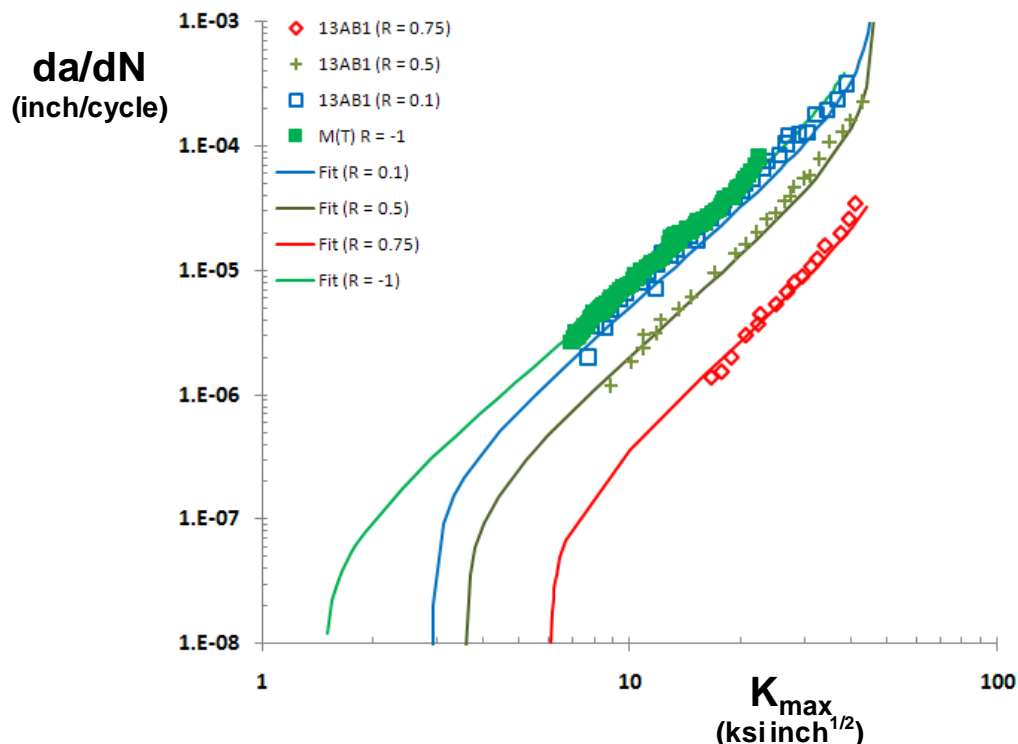


Figure 6.8-2. NASGRO® material model 13AB1 for 6061-T62 aluminum fit to data for four stress ratios

The NASGRO® FCG predictions were made for the elastically responding tests that included all of the cracks in the COPV tests and the two uniaxial tests conducted at the strain levels predicted for the COPV tests (UNI-090-40-06 and UNI-090-40-07). The initial crack length and shape used in the NASGRO® FCG prediction were obtained from the measurement of the crack front boundary between the precrack and fatigue regions, as identified in Figure 6.4-8. The NASGRO® FCG analysis was performed for the same number of cycles as applied in the test

| | | | |
|--|---|---|------------------------|
|  | NASA Engineering and Safety Center Technical Assessment Report | Document #: NESC-RP- 06-065 | Version: 1.0 |
| Title: Fracture Mechanics Based Methods Development for COPVs with Metallic Liners | | Page #: 70 of 164 | |

and the resulting crack length and shape was compared with the measurement of the crack front boundary between the fatigue and ductile fracture region, as identified in Figure 6.4-8. The stresses used ($S_{\max} = 24$ ksi and $R = -0.7$) in the NASGRO® predictions were obtained from the stresses obtained from the uniaxial tests, as shown in Figure 6.4-10. The NASGRO® material model used in the analyses was for 6061-T6 plate in the T-L orientation (M6AB13AB1). The models available in NASGRO® did not distinguish between the FCG rate in the surface (dc/dN) and depth (da/dN) directions.

The average FCG rate measured for the individual cracks in the COPV tests and the NASGRO® material model for $R = -0.7$ are shown in Figure 6.8-3 as a function of K_{\max} . The majority of the FCG rates for the cracks in the COPVs were above the NASGRO® curve, indicating that the resulting NASGRO® predictions would predict less FCG than observed in the tests. The K for the starting length and shape of the COPV cracks and the associated FCG rates, as calculated by the NASGRO® material model, are shown as open symbols in Figure 6.8.3. The smaller initial crack lengths have K values that are in the threshold influenced region (shaded region) of the NASGRO® M6AB13AB1 material model and one crack is below ΔK_{th} . The average FCG rate measurements from the small ID cracks in the COPV tests do not exhibit a threshold behavior for $K_{\max} > 1.8$ ksi inch^{1/2}, $R = -0.7$. This indicates that the threshold extrapolation in the NASGRO® material model M6AB13AB1 may limit the crack growth rate at too high of a K or that the physically small cracks present in the COPV liners do not exhibit a ΔK_{th} behavior.



Title:

Fracture Mechanics Based Methods Development for COPVs with Metallic Liners

Page #:
 71 of 164

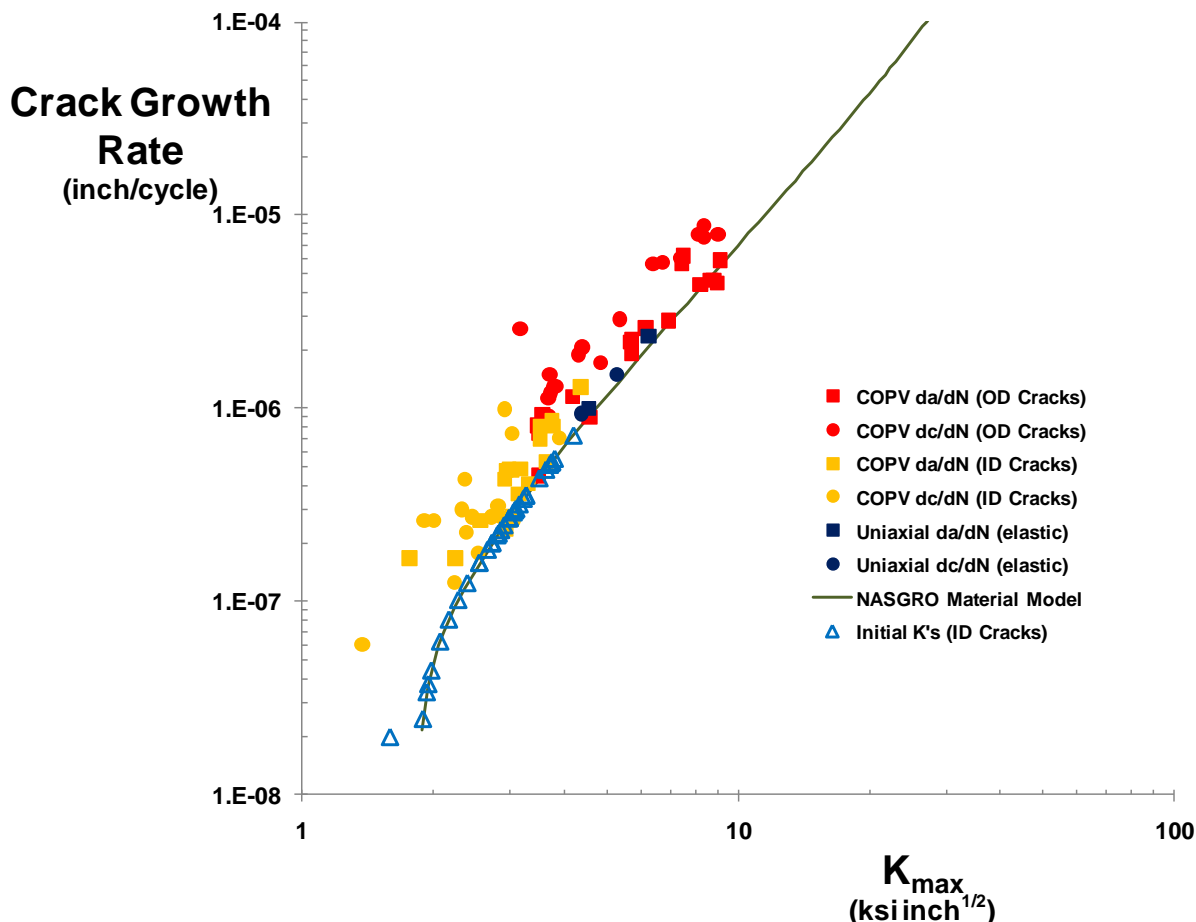


Figure 6.8-3. NASGRO® material model M6AB13AB1 for 6061-T62 aluminum for $R = -0.7$ and the measurements from the COPV tests

The percent difference between the predicted amount of crack extension and the amount measured in the tests was defined as:

$$\text{percent error} = \frac{(\Delta a_{\text{prediction}} - \Delta a_{\text{test}})}{\Delta a_{\text{test}}} \times 100 \quad (3)$$

Tables 6.8-1 and 6.8-2 contain the percent error for the NASGRO® predictions of the tests with OD and ID cracks, respectively. The calculated percent error for almost all of the predictions was negative, indicating that NASGRO® was predicting less crack growth than observed in the tests. The NASGRO® predictions for the depth direction of all of the cracks had a percent error closer to zero than that of the surface direction. The calculated standard deviations for the



**NASA Engineering and Safety Center
Technical Assessment Report**

Document #:
**NESC-RP-
06-065**

Version:
1.0

Title:

**Fracture Mechanics Based Methods Development for
COPVs with Metallic Liners**

Page #:
72 of 164

percent error of the prediction were large and illustrate the scatter that is typical in the FCG behavior of small cracks [ref. 13, 14].

Table 6.8-1. Percent Error for the NASGRO® Predictions (13AB1 material model) for the Tests with OD Cracks

| Specimen | Crack | NASGRO Predictions (Percent Error) | |
|----------------|-------|---------------------------------------|--------------|
| | | Depth | Surface |
| UNI-090-40-06 | 1 | -13.1 | -31.6 |
| UNI-090-40-07 | 1 | -23.0 | -51.1 |
| 18118 | 1 | -33.0 | -61.1 |
| 18118 | 3 | -13.8 | -52.7 |
| 18117 | 1 | -59.5 | -79.9 |
| 18117 | 2 | -57.5 | -81.1 |
| 18117 | 3 | -10.3 | -64.3 |
| 18107 | 1 | -21.2 | -62.4 |
| 18107 | 2 | -16.0 | -64.7 |
| 18107 | 3 | -18.0 | -64.2 |
| 18105 | 1 | -39.3 | -81.0 |
| 18105 | 2 | -32.6 | -74.9 |
| 18105 | 3 | -19.6 | -70.7 |
| 18103 | 1 | -58.0 | -70.6 |
| 18103 | 2 | -13.5 | -52.9 |
| 18103 | 3 | -16.0 | -58.3 |
| 18103 | 1a | -50.4 | -95.0 |
| 18119 | 1 | -50.5 | -69.1 |
| 18119 | 2 | -47.8 | -71.9 |
| 18119 | 3 | -58.1 | -71.1 |
| Average | | -32.6 | -66.4 |
| STDEV | | 18.2 | 13.6 |

| | | | |
|--|---|-----------------------|----------------------|
|  | NASA Engineering and Safety Center Technical Assessment Report | Document #: | Version: |
| | | NESC-RP-06-065 | 1.0 |
| Title: Fracture Mechanics Based Methods Development for COPVs with Metallic Liners | | | Page #: 73 of 164 |

Table 6.8-2. Percent Error for the NASGRO® Predictions for the Tests with ID Cracks

| Specimen | Crack | NASGRO Predictions (Percent Error) | |
|----------------|-------|---------------------------------------|--------------|
| | | Depth | Surface |
| 18118 | ID6 | -5.1 | -29.5 |
| 18119 | ID1 | -36.5 | -60.4 |
| 18119 | ID2 | -45.5 | -75.6 |
| 18119 | ID3 | -38.8 | -37.4 |
| 18119 | ID4 | -50.1 | -64.8 |
| 18119 | ID5 | -38.8 | -27.0 |
| 18119 | ID6 | -38.3 | -70.3 |
| 18119 | ID7 | -29.8 | -93.5 |
| 18119 | ID8 | -40.7 | -98.2 |
| 18119 | ID9 | -1.1 | -44.7 |
| 18119 | ID10 | -4.6 | -68.4 |
| 18119 | ID11 | -70.4 | -100.1 |
| 18119 | ID12 | -26.1 | -87.1 |
| 18118 | ID1a | -48.9 | -96.0 |
| 18118 | ID2 | 22.3 | 5.8 |
| 18118 | ID4 | 12.4 | -17.9 |
| 18118 | ID5 | -40.1 | -83.2 |
| 18118 | ID1b | -48.4 | -78.0 |
| Average | | -29.4 | -62.6 |
| STDEV | | 24.4 | 30.9 |

The NASGRO® material model M6AB13AB1 was modified to remove the influence of ΔK_{th} by setting the input parameter “p” equal to zero. This effectively creates a power law relationship between the FCG rate and K in the region of the elastic uniaxial and COPV tests. The percent errors for the NASGRO® predictions using the material model without a threshold were smaller than the predictions using the M6AB13AB1 material model that included threshold effects. The predictions for the FCG in the depth direction shown in Tables 6.8-1 through 6.8-4 indicate that the inclusion of a threshold, without specific data applicable to the material, crack sizes, stress levels, environment, etc. for the application being investigated, could result in unconservative safe-life predictions.

The NASGRO® predictions of the FCG in the depth direction were, on average, unconservative (-13 percent) for the OD cracks and conservative (10 percent) for the ID cracks. The mean of the

| | | | |
|--|---|--------------------------------------|------------------------|
|  | NASA Engineering and Safety Center Technical Assessment Report | Document #: NESC-RP-06-065 | Version: 1.0 |
| Title: Fracture Mechanics Based Methods Development for COPVs with Metallic Liners | | Page #: 74 of 164 | |

combined ID and OD predictions in the depth direction was about -0.9 percent with a standard deviation of 36 percent. The NASGRO® predictions of the FCG in the surface direction were unconservative for both the OD cracks (-53 percent) and ID cracks (-10 percent). A consistent difference between the percent error in the NASGRO® predictions of FCG in the depth and surface directions was observed with the percent errors in the surface FCG being greater than that of the depth direction. The root cause of this difference was not determined, but the following observations could be contributing factors:

1. The surface crack lengths were more difficult to measure than the crack depths, potentially resulting in greater measurement errors.
2. The through-the-thickness stress gradient was not known, but would likely result in a greater stress on the OD surface.
3. The crack growth rate behavior may be different in the surface and depth directions may be different due to manufacturing and/or microstructural differences.
4. The composite overwrap may influence the crack growth rate of the surface and depth directions differently.



**NASA Engineering and Safety Center
Technical Assessment Report**

Document #:
**NESC-RP-
06-065**

Version:
1.0

Title:

**Fracture Mechanics Based Methods Development for
COPVs with Metallic Liners**

Page #:
75 of 164

Table 6.8-3. Percent Error for the NASGRO® Predictions (no threshold material model) for the Tests with OD Cracks

| Specimen | Crack | NASGRO Predictions (Percent Error) | |
|----------------|-------|---------------------------------------|--------------|
| | | Depth | Surface |
| UNI-090-40-06 | 1 | 16.8 | -10.0 |
| UNI-090-40-07 | 1 | -2.6 | -15.6 |
| 18118 | 1 | -20.6 | -51.0 |
| 18118 | 3 | 2.2 | -50.6 |
| 18117 | 1 | -52.8 | -73.1 |
| 18117 | 2 | -48.7 | -74.4 |
| 18117 | 3 | 8.0 | -51.3 |
| 18107 | 1 | -6.5 | -53.0 |
| 18107 | 2 | -2.0 | -57.0 |
| 18107 | 3 | -4.1 | -56.2 |
| 18105 | 1 | -21.7 | -67.2 |
| 18105 | 2 | -15.6 | -61.2 |
| 18105 | 3 | 2.4 | -51.6 |
| 18103 | 1 | -35.3 | -54.3 |
| 18103 | 2 | 17.3 | -36.3 |
| 18103 | 3 | 27.0 | -36.9 |
| 18103 | 1a | -31.8 | -88.4 |
| 18119 | 1 | -25.7 | -54.6 |
| 18119 | 2 | -27.8 | -60.8 |
| 18119 | 3 | -38.1 | -56.7 |
| Average | | -13.0 | -53.0 |
| STDEV | | 22.4 | 18.2 |

| | | | |
|--|---|-----------------------|----------------------|
|  | NASA Engineering and Safety Center Technical Assessment Report | Document #: | Version: |
| | | NESC-RP-06-065 | 1.0 |
| Title: Fracture Mechanics Based Methods Development for COPVs with Metallic Liners | | | Page #: 76 of 164 |

Table 6.8-4. Percent Error for the NASGRO® Predictions (no threshold material model) for the Tests with ID Cracks

| Specimen | Crack | NASGRO Predictions (Percent Error) | |
|----------------|-------|---------------------------------------|--------------|
| | | Depth | Surface |
| 18118 | ID6 | 44.1 | 34.8 |
| 18119 | ID1 | -8.5 | -43.0 |
| 18119 | ID2 | -13.3 | -44.8 |
| 18119 | ID3 | -17.9 | -5.2 |
| 18119 | ID4 | -25.7 | -14.2 |
| 18119 | ID5 | -12.9 | 36.3 |
| 18119 | ID6 | -10.3 | -47.9 |
| 18119 | ID7 | 19.1 | -48.3 |
| 18119 | ID8 | -4.9 | -56.6 |
| 18119 | ID9 | 47.5 | 33.1 |
| 18119 | ID10 | 46.0 | -10.8 |
| 18119 | ID11 | -31.0 | -32.6 |
| 18119 | ID12 | 36.3 | -47.8 |
| 18118 | ID1a | -8.2 | 3.4 |
| 18118 | ID2 | 98.2 | 74.0 |
| 18118 | ID4 | 78.1 | 46.5 |
| 18118 | ID5 | 0.3 | -29.6 |
| 18118 | ID1b | -12.9 | -27.5 |
| Average | | 12.4 | -10.0 |
| STDEV | | 37.3 | 39.5 |

6.9 Eddy Current NDE

The presence of manufacturing defects in the bare liners and the subsequent nucleation of fatigue cracks from these defects caused liners to leak during precracking. A method was needed to detect cracks on the ID surface, from observations on the OD surface, of bare liners so that the precracking could be stopped prior to the cracks growing through the thickness and leaking. An eddy current system was developed and successfully used to detect ID cracks in bare liners and the system was also evaluated to determine the feasibility of detecting ID and OD cracks through the composite overwrap.

| | | | |
|--|---|--------------------------------------|------------------------|
|  | NASA Engineering and Safety Center Technical Assessment Report | Document #: NESC-RP-06-065 | Version: 1.0 |
| Title: Fracture Mechanics Based Methods Development for COPVs with Metallic Liners | | | Page #: 77 of 164 |

The eddy current system consisted of an eddy current probe that scanned longitudinally along the COPVs and liners and a motor that automatically rotated the COPVs and liners, and is shown in Figure 6.9-1. The following types of inspections were performed:

1. Low frequency eddy current (~5 kHz) inspections were performed to locate ID cracks in bare liners.
2. High frequency eddy current (~100 kHz) inspections were performed to detect OD cracks in wrapped COPVs.
3. Low frequency eddy current (~5 kHz) inspections were performed to detect ID cracks in wrapped COPVs.
4. High frequency eddy current (~1 MHz) inspections were performed to detect ID cracks in COPVs that were sectioned to allow direct access to the ID surface.

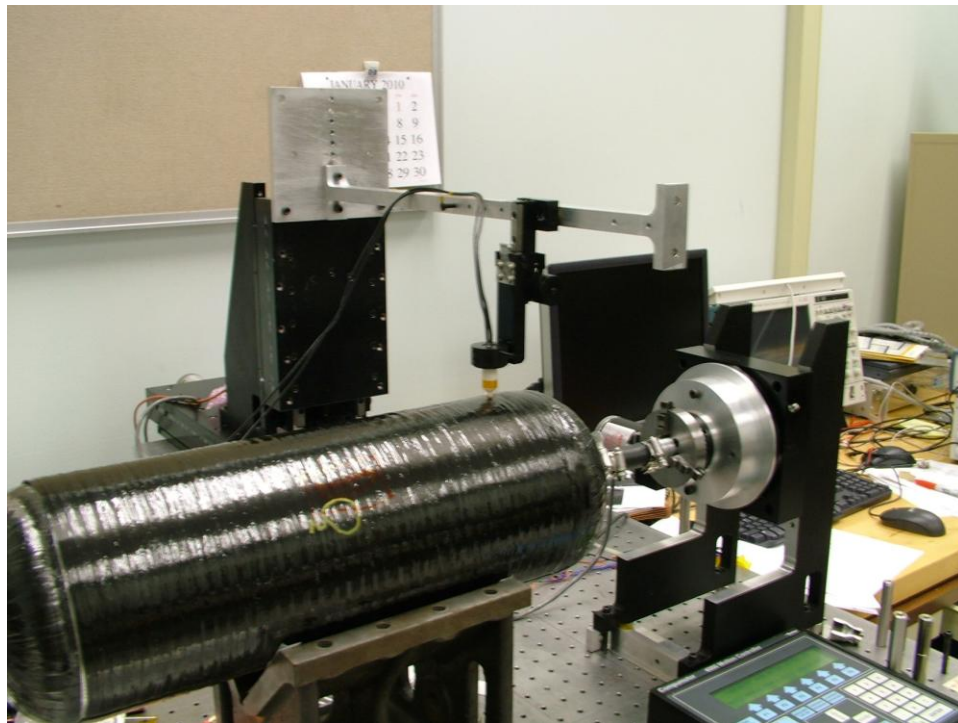


Figure 6.9-1. Photograph of the eddy current inspection system

6.9.1 Location of ID Cracks in Bare Liners

Four bare liners (18115, 18116, 18103, and 18119) were examined with the eddy current system and ID cracks detected in two (18115 and 18119) from measurements made on the liner OD



NASA Engineering and Safety Center Technical Assessment Report

Document #:
**NESC-RP-
06-065**

Version:
1.0

Title:

Fracture Mechanics Based Methods Development for COPVs with Metallic Liners

Page #:
78 of 164

surface. All four of these liners had the small semi-circular notches that required 10,000 cycles to initiate and grow the cracks to the desired length. All four of the liners were subsequently wrapped and tested, but 18115 leaked after only a few cycles and 18116 was only fatigue cycled for 200 cycles. Neither 18115 nor 18116 had sufficient FCG following precracking to produce usable crack growth measurements. The eddy current results for liner 18119 during the precracking revealed an indication that was determined to be two co-linear cracks after post-test examination, as previously shown in Figure 6.5-1. The larger of the two cracks was 0.035 inches deep by 0.190 inches long, and the smaller was 0.012 inches deep by 0.082 inches long.

The eddy current results during the precracking of bare liner 18115 revealed two independent ID cracks located about 5 inches apart in the circumferential direction, as shown in Figure 6.9-2. The first crack, ID01, and second, ID02, cracks were located about 5 inches and 2 inches from the end of the cylindrical portion of the ported end of the liner, respectively. Crack ID01 was 0.125 inches long and 0.039 inches deep after precracking, as shown in Figure 6.9-3. Crack ID02 consisted of four co-linear cracks with a total length of 0.818 inches and a maximum depth of 0.036 inches, as shown in Figure 6.9-4. Liner 18115 was wrapped and the four co-linear cracks of ID02 rapidly coalesced and leaked after a few fatigue cycles.

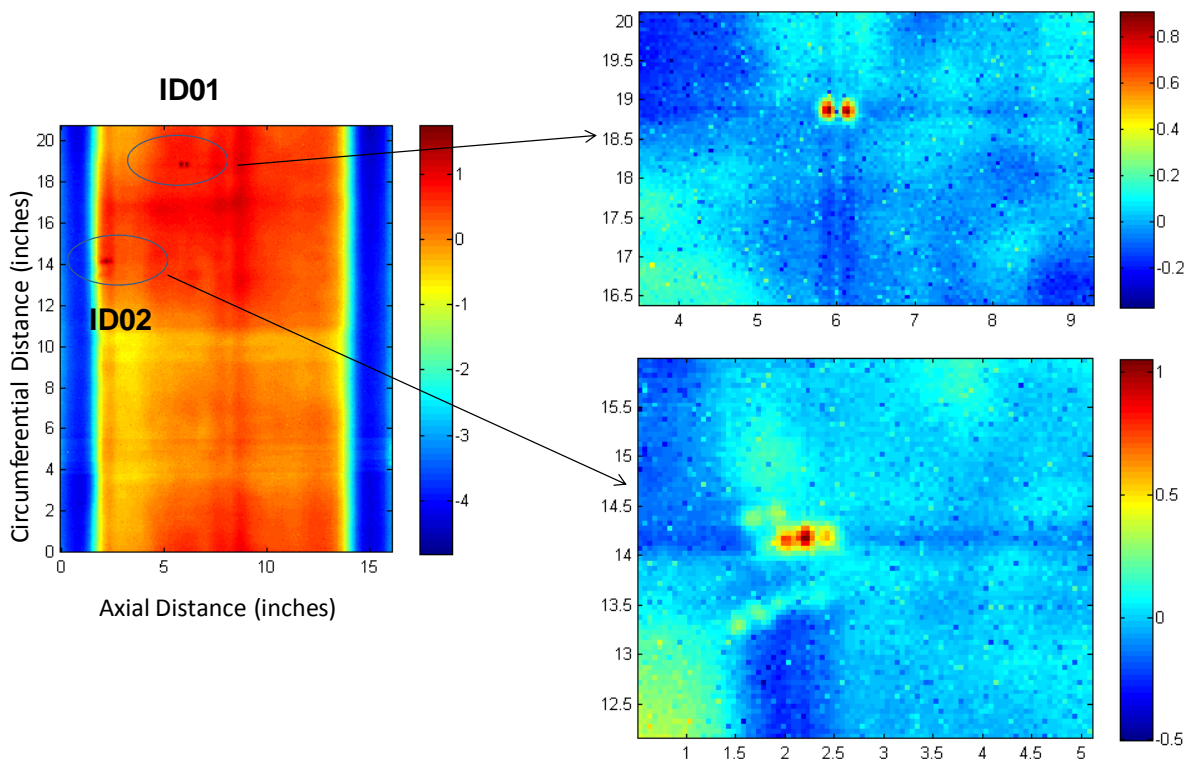


Figure 6.9-2. Eddy current scan of bare liner COPV 18115 after 10,000 precrack cycles



Title:

Fracture Mechanics Based Methods Development for
COPVs with Metallic Liners

Page #:
79 of 164

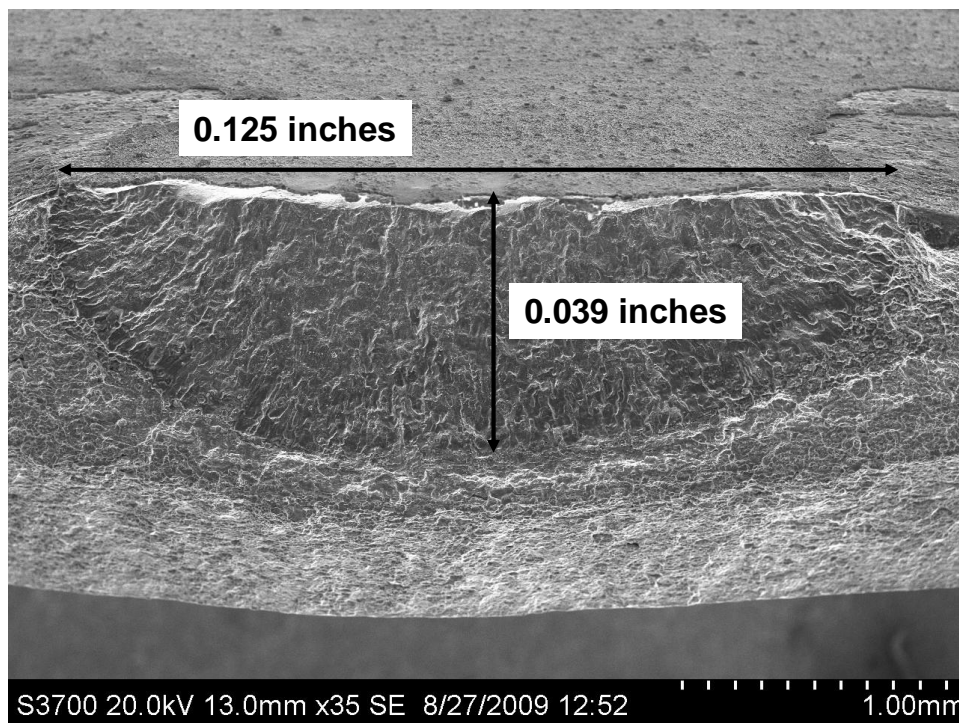


Figure 6.9-3. Crack ID01 of COPV 18115

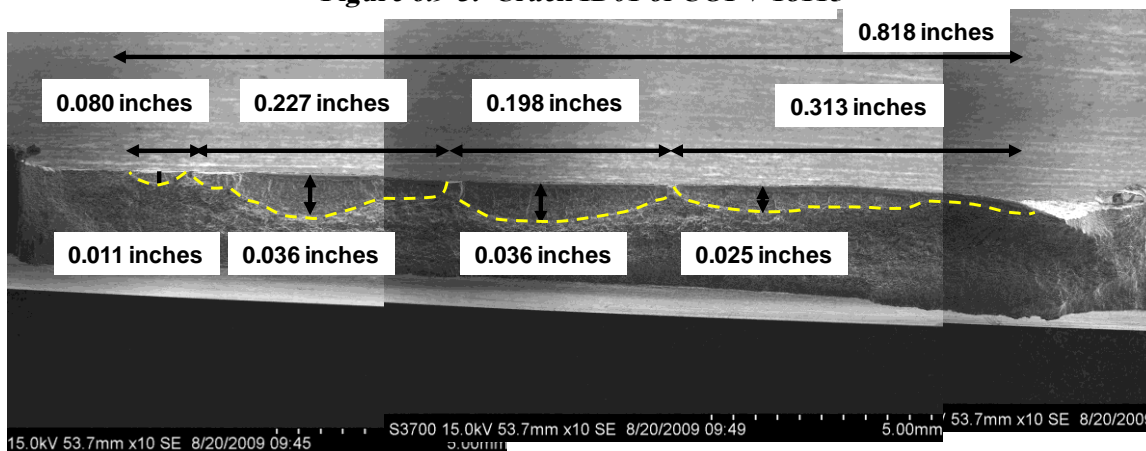


Figure 6.9-4. The four co-linear cracks that coalesced into crack ID02 of COPV 18115

6.9.2 Location of OD Cracks in Wrapped COPVs

High frequency (100 kHz) eddy current was used to inspect wrapped COPVs for OD cracks. The OD cracks were generated by fatigue precracking from the laser notches. While the laser notches were small (~0.003 to 0.005 inches wide at the surface), they were not as tight as a



Title:

**Fracture Mechanics Based Methods Development for
COPVs with Metallic Liners**

Page #:
80 of 164

fatigue crack. Only one of the three small, semi-circular OD fatigue cracks of wrapped COPV 18115 was detected through the composite wrap, as shown in Figure 6.9-5. The detected crack (OD03) was located in the cylindrical section, near the un-ported end of the COPV. The detected crack was 0.027 inches long and 0.017 inches deep and not significantly different in size from the two cracks that were not detected. All three of the long, shallow OD cracks from COPV 18118 were detected through the composite overwrap, as shown in Figure 6.9-6. The cracks at the end of the precracking of 18118 were about 0.12 inches long by 0.035 inches deep, exceeding both the target length and depth of 0.1 inches and 0.01 inches, respectively.

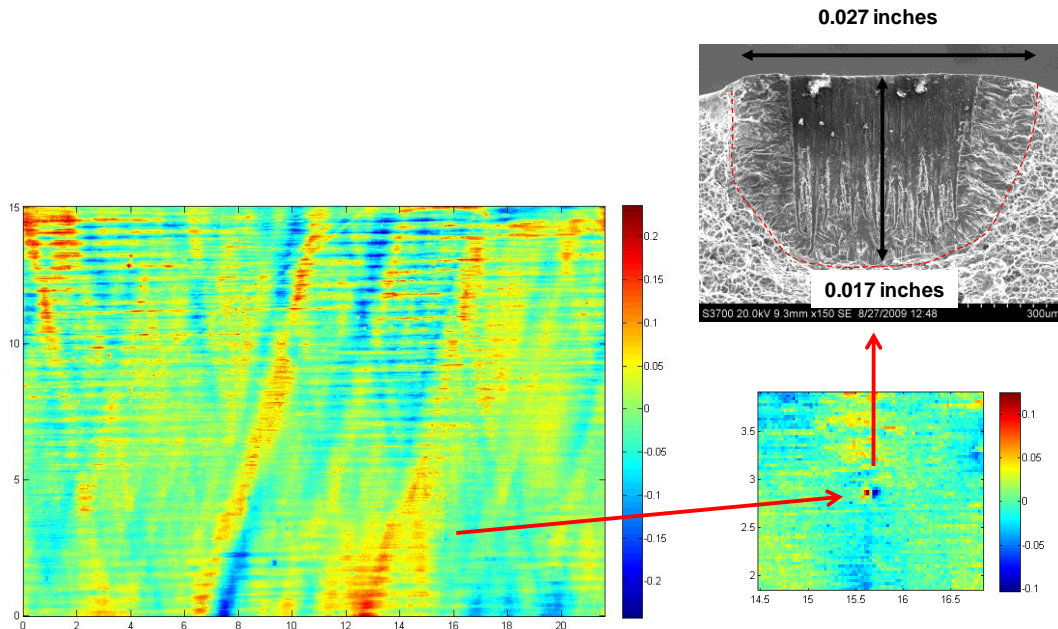


Figure 6.9-5. High frequency eddy current scan of wrapped COPV 18115



Title:

Fracture Mechanics Based Methods Development for
COPVs with Metallic Liners

Page #:
81 of 164

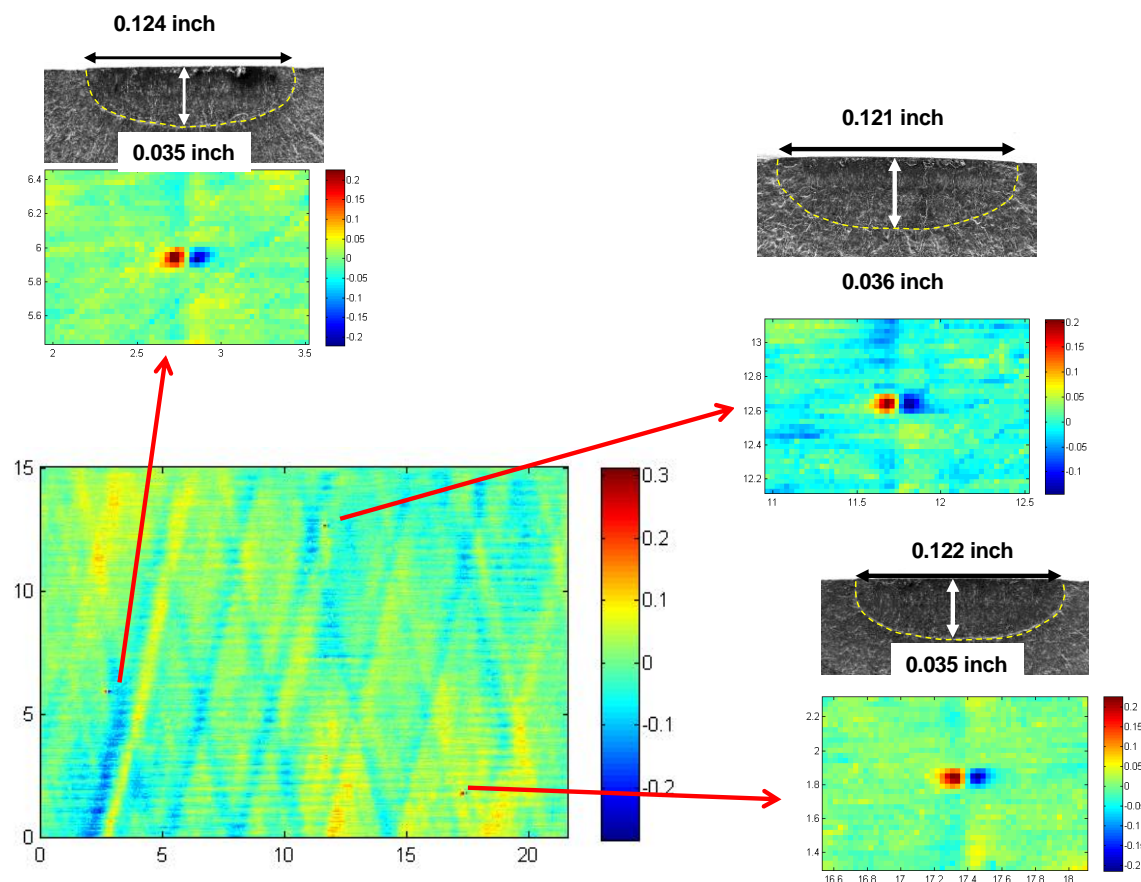


Figure 6.9-6. High frequency eddy current scan of wrapped COPV 18118 prior to fatigue testing

6.9.3 Location of ID Cracks in Wrapped COPVs

Low frequency (2 to 5 kHz) eddy current was used to inspect wrapped COPVs for ID cracks. The ID cracks were generated by precracking from manufacturing defects. COPV 18115 had two ID cracks that were detected in the bare liners and were rescanned after applying the composite overwrap. The crack ID01 was 0.125 inches long and 0.039 inches deep and was easily detected in the bare liner, but only marginally detectable in the post-wrap scan, as shown in Figure 6.9-7. The crack ID02 consisted of four co-linear cracks that may have been linked prior to the post-wrap fatigue cycling. The total crack length was 0.818 inches and the maximum crack depth was 0.036 inches. The post-wrapping inspection of ID02 was more detectable than that of ID01, as shown in Figure 6.9-8.



Title:

Fracture Mechanics Based Methods Development for
COPVs with Metallic Liners

Page #:
82 of 164

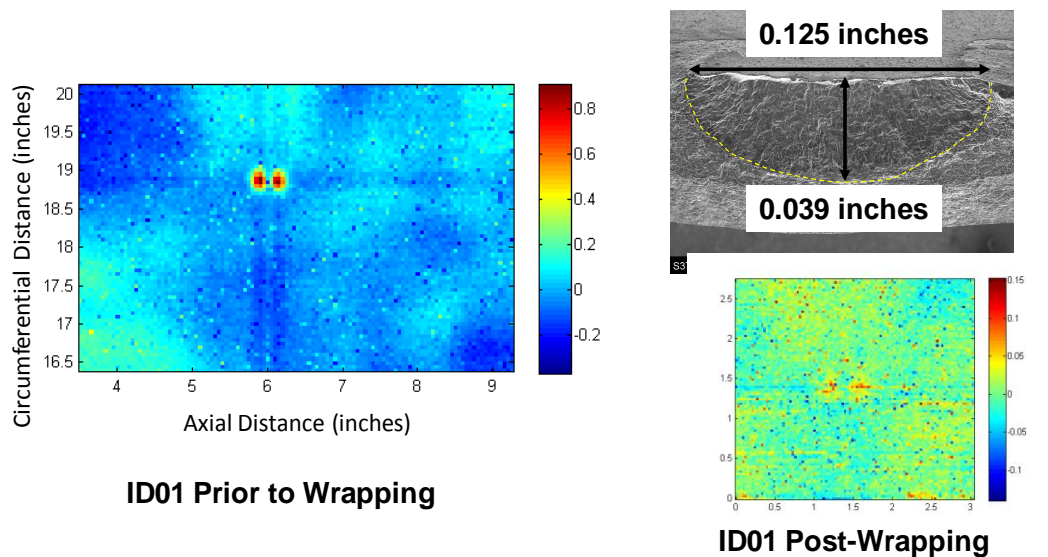


Figure 6.9-7. Low frequency eddy current scan of crack ID01 in the wrapped and un-wrapped COPV 18115 prior to fatigue testing

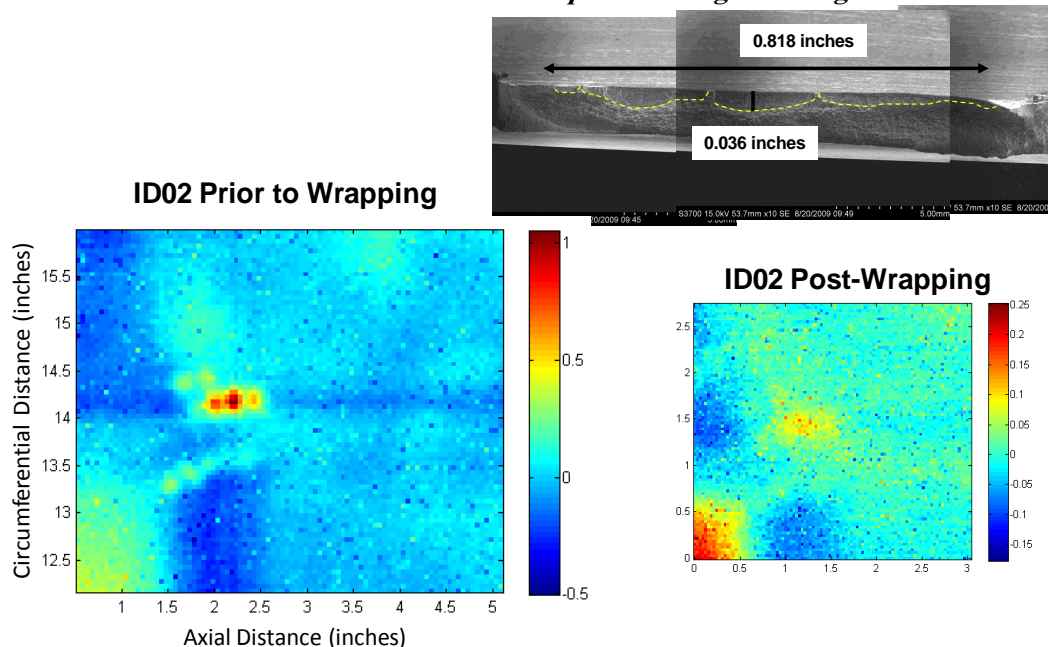


Figure 6.9-8. Low frequency eddy current scan of crack ID02 in the wrapped and un-wrapped COPV 18115 prior to fatigue testing

| | | | |
|--|---|-----------------------|----------------------|
|  | NASA Engineering and Safety Center Technical Assessment Report | Document #: | Version: |
| | | NESC-RP-06-065 | 1.0 |
| Title: Fracture Mechanics Based Methods Development for COPVs with Metallic Liners | | | Page #: 83 of 164 |

6.9.4 Location of ID Cracks in Tested COPVs

High frequency (1 MHz) eddy current was used to inspect the ID surface of tested COPVs for ID cracks that had previously not been detected either in the bare liner or wrapped liner from the OD surface. The tested COPVs were cut lengthwise in half and the known cracks were removed and examined. The exposed ID surface was directly inspected and five crack indications were detected, as shown in Figures 6.9-9 and 6.9-10. The five locations were destructively examined by cutting out small squares in the vicinity of the crack indications, identifying the cracks optically, making small saw cuts to within 0.05 inches of the crack tips, and fracturing the remaining ligaments. This method successfully located cracks at all locations except for ID03, where it was believed that a crack was present, but the fracture did not go through the crack plane. Cracks with surface lengths less than 0.05 inches and depths less than 0.008 inches were found at the remaining four locations and the fracture surfaces are shown in Figures C.42 – C.48 of Appendix C. Crack location ID01 had two nearly co-linear cracks, identified as ID01a and ID01b, as shown in Figure 6.9-11.

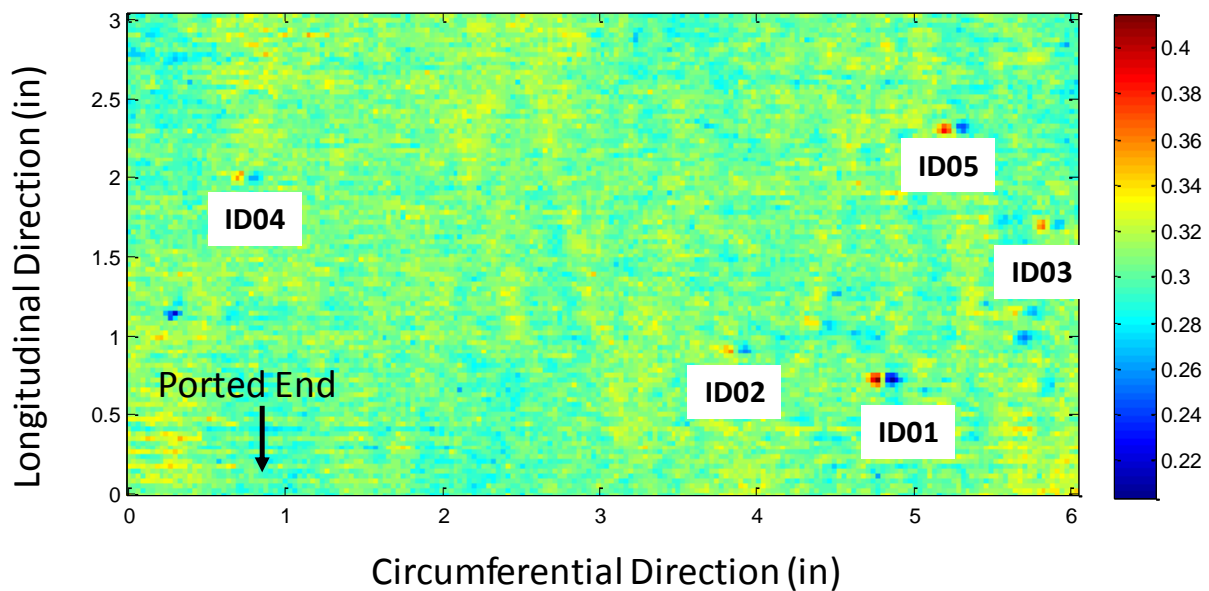


Figure 6.9-9. Five crack locations on the ID surface of COPV 18118 determined by post-test eddy current inspection of the ID surface



Title:

**Fracture Mechanics Based Methods Development for
COPVs with Metallic Liners**

Page #:
84 of 164

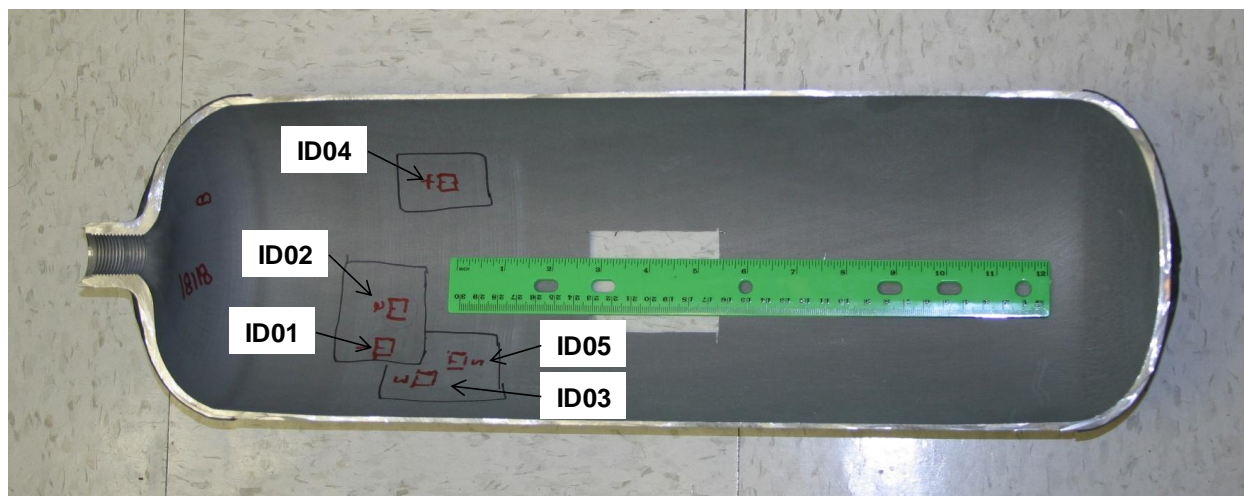


Figure 6.9-10. Location of the five ID cracks in COPV 18118 that were identified in the post-test eddy current inspection of the ID surface

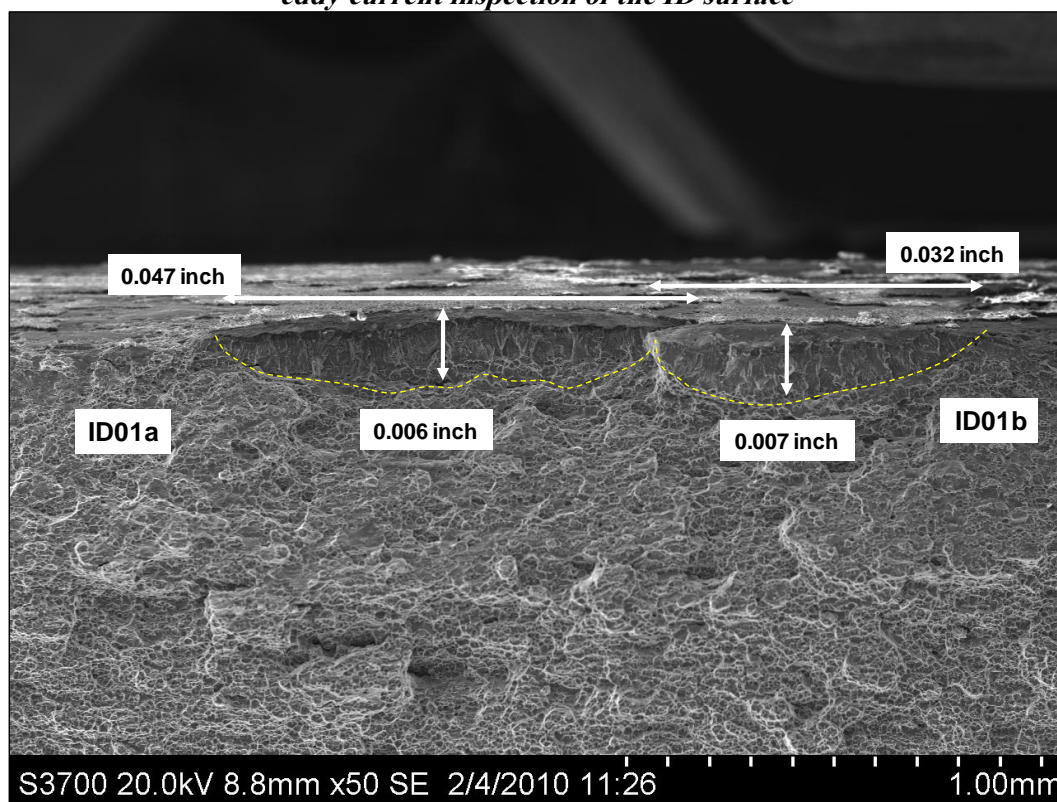


Figure 6.9-11. Photograph (50x) of the fracture surface of cracks ID01a and ID01b of COPV 18118

| | | | |
|--|---|--------------------------------------|------------------------|
|  | NASA Engineering and Safety Center Technical Assessment Report | Document #: NESC-RP-06-065 | Version: 1.0 |
| Title: Fracture Mechanics Based Methods Development for COPVs with Metallic Liners | | Page #: 85 of 164 | |

7.0 Findings, Conclusions, and NESC Recommendations

A study was performed to investigate the viability of a test method for the qualification of plastically responding COPV liners using uniaxial coupons. The investigation of the test method required the development of new test procedures to provide a first-of-kind methodology to predict the safe-life behavior of COPVs containing plastically responding metallic liners. Aluminum alloy 6061-T62, a common COPV liner material, was selected for this study. Features of the test method included: (1) laser induced notches (artificial crack starters) in the OD surface of thin cylindrical COPV liners (Note: manufacturing induced surface flaws that nucleated fatigue cracks were also observed and used in this study), (2) coupon test methods for simulating COPV liner cyclic tensile/compressive loading, (3) unique fractographic-based measurements for determining the FCG rates of small surface cracks, and (4) special eddy current inspection methods for detecting small surface cracks.

The results of this study are summarized below:

1. A new test procedure for the characterization of small (depths ranging from 0.001 to 0.03 inches) surface fatigue cracks contained in both thin uniaxial test coupons and COPV metallic liners was developed. This test procedure uniquely characterized the growth of small fatigue cracks subjected to strains that replicated the hoop strains due to the autofrettage, proof, and MDP cycling of both plastically and elastically responding COPVs. The test procedure was validated for elastically responding COPVs by demonstrating correlation between the behavior of the surface cracks in the uniaxial test coupons and both artificial and manufacturing cracks in the COPV liners.
2. The new test procedure was used to successfully test uniaxial coupons subjected to fully reversed, fully plastic conditions that simulated the hoop strains in the liner of a plastically responding COPV. The resulting FCG rate measurements under plastic conditions were at least an order of magnitude larger than similar tests conducted under elastic conditions. However, the COPVs used in this study were incapable of achieving plastically responding behavior; therefore correlation of plastic response in COPV liners with the plastically strained uniaxial coupons was not yet demonstrated. Additional testing of COPVs with plastically responding liners will be required to fully demonstrate correlation between coupon tests and plastically responding COPVs for safe-life qualification.
3. The existence of unexpected manufacturing induced flaws in the ID and OD liner surfaces presented difficulties that were overcome by the development of a special eddy current inspection method capable of detecting fatigue cracks nucleating from these

| | | | |
|--|---|--------------------------------------|------------------------|
|  | NASA Engineering and Safety Center Technical Assessment Report | Document #: NESC-RP-06-065 | Version: 1.0 |
| Title: Fracture Mechanics Based Methods Development for COPVs with Metallic Liners | | Page #: 86 of 164 | |

flaws. The assessment scope was expanded to include an investigation into the feasibility of detecting cracks in the liner that nucleated from manufacturing defects and laser notches from an examination of the bare liner OD and an examination through the composite after wrapping.

7.2 Findings

The following Findings were identified:

- F-1.** Fatigue cracks nucleated from manufacturing defects on the ID and OD of the liners during the precracking process. This occurred before the intended cracks from the laser notches on the liners OD nucleated and grew to the desired size. The size of some of the manufacturing defects exceeded the sensitivity limits of the NSTS Orbiter SPI and Orbiter EPI processes.
- F-2.** The FCG rate behavior in the depth direction for the small ID and OD surface cracks in the COPV liners correlated with the LEFM long crack data. The FCG rate behavior in the surface direction did not correlate with the long crack behavior as well as the FCG rate behavior in the depth direct. The depth direction crack growth has a greater impact on the safe-life performance than the surface crack growth direction.
- F-3.** The FCG rate behavior of the small surface cracks in the COPV liners did not exhibit a ΔK_{th} as low as $K_{max} = 1.7 \text{ ksi inch}^{1/2}$ and $R = -0.7$. This suggests the presence of a “small crack effect”, a document effect where small fatigue cracks exhibit accelerated growth rates compared to long crack threshold FCG data [ref. 13].
- F-4.** A laboratory test method was developed to test thin (0.032 inch) uniaxial coupons subjected to loading conditions that are representative of the loading conditions in a plastically responding COPV.
- F-5.** The FCG rate measurements from the uniaxial tests subjected to fully plastic, fully reversed loading conditions were more than an order of magnitude higher than those measured for the elastically responding COPV liners and elastic uniaxial tests.
- F-6.** An automated eddy current NDE method was developed to detect cracks on the ID surface of the bare liners during the precracking process. Several cracks that nucleated from manufacturing cracks were detected using the NDE system and no liners leaked during the precracking process after the NDE inspections were implemented.

| | | | |
|--|---|--------------------------------------|------------------------|
|  | NASA Engineering and Safety Center Technical Assessment Report | Document #: NESC-RP-06-065 | Version: 1.0 |
| Title: Fracture Mechanics Based Methods Development for COPVs with Metallic Liners | | Page #: 87 of 164 | |

- F-7.** The eddy current NDE method detected cracks on the liner OD from measurements made on the outside surface of the composite overwrap. All of the larger cracks (length $2c \sim 0.12$ inches and depth $a \sim 0.035$ inches) were located by the eddy current method, but only one of three smaller cracks (length $2c \sim 0.027$ inch and depth $a \sim 0.017$ inch) was detected when inspecting through the composite overwrap.
- F-8.** The eddy current NDE method detected cracks on the liner ID from measurements made on the composite overwrap OD.
- F-9.** The eddy current NDE method detected small fatigue cracks that nucleated from manufacturing defects from direct measurements on the surface containing the cracks.
- F-10.** Internal crack face pressure will influence the fatigue crack driving force. A 15 percent increase in the crack tip driving force for the ID cracks was calculated at MDP loading of the COPVs.
- F-11.** The mean percent error of the NASGRO® LEFM FCG predictions for the crack growth in the depth direction for all of the ID and OD cracks in the elastically responding COPV liners was -0.9 percent with a standard deviation of about 36 percent. The mean percent error of the NASGRO® predictions for the FCG for crack growth in the surface direction was unconservative by more than 30 percent with a standard deviation of about 36 percent.
- F-12.** The COPV liners were elastically responding, unable to achieve tensile and compressive plastic deformation during the cyclic loading after autofrettage due to the liner diameter and thickness and test pressure limitations.

7.1 Conclusions

The following conclusions were identified:

- C-1.** Uniaxial tests (simple and inexpensive relative to full-scale or sub-scale COPV testing) can be used to replicate the FCG behavior in COPVs with elastically responding liners. The FCG rates for the crack depth direction on both the ID and OD surfaces of the liner correlated with the measurements from the long crack tests. The NASGRO® LEFM crack growth analysis code predictions were in good agreement with the observed FCG behavior in the depth direction. (**F-2, F-10, F-11**)

| | | | |
|--|---|--------------------------------------|------------------------|
|  | NASA Engineering and Safety Center Technical Assessment Report | Document #: NESC-RP-06-065 | Version: 1.0 |
| Title: Fracture Mechanics Based Methods Development for COPVs with Metallic Liners | | Page #: 88 of 164 | |

- C-2.** Laboratory uniaxial coupon tests conducted under loading conditions representative of plastically responding COPV liners resulted in FCG rates that were more than an order of magnitude faster than similar tests conducted under elastic conditions. LEFM techniques are not sufficient to predict this faster FCG rate. **(F-4, F-5)**
- C-3.** Eddy current is a potential NDE technique for detecting small ID and OD surface cracks in the liner of COPVs. The NDE method detected fatigue cracks that nucleated from manufacturing defects **(F-1)** and cracks that initiated from small laser notches. **(F-6, F-7, F-8, F-9)**

7.3 NESC Recommendations

The following NESC recommendations were identified for the CPV WG:

- R-1.** The methodology developed in this study provides the test procedures for safe-life qualification of COPVs, but additional validation work will be required for plastically responding conditions. Validation will require the testing of several COPVs that are designed to have a near zero liner strain at 0 pressure after autofrettage. Additional COPV tests should be conducted using liners that are 0.05 inches to 0.03 inches thick to provide crack growth rate data for plastically responding liners. **(F-12, C-1)**
- R-2.** The success of the eddy current system indicates that it is feasible to detect cracks on hidden surfaces (both on the inside of a bare liner from the OD, and on the ID or OD of a wrapped liner from outside of the composite wrap). Additional investigations should be performed to characterize the detectability of cracks by size, shape, and location. **(F-1, F-6, F-7, F-8, F-9, C-3)**
- R-3.** EPFM techniques have been proposed for predicting the FCG behavior under conditions of high plasticity. The data generated in this study should be used to evaluate existing EPFM techniques and guide the development of new EPFM tools. **(F-5, C-2)**

8.0 Alternate Viewpoints

There were no alternate viewpoints identified during the course of this assessment by the NESC team.

9.0 Other Deliverables

Deliverables will be the final NESC report which will be provided to the key stakeholders.

| | | | |
|--|---|--------------------------------------|------------------------|
|  | NASA Engineering and Safety Center Technical Assessment Report | Document #: NESC-RP-06-065 | Version: 1.0 |
| Title: Fracture Mechanics Based Methods Development for COPVs with Metallic Liners | | Page #: 89 of 164 | |

10.0 Lessons Learned

No applicable lessons learned were identified for entry into the NASA Lessons Learned Information System (LLIS).

11.0 Definition of Terms

| | |
|--------------------|--|
| Corrective Actions | Changes to design processes, work instructions, workmanship practices, training, inspections, tests, procedures, specifications, drawings, tools, equipment, facilities, resources, or material that result in preventing, minimizing, or limiting the potential for recurrence of a problem. |
| Finding | A conclusion based on facts established by the investigating authority. |
| Lessons Learned | Knowledge or understanding gained by experience. The experience may be positive, as in a successful test or mission, or negative, as in a mishap or failure. A lesson must be significant in that it has real or assumed impact on operations; valid in that it is factually and technically correct; and applicable in that it identifies a specific design, process, or decision that reduces or limits the potential for failures and mishaps, or reinforces a positive result. |
| Observation | A factor, event, or circumstance identified during the assessment that did not contribute to the problem, but if left uncorrected has the potential to cause a mishap, injury, or increase the severity should a mishap occur. Alternatively, an observation could be a positive acknowledgement of a Center/Program/Project/Organization's operational structure, tools, and/or support provided. |
| Problem | The subject of the independent technical assessment. |
| Proximate Cause | The event(s) that occurred, including any condition(s) that existed immediately before the undesired outcome, directly resulted in its occurrence and, if eliminated or modified, would have prevented the undesired outcome. |
| Recommendation | An action identified by the NESC to correct a root cause or deficiency identified during the investigation. The recommendations may be used by the responsible Center/Program/Project/Organization in the preparation of a corrective action plan. |



NASA Engineering and Safety Center Technical Assessment Report

Document #:
**NESC-RP-
06-065**

Version:
1.0

Title:

Fracture Mechanics Based Methods Development for COPVs with Metallic Liners

Page #:
90 of 164

Root Cause One of multiple factors (events, conditions, or organizational factors) that contributed to or created the proximate cause and subsequent undesired outcome and, if eliminated or modified, would have prevented the undesired outcome. Typically, multiple root causes contribute to an undesired outcome.

12.0 Acronyms List

| | |
|-----------|--|
| a | Crack depth |
| a_f | Final crack depth |
| a_i | Initial crack depth |
| AIAA | American Institute of Aeronautics and Astronautics, Inc. |
| ANSI | American National Standards Institute |
| ASTM | American Society for Testing and Materials |
| B | Coupon thickness |
| c | Half crack length |
| CEV | Crew Exploration Vehicle |
| c_f | Final half crack length |
| c_i | Initial half crack length |
| COPV | Composite Overwrapped Pressure Vessel |
| CPV WG | Composite Pressure Vessel Working Group |
| CxP | Constellation Program |
| da/dN | Crack growth rate in the depth direction |
| dc/dN | Crack growth rate in the length direction |
| DI | Deionized |
| E | Elastic modulus |
| FCG | Fatigue Crack Growth |
| FEA | Finite Element Analysis |
| ID | inside |
| ISS | International Space Station |
| JPL | Jet Propulsion Laboratory |
| K | Stress intensity factor |
| KHz | Kilohertz |
| K_{max} | Maximum cyclic stress intensity factor |
| K_{min} | Minimum cyclic stress intensity factor |
| LaRC | Langley Research Center |
| LBB | Leak Before Burst |
| LEFM | Linear Elastic Fracture Mechanics |

| | | | |
|---|--|--------------------------------------|------------------------|
|  | NASA Engineering and Safety Center Technical Assessment Report | Document #: NESC-RP-06-065 | Version: 1.0 |
| | Title: Fracture Mechanics Based Methods Development for COPVs with Metallic Liners | | Page #: 91 of 164 |

| | |
|------------|---|
| LLIS | NASA Lessons Learned Information System |
| MDP | Maximum Design Pressure |
| MSL | Mars Science Laboratory |
| NASA | NASA Aeronautics and Space Administration |
| NDE | Nondestructive Examination |
| NESC | NASA Engineering and Safety Center |
| NRB | NESC Review Board |
| OD | outside |
| psid | lbs per square inch difference |
| R | S_{\min}/S_{\max} |
| S | Applied stress |
| SEM | Scanning Electron Microscope |
| S_{\max} | Maximum cyclic stress |
| S_{\min} | Minimum cyclic stress |
| S_o | Yield stress |
| S_{ult} | Ultimate stress |
| W | Coupon width |
| ΔK | $K_{\max} - K_{\min}$ |

13.0 References

1. ANSI/AIAA S-081A-2006, "Space Systems-Composite Overwrapped Pressure Vessels (COPVs)" dated July 24, 2006.
2. ANSI/AIAA-S081-2000, "Space Systems-Composite Overwrapped Pressure Vessels (COPVs)" dated December 19, 2000.
3. ASTM, "E8 Standard Test Methods of Tension Testing of Metallic Materials," Annual Book or ASTM Standards, American Society for Testing and Materials, Vol. 3.01, 2008.
4. ASTM, "E647 Standard Test Method for Measurement of Fatigue Crack Growth Rates," Annual Book or ASTM Standards, American Society for Testing and Materials, Vol. 3.01.
5. Forsyth, J. J. E. and Ryder, D. A., "Some Results Derived from the Microscopic Examination of Crack Surfaces," *Aircraft Eng* **32** (1960), pp. 96–103.
6. B. Wincheski, J.P. Fulton, M. Namkung, S. Nath and J.W Simpson, "Self-Nulling Eddy Current Probe for Surface and Subsurface Flaw Detection," *Materials Evaluation*, Vol. 52, No. 1, January 1994.
7. Shih, J. and Harris, J., "Overwrapping of Seamless 6061-T6 Aluminum Liners," Report No. 5456, Carleton Technologies, Inc., April 6, 2009.

| | | | |
|--|---|---|------------------------|
|  | NASA Engineering and Safety Center Technical Assessment Report | Document #: NESC-RP- 06-065 | Version: 1.0 |
| Title: Fracture Mechanics Based Methods Development for COPVs with Metallic Liners | | Page #: 92 of 164 | |

8. "NASGRO Fracture Mechanics and Fatigue Crack Growth Analysis Software," v6.0, Southwest Research Institute, March 2009.
9. Tada, H., Paris P. C., and Irwin, G. R., "The Stress Analysis of Cracks Handbook," 1985.
10. King, J. P., Jr. and Johnson, K. R., "Shuttle Orbiter Fracture Control Plan," NASA Document SD73-SH-0082A, September 1974.
11. Prosser, W., "Composite Pressure Vessel Working Group (CPVWG) Mars Science Laboratory (MSL) Cruise-Stage Propellant Tank Penetrant Non Destructive Evaluation (NDE) Probability of Detection (POD) Assessment," NASA Engineering and Safety Center Report, August 2009.
12. "Nondestructive Evaluation Requirements for Fracture Critical Metallic Components." NASA STD-5009, April 7, 2008.
13. Newman, J. C., Jr., Swain, M. H., and Phillips, E. P., "An Assessment of the Small-Crack Effect for 2024-T3 Aluminum Alloy," 2nd Engineering Foundation International Conference, The Metallurgical Society, January 1986.
14. Harris, C. E., Piascik, R. S., and Newman, J. C., Jr., "A Practical Engineering Approach to Predicting Fatigue Crack Growth in Riveted Lap Joints," NASA TM-2000-210106, May 2000.

Volume II: Appendices

- Appendix A. LEFM Fatigue Crack Growth Rate Data
- Appendix B. Fracture Surfaces from the Uniaxial Tests
- Appendix C. Fracture Surfaces from the COPV Tests
- Appendix D. Calculated Stress Intensity Factor Values for the Uniaxial and COPV Tests



**NASA Engineering and Safety Center
Technical Assessment Report**

Document #:
**NESC-RP-
06-065**

Version:
1.0

Title:

**Fracture Mechanics Based Methods Development for
COPVs with Metallic Liners**

Page #:
93 of 164

Appendix A. LEFM FCG Rate Data

| Specimen 1 | | | | | |
|------------|---------|--------|--------|-------------------------|----------|
| W | 3.0300 | in | | | |
| B | 0.0900 | in | | | |
| Notch | 0.4805 | in | | | |
| Pmax | 1.5000 | kips | | | |
| Pmain | -1.5000 | kips | | | |
| Cycle | Left | Right | Total | Kmax | da/dN |
| | inch | inch | inch | ksi inch ^{1/2} | in/cycle |
| 0 | 0.0000 | 0.0000 | 0.4805 | 4.8542 | |
| 30000 | 0.0130 | 0.0120 | 0.5055 | 4.9873 | 4.50E-07 |
| 35000 | 0.0170 | 0.0145 | 0.5120 | 5.0216 | 5.50E-07 |
| 40000 | 0.0195 | 0.0165 | 0.5165 | 5.0452 | 4.75E-07 |
| 45000 | 0.0225 | 0.0185 | 0.5215 | 5.0714 | 4.25E-07 |
| 50000 | 0.0240 | 0.0205 | 0.5250 | 5.0897 | 4.83E-07 |
| 60000 | 0.0300 | 0.0255 | 0.5360 | 5.1469 | 4.63E-07 |
| 70000 | 0.0305 | 0.0325 | 0.5435 | 5.1856 | 3.50E-07 |
| 80000 | 0.0345 | 0.0350 | 0.5500 | 5.2191 | 4.12E-07 |
| 90000 | 0.0410 | 0.0385 | 0.5600 | 5.2704 | 5.62E-07 |
| 100000 | 0.0500 | 0.0420 | 0.5725 | 5.3341 | 5.38E-07 |
| 110000 | 0.0540 | 0.0470 | 0.5815 | 5.3797 | 4.62E-07 |
| 120000 | 0.0600 | 0.0505 | 0.5910 | 5.4277 | 3.62E-07 |
| 130000 | 0.0610 | 0.0545 | 0.5960 | 5.4528 | 3.87E-07 |
| 140000 | 0.0665 | 0.0595 | 0.6065 | 5.5055 | 4.25E-07 |
| 150000 | 0.0690 | 0.0635 | 0.6130 | 5.5380 | 4.50E-07 |
| 160000 | 0.0760 | 0.0680 | 0.6245 | 5.5952 | 6.62E-07 |
| 170000 | 0.0860 | 0.0730 | 0.6395 | 5.6695 | 7.12E-07 |
| 180000 | 0.0930 | 0.0795 | 0.6530 | 5.7360 | 6.50E-07 |
| 190000 | 0.1000 | 0.0850 | 0.6655 | 5.7973 | 5.62E-07 |
| 200000 | 0.1085 | 0.0865 | 0.6755 | 5.8462 | 7.13E-07 |
| 210000 | 0.1160 | 0.0975 | 0.6940 | 5.9363 | 8.62E-07 |
| 220000 | 0.1245 | 0.1050 | 0.7100 | 6.0138 | 9.00E-07 |
| 230000 | 0.1380 | 0.1115 | 0.7300 | 6.1103 | 1.05E-06 |
| 235000 | 0.1445 | 0.1165 | 0.7415 | 6.1656 | 1.25E-06 |
| 240000 | 0.1520 | 0.1225 | 0.7550 | 6.2304 | 1.30E-06 |
| 245000 | 0.1590 | 0.1280 | 0.7675 | 6.2902 | 1.30E-06 |
| 250000 | 0.1665 | 0.1340 | 0.7810 | 6.3548 | 1.50E-06 |
| 255000 | 0.1760 | 0.1410 | 0.7975 | 6.4334 | 1.60E-06 |
| 260000 | 0.1845 | 0.1480 | 0.8130 | 6.5073 | 1.78E-06 |
| 265000 | 0.1950 | 0.1575 | 0.8330 | 6.6023 | 2.00E-06 |
| 267000 | 0.1985 | 0.1620 | 0.8410 | 6.6404 | 1.88E-06 |
| 269000 | 0.2030 | 0.1645 | 0.8480 | 6.6736 | 1.69E-06 |
| 271000 | 0.2065 | 0.1675 | 0.8545 | 6.7045 | 1.69E-06 |
| 273000 | 0.2100 | 0.1710 | 0.8615 | 6.7377 | 1.88E-06 |
| 275000 | 0.2145 | 0.1745 | 0.8695 | 6.7757 | 2.00E-06 |



**NASA Engineering and Safety Center
Technical Assessment Report**

Document #:
**NESC-RP-
06-065**

Version:
1.0

Title:

**Fracture Mechanics Based Methods Development for
COPVs with Metallic Liners**

Page #:
94 of 164

| | | | | | |
|--------|--------|--------|--------|--------|----------|
| 277000 | 0.2185 | 0.1785 | 0.8775 | 6.8136 | 2.31E-06 |
| 279000 | 0.2240 | 0.1835 | 0.8880 | 6.8635 | 2.63E-06 |
| 281000 | 0.2305 | 0.1875 | 0.8985 | 6.9133 | 2.87E-06 |
| 283000 | 0.2380 | 0.1925 | 0.9110 | 6.9727 | 3.00E-06 |
| 285000 | 0.2420 | 0.2000 | 0.9225 | 7.0273 | 2.58E-06 |
| 286000 | 0.2450 | 0.2010 | 0.9265 | 7.0463 | 2.63E-06 |
| 287000 | 0.2480 | 0.2045 | 0.9330 | 7.0772 | 3.12E-06 |
| 288000 | 0.2510 | 0.2075 | 0.9390 | 7.1058 | 3.25E-06 |
| 289000 | 0.2545 | 0.2110 | 0.9460 | 7.1391 | 3.87E-06 |
| 290000 | 0.2590 | 0.2150 | 0.9545 | 7.1796 | 3.13E-06 |
| 291000 | 0.2610 | 0.2170 | 0.9585 | 7.1987 | 2.50E-06 |
| 292000 | 0.2645 | 0.2195 | 0.9645 | 7.2273 | 3.13E-06 |
| 293000 | 0.2690 | 0.2215 | 0.9710 | 7.2583 | 2.62E-06 |
| 294000 | 0.2705 | 0.2240 | 0.9750 | 7.2774 | 3.25E-06 |
| 295000 | 0.2745 | 0.2290 | 0.9840 | 7.3204 | 3.50E-06 |
| 296000 | 0.2775 | 0.2310 | 0.9890 | 7.3443 | 3.00E-06 |
| 297000 | 0.2805 | 0.2350 | 0.9960 | 7.3778 | 3.37E-06 |
| 298000 | 0.2840 | 0.2380 | 1.0025 | 7.4090 | 3.12E-06 |
| 299000 | 0.2870 | 0.2410 | 1.0085 | 7.4377 | 3.38E-06 |
| 300000 | 0.2910 | 0.2445 | 1.0160 | 7.4738 | 3.62E-06 |
| 301000 | 0.2945 | 0.2480 | 1.0230 | 7.5074 | 3.50E-06 |
| 302000 | 0.2975 | 0.2520 | 1.0300 | 7.5411 | 3.88E-06 |
| 303000 | 0.3020 | 0.2560 | 1.0385 | 7.5821 | 3.62E-06 |
| 304000 | 0.3055 | 0.2585 | 1.0445 | 7.6110 | 3.12E-06 |
| 305000 | 0.3085 | 0.2620 | 1.0510 | 7.6425 | 3.62E-06 |
| 306000 | 0.3120 | 0.2665 | 1.0590 | 7.6812 | 3.88E-06 |
| 307000 | 0.3160 | 0.2700 | 1.0665 | 7.7175 | 4.00E-06 |
| 308000 | 0.3205 | 0.2740 | 1.0750 | 7.7588 | 3.88E-06 |
| 309000 | 0.3235 | 0.2780 | 1.0820 | 7.7929 | 3.75E-06 |
| 310000 | 0.3275 | 0.2820 | 1.0900 | 7.8319 | 4.50E-06 |
| 311000 | 0.3335 | 0.2860 | 1.1000 | 7.8807 | 4.62E-06 |
| 312000 | 0.3380 | 0.2900 | 1.1085 | 7.9224 | 4.37E-06 |
| 313000 | 0.3425 | 0.2945 | 1.1175 | 7.9666 | 4.87E-06 |
| 314000 | 0.3470 | 0.3005 | 1.1280 | 8.0183 | 4.75E-06 |
| 315000 | 0.3515 | 0.3045 | 1.1365 | 8.0602 | 4.00E-06 |
| 316000 | 0.3550 | 0.3085 | 1.1440 | 8.0973 | 4.13E-06 |
| 317000 | 0.3595 | 0.3130 | 1.1530 | 8.1420 | 4.75E-06 |
| 318000 | 0.3640 | 0.3185 | 1.1630 | 8.1917 | 5.00E-06 |
| 319000 | 0.3700 | 0.3225 | 1.1730 | 8.2416 | 5.00E-06 |
| 320000 | 0.3745 | 0.3280 | 1.1830 | 8.2917 | 4.88E-06 |
| 321000 | 0.3800 | 0.3320 | 1.1925 | 8.3395 | 5.12E-06 |
| 322000 | 0.3860 | 0.3370 | 1.2035 | 8.3950 | 5.12E-06 |
| 323000 | 0.3905 | 0.3420 | 1.2130 | 8.4431 | 5.12E-06 |
| 324000 | 0.3970 | 0.3465 | 1.2240 | 8.4990 | 5.62E-06 |
| 325000 | 0.4030 | 0.3520 | 1.2355 | 8.5577 | 5.50E-06 |
| 326000 | 0.4080 | 0.3575 | 1.2460 | 8.6115 | 5.25E-06 |
| 327000 | 0.4130 | 0.3630 | 1.2565 | 8.6656 | 5.38E-06 |
| 328000 | 0.4185 | 0.3685 | 1.2675 | 8.7225 | 5.62E-06 |
| 329000 | 0.4240 | 0.3745 | 1.2790 | 8.7823 | 5.75E-06 |
| 330000 | 0.4300 | 0.3800 | 1.2905 | 8.8423 | 6.13E-06 |



NASA Engineering and Safety Center Technical Assessment Report

Document #:
**NESC-RP-
06-065**

Version:
1.0

Title:

Fracture Mechanics Based Methods Development for COPVs with Metallic Liners

Page #:
95 of 164

| | | | | | |
|--------|--------|--------|--------|---------|----------|
| 331000 | 0.4360 | 0.3870 | 1.3035 | 8.9106 | 6.00E-06 |
| 332000 | 0.4425 | 0.3915 | 1.3145 | 8.9687 | 6.12E-06 |
| 333000 | 0.4510 | 0.3965 | 1.3280 | 9.0405 | 6.25E-06 |
| 334000 | 0.4560 | 0.4030 | 1.3395 | 9.1020 | 5.62E-06 |
| 335000 | 0.4610 | 0.4090 | 1.3505 | 9.1611 | 6.50E-06 |
| 336000 | 0.4690 | 0.4160 | 1.3655 | 9.2423 | 7.00E-06 |
| 337000 | 0.4760 | 0.4220 | 1.3785 | 9.3132 | 7.12E-06 |
| 338000 | 0.4835 | 0.4300 | 1.3940 | 9.3984 | 7.00E-06 |
| 339000 | 0.4900 | 0.4360 | 1.4065 | 9.4676 | 6.75E-06 |
| 340000 | 0.4970 | 0.4435 | 1.4210 | 9.5486 | 7.12E-06 |
| 341000 | 0.5045 | 0.4500 | 1.4350 | 9.6274 | 6.87E-06 |
| 342000 | 0.5120 | 0.4560 | 1.4485 | 9.7040 | 7.88E-06 |
| 343000 | 0.5210 | 0.4650 | 1.4665 | 9.8071 | 7.50E-06 |
| 344000 | 0.5270 | 0.4710 | 1.4785 | 9.8765 | 7.75E-06 |
| 345000 | 0.5360 | 0.4810 | 1.4975 | 9.9875 | 8.13E-06 |
| 346000 | 0.5430 | 0.4875 | 1.5110 | 10.0671 | 7.50E-06 |
| 347000 | 0.5520 | 0.4950 | 1.5275 | 10.1655 | 8.25E-06 |
| 348000 | 0.5595 | 0.5040 | 1.5440 | 10.2651 | 9.13E-06 |
| 349000 | 0.5705 | 0.5130 | 1.5640 | 10.3872 | 9.63E-06 |
| 350000 | 0.5780 | 0.5240 | 1.5825 | 10.5019 | 8.62E-06 |
| 351000 | 0.5870 | 0.5310 | 1.5985 | 10.6023 | 7.87E-06 |
| 352000 | 0.5960 | 0.5375 | 1.6140 | 10.7007 | 8.37E-06 |
| 353000 | 0.6030 | 0.5485 | 1.6320 | 10.8165 | |



**NASA Engineering and Safety Center
Technical Assessment Report**

Document #:
**NESC-RP-
06-065**

Version:
1.0

Title:

**Fracture Mechanics Based Methods Development for
COPVs with Metallic Liners**

Page #:
96 of 164

| Specimen 2 | | | | | |
|------------|--------------|---------------|---------------|---------------------------------|-------------------|
| | W | 3.0300 | in | | |
| | B | 0.0900 | in | | |
| | Notch | 0.4835 | in | | |
| | Pmax | 2.0000 | kips | | |
| | Pmain | -2.0000 | kips | | |
| Cycle | Left inch | Right inch | Total inch | Kmax ksi inch ^{1/2} | da/dN in/cycle |
| 0 | 0.0000 | 0.0000 | 0.4835 | 6.4938 | |
| 10000 | 0.0250 | 0.0270 | 0.5355 | 6.8590 | 2.68E-06 |
| 20000 | 0.0535 | 0.0535 | 0.5905 | 7.2336 | 2.85E-06 |
| 25000 | 0.0675 | 0.0700 | 0.6210 | 7.4371 | 3.18E-06 |
| 27000 | 0.0765 | 0.0750 | 0.6350 | 7.5297 | 3.56E-06 |
| 29000 | 0.0825 | 0.0835 | 0.6495 | 7.6251 | 3.69E-06 |
| 31000 | 0.0900 | 0.0910 | 0.6645 | 7.7232 | 3.94E-06 |
| 33000 | 0.0985 | 0.0990 | 0.6810 | 7.8307 | 4.08E-06 |
| 34000 | 0.1025 | 0.1030 | 0.6890 | 7.8826 | 4.00E-06 |
| 35000 | 0.1065 | 0.1070 | 0.6970 | 7.9344 | 4.50E-06 |
| 36000 | 0.1110 | 0.1125 | 0.7070 | 7.9991 | 4.75E-06 |
| 37000 | 0.1160 | 0.1165 | 0.7160 | 8.0571 | 4.63E-06 |
| 38000 | 0.1205 | 0.1215 | 0.7255 | 8.1182 | 4.12E-06 |
| 39000 | 0.1250 | 0.1240 | 0.7325 | 8.1631 | 4.12E-06 |
| 40000 | 0.1290 | 0.1295 | 0.7420 | 8.2240 | 5.50E-06 |
| 41000 | 0.1350 | 0.1360 | 0.7545 | 8.3040 | 4.88E-06 |
| 42000 | 0.1400 | 0.1380 | 0.7615 | 8.3487 | 4.12E-06 |
| 43000 | 0.1440 | 0.1435 | 0.7710 | 8.4093 | 5.12E-06 |
| 44000 | 0.1490 | 0.1495 | 0.7820 | 8.4794 | 5.00E-06 |
| 45000 | 0.1545 | 0.1530 | 0.7910 | 8.5366 | 4.87E-06 |
| 46000 | 0.1595 | 0.1585 | 0.8015 | 8.6033 | 5.00E-06 |
| 47000 | 0.1640 | 0.1635 | 0.8110 | 8.6636 | 5.25E-06 |
| 48000 | 0.1695 | 0.1695 | 0.8225 | 8.7366 | 5.50E-06 |
| 49000 | 0.1755 | 0.1740 | 0.8330 | 8.8031 | 5.37E-06 |
| 50000 | 0.1805 | 0.1800 | 0.8440 | 8.8728 | 5.25E-06 |
| 51000 | 0.1850 | 0.1855 | 0.8540 | 8.9361 | 5.63E-06 |
| 52000 | 0.1930 | 0.1900 | 0.8665 | 9.0152 | 6.25E-06 |
| 53000 | 0.1990 | 0.1965 | 0.8790 | 9.0943 | 6.37E-06 |
| 54000 | 0.2065 | 0.2020 | 0.8920 | 9.1766 | 6.50E-06 |
| 55000 | 0.2130 | 0.2085 | 0.9050 | 9.2589 | 6.75E-06 |
| 56000 | 0.2200 | 0.2155 | 0.9190 | 9.3476 | 6.87E-06 |
| 57000 | 0.2270 | 0.2220 | 0.9325 | 9.4332 | 6.87E-06 |
| 58000 | 0.2340 | 0.2290 | 0.9465 | 9.5220 | 7.37E-06 |
| 59000 | 0.2425 | 0.2360 | 0.9620 | 9.6205 | 8.00E-06 |
| 60000 | 0.2510 | 0.2440 | 0.9785 | 9.7255 | 7.88E-06 |
| 61000 | 0.2590 | 0.2510 | 0.9935 | 9.8211 | 7.00E-06 |
| 62000 | 0.2635 | 0.2595 | 1.0065 | 9.9042 | 6.62E-06 |
| 63000 | 0.2705 | 0.2660 | 1.0200 | 9.9906 | 7.75E-06 |
| 64000 | 0.2795 | 0.2745 | 1.0375 | 10.1030 | 8.75E-06 |
| 65000 | 0.2880 | 0.2835 | 1.0550 | 10.2157 | 8.50E-06 |
| 66000 | 0.2970 | 0.2910 | 1.0715 | 10.3224 | 8.88E-06 |



NASA Engineering and Safety Center Technical Assessment Report

Document #:
**NESC-RP-
06-065**

Version:
1.0

Title:

Fracture Mechanics Based Methods Development for COPVs with Metallic Liners

Page #:
97 of 164

| | | | | | |
|-------|--------|--------|--------|---------|----------|
| 67000 | 0.3065 | 0.3005 | 1.0905 | 10.4458 | 1.03E-05 |
| 68000 | 0.3175 | 0.3115 | 1.1125 | 10.5893 | 9.63E-06 |
| 69000 | 0.3250 | 0.3205 | 1.1290 | 10.6976 | 8.62E-06 |
| 70000 | 0.3340 | 0.3295 | 1.1470 | 10.8163 | 1.06E-05 |
| 71000 | 0.3455 | 0.3425 | 1.1715 | 10.9789 | 1.08E-05 |
| 72000 | 0.3565 | 0.3500 | 1.1900 | 11.1025 | 1.01E-05 |
| 73000 | 0.3670 | 0.3615 | 1.2120 | 11.2506 | 1.13E-05 |
| 74000 | 0.3785 | 0.3730 | 1.2350 | 11.4068 | 1.14E-05 |
| 75000 | 0.3900 | 0.3840 | 1.2575 | 11.5610 | 1.26E-05 |
| 76000 | 0.4035 | 0.3985 | 1.2855 | 11.7549 | 1.20E-05 |
| 77000 | 0.4145 | 0.4075 | 1.3055 | 11.8949 | 1.11E-05 |
| 78000 | 0.4265 | 0.4200 | 1.3300 | 12.0682 | 1.25E-05 |
| 79000 | 0.4385 | 0.4335 | 1.3555 | 12.2508 | 1.31E-05 |
| 80000 | 0.4520 | 0.4470 | 1.3825 | 12.4469 | 1.40E-05 |
| 81000 | 0.4660 | 0.4620 | 1.4115 | 12.6606 | 1.49E-05 |
| 82000 | 0.4815 | 0.4770 | 1.4420 | 12.8893 | 1.56E-05 |
| 83000 | 0.4980 | 0.4925 | 1.4740 | 13.1339 | 1.59E-05 |
| 84000 | 0.5140 | 0.5080 | 1.5055 | 13.3795 | 1.69E-05 |
| 85000 | 0.5320 | 0.5260 | 1.5415 | 13.6665 | 1.78E-05 |
| 86000 | 0.5500 | 0.5430 | 1.5765 | 13.9527 | 1.78E-05 |
| 87000 | 0.5695 | 0.5595 | 1.6125 | 14.2548 | |



**NASA Engineering and Safety Center
Technical Assessment Report**

Document #:
**NESC-RP-
06-065**

Version:
1.0

Title:

**Fracture Mechanics Based Methods Development for
COPVs with Metallic Liners**

Page #:
98 of 164

| Specimen 3 | | | | | |
|------------|--------------|---------------|---------------|---------------------------------|--------------------------|
| | W | 2.9900 | in | | |
| | B | 0.0870 | in | | |
| | Notch | 0.5520 | in | | |
| | Pmax | 3.0000 | kips | | |
| | Pmain | -3.0000 | Kips | | |
| Cycle | Left inch | Right inch | Total inch | Kmax ksi inch ^{1/2} | da/dN (3-pt) in/cycle |
| 0 | 0.0000 | 0.0000 | 0.5520 | 10.9704 | |
| 500 | 0.011 | 0.0095 | 0.5725 | 11.1906 | 2.73E-05 |
| 1000 | 0.0285 | 0.026 | 0.6065 | 11.5510 | 3.07E-05 |
| 1250 | 0.0320 | 0.0345 | 0.6185 | 11.6770 | 2.40E-05 |
| 1500 | 0.037 | 0.0415 | 0.6305 | 11.8024 | 2.30E-05 |
| 1750 | 0.0415 | 0.048 | 0.6415 | 11.9168 | 2.10E-05 |
| 2000 | 0.0465 | 0.053 | 0.6515 | 12.0205 | 2.00E-05 |
| 2250 | 0.0505 | 0.059 | 0.6615 | 12.1239 | 1.85E-05 |
| 2500 | 0.055 | 0.063 | 0.6700 | 12.2114 | 1.90E-05 |
| 2750 | 0.06 | 0.0685 | 0.6805 | 12.3193 | 1.70E-05 |
| 3000 | 0.063 | 0.072 | 0.6870 | 12.3860 | 1.35E-05 |
| 3250 | 0.066 | 0.076 | 0.6940 | 12.4576 | 1.75E-05 |
| 3500 | 0.071 | 0.0815 | 0.7045 | 12.5648 | 1.65E-05 |
| 3750 | 0.074 | 0.0845 | 0.7105 | 12.6260 | 1.55E-05 |
| 4000 | 0.079 | 0.089 | 0.7200 | 12.7226 | 1.95E-05 |



**NASA Engineering and Safety Center
Technical Assessment Report**

Document #:
**NESC-RP-
06-065**

Version:
1.0

Title:

**Fracture Mechanics Based Methods Development for
COPVs with Metallic Liners**

Page #:
99 of 164

| | | | | | |
|-------|--------|--------|--------|---------|----------|
| 4250 | 0.0845 | 0.0935 | 0.7300 | 12.8241 | 1.65E-05 |
| 4500 | 0.088 | 0.0965 | 0.7365 | 12.8900 | 1.65E-05 |
| 4750 | 0.0925 | 0.102 | 0.7465 | 12.9912 | 2.05E-05 |
| 5000 | 0.0975 | 0.1075 | 0.7570 | 13.0973 | 1.90E-05 |
| 5250 | 0.1025 | 0.111 | 0.7655 | 13.1831 | 2.00E-05 |
| 5500 | 0.1075 | 0.1175 | 0.7770 | 13.2990 | 1.80E-05 |
| 5750 | 0.1115 | 0.12 | 0.7835 | 13.3644 | 1.80E-05 |
| 6000 | 0.116 | 0.127 | 0.7950 | 13.4800 | 1.85E-05 |
| 6250 | 0.12 | 0.13 | 0.8020 | 13.5504 | 1.70E-05 |
| 6500 | 0.1245 | 0.1355 | 0.8120 | 13.6507 | 1.95E-05 |
| 6750 | 0.13 | 0.1395 | 0.8215 | 13.7461 | 2.15E-05 |
| 7000 | 0.136 | 0.1455 | 0.8335 | 13.8664 | 2.00E-05 |
| 7250 | 0.1405 | 0.149 | 0.8415 | 13.9465 | 1.75E-05 |
| 7500 | 0.144 | 0.155 | 0.8510 | 14.0417 | 2.00E-05 |
| 7750 | 0.149 | 0.1605 | 0.8615 | 14.1469 | 2.15E-05 |
| 8000 | 0.1545 | 0.166 | 0.8725 | 14.2571 | 2.15E-05 |
| 8250 | 0.1595 | 0.1715 | 0.8830 | 14.3623 | 2.40E-05 |
| 8500 | 0.1675 | 0.177 | 0.8965 | 14.4976 | 2.15E-05 |
| 8750 | 0.1725 | 0.18 | 0.9045 | 14.5778 | 1.95E-05 |
| 9000 | 0.177 | 0.187 | 0.9160 | 14.6932 | 1.85E-05 |
| 9250 | 0.181 | 0.19 | 0.9230 | 14.7635 | 2.05E-05 |
| 9500 | 0.1875 | 0.197 | 0.9365 | 14.8991 | 2.65E-05 |
| 9750 | 0.1945 | 0.203 | 0.9495 | 15.0298 | 2.45E-05 |
| 10000 | 0.2 | 0.209 | 0.9610 | 15.1457 | 2.30E-05 |
| 10250 | 0.204 | 0.2165 | 0.9725 | 15.2617 | 2.10E-05 |
| 10500 | 0.211 | 0.219 | 0.9820 | 15.3576 | 2.75E-05 |
| 10750 | 0.2205 | 0.2275 | 1.0000 | 15.5398 | 2.85E-05 |
| 11000 | 0.2255 | 0.233 | 1.0105 | 15.6463 | 2.10E-05 |
| 11250 | 0.2295 | 0.2395 | 1.0210 | 15.7531 | 2.05E-05 |
| 11500 | 0.2345 | 0.2445 | 1.0310 | 15.8549 | 2.55E-05 |
| 11750 | 0.2425 | 0.252 | 1.0465 | 16.0132 | 2.85E-05 |
| 12000 | 0.2495 | 0.258 | 1.0595 | 16.1463 | 2.45E-05 |
| 12250 | 0.256 | 0.263 | 1.0710 | 16.2645 | 2.50E-05 |
| 12500 | 0.263 | 0.2695 | 1.0845 | 16.4036 | 2.75E-05 |
| 12750 | 0.271 | 0.2755 | 1.0985 | 16.5484 | 2.95E-05 |
| 13000 | 0.2785 | 0.2835 | 1.1140 | 16.7094 | 2.95E-05 |
| 13250 | 0.2835 | 0.2925 | 1.1280 | 16.8554 | 2.95E-05 |
| 13500 | 0.293 | 0.2985 | 1.1435 | 17.0178 | 2.95E-05 |
| 13750 | 0.3005 | 0.305 | 1.1575 | 17.1652 | 3.00E-05 |
| 14000 | 0.308 | 0.3135 | 1.1735 | 17.3345 | 3.20E-05 |
| 14250 | 0.317 | 0.3205 | 1.1895 | 17.5048 | 3.10E-05 |
| 14500 | 0.3255 | 0.327 | 1.2045 | 17.6654 | 3.20E-05 |
| 14750 | 0.335 | 0.3345 | 1.2215 | 17.8485 | 3.64E-05 |
| 15000 | 0.3445 | 0.3444 | 1.2409 | 18.0591 | 3.95E-05 |
| 15250 | 0.3555 | 0.3535 | 1.2610 | 18.2790 | 4.16E-05 |
| 15500 | 0.3665 | 0.364 | 1.2825 | 18.5166 | 3.90E-05 |
| 15750 | 0.376 | 0.372 | 1.3000 | 18.7117 | 3.55E-05 |
| 16000 | 0.3865 | 0.3795 | 1.3180 | 18.9141 | 4.10E-05 |
| 16250 | 0.3985 | 0.3905 | 1.3410 | 19.1754 | 4.05E-05 |



NASA Engineering and Safety Center Technical Assessment Report

Document #:
**NESC-RP-
06-065**

Version:
1.0

Title:

Fracture Mechanics Based Methods Development for COPVs with Metallic Liners

Page #:
100 of 164

| | | | | | |
|-------|--------|--------|--------|---------|----------|
| 16500 | 0.406 | 0.4005 | 1.3585 | 19.3764 | 4.05E-05 |
| 16750 | 0.4205 | 0.409 | 1.3815 | 19.6435 | 5.10E-05 |
| 17000 | 0.436 | 0.4215 | 1.4095 | 19.9734 | 5.15E-05 |
| 17250 | 0.447 | 0.434 | 1.4330 | 20.2546 | 5.25E-05 |
| 17500 | 0.4635 | 0.4465 | 1.4620 | 20.6073 | 5.40E-05 |
| 17750 | 0.478 | 0.457 | 1.4870 | 20.9168 | 5.55E-05 |
| 18000 | 0.4935 | 0.472 | 1.5175 | 21.3015 | 6.75E-05 |
| 18250 | 0.5165 | 0.486 | 1.5545 | 21.7795 | 7.40E-05 |
| 18500 | 0.536 | 0.5035 | 1.5915 | 22.2709 | 8.60E-05 |
| 18750 | 0.565 | 0.5235 | 1.6405 | 22.9442 | 1.02E-04 |
| 19000 | 0.5955 | 0.5455 | 1.6930 | 23.6971 | |



Title:

Fracture Mechanics Based Methods Development for
COPVs with Metallic Liners

Page #:
101 of 164

Appendix B. Fracture Surfaces from the Uniaxial Tests

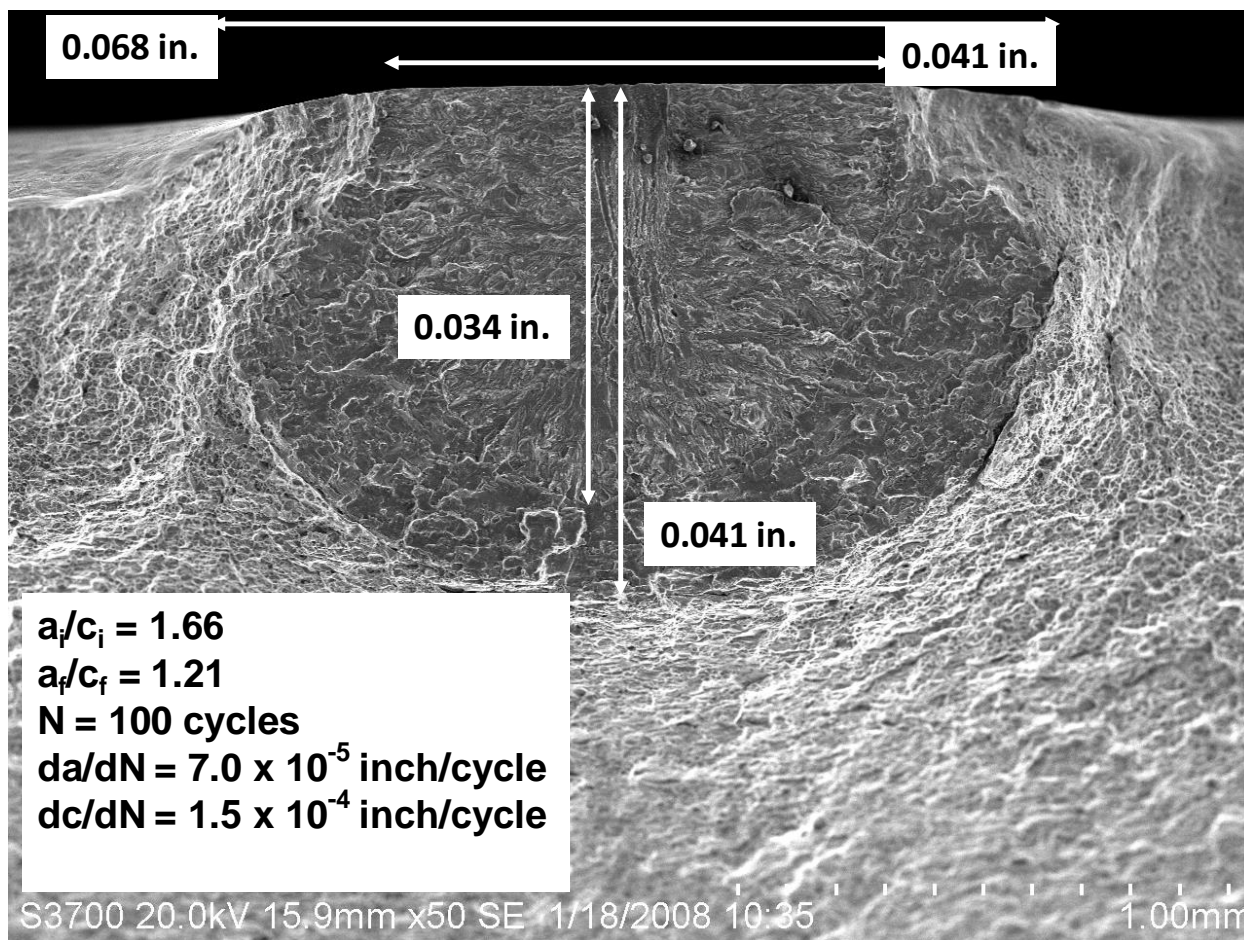


Figure B.1. SEM photograph (50x) of the fracture surface from uniaxial test UNI-125-35-01.



**NASA Engineering and Safety Center
Technical Assessment Report**

Document #:
**NESC-RP-
06-065**

Version:
1.0

Title:

**Fracture Mechanics Based Methods Development for
COPVs with Metallic Liners**

Page #:
102 of 164

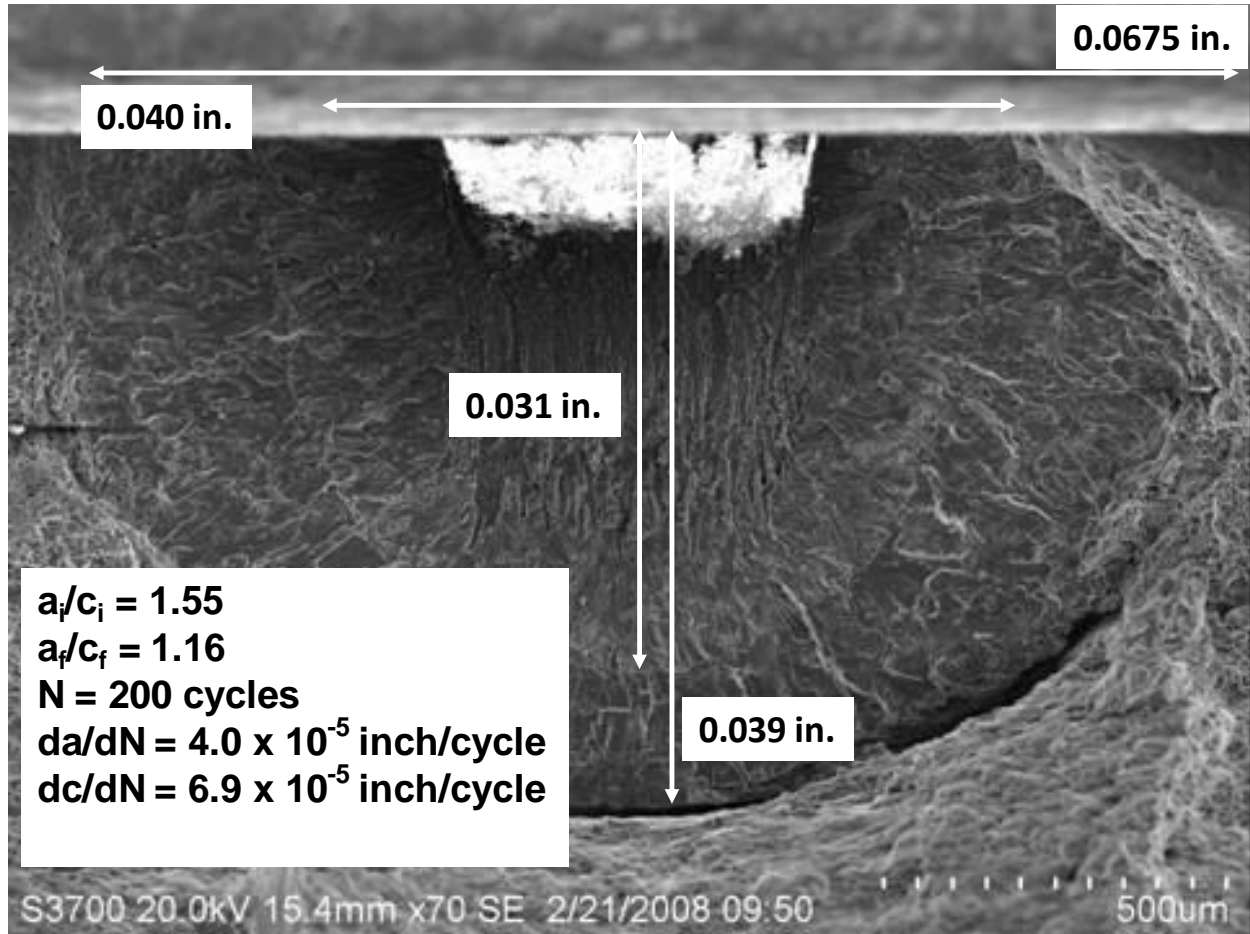


Figure B.2. SEM photograph (70x) of the fracture surface from uniaxial test UNI-125-35-02.



Title:

Fracture Mechanics Based Methods Development for
COPVs with Metallic Liners

Page #:
103 of 164

$a_i/c_i = 1.36$
 $a_f/c_f = 1.07$
 $N = 200$ cycles
 $da/dN = 9.5 \times 10^{-5}$ inch/cycle
 $dc/dN = 1.2 \times 10^{-4}$ inch/cycle

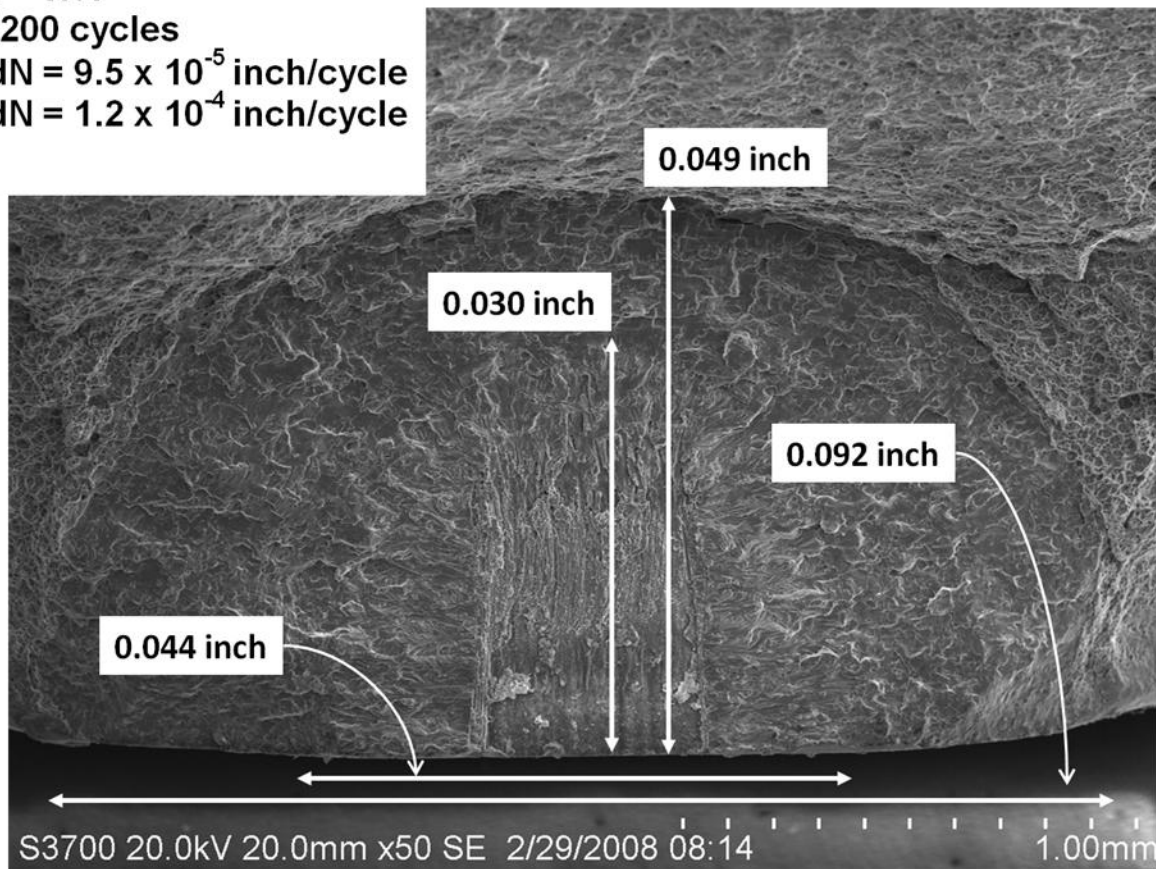


Figure B.3. SEM photograph (50x) of the fracture surface from uniaxial test UNI-125-35-03.



**NASA Engineering and Safety Center
Technical Assessment Report**

Document #:
**NESC-RP-
06-065**

Version:
1.0

Title:

**Fracture Mechanics Based Methods Development for
COPVs with Metallic Liners**

Page #:
104 of 164

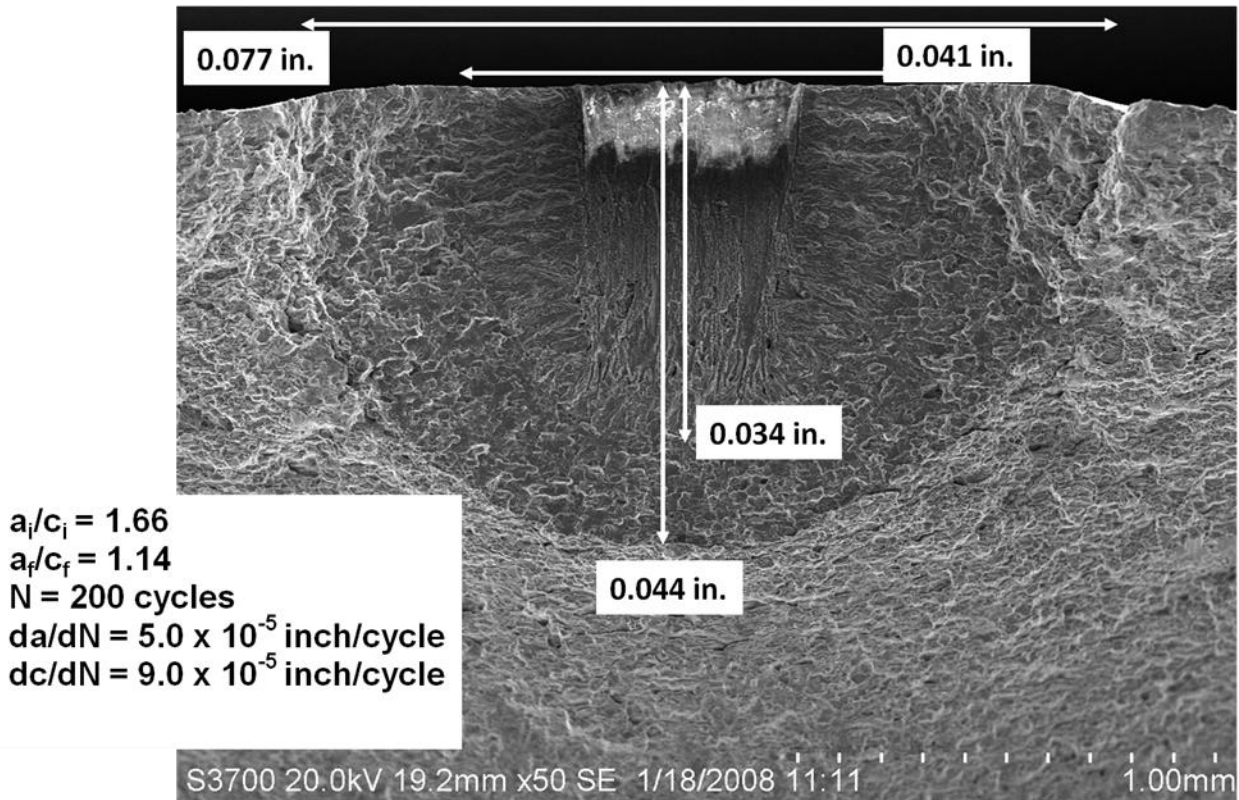


Figure B.4. SEM photograph (50x) of the fracture surface from uniaxial test UNI-090-35-01.



Title:

**Fracture Mechanics Based Methods Development for
COPVs with Metallic Liners**

Page #:
105 of 164

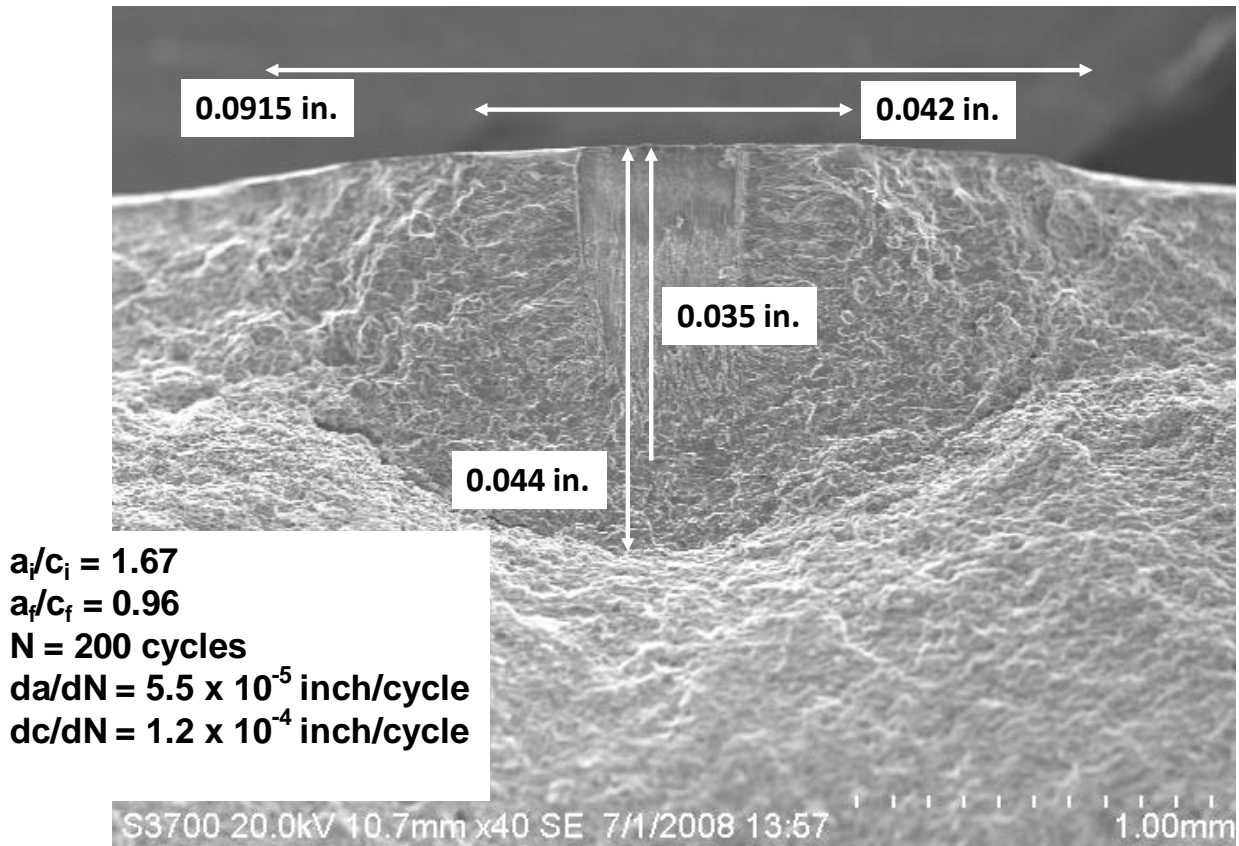


Figure B.5. SEM photograph (40x) of the fracture surface from uniaxial test UNI-090-35-02.



Title:

**Fracture Mechanics Based Methods Development for
COPVs with Metallic Liners**

Page #:
106 of 164

$a_i/c_i = 1.68$
 $a_f/c_f = 1.09$
 $N = 200$ cycles
 $da/dN = 6.0 \times 10^{-5}$ inch/cycle
 $dc/dN = 1.1 \times 10^{-4}$ inch/cycle

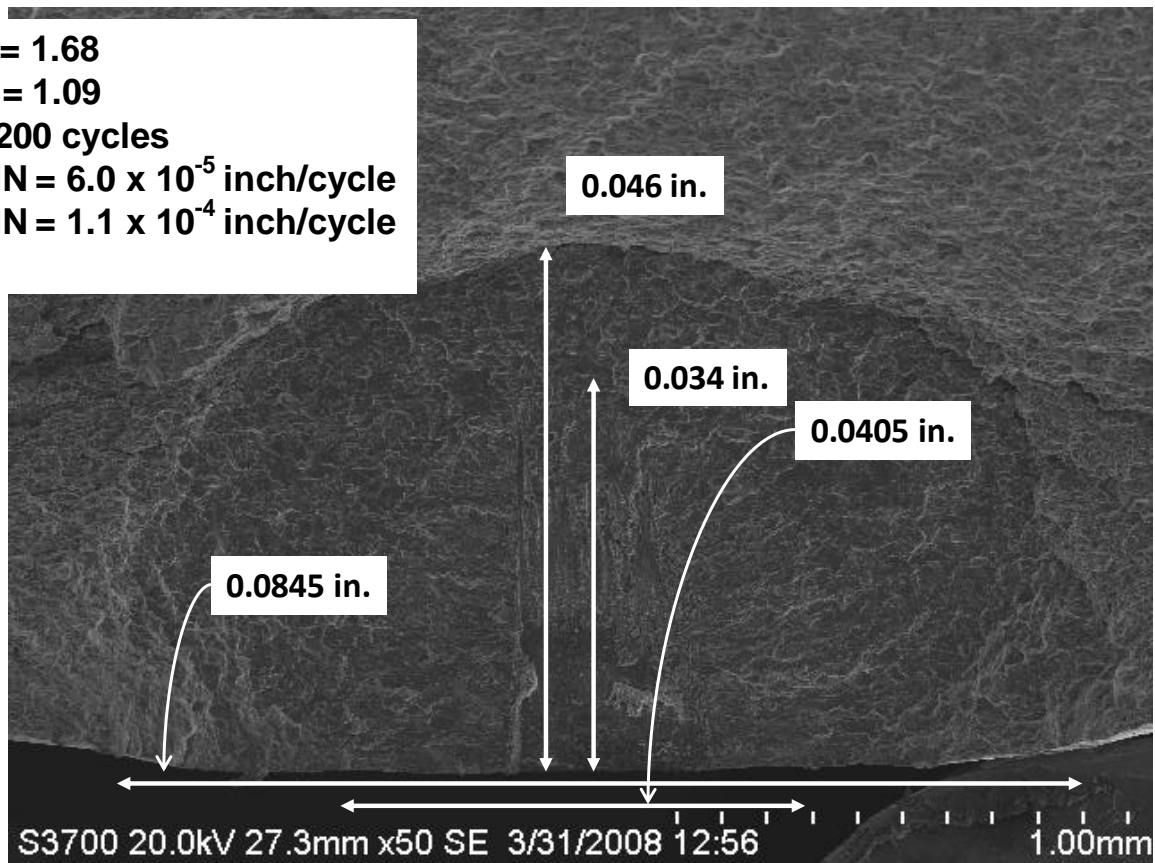


Figure B.6. SEM photograph (50x) of the fracture surface from uniaxial test UNI-090-35-03.



**NASA Engineering and Safety Center
Technical Assessment Report**

Document #:
**NESC-RP-
06-065**

Version:
1.0

Title:

**Fracture Mechanics Based Methods Development for
COPVs with Metallic Liners**

Page #:
107 of 164

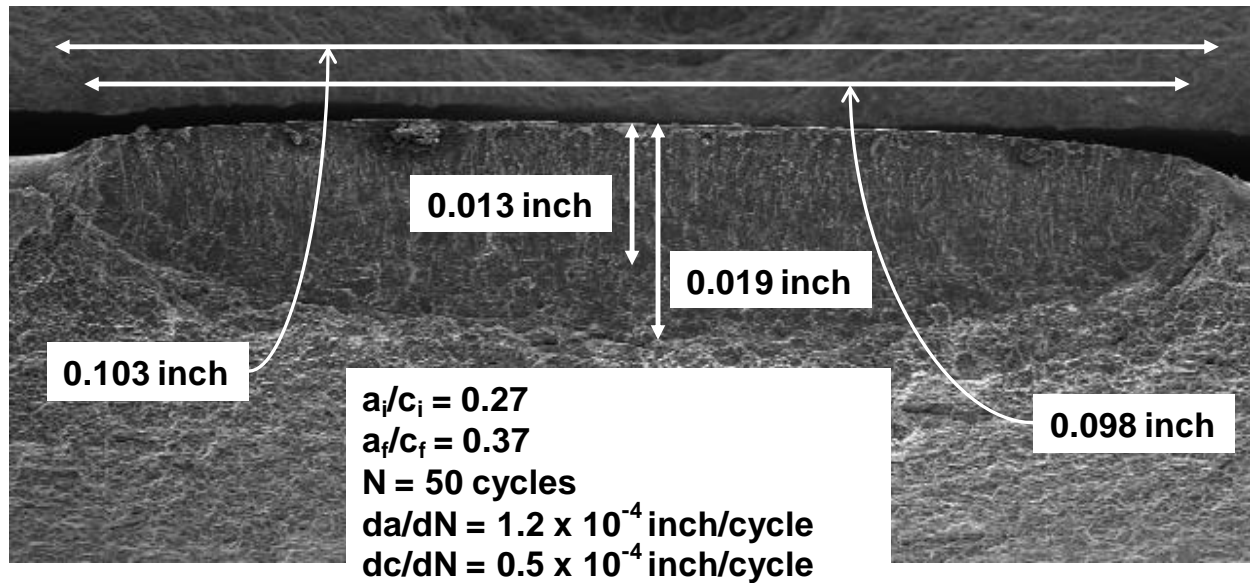


Figure B.7. SEM photograph (45x) of the fracture surface from uniaxial test UNI-090-36-01.



**NASA Engineering and Safety Center
Technical Assessment Report**

Document #:
**NESC-RP-
06-065**

Version:
1.0

Title:

**Fracture Mechanics Based Methods Development for
COPVs with Metallic Liners**

Page #:
108 of 164

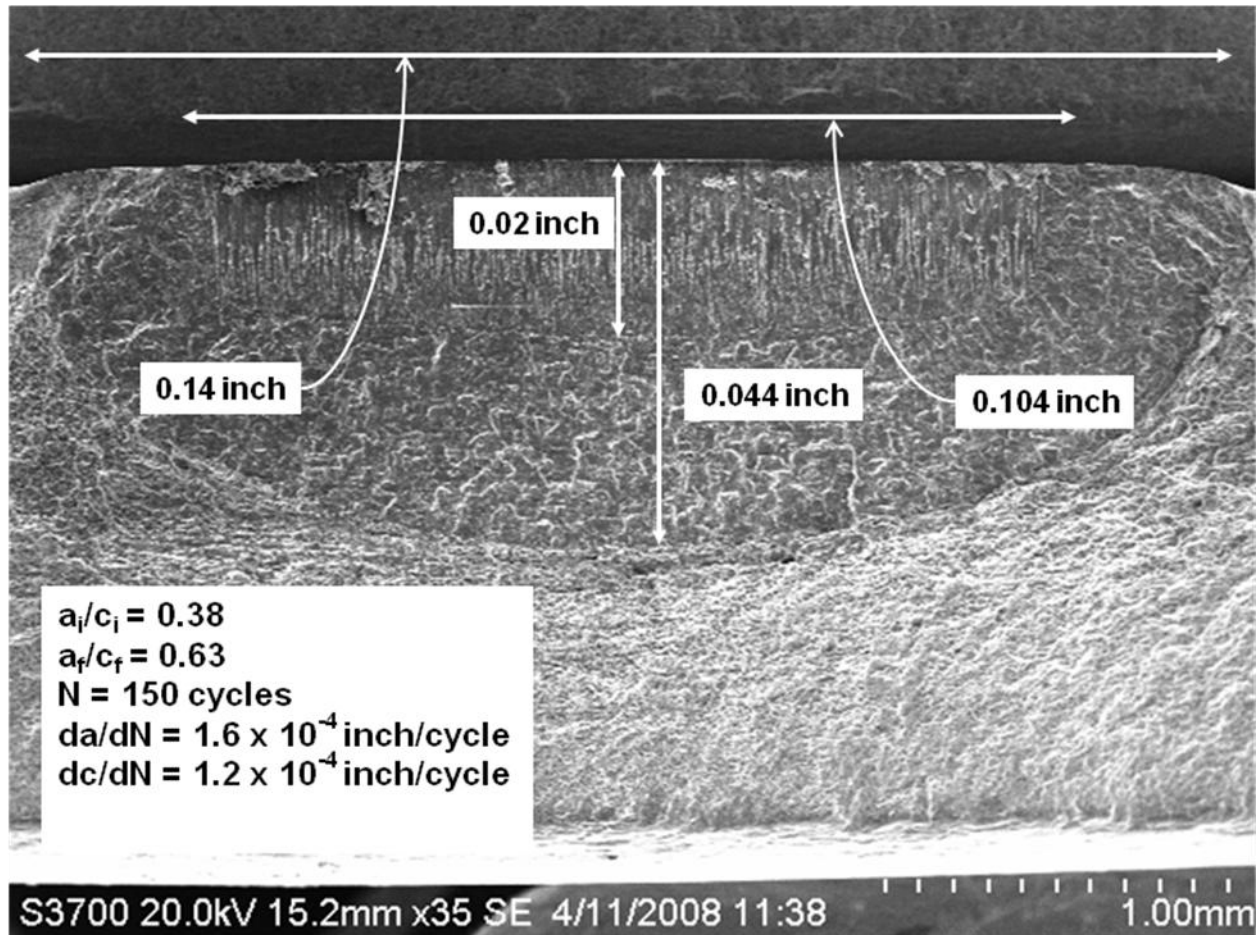


Figure B.8. SEM photograph (35x) of the fracture surface from uniaxial test UNI-090-36-02.



Title:

Fracture Mechanics Based Methods Development for
COPVs with Metallic Liners

Page #:
109 of 164

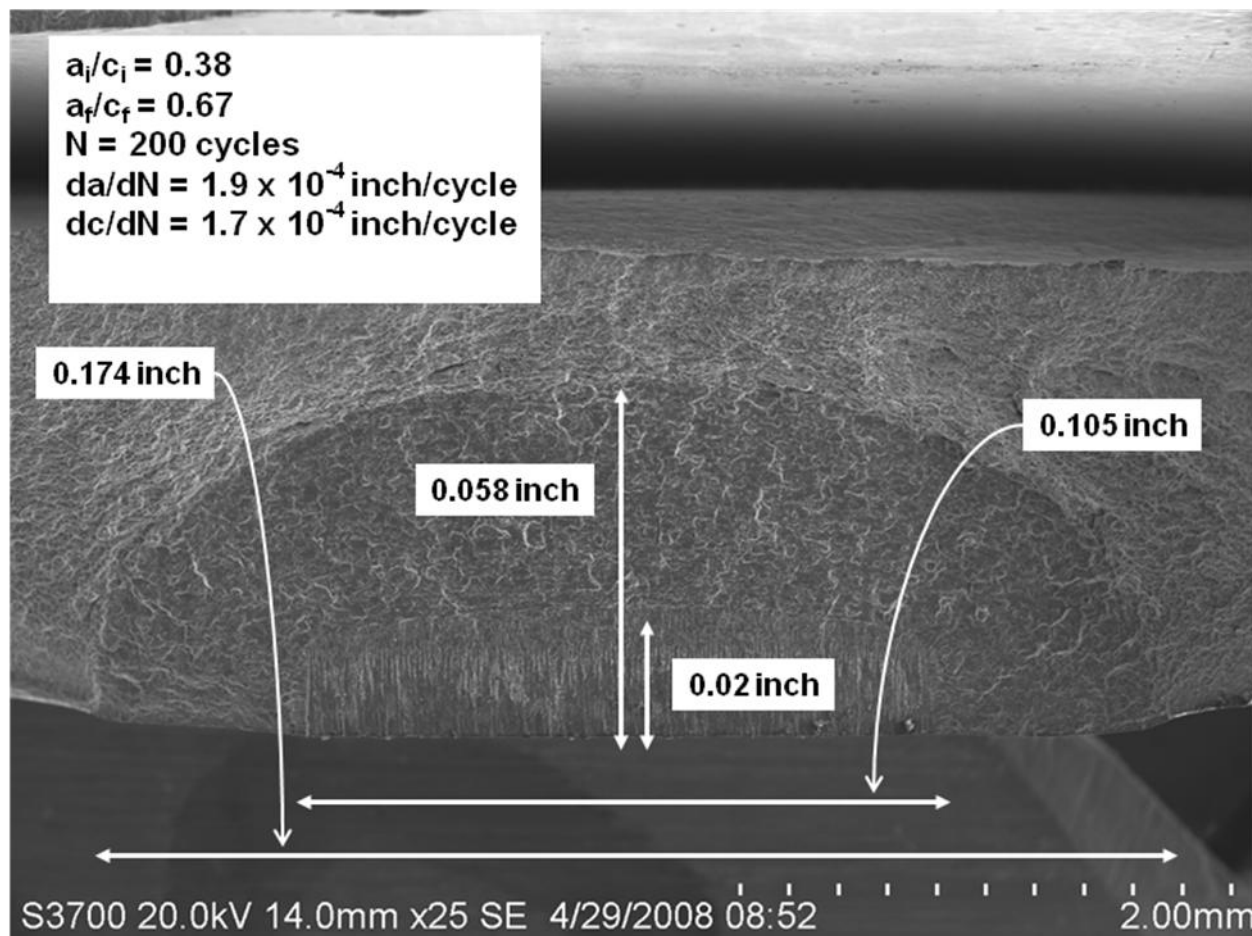


Figure B.9. SEM photograph (25x) of the fracture surface from uniaxial test UNI-090-36-04.



Title:

**Fracture Mechanics Based Methods Development for
COPVs with Metallic Liners**

Page #:
110 of 164

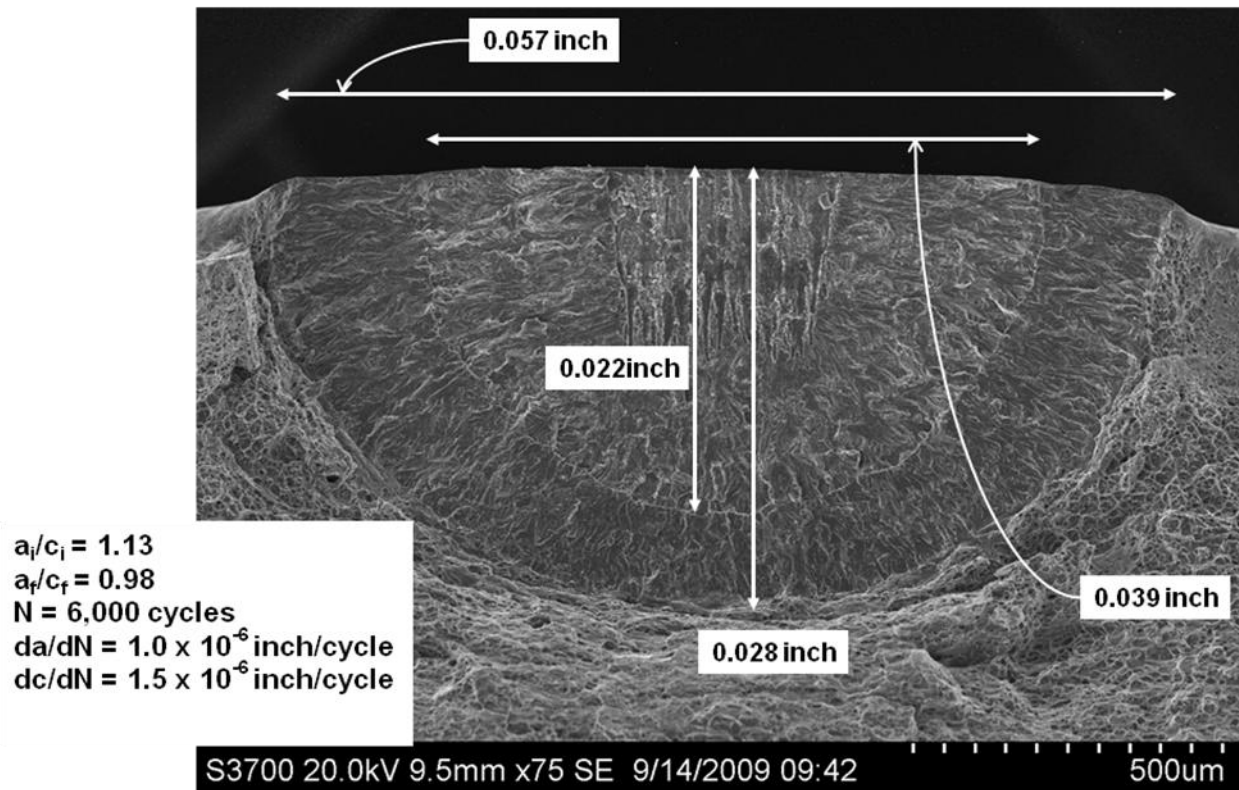


Figure B.10. SEM photograph (75x) of the fracture surface from uniaxial test UNI-090-40-06.



**NASA Engineering and Safety Center
Technical Assessment Report**

Document #:
**NESC-RP-
06-065**

Version:
1.0

Title:

**Fracture Mechanics Based Methods Development for
COPVs with Metallic Liners**

Page #:
111 of 164

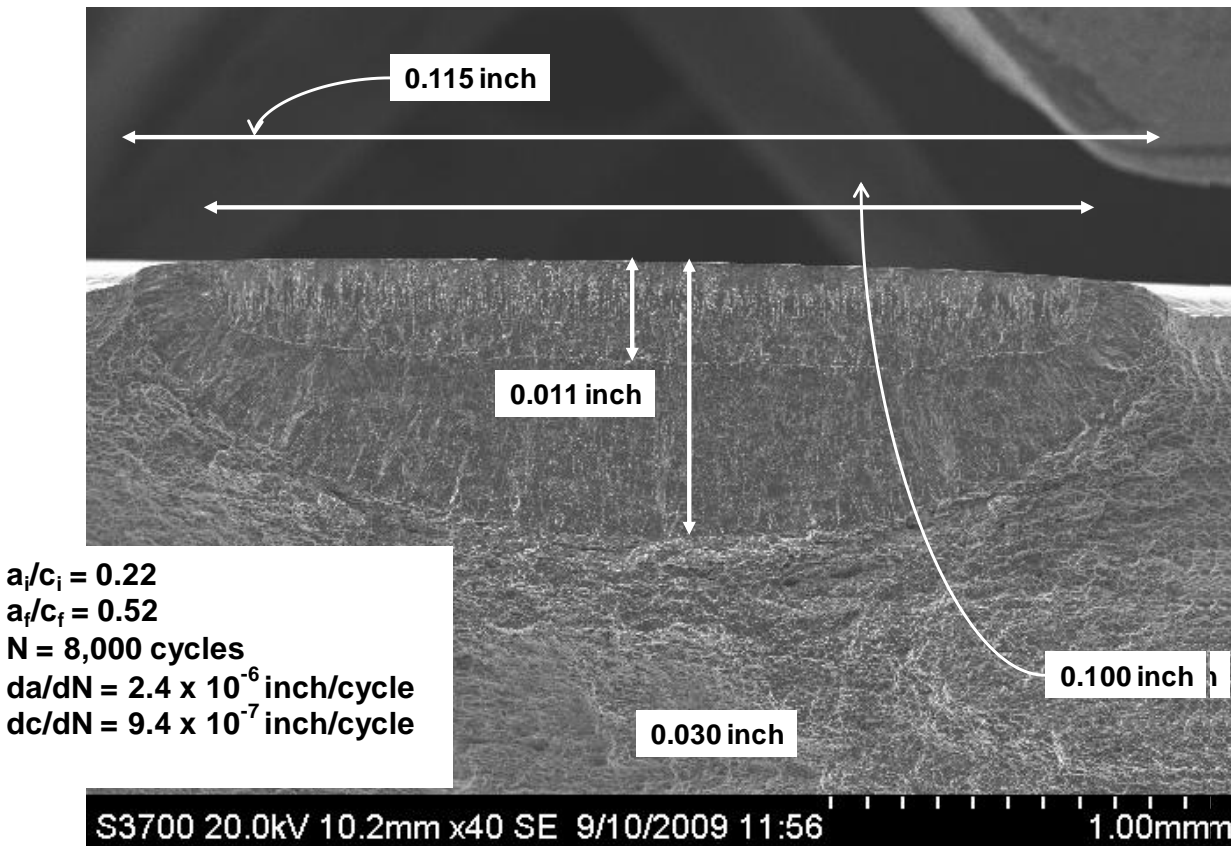


Figure B.11. SEM photograph (40x) of the fracture surface from uniaxial test UNI-090-40-07.



**NASA Engineering and Safety Center
Technical Assessment Report**

Document #:
**NESC-RP-
06-065**

Version:
1.0

Title:

**Fracture Mechanics Based Methods Development for
COPVs with Metallic Liners**

Page #:
112 of 164

$a_i/c_i = 1.30$
 $a_f/c_f = 1.10$
 $N = 200$ cycles
 $da/dN = 5.5 \times 10^{-5}$ inch/cycle
 $dc/dN = 6.8 \times 10^{-5}$ inch/cycle

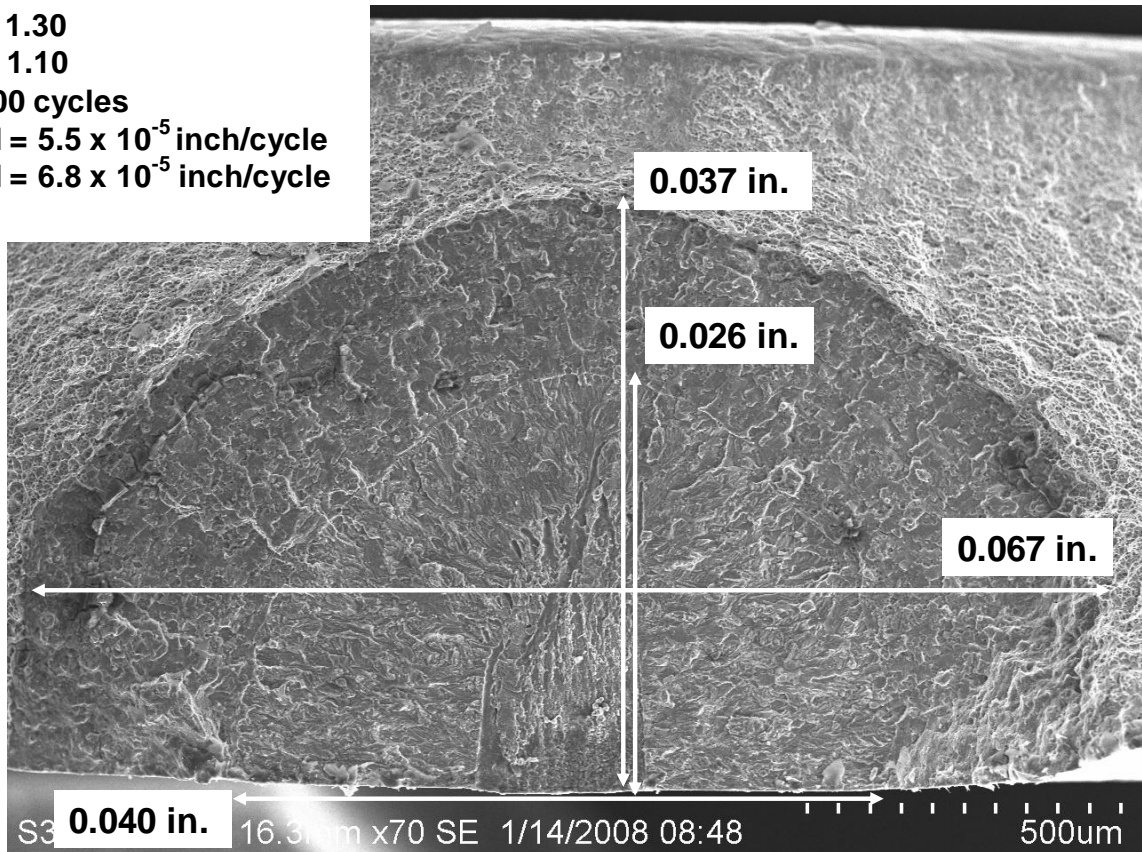


Figure B.12. SEM photograph (70x) of the fracture surface from uniaxial test UNI-050-35-01.



Title:

**Fracture Mechanics Based Methods Development for
COPVs with Metallic Liners**

Page #:
113 of 164

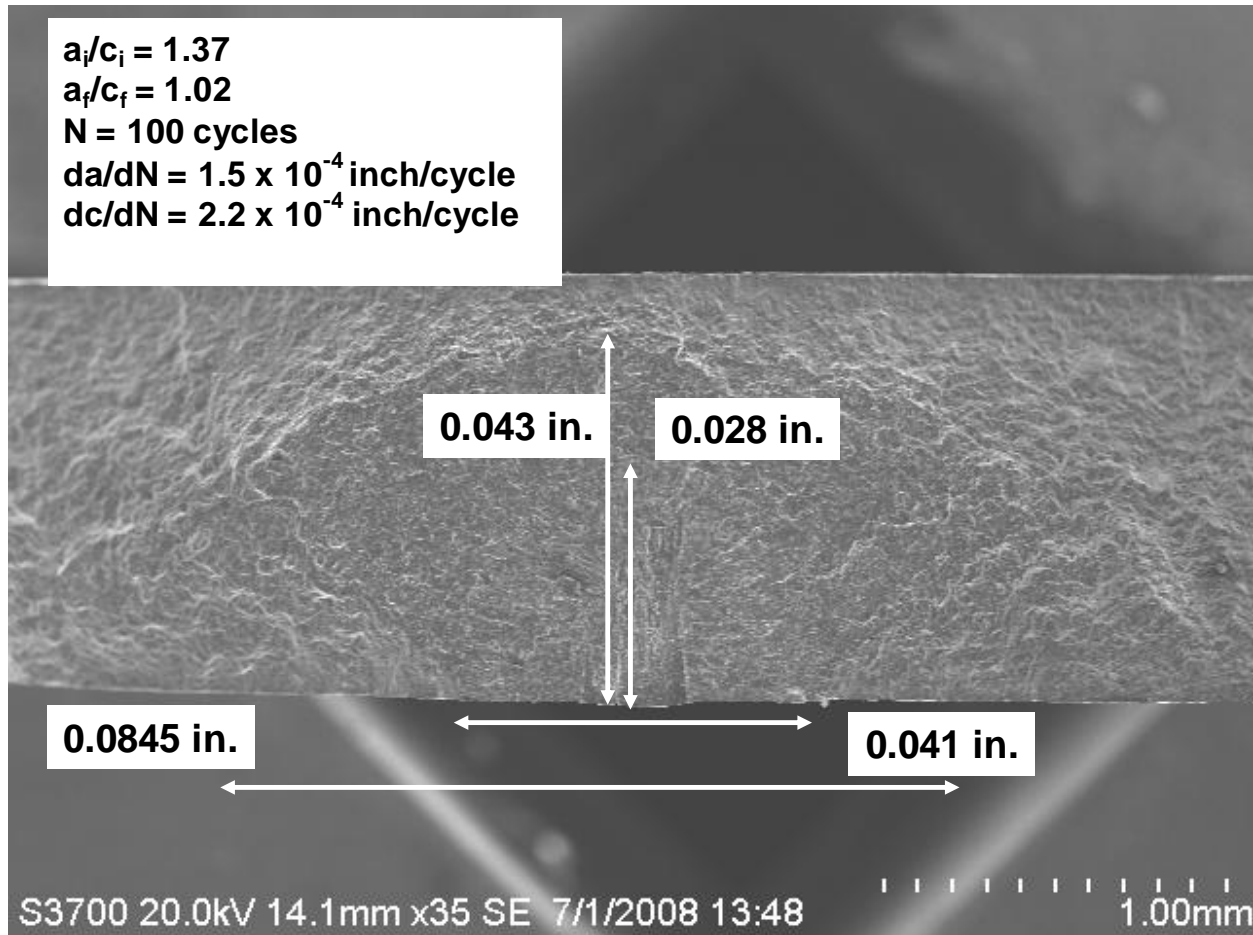


Figure B.13. SEM photograph (35x) of the fracture surface from uniaxial test UNI-050-35-04.



**NASA Engineering and Safety Center
Technical Assessment Report**

Document #:
**NESC-RP-
06-065**

Version:
1.0

Title:

**Fracture Mechanics Based Methods Development for
COPVs with Metallic Liners**

Page #:
114 of 164

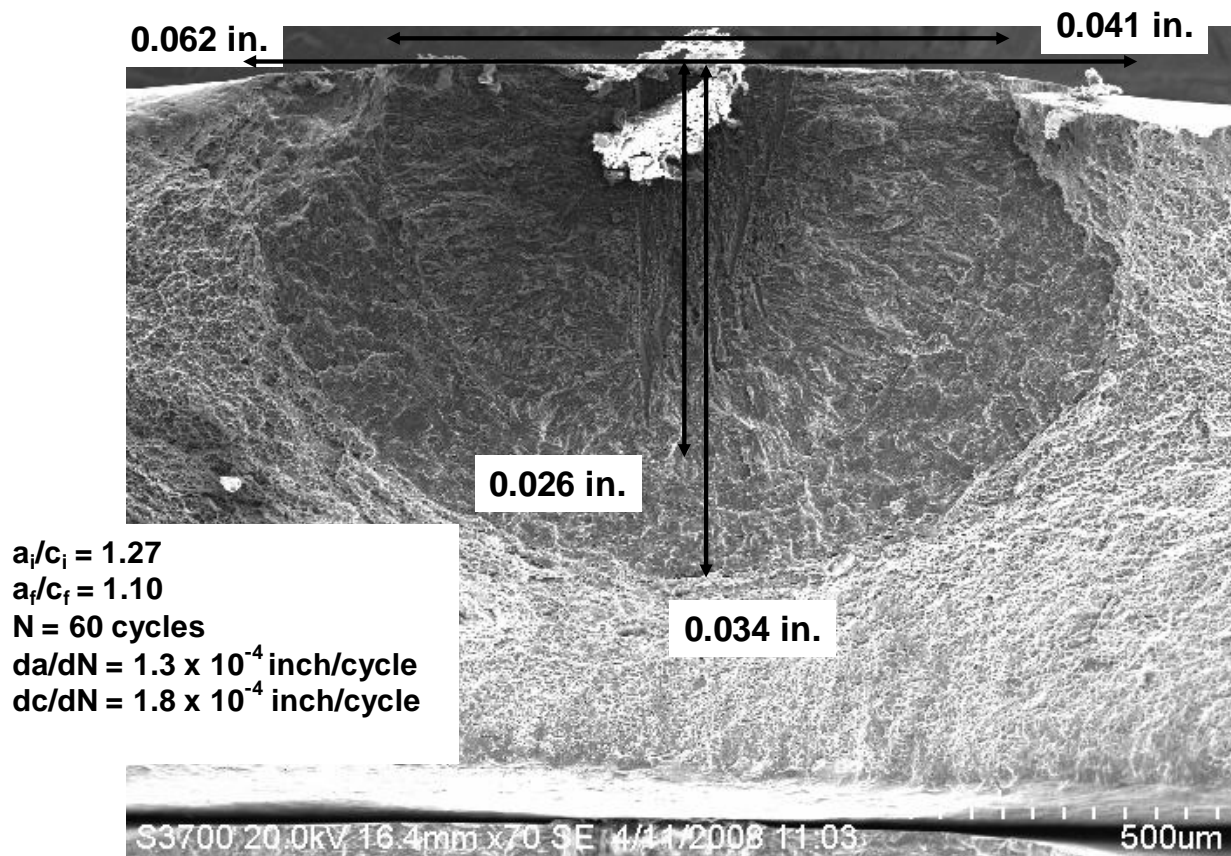


Figure B.14. SEM photograph (70x) of the fracture surface from uniaxial test UNI-050-35-05.



**NASA Engineering and Safety Center
Technical Assessment Report**

Document #:
**NESC-RP-
06-065**

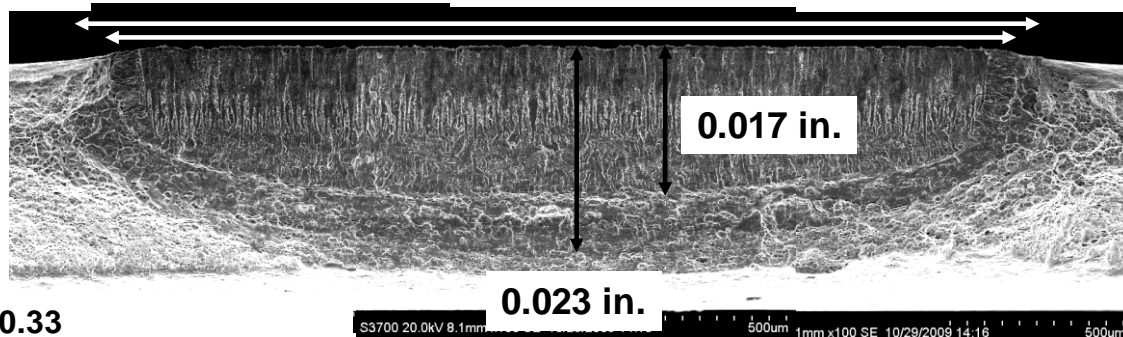
Version:
1.0

Title:

**Fracture Mechanics Based Methods Development for
COPVs with Metallic Liners**

Page #:
115 of 164

0.109 in.



$$a_i/c_i = 0.33$$

$$a_f/c_f = 0.42$$

$$N = 10 \text{ cycles}$$

$$da/dN = 6.0 \times 10^{-4} \text{ inch/cycle}$$

$$dc/dN = 3.0 \times 10^{-4} \text{ inch/cycle}$$

Figure B.15. SEM photograph (100x montage) of the fracture surface from uniaxial test UNI-032-36-05.



Title:

Fracture Mechanics Based Methods Development for
COPVs with Metallic Liners

Page #:
116 of 164

$a_i/c_i = 1.20$
 $a_f/c_f = 1.11$
 $N = 50$ cycles
 $da/dN = 4.0 \times 10^{-5}$ inch/cycle
 $dc/dN = 6.0 \times 10^{-5}$ inch/cycle

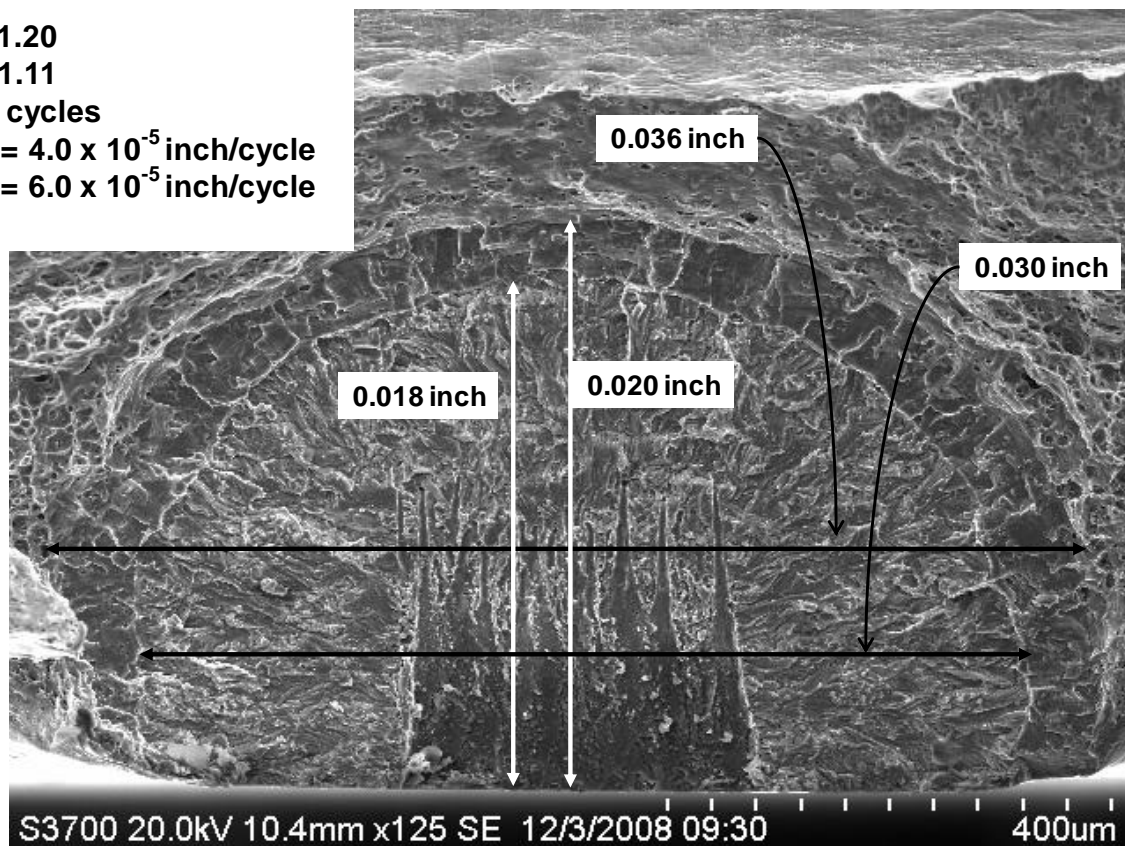


Figure B.16. SEM photograph (125x) of the fracture surface from uniaxial test UNI-032-37-03.



Title:

Fracture Mechanics Based Methods Development for
COPVs with Metallic Liners

Page #:
117 of 164

Appendix C. Fracture Surfaces from the COPV Tests

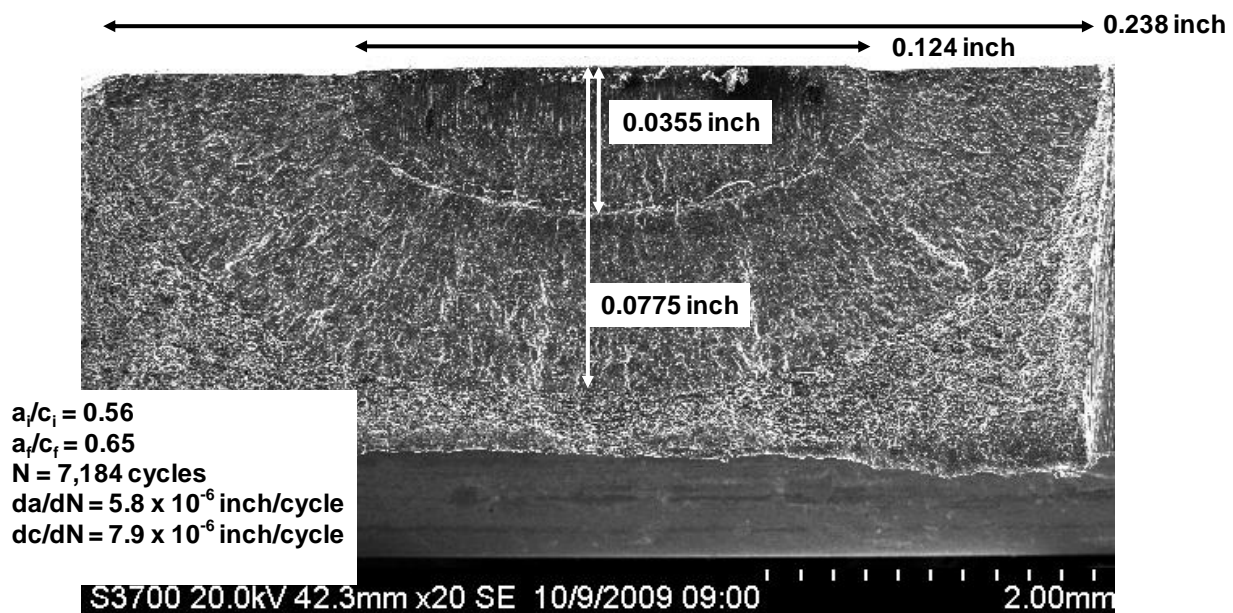


Figure C.1. SEM photograph (20x) of the fracture surface from crack #1 of COPV test 18118.



**NASA Engineering and Safety Center
Technical Assessment Report**

Document #:
**NESC-RP-
06-065**

Version:
1.0

Title:

**Fracture Mechanics Based Methods Development for
COPVs with Metallic Liners**

Page #:
118 of 164

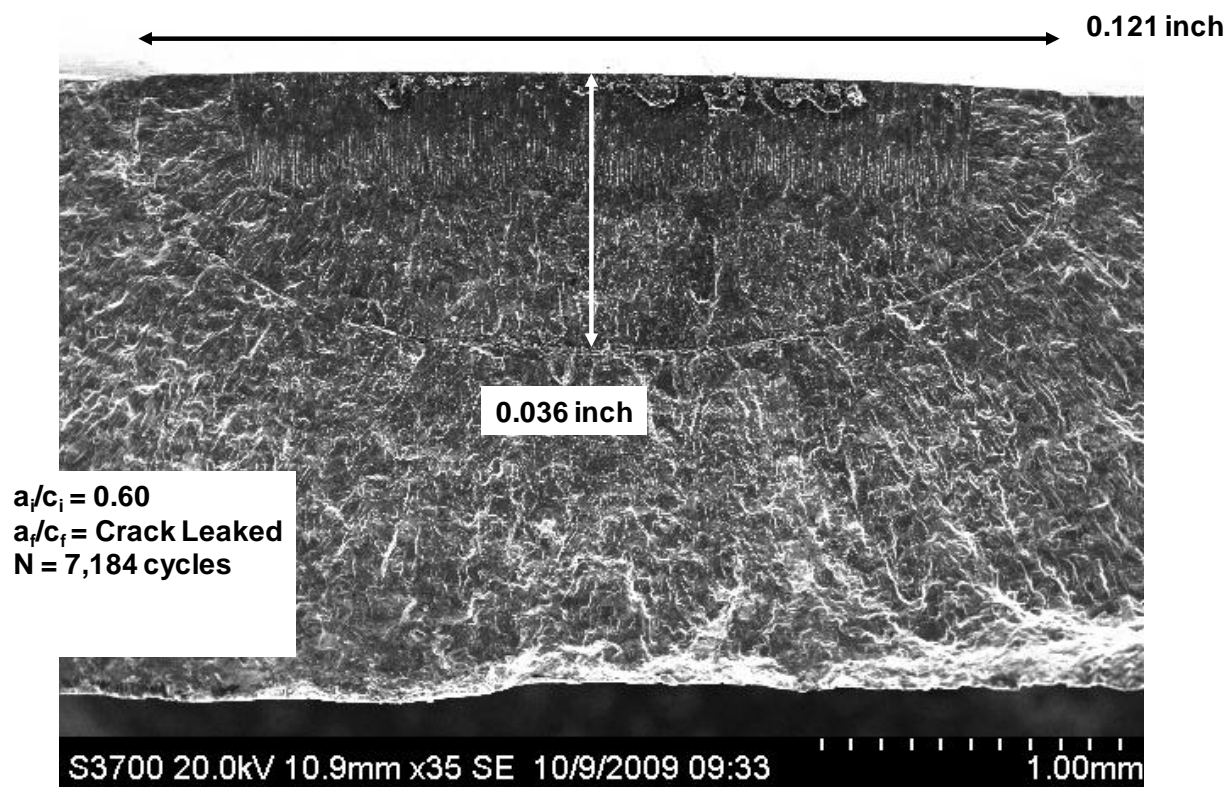


Figure C.2. SEM photograph (35x) of the fracture surface of crack #2 of COPV 18118. This cracked leaked after 7,184 fatigue cycles.



**NASA Engineering and Safety Center
Technical Assessment Report**

Document #:
**NESC-RP-
06-065**

Version:
1.0

Title:

**Fracture Mechanics Based Methods Development for
COPVs with Metallic Liners**

Page #:
119 of 164

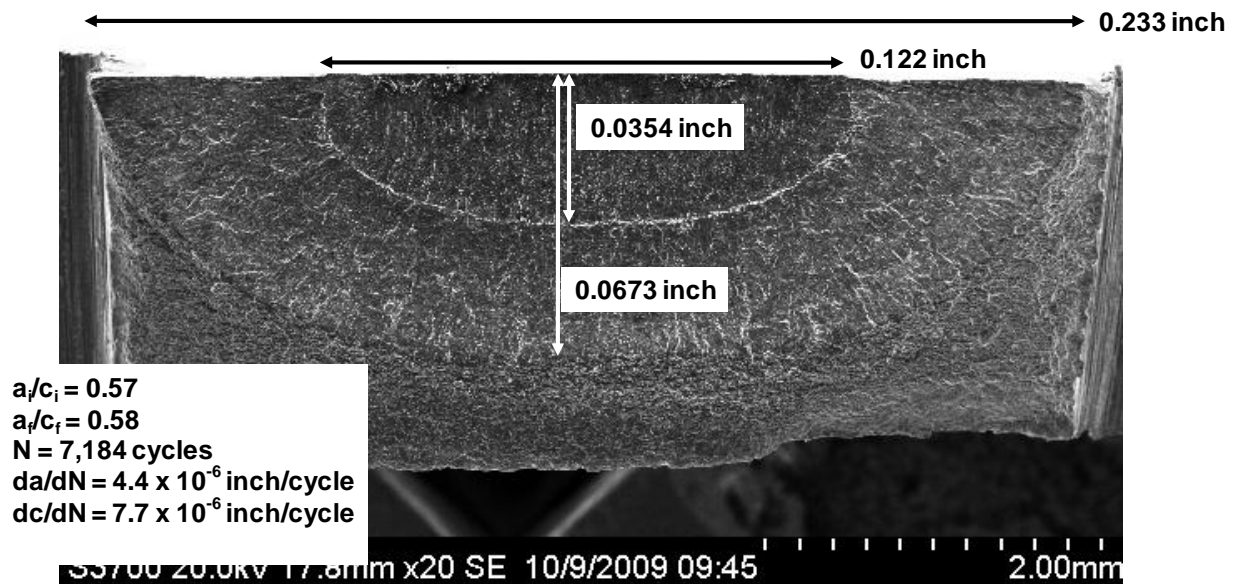


Figure C.3. SEM photograph (20x) of the fracture surface from crack #3 of COPV test 18118.



**NASA Engineering and Safety Center
Technical Assessment Report**

Document #:
**NESC-RP-
06-065**

Version:
1.0

Title:

**Fracture Mechanics Based Methods Development for
COPVs with Metallic Liners**

Page #:
120 of 164

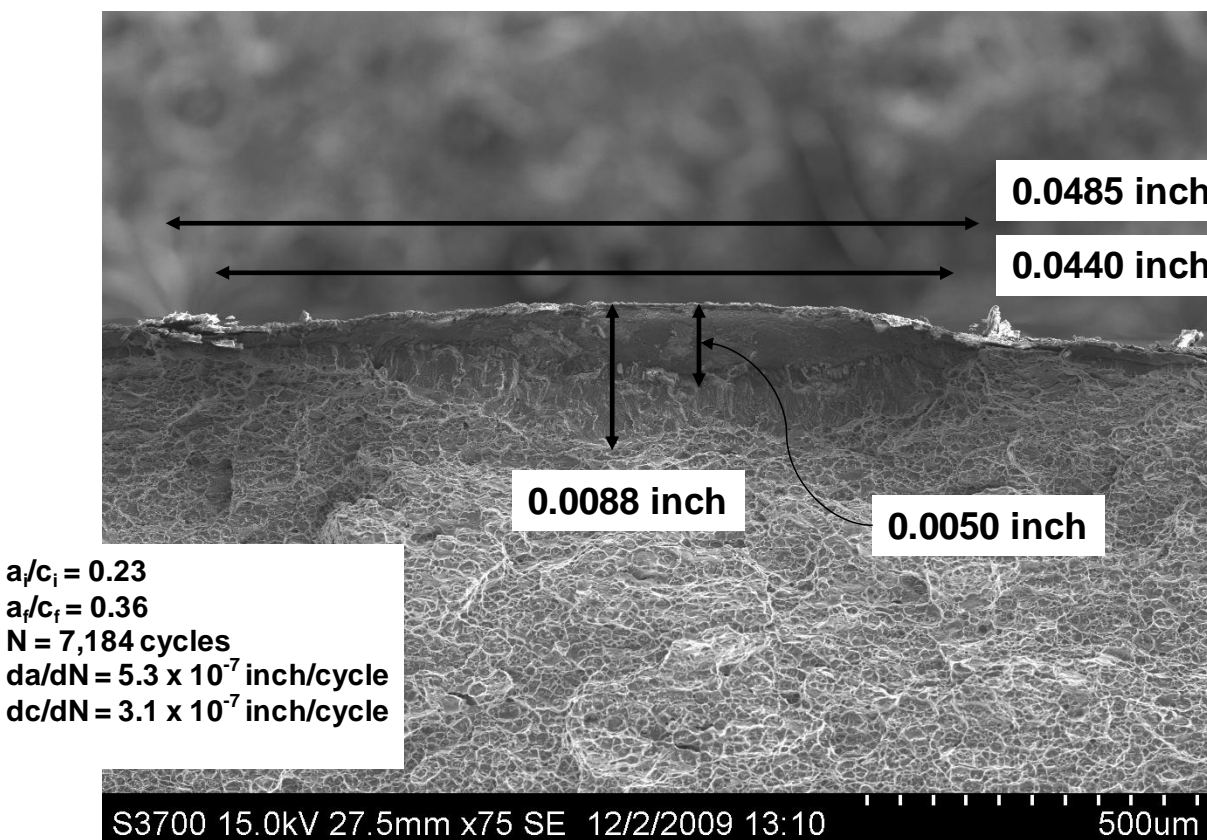


Figure C.4. SEM photograph (75x) of the fracture surface of an ID crack in COPV test 18118.



Title:

Fracture Mechanics Based Methods Development for
COPVs with Metallic Liners

Page #:
121 of 164

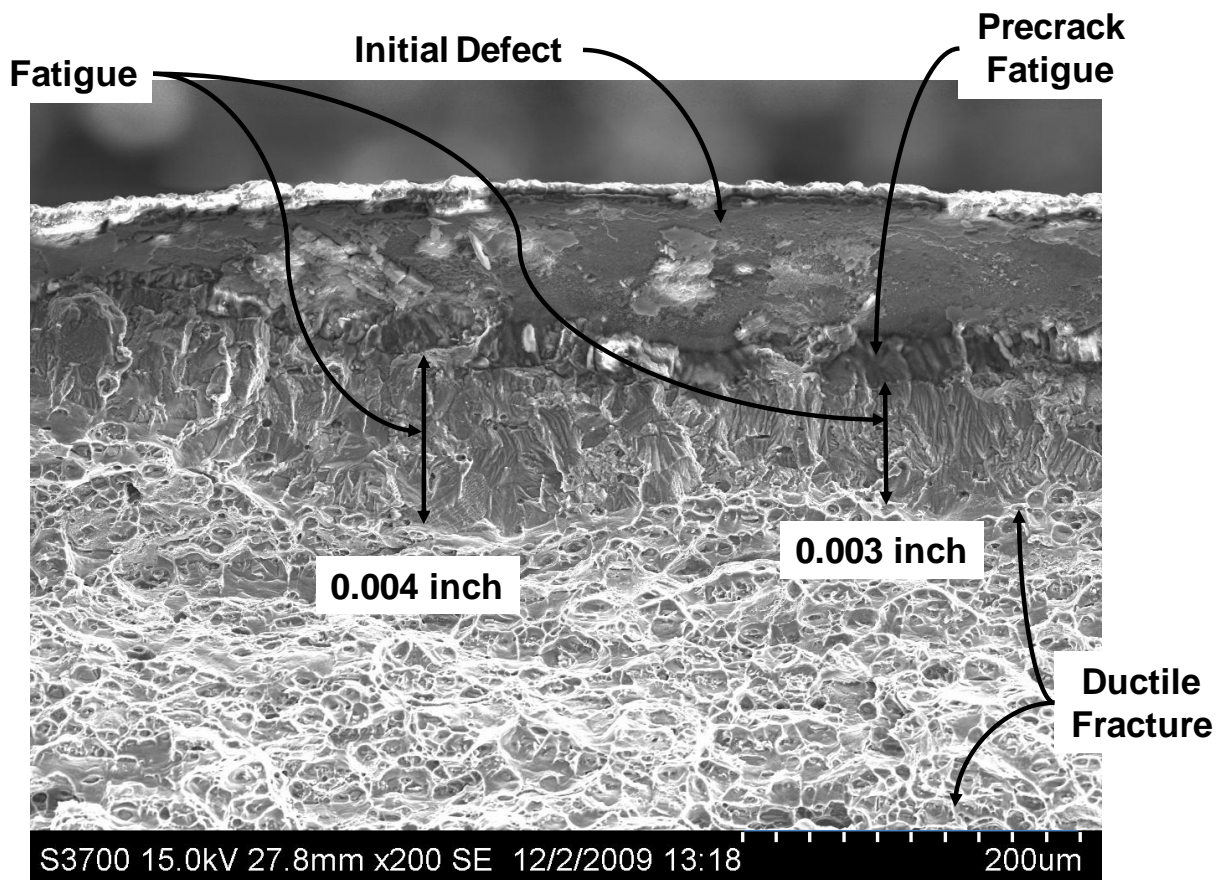


Figure C.5. SEM photograph (200x) of the fracture surface details for the ID crack in COPV test 18118.



**NASA Engineering and Safety Center
Technical Assessment Report**

Document #:
**NESC-RP-
06-065**

Version:
1.0

Title:

**Fracture Mechanics Based Methods Development for
COPVs with Metallic Liners**

Page #:
122 of 164

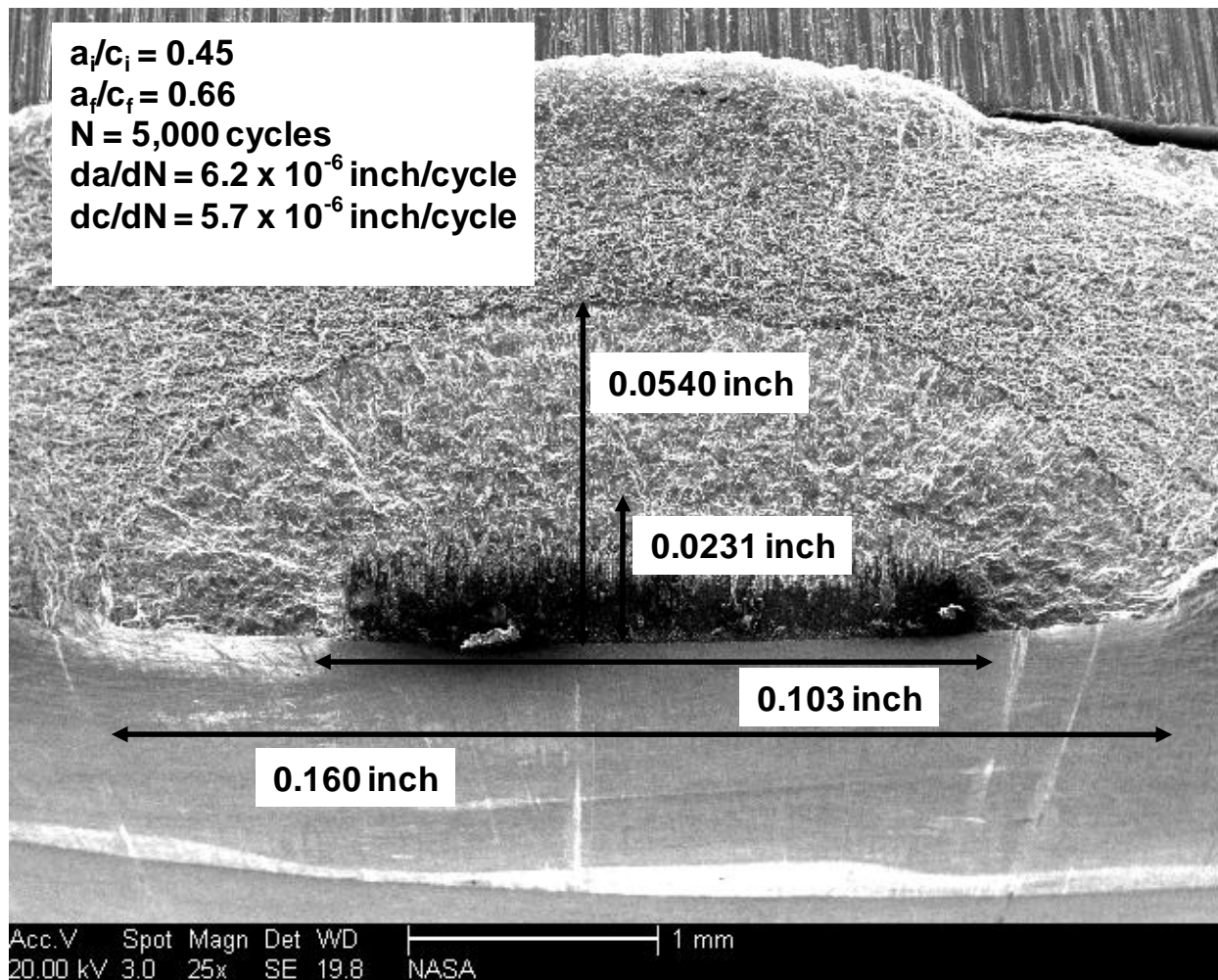


Figure C.6. SEM photograph (25x) of the fracture surface from crack #1 of COPV test 18117.



**NASA Engineering and Safety Center
Technical Assessment Report**

Document #:
**NESC-RP-
06-065**

Version:
1.0

Title:

**Fracture Mechanics Based Methods Development for
COPVs with Metallic Liners**

Page #:
123 of 164

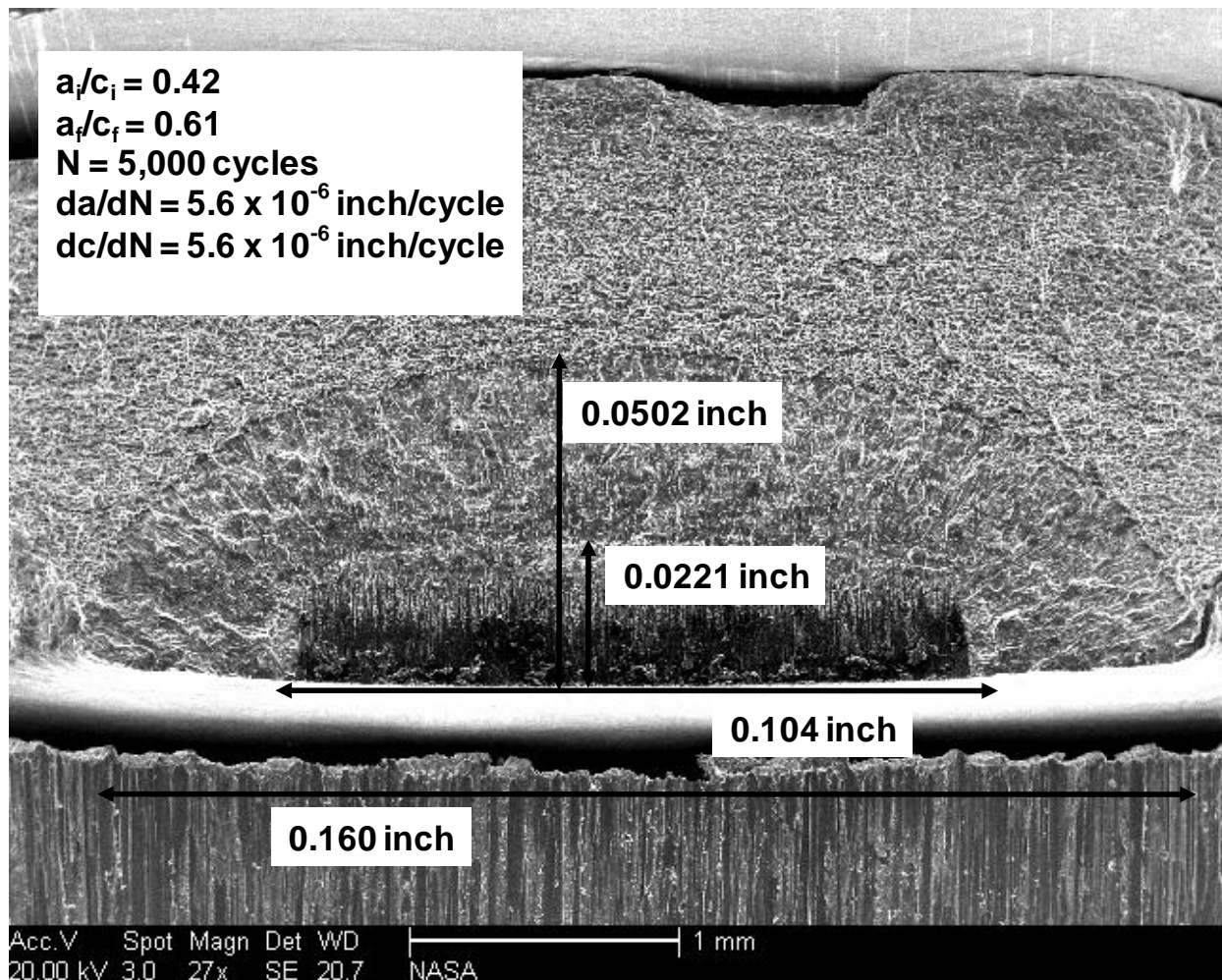


Figure C.7. SEM photograph (27x) of the fracture surface from crack #2 of COPV test 18117.



**NASA Engineering and Safety Center
Technical Assessment Report**

Document #:
**NESC-RP-
06-065**

Version:
1.0

Title:

**Fracture Mechanics Based Methods Development for
COPVs with Metallic Liners**

Page #:
124 of 164

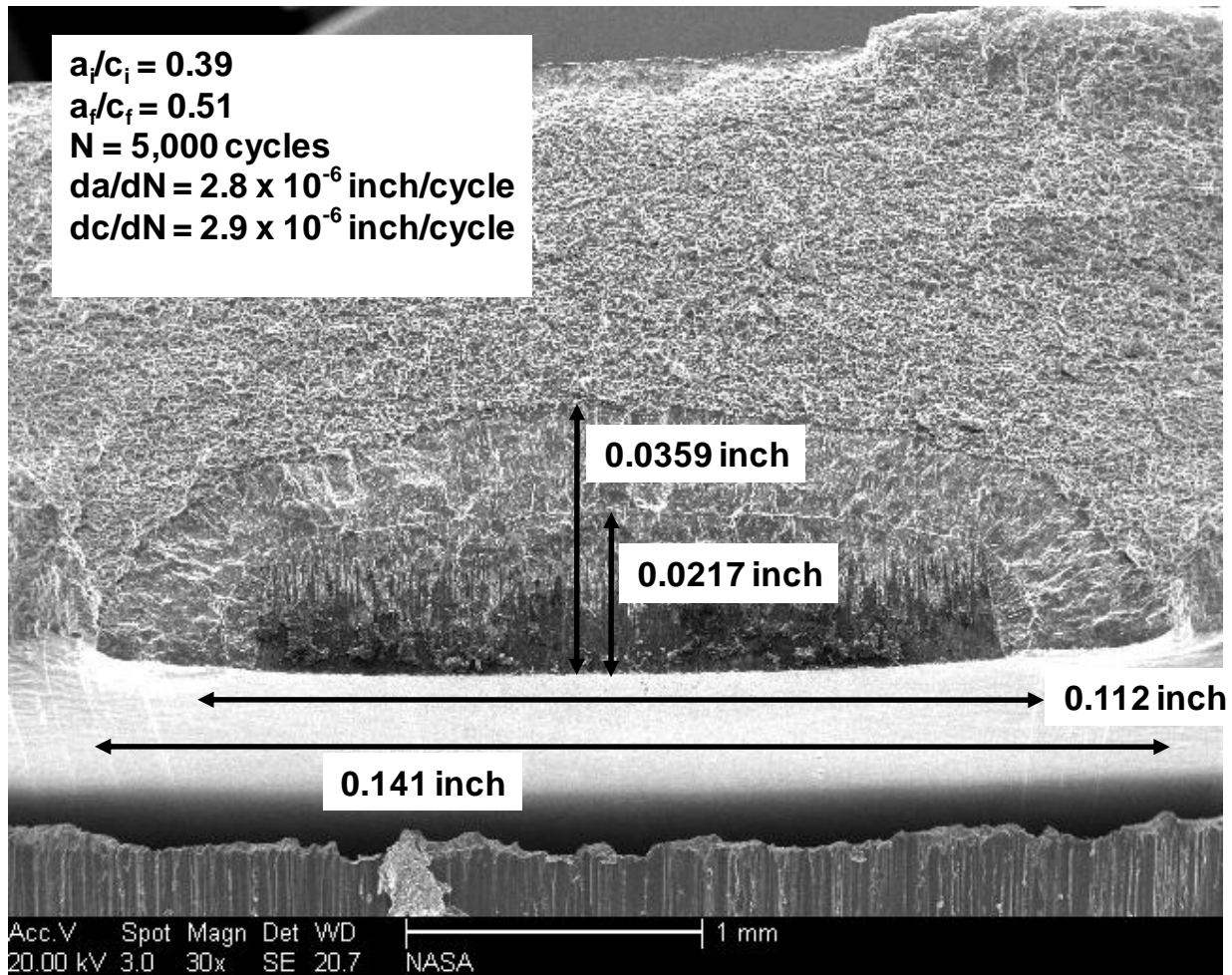


Figure C.8. SEM photograph (30x) of the fracture surface from crack #3 of COPV test 18117.



**NASA Engineering and Safety Center
Technical Assessment Report**

Document #:
**NESC-RP-
06-065**

Version:
1.0

Title:

**Fracture Mechanics Based Methods Development for
COPVs with Metallic Liners**

Page #:
125 of 164

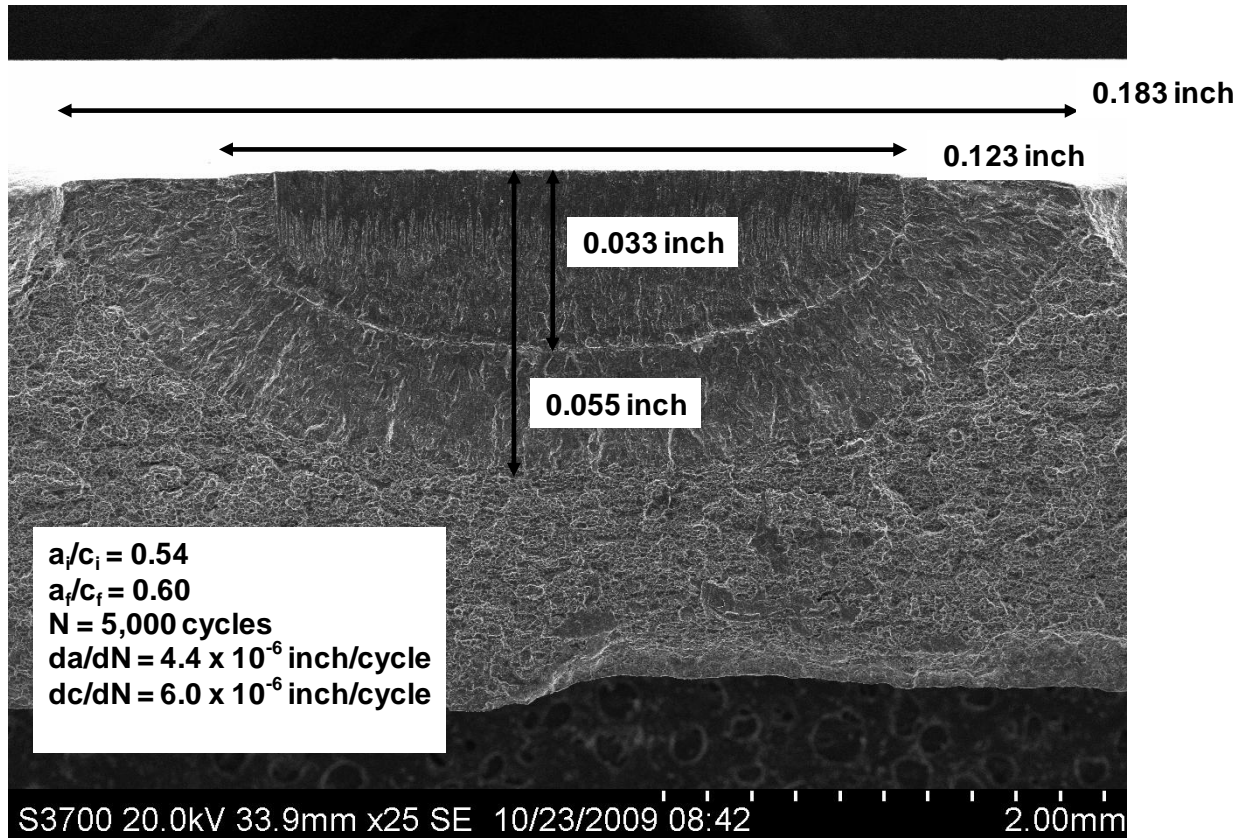


Figure C.9. SEM photograph (25x) of the fracture surface from crack #1 of COPV test 18107.



**NASA Engineering and Safety Center
Technical Assessment Report**

Document #:
**NESC-RP-
06-065**

Version:
1.0

Title:

**Fracture Mechanics Based Methods Development for
COPVs with Metallic Liners**

Page #:
126 of 164

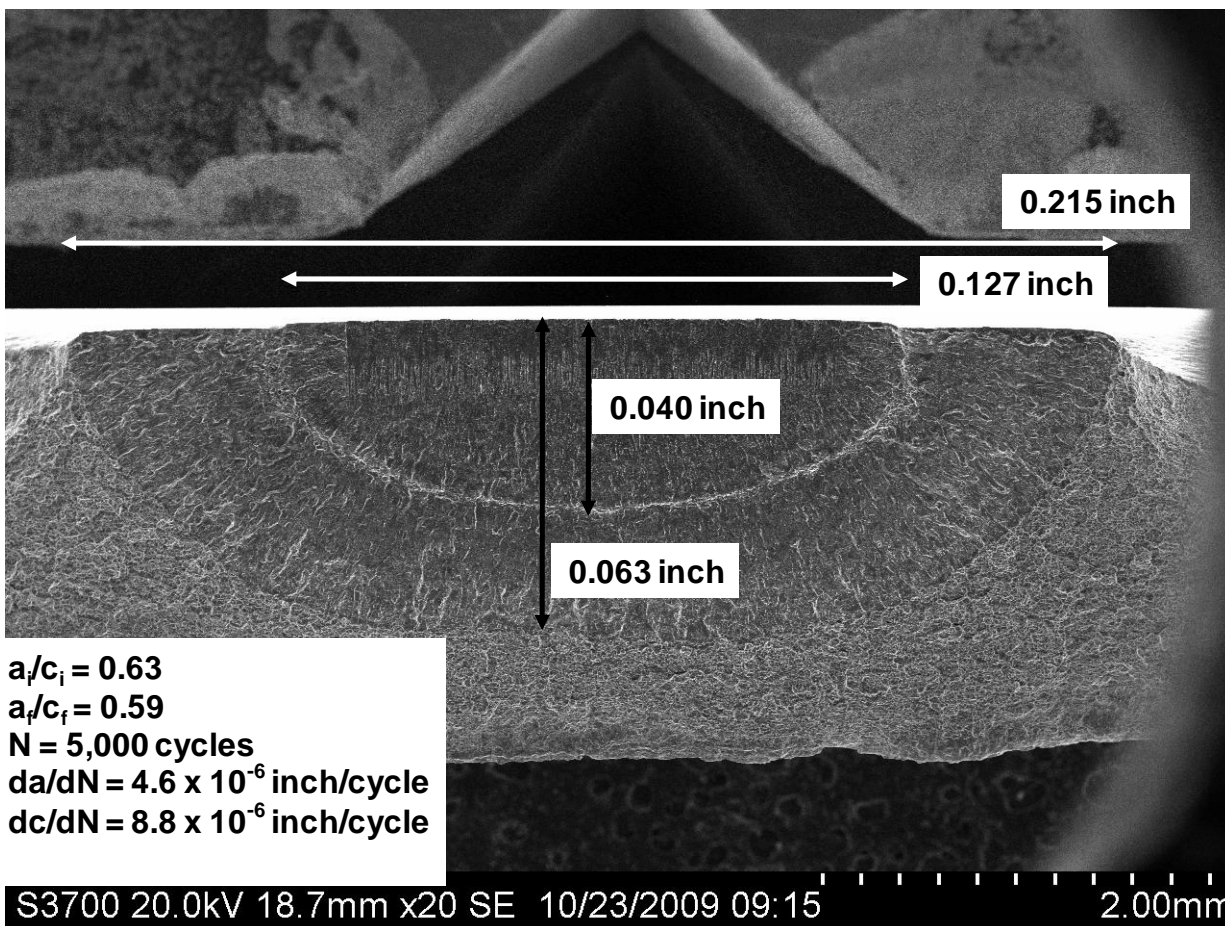


Figure C.10. SEM photograph (20x) of the fracture surface from crack #2 of COPV test 18107.



Title:

Fracture Mechanics Based Methods Development for
COPVs with Metallic Liners

Page #:
127 of 164

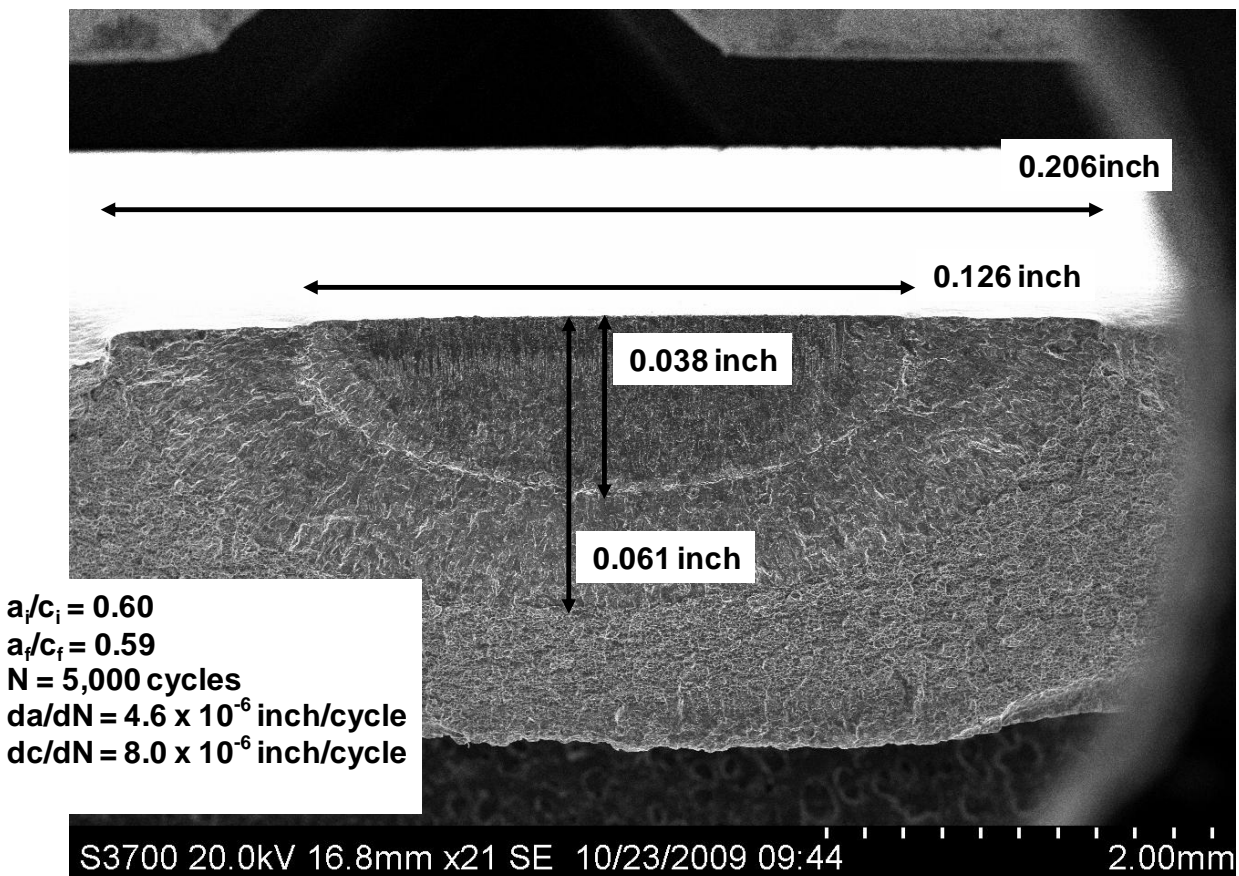


Figure C.11. SEM photograph (21x) of the fracture surface from crack #3 of COPV test 18107.



Title:

**Fracture Mechanics Based Methods Development for
COPVs with Metallic Liners**

Page #:
128 of 164

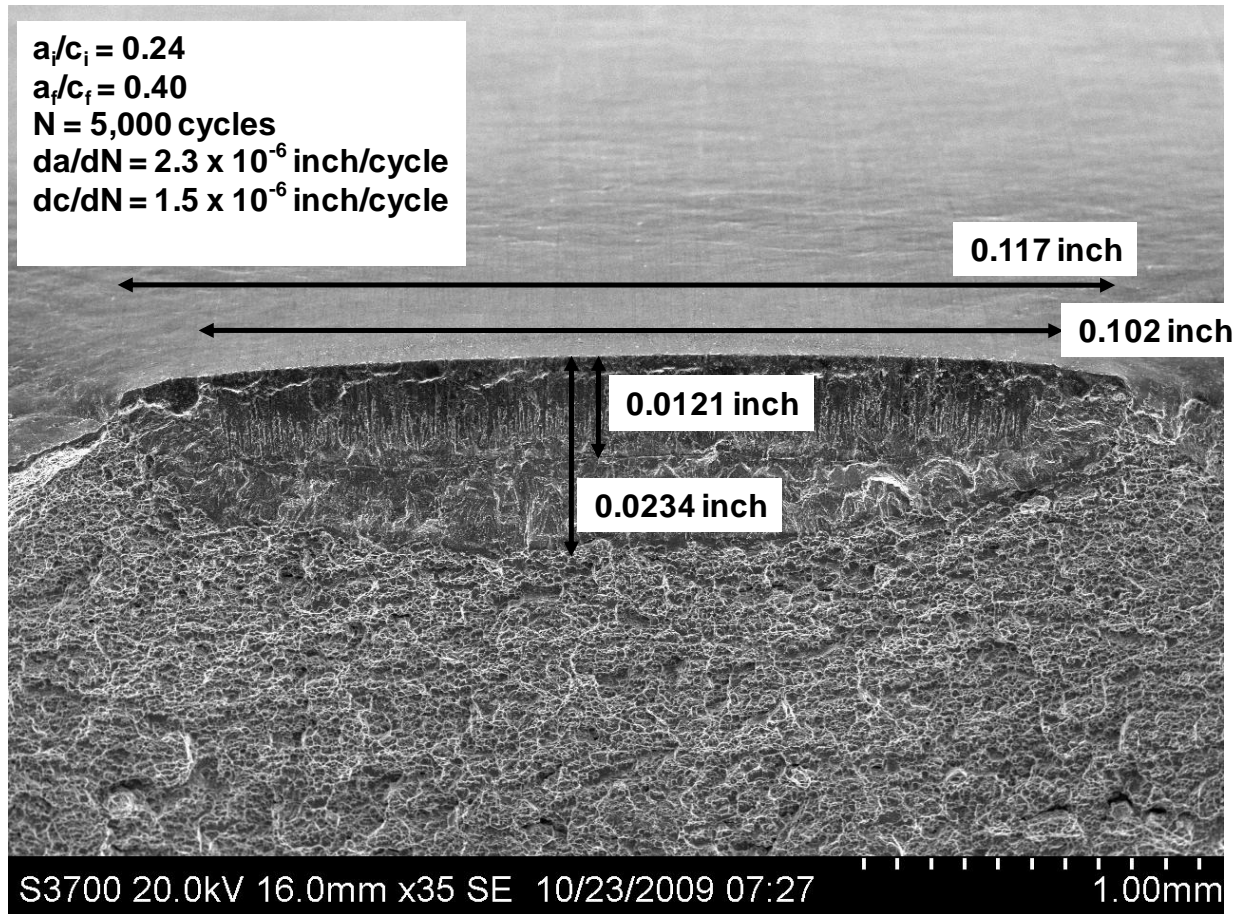


Figure C.12. SEM photograph (35x) of the fracture surface from crack #1 of COPV test 18105.



**NASA Engineering and Safety Center
Technical Assessment Report**

Document #:
**NESC-RP-
06-065**

Version:
1.0

Title:

**Fracture Mechanics Based Methods Development for
COPVs with Metallic Liners**

Page #:
129 of 164

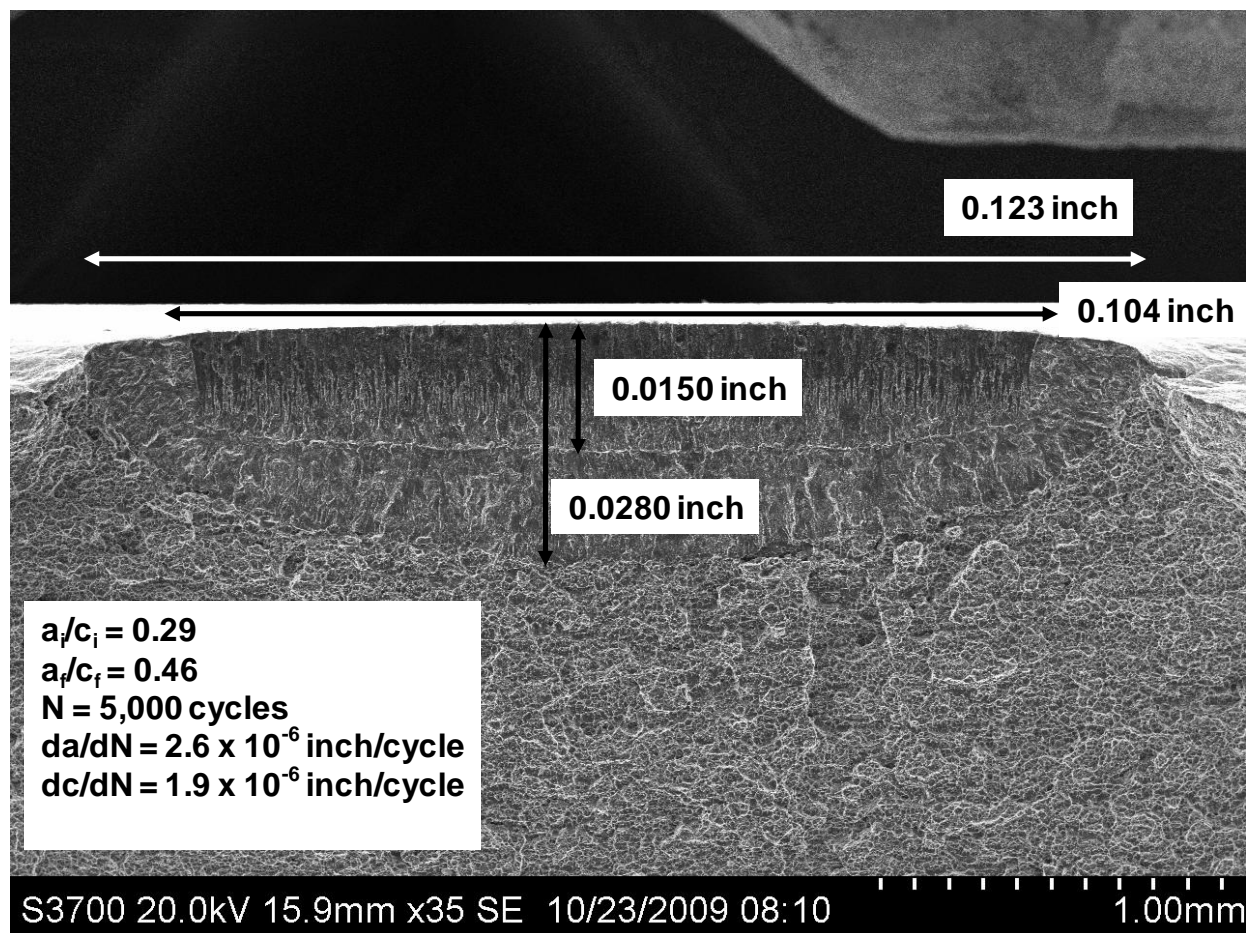


Figure C.13. SEM photograph (35x) of the fracture surface from crack #2 of COPV test 18105.



**NASA Engineering and Safety Center
Technical Assessment Report**

Document #:
**NESC-RP-
06-065**

Version:
1.0

Title:

**Fracture Mechanics Based Methods Development for
COPVs with Metallic Liners**

Page #:
130 of 164

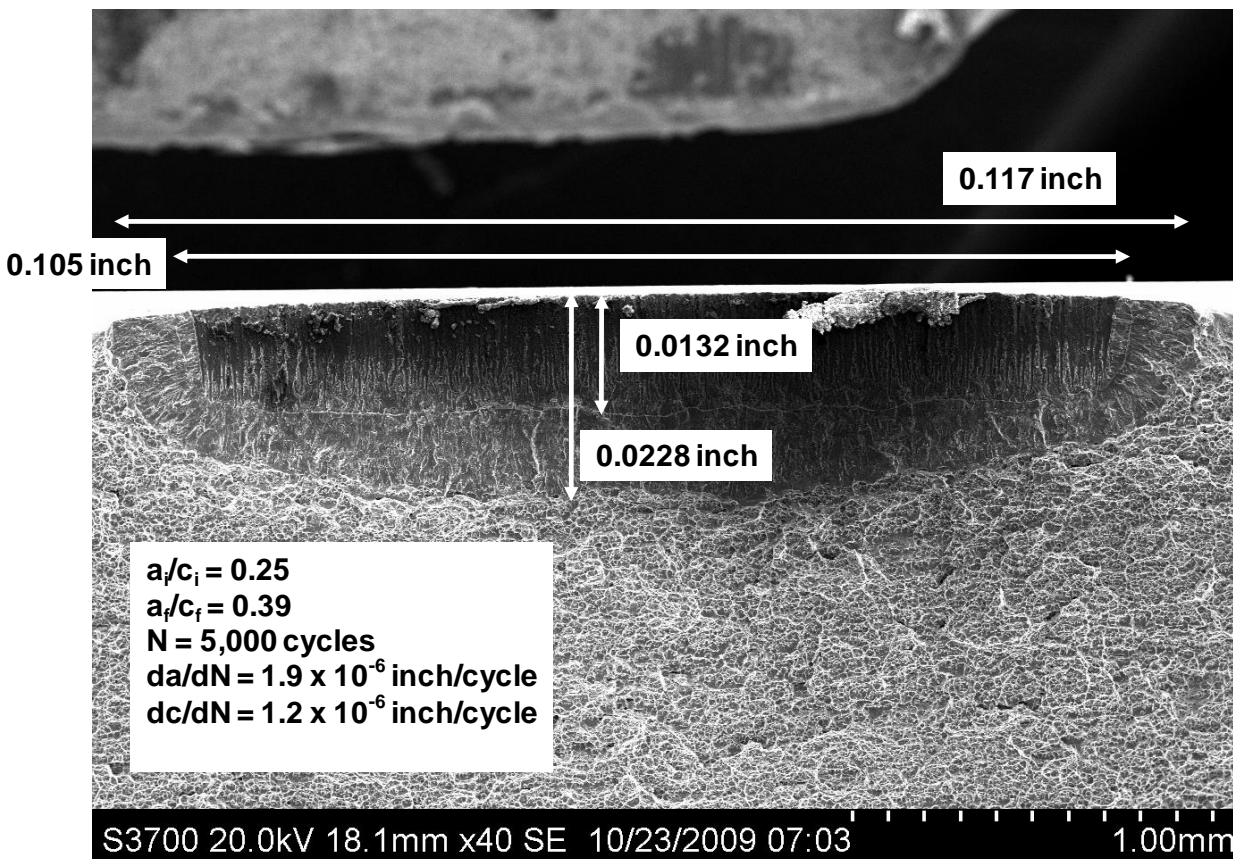


Figure C.14. SEM photograph (40x) of the fracture surface from crack #3 of COPV test 18105.



Title:

Fracture Mechanics Based Methods Development for
COPVs with Metallic Liners

Page #:
131 of 164

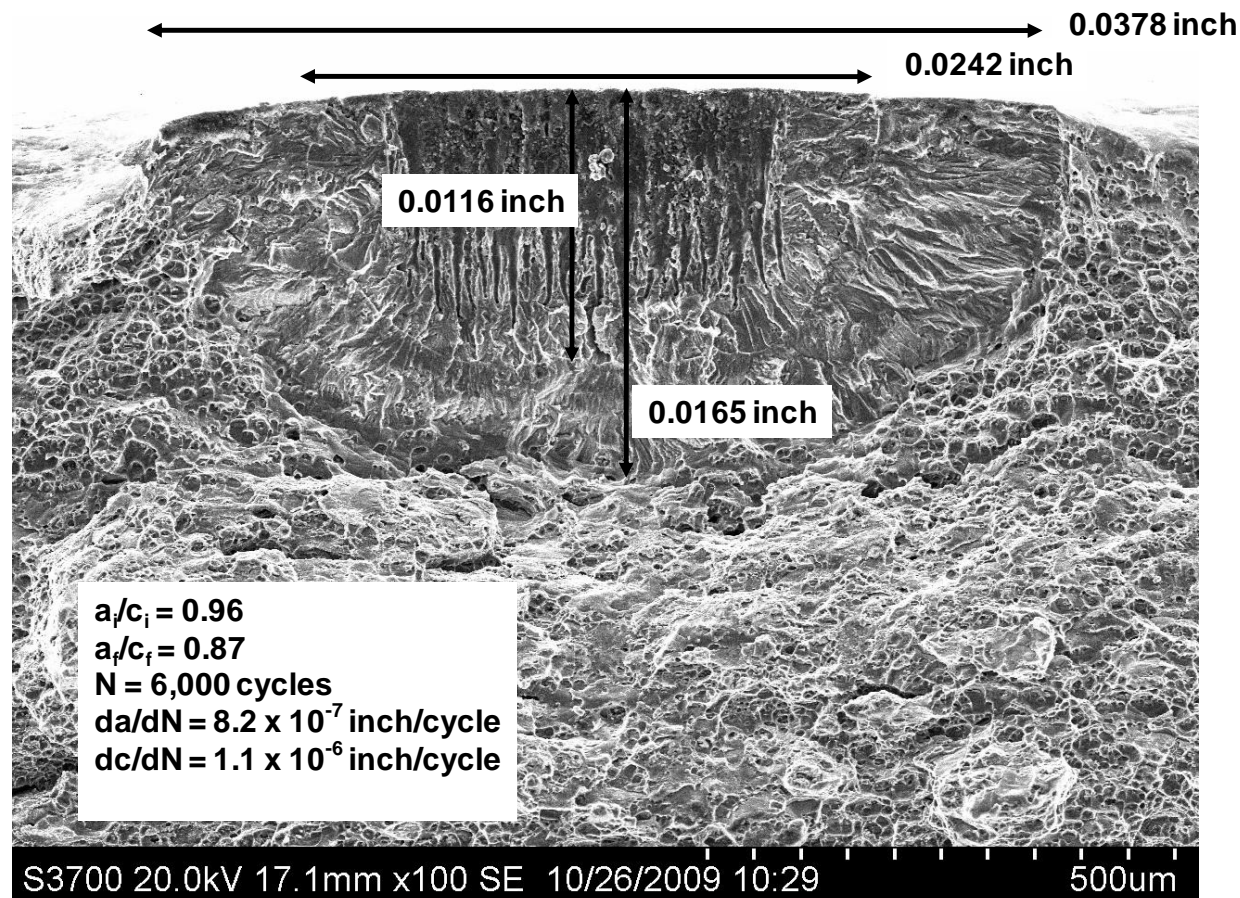


Figure C.15. SEM photograph (100x) of the fracture surface from crack #1 of COPV test 18103.



Title:

Fracture Mechanics Based Methods Development for
COPVs with Metallic Liners

Page #:
132 of 164

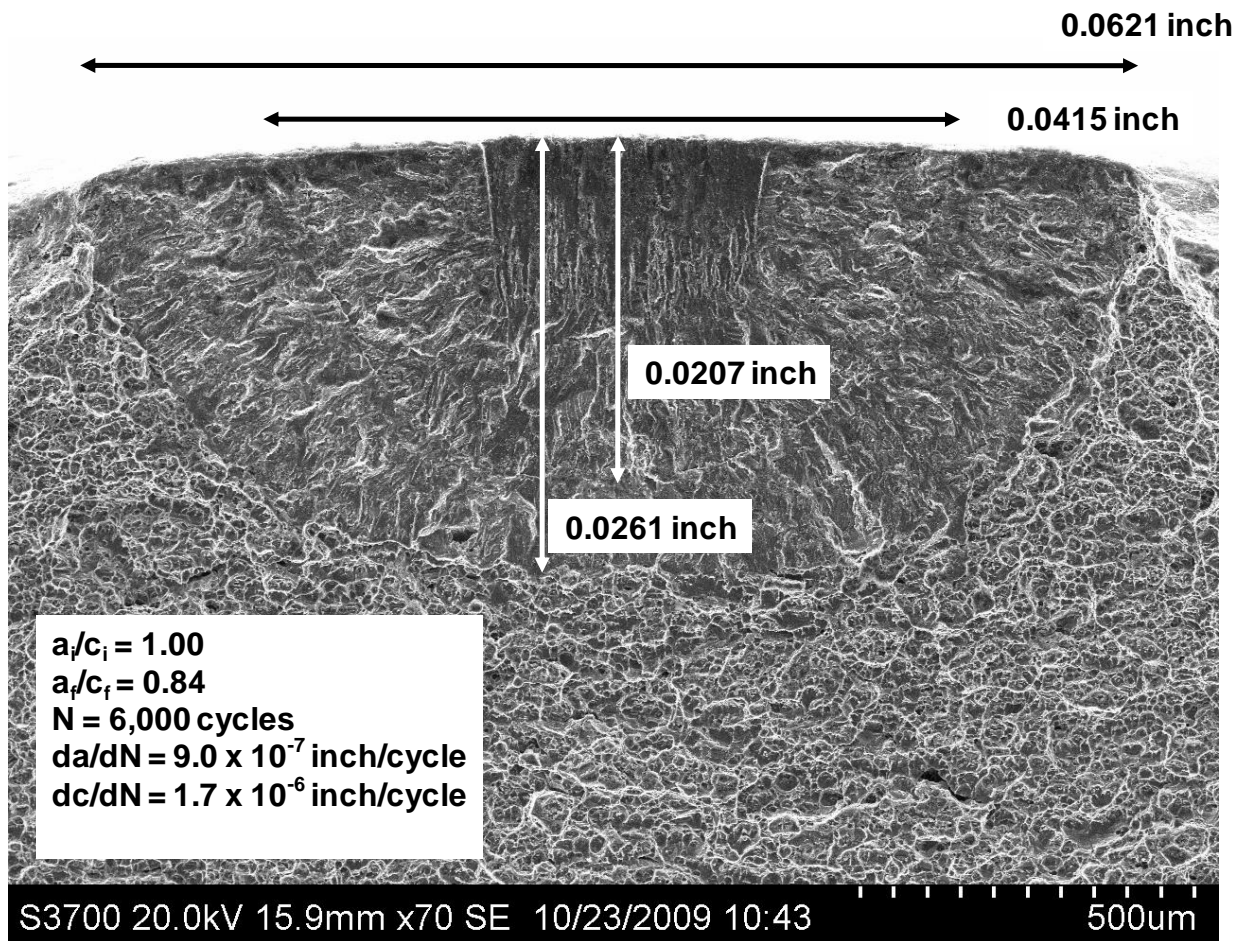


Figure C.16. SEM photograph (70x) of the fracture surface from crack #2 of COPV test 18103.



**NASA Engineering and Safety Center
Technical Assessment Report**

Document #:
**NESC-RP-
06-065**

Version:
1.0

Title:

**Fracture Mechanics Based Methods Development for
COPVs with Metallic Liners**

Page #:
133 of 164

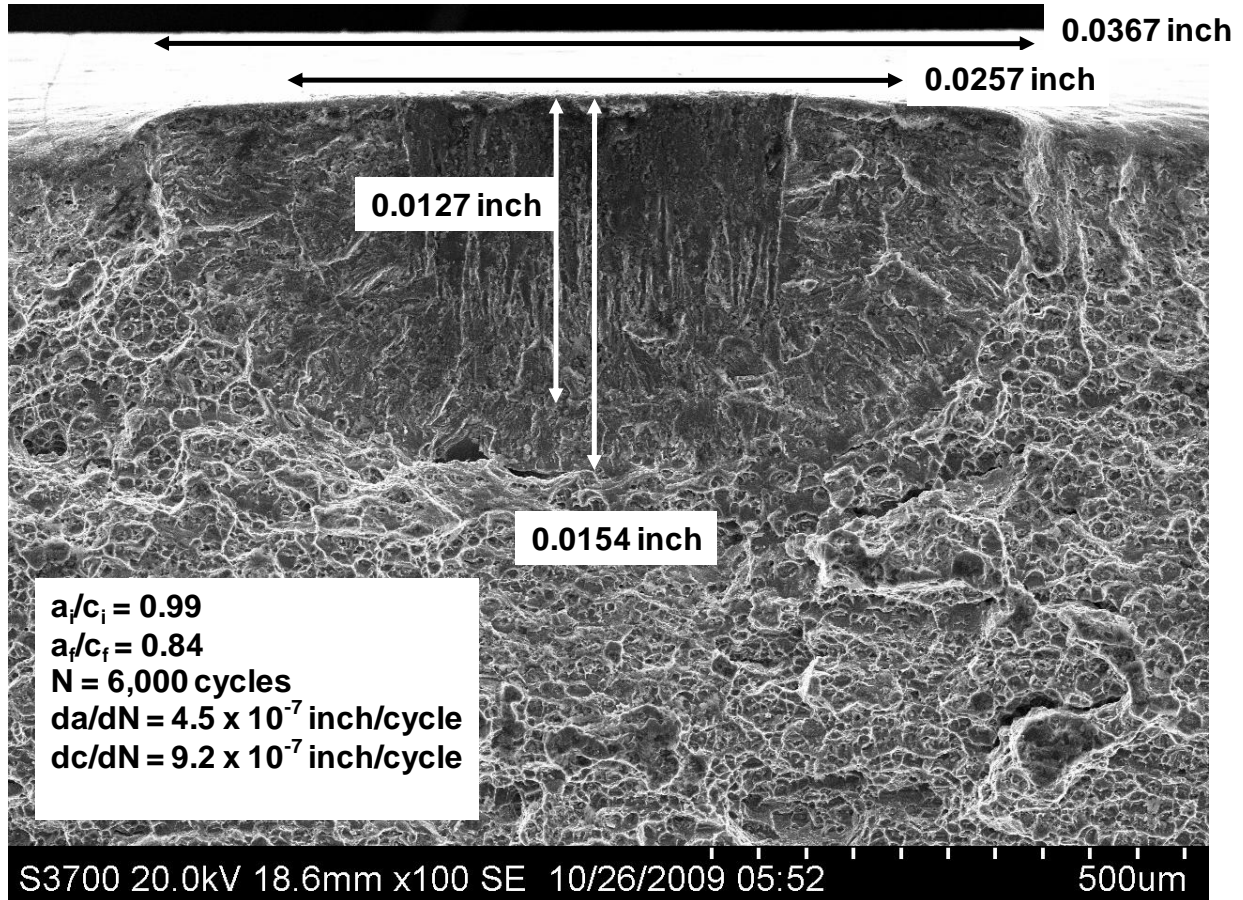


Figure C.17. SEM photograph (100x) of the fracture surface from crack #3 of COPV test 18103.



**NASA Engineering and Safety Center
Technical Assessment Report**

Document #:
**NESC-RP-
06-065**

Version:
1.0

Title:

**Fracture Mechanics Based Methods Development for
COPVs with Metallic Liners**

Page #:
134 of 164

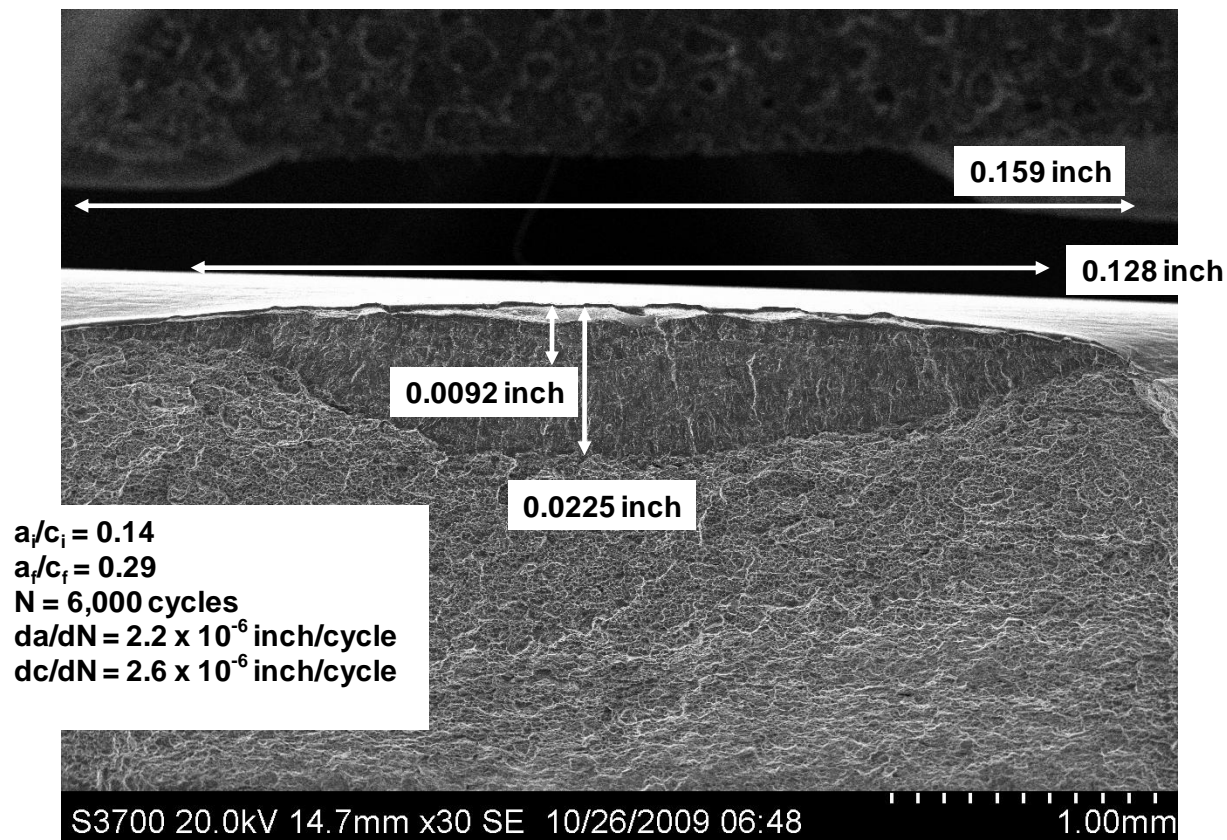


Figure C.18. SEM photograph (30x) of the fracture surface from exterior crack #1a of COPV test 18103 that initiated from a manufacturing defect.



**NASA Engineering and Safety Center
Technical Assessment Report**

Document #:
**NESC-RP-
06-065**

Version:
1.0

Title:

**Fracture Mechanics Based Methods Development for
COPVs with Metallic Liners**

Page #:
135 of 164

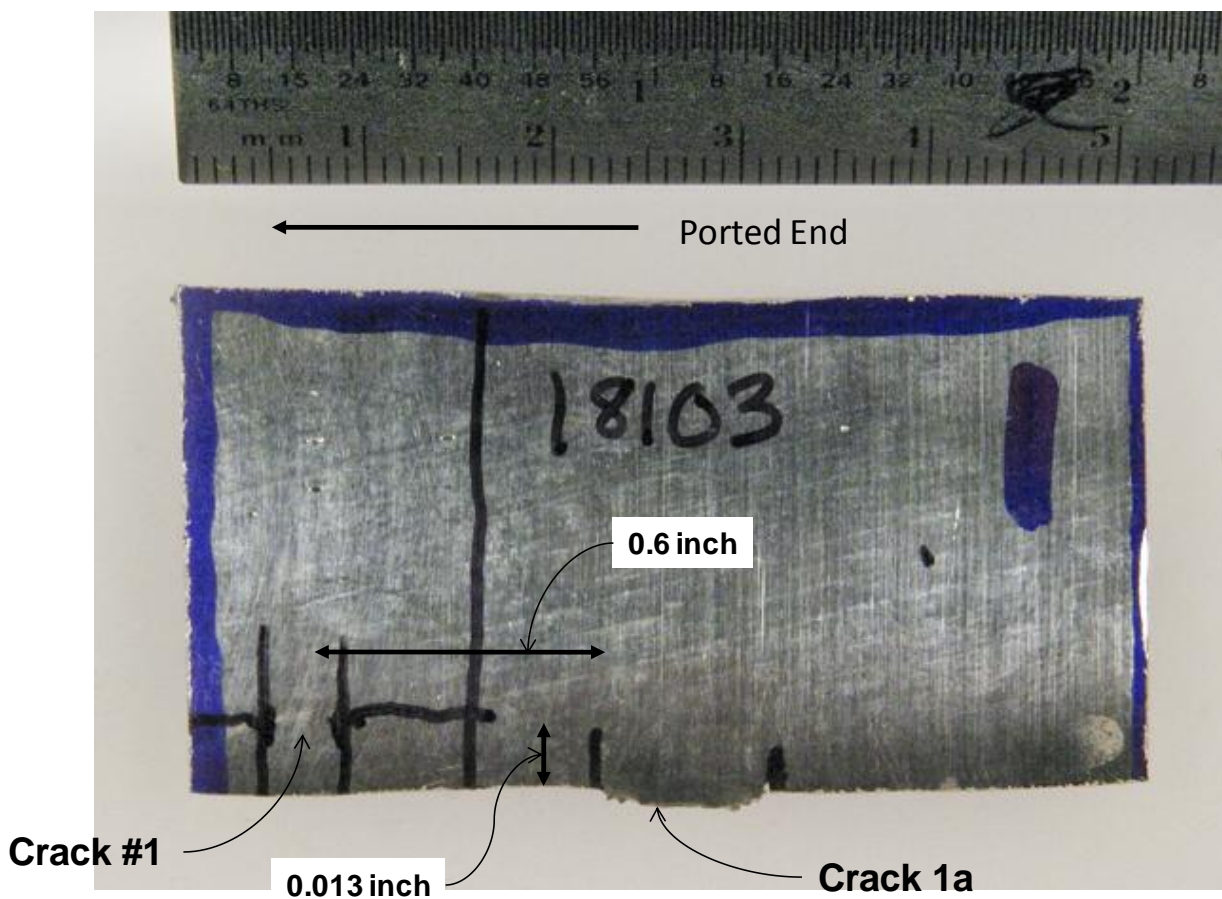


Figure C.19. Location of the exterior crack #1a that initiated from a manufacturing defect in COPV test 18103.



Title:

Fracture Mechanics Based Methods Development for
COPVs with Metallic Liners

Page #:
136 of 164

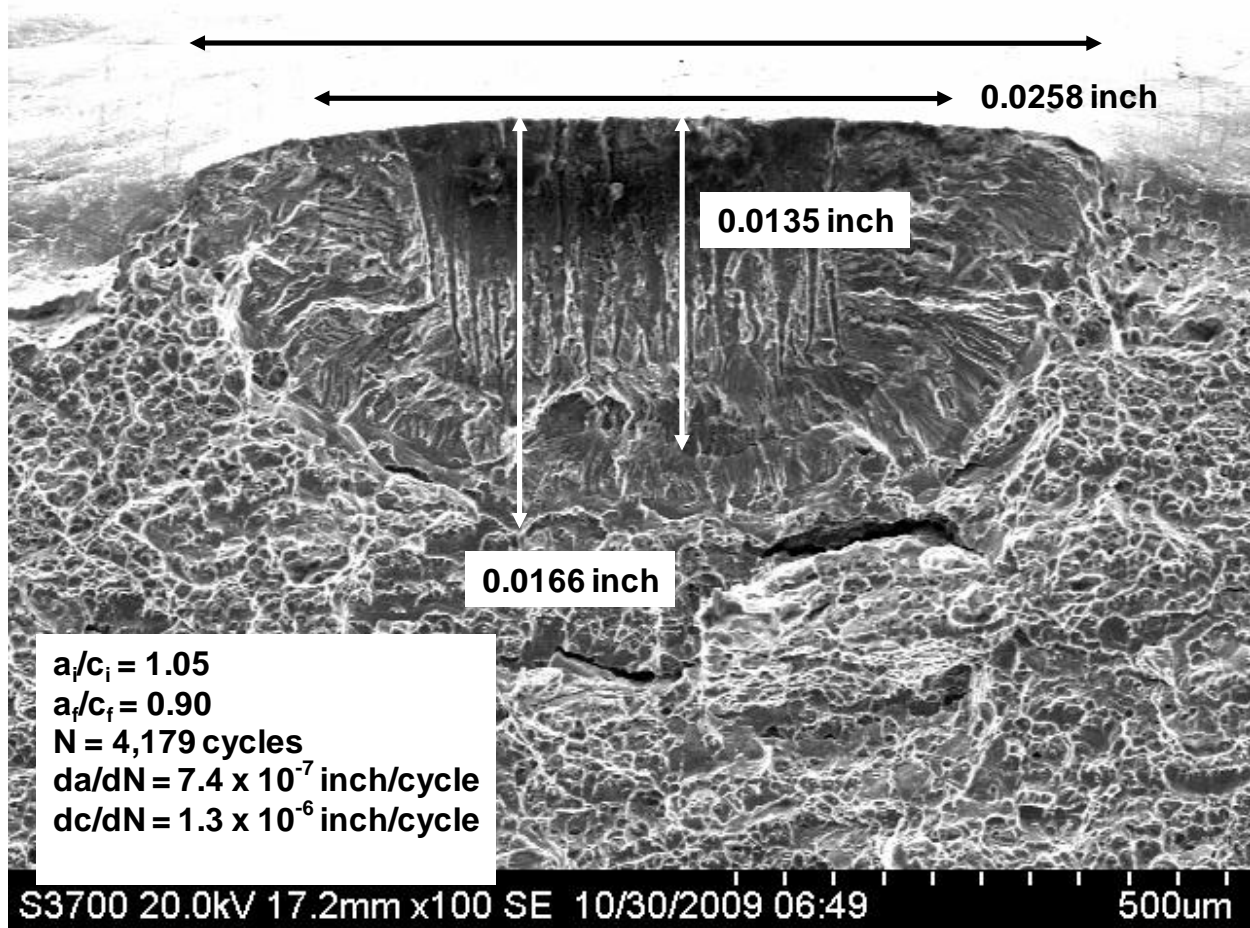


Figure C.20. SEM photograph (100x) of the fracture surface from crack #1 of COPV test 18119.



NASA Engineering and Safety Center
Technical Assessment Report

Document #:
**NESC-RP-
06-065**

Version:
1.0

Title:

**Fracture Mechanics Based Methods Development for
COPVs with Metallic Liners**

Page #:
137 of 164

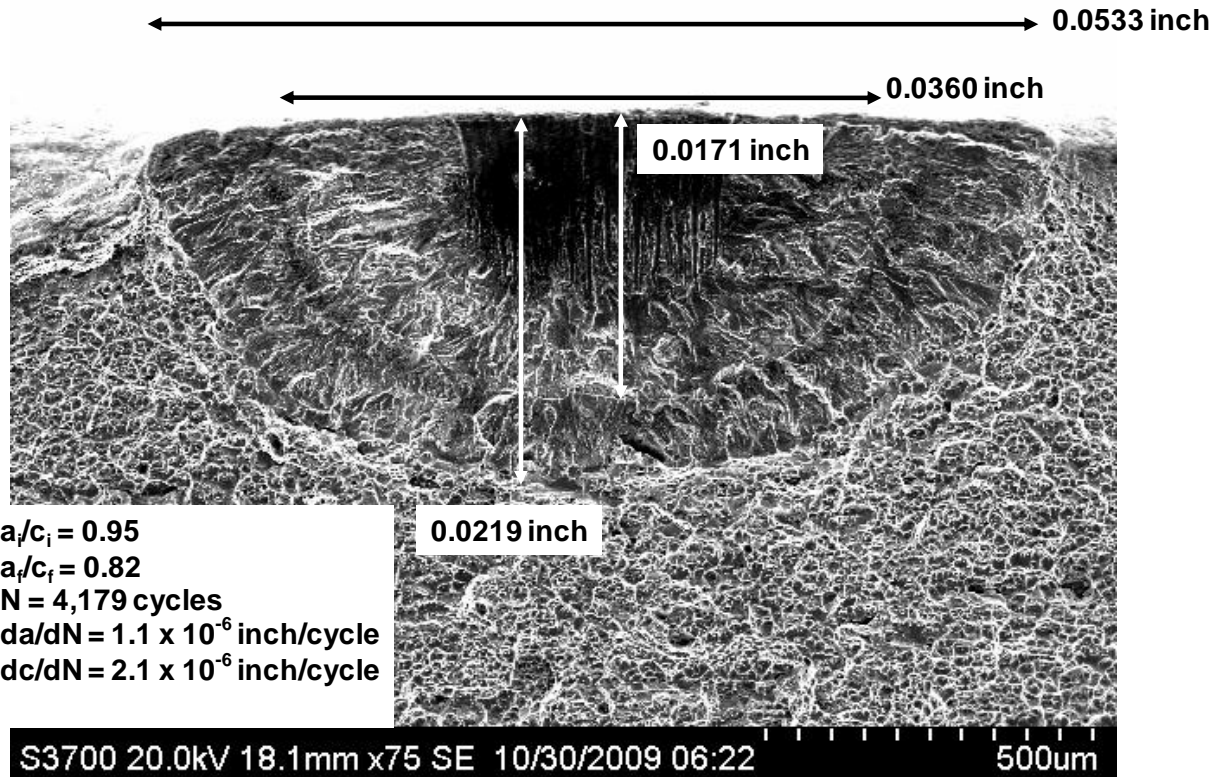


Figure C.21. SEM photograph (75x) of the fracture surface from crack #2 of COPV test 18119.



Title:

Fracture Mechanics Based Methods Development for
COPVs with Metallic Liners

Page #:
138 of 164

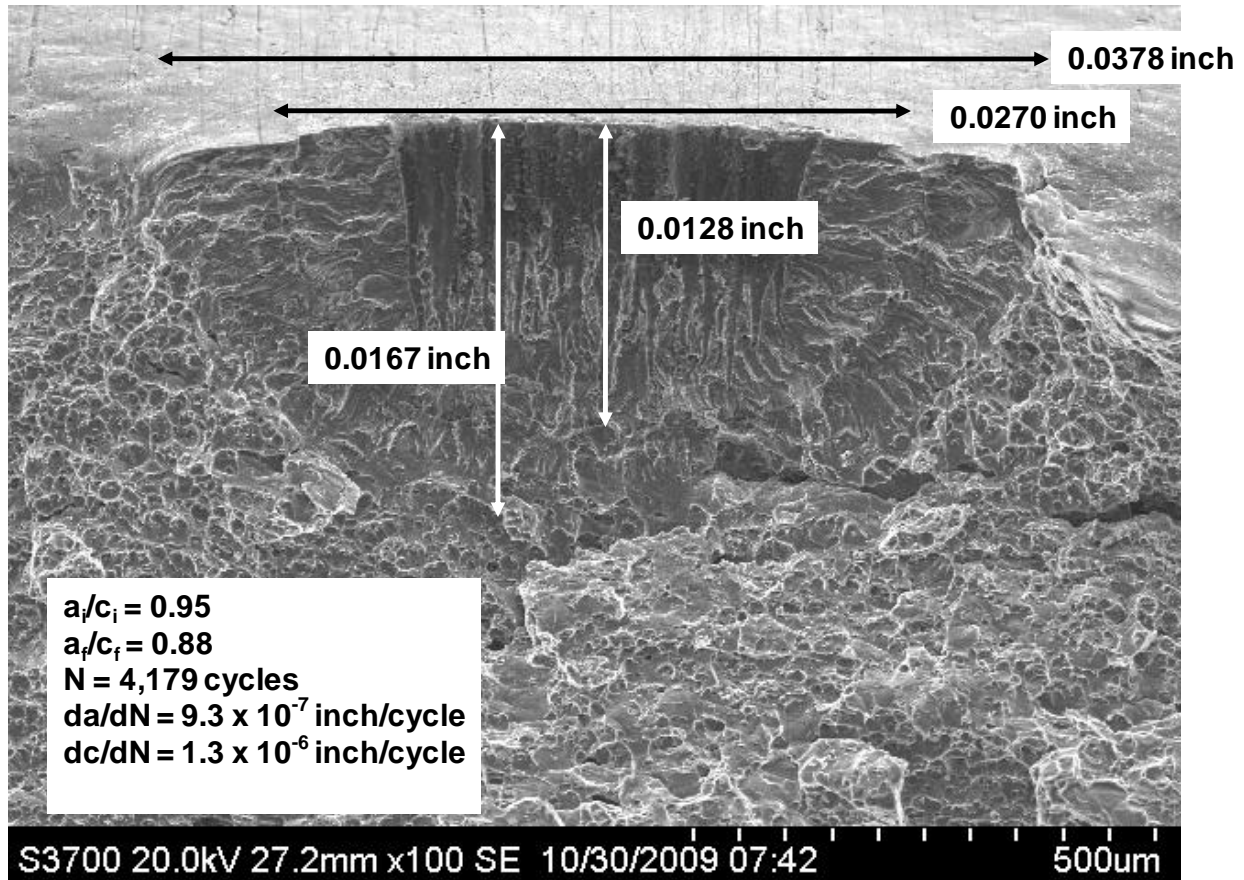


Figure C.22. SEM photograph (100x) of the fracture surface from crack #3 of COPV test 18119.



**NASA Engineering and Safety Center
Technical Assessment Report**

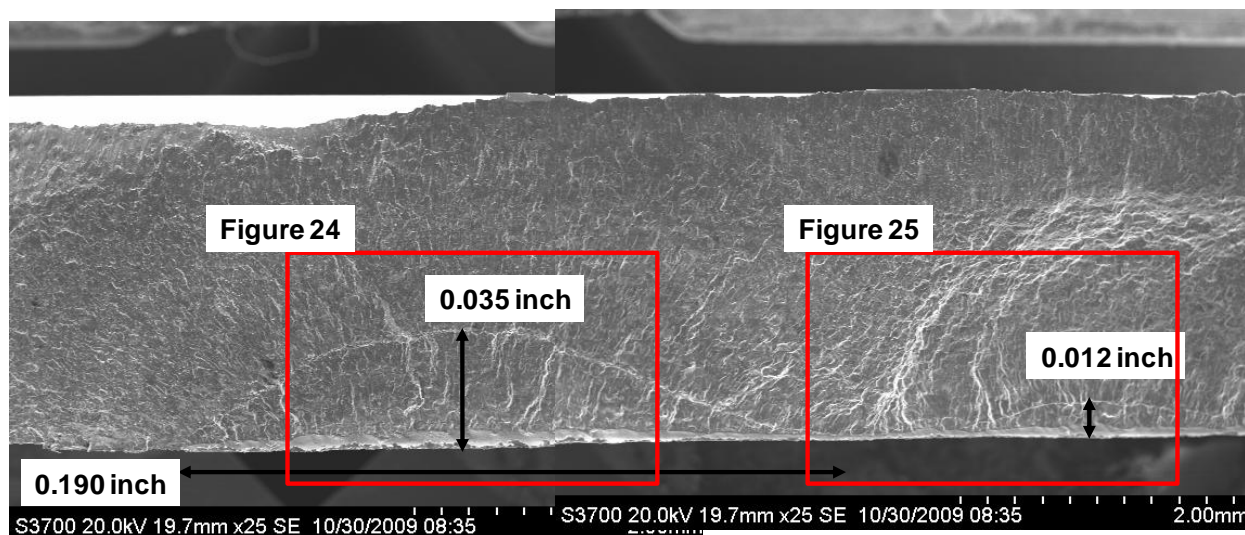
Document #:
**NESC-RP-
06-065**

Version:
1.0

Title:

**Fracture Mechanics Based Methods Development for
COPVs with Metallic Liners**

Page #:
139 of 164



$a/c_i = 0.37$
 $N = 4,179$ cycles

Figure C.23. SEM photograph (25x montage) of the leak site that initiated from an interior manufacturing defect of COPV test 18119.



**NASA Engineering and Safety Center
Technical Assessment Report**

Document #:
**NESC-RP-
06-065**

Version:
1.0

Title:

**Fracture Mechanics Based Methods Development for
COPVs with Metallic Liners**

Page #:
140 of 164

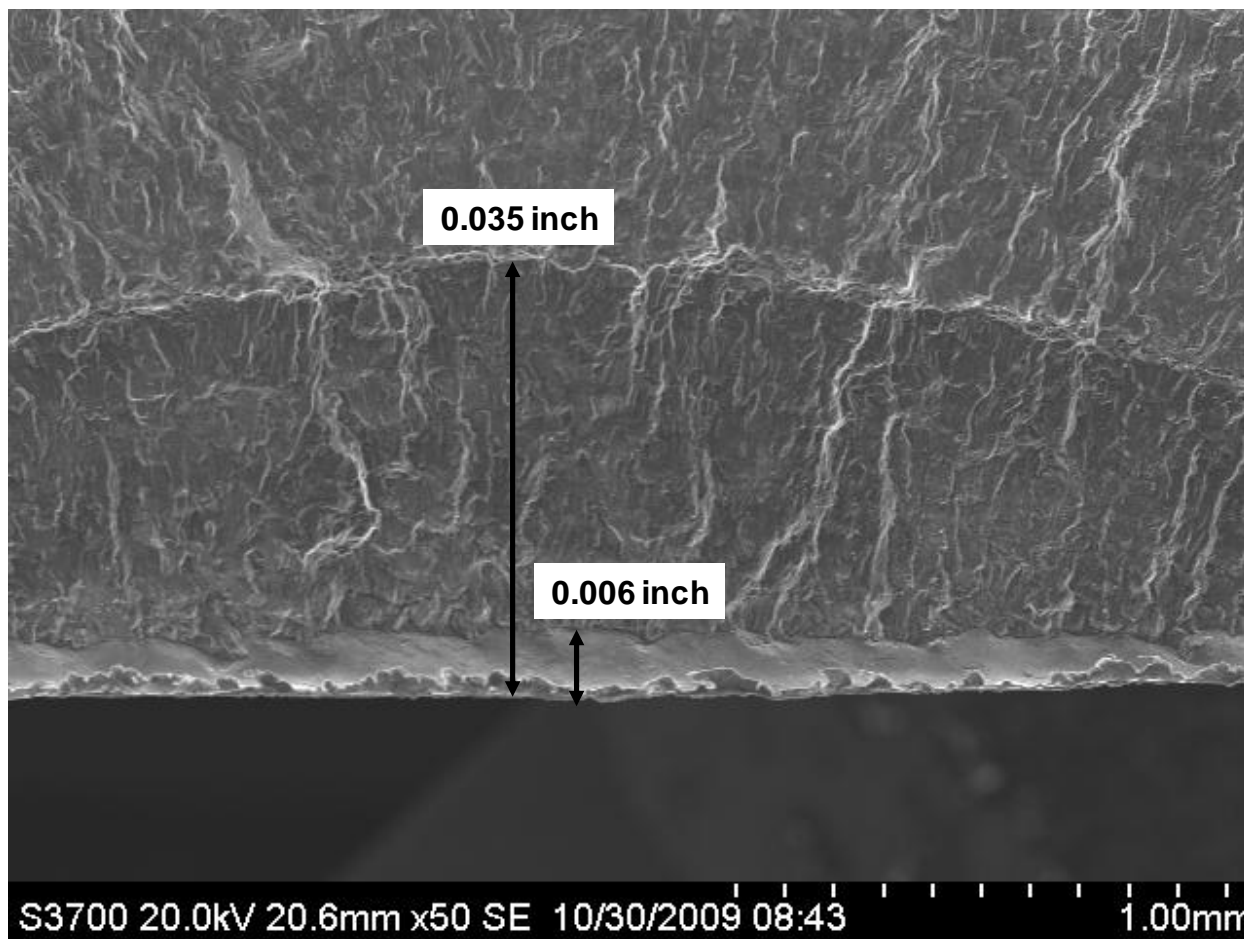


Figure C.24. SEM photograph (50x) of the large interior crack of COPV test 18119 that leaked during fatigue.



**NASA Engineering and Safety Center
Technical Assessment Report**

Document #:
**NESC-RP-
06-065**

Version:
1.0

Title:

**Fracture Mechanics Based Methods Development for
COPVs with Metallic Liners**

Page #:
141 of 164

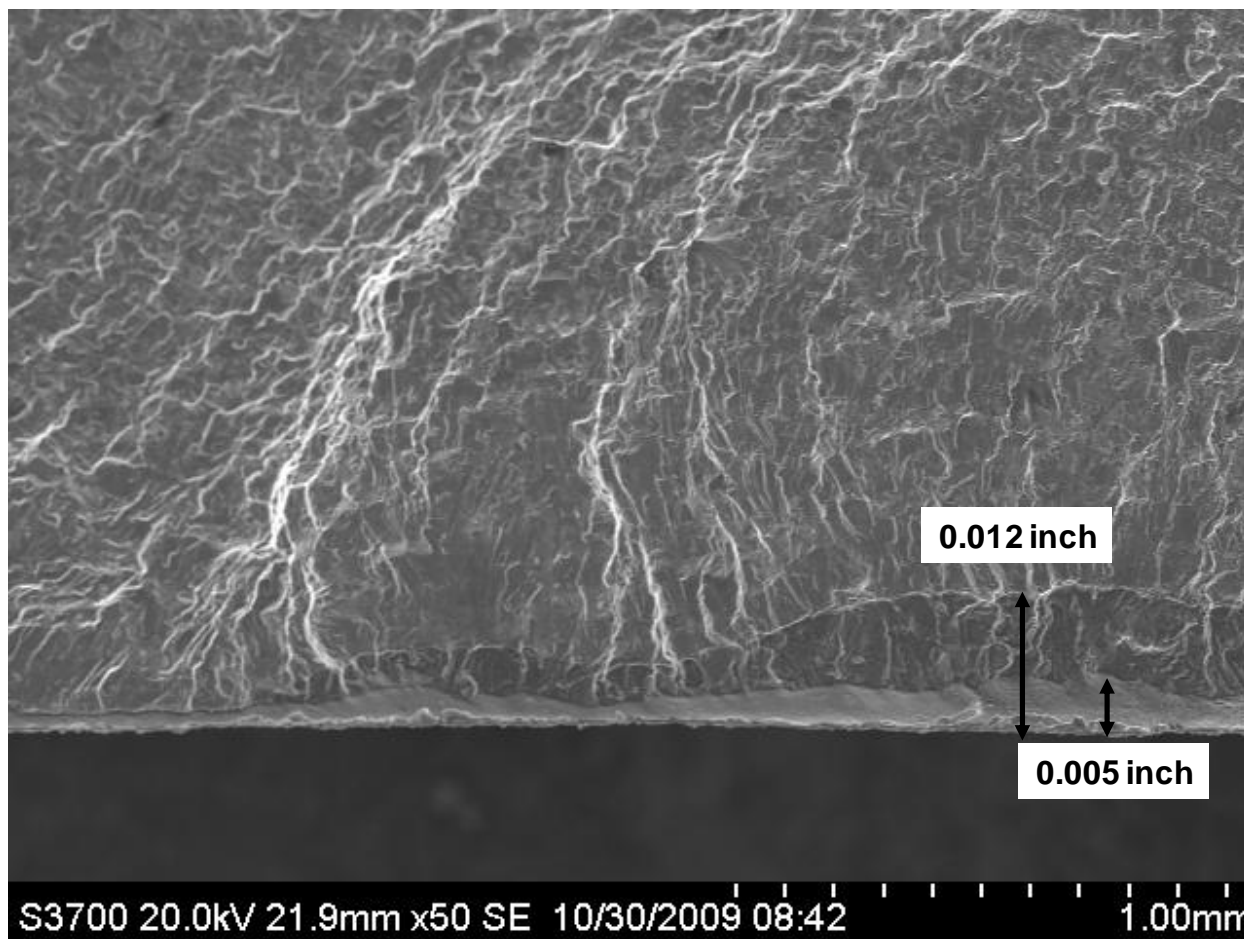


Figure C.25. SEM photograph (50x) of the smaller portion of the interior crack of COPV test 18119 that leaked during fatigue.



**NASA Engineering and Safety Center
Technical Assessment Report**

Document #:
**NESC-RP-
06-065**

Version:
1.0

Title:

**Fracture Mechanics Based Methods Development for
COPVs with Metallic Liners**

Page #:
142 of 164

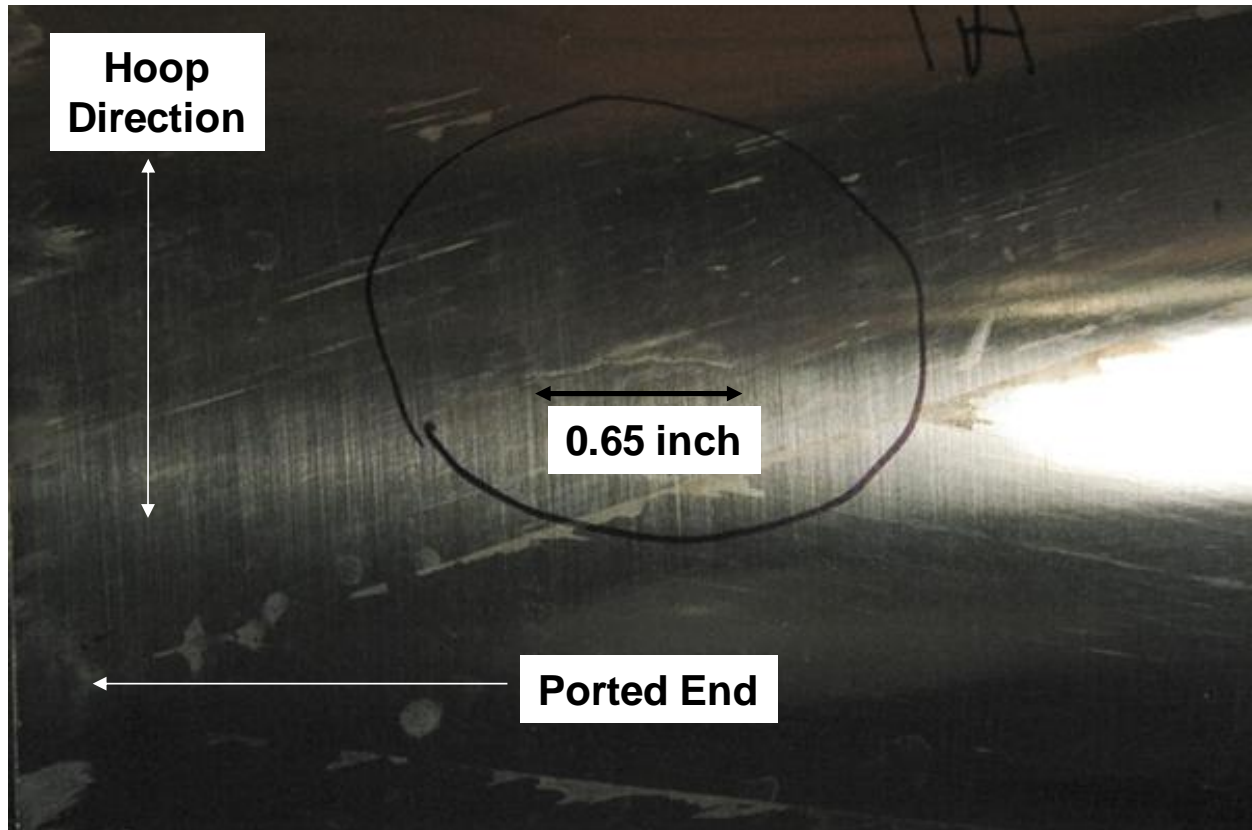


Figure C.26. Exterior view of the fatigue crack that initiated from an internal defect and leaked during the fatigue cycling of COPV test 18119.



**NASA Engineering and Safety Center
Technical Assessment Report**

Document #:
**NESC-RP-
06-065**

Version:
1.0

Title:

**Fracture Mechanics Based Methods Development for
COPVs with Metallic Liners**

Page #:
143 of 164

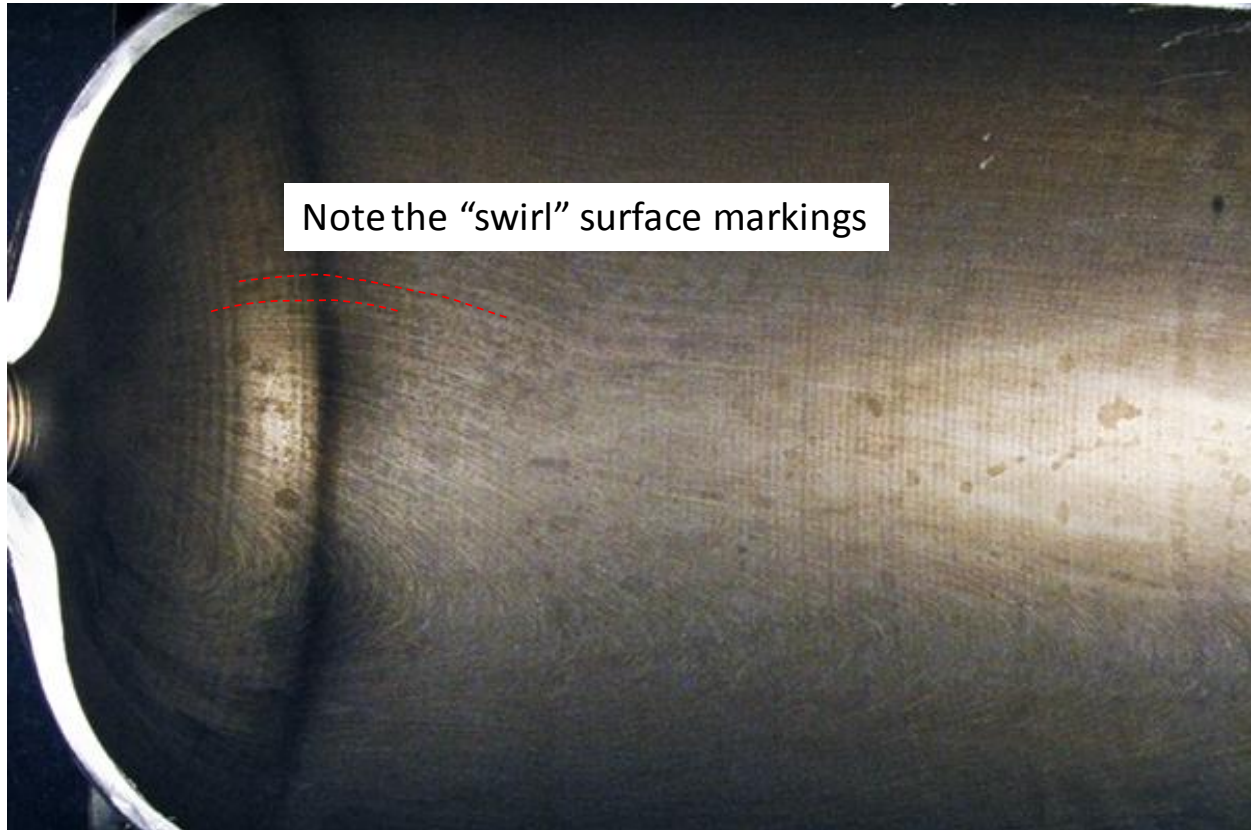


Figure C.27. View of the interior of the liner of COPV 18119 near the internal defect that initiated the crack that leaked during the fatigue cycling.



NASA Engineering and Safety Center Technical Assessment Report

Document #:
**NESC-RP-
06-065**

Version:
1.0

Title:

Fracture Mechanics Based Methods Development for COPVs with Metallic Liners

Page #:
144 of 164

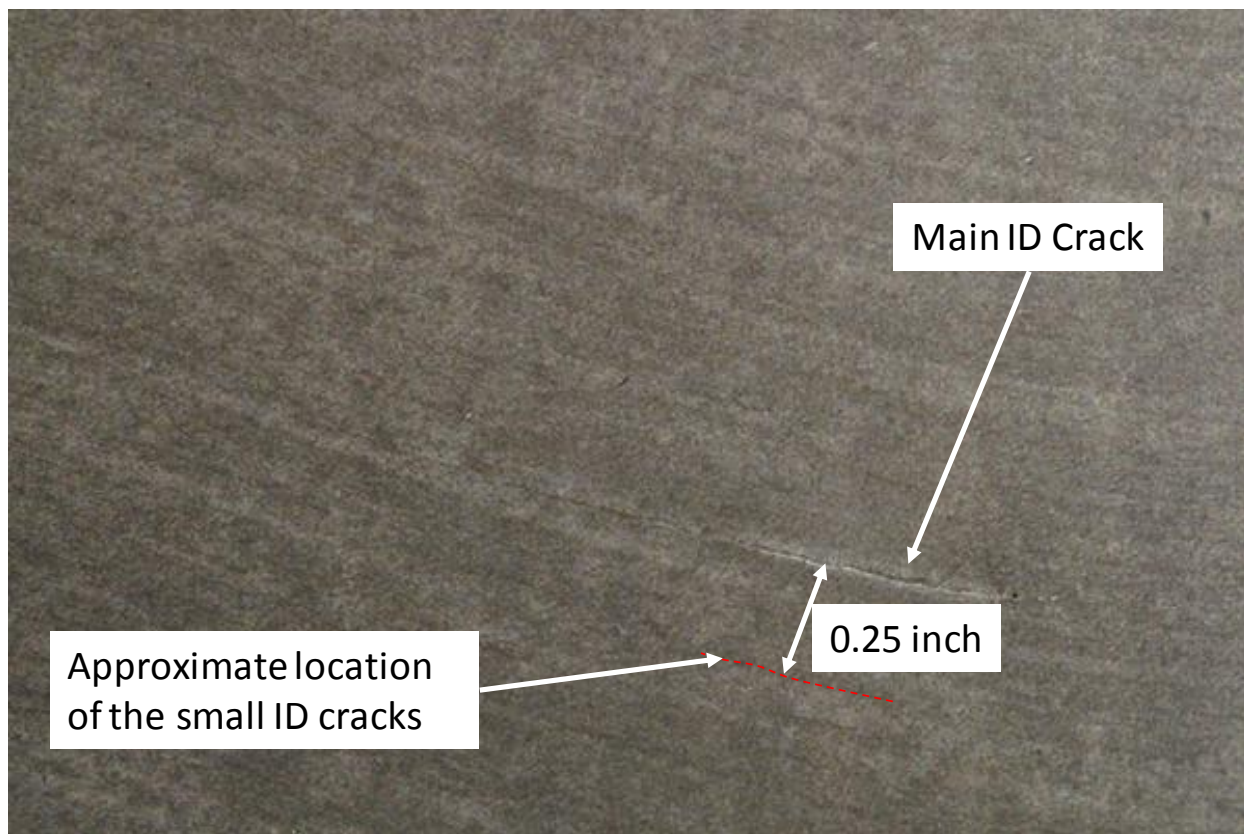


Figure C.28 Close up of the interior of the liner of COPV test 18119 showing the crack that leaked follows the “swirl” pattern on the interior surface and the approximate location of the smaller ID cracks.

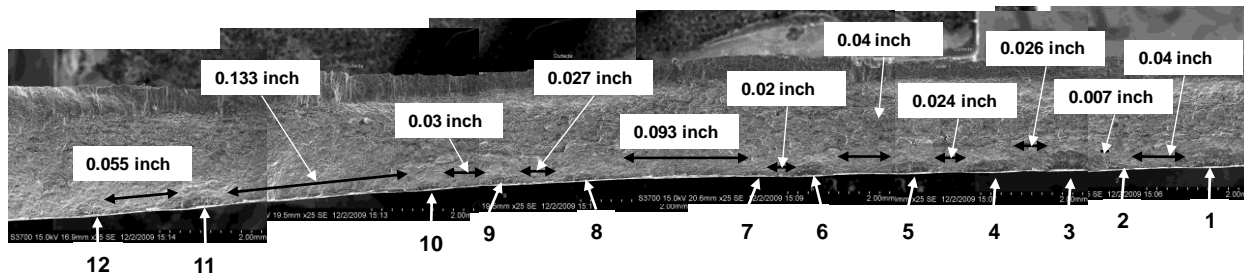


Figure C.29. SEM photograph (25x montage) of the location of the 12 small cracks found on the interior of the liner of COPV test 18119 and the approximate distances between the cracks.



**NASA Engineering and Safety Center
Technical Assessment Report**

Document #:
**NESC-RP-
06-065**

Version:
1.0

Title:

**Fracture Mechanics Based Methods Development for
COPVs with Metallic Liners**

Page #:
145 of 164

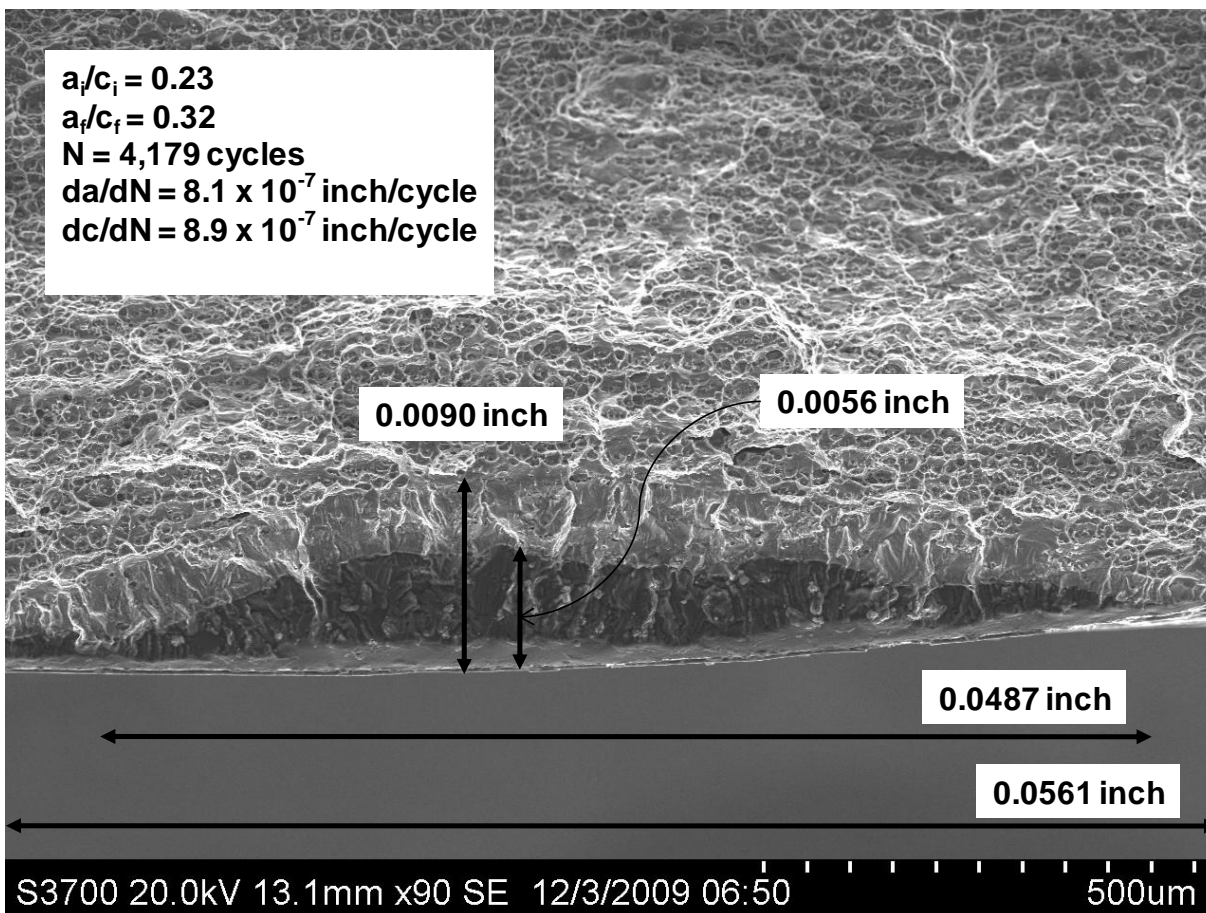


Figure C.30. SEM photograph (90x) of the interior crack ID1 found on the liner of COPV test 18119.



**NASA Engineering and Safety Center
Technical Assessment Report**

Document #:
**NESC-RP-
06-065**

Version:
1.0

Title:

**Fracture Mechanics Based Methods Development for
COPVs with Metallic Liners**

Page #:
146 of 164

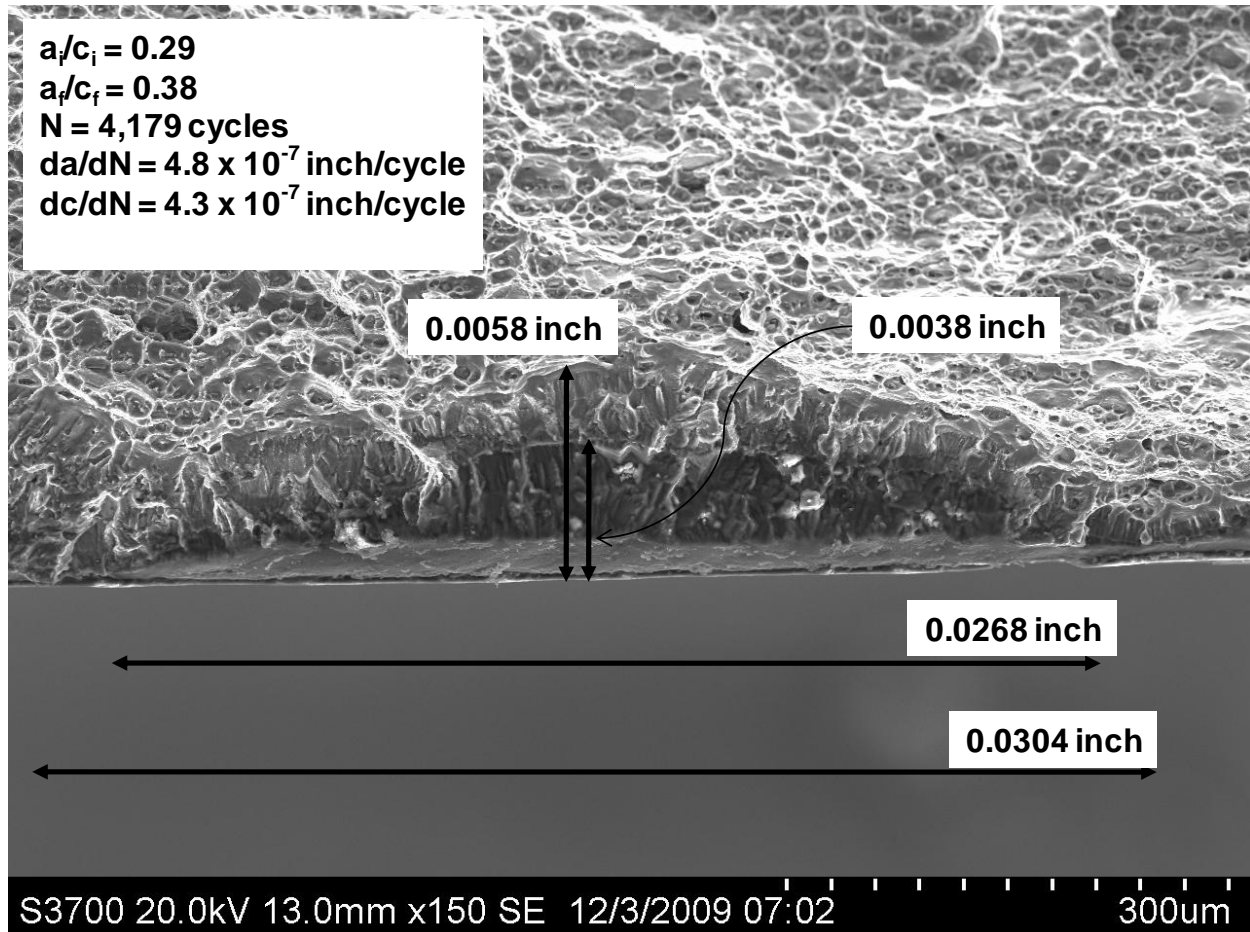


Figure C.31. SEM photograph (150x) of the interior crack ID2 found on the liner of COPV test 18119.



**NASA Engineering and Safety Center
Technical Assessment Report**

Document #:
**NESC-RP-
06-065**

Version:
1.0

Title:

**Fracture Mechanics Based Methods Development for
COPVs with Metallic Liners**

Page #:
147 of 164

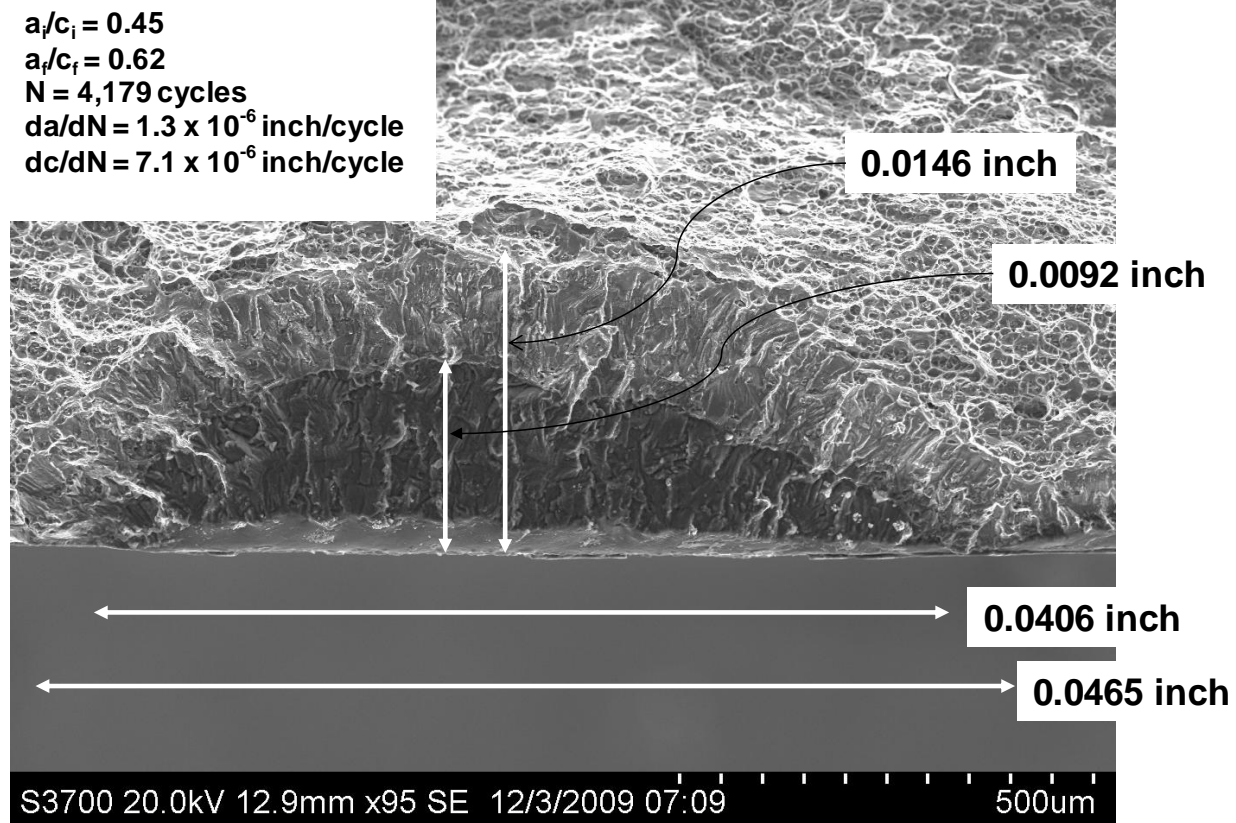


Figure C.32. SEM photograph (95x) of the interior crack ID3 found on the liner of COPV test 18119.



**NASA Engineering and Safety Center
Technical Assessment Report**

Document #:
**NESC-RP-
06-065**

Version:
1.0

Title:

**Fracture Mechanics Based Methods Development for
COPVs with Metallic Liners**

Page #:
148 of 164

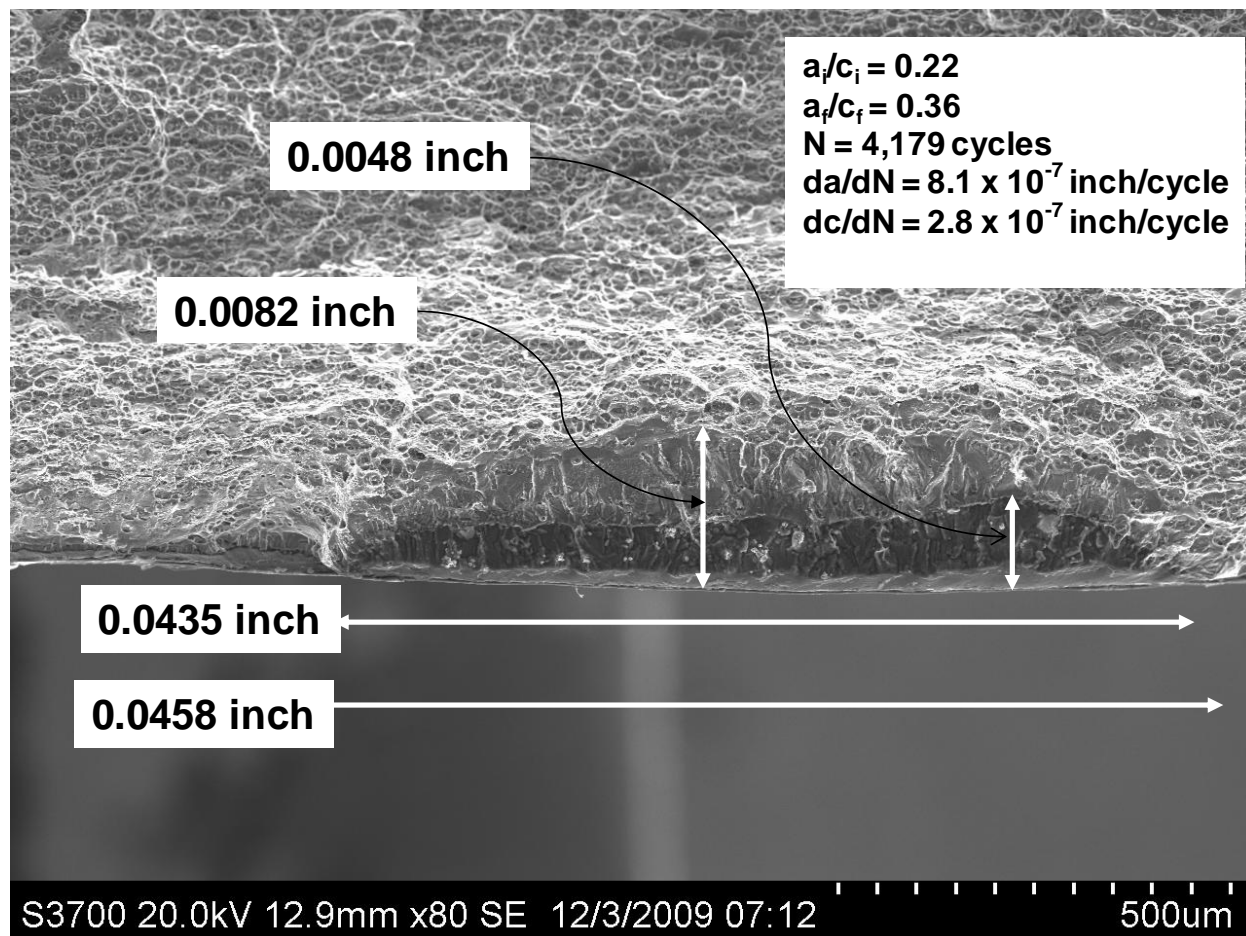


Figure C.33. SEM photograph (80x) of the interior crack ID4 found on the liner of COPV test 18119.



**NASA Engineering and Safety Center
Technical Assessment Report**

Document #:
**NESC-RP-
06-065**

Version:
1.0

Title:

**Fracture Mechanics Based Methods Development for
COPVs with Metallic Liners**

Page #:
149 of 164

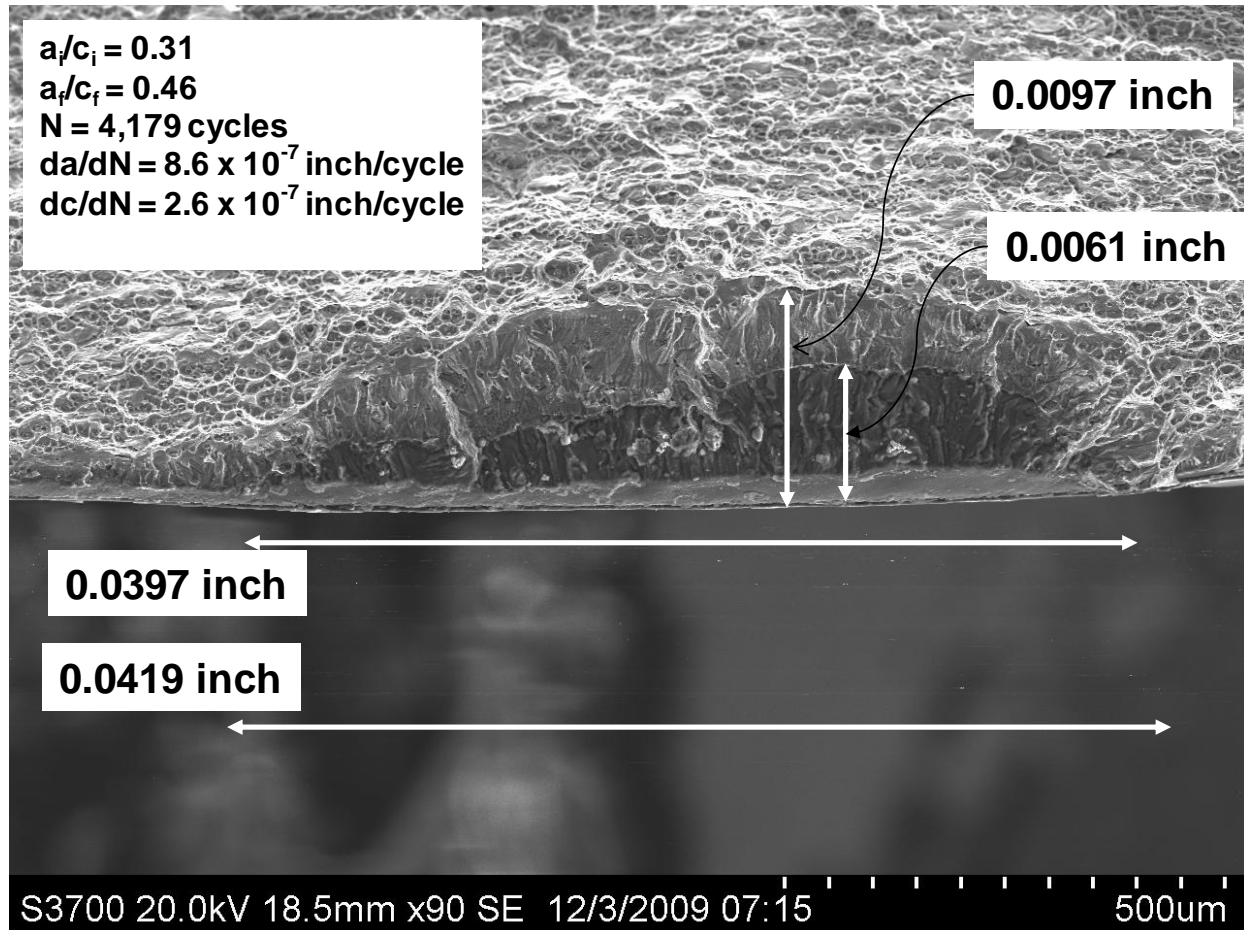


Figure C.34. SEM photograph (90x) of the interior crack ID5 found on the liner of COPV test 18119.



**NASA Engineering and Safety Center
Technical Assessment Report**

Document #:
**NESC-RP-
06-065**

Version:
1.0

Title:

**Fracture Mechanics Based Methods Development for
COPVs with Metallic Liners**

Page #:
150 of 164

$$a_i/c_i = 0.45$$

$$a_f/c_f = 0.54$$

$$N = 4,179 \text{ cycles}$$

$$da/dN = 6.9 \times 10^{-7} \text{ inch/cycle}$$

$$dc/dN = 7.4 \times 10^{-7} \text{ inch/cycle}$$

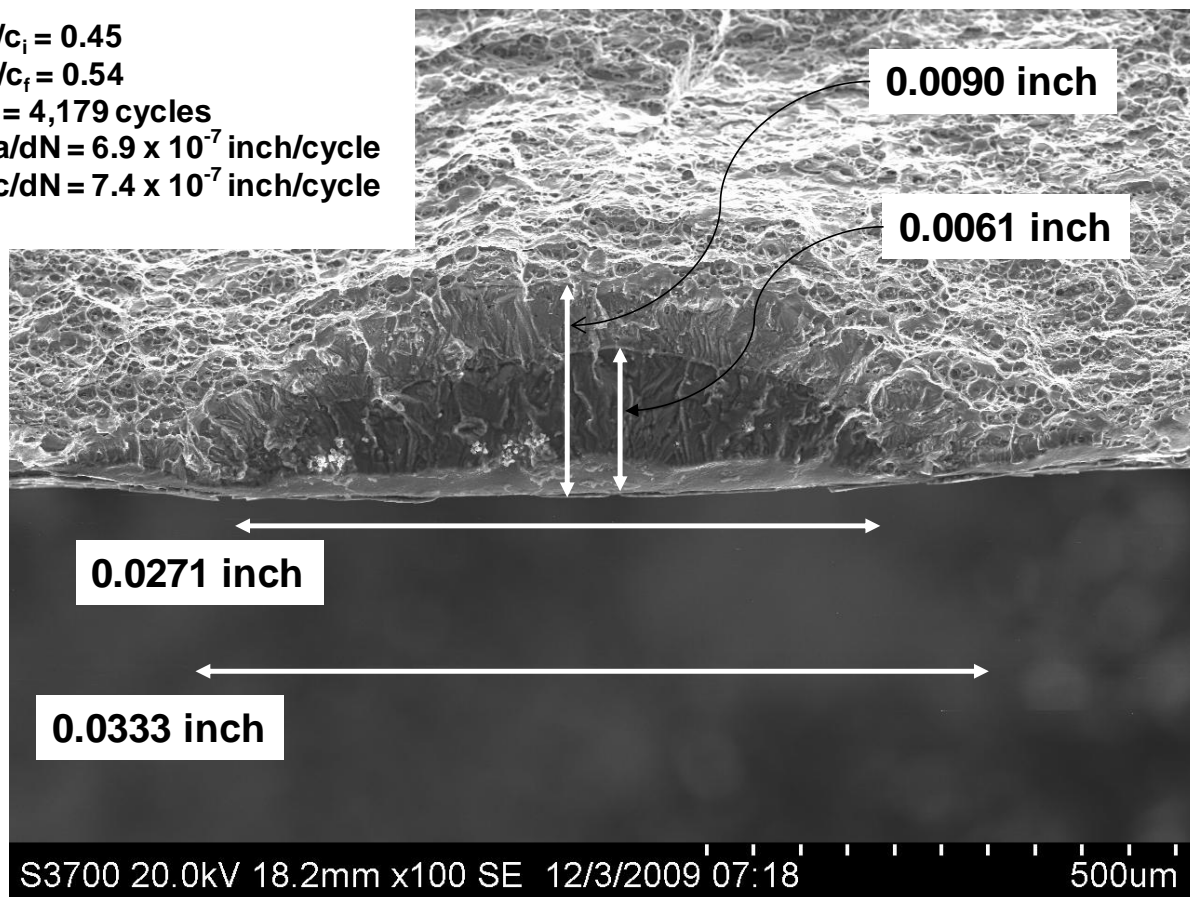


Figure C.35. SEM photograph (100x) of the interior crack ID6 found on the liner of COPV test 18119.



**NASA Engineering and Safety Center
Technical Assessment Report**

Document #:
**NESC-RP-
06-065**

Version:
1.0

Title:

**Fracture Mechanics Based Methods Development for
COPVs with Metallic Liners**

Page #:
151 of 164

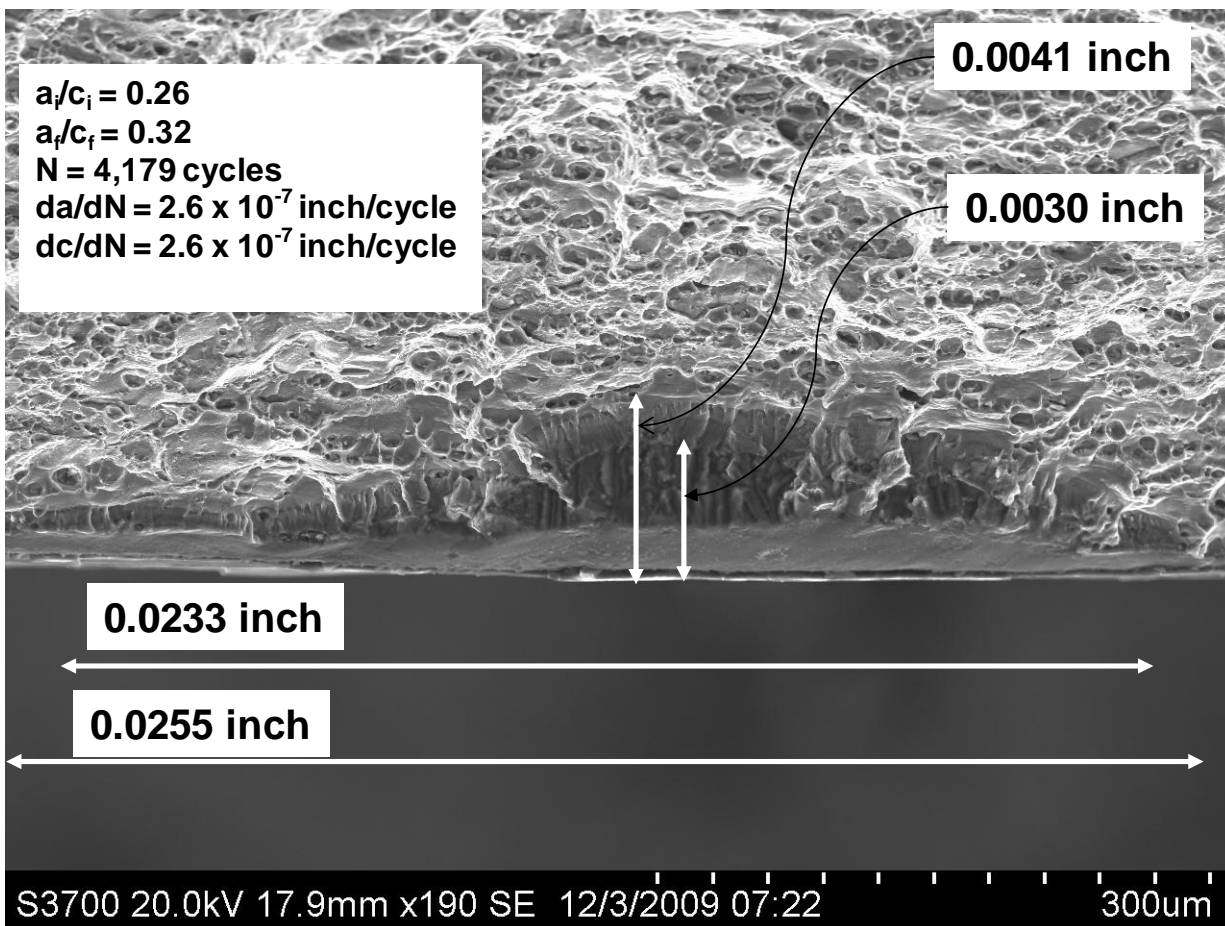


Figure C.36. SEM photograph (190x) of interior crack ID7 found on the liner of COPV test 18119.



**NASA Engineering and Safety Center
Technical Assessment Report**

Document #:
**NESC-RP-
06-065**

Version:
1.0

Title:

**Fracture Mechanics Based Methods Development for
COPVs with Metallic Liners**

Page #:
152 of 164

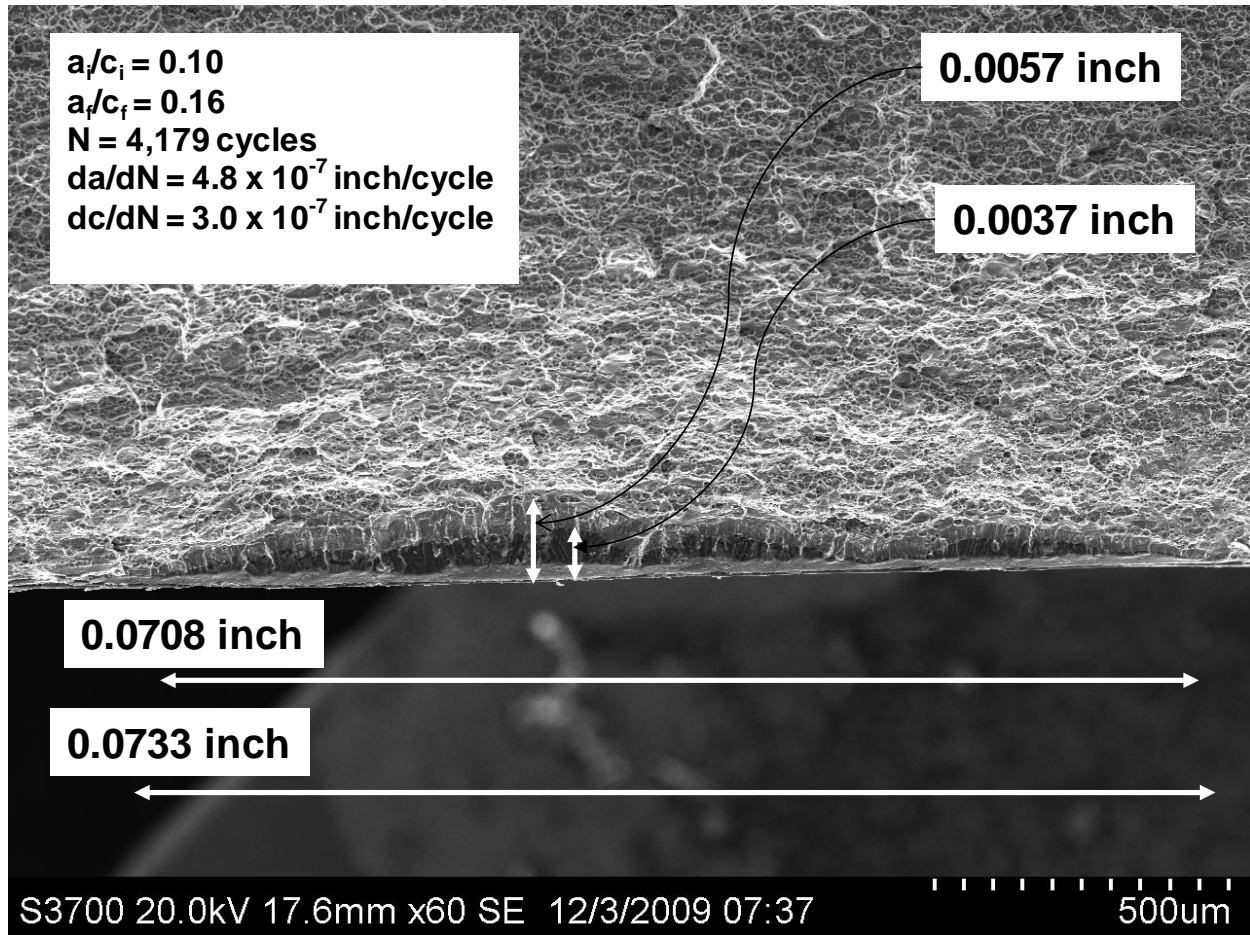


Figure C.37. SEM photograph (60x) of the interior crack ID8 found on the liner of COPV test 18119.



**NASA Engineering and Safety Center
Technical Assessment Report**

Document #:
**NESC-RP-
06-065**

Version:
1.0

Title:

**Fracture Mechanics Based Methods Development for
COPVs with Metallic Liners**

Page #:
153 of 164

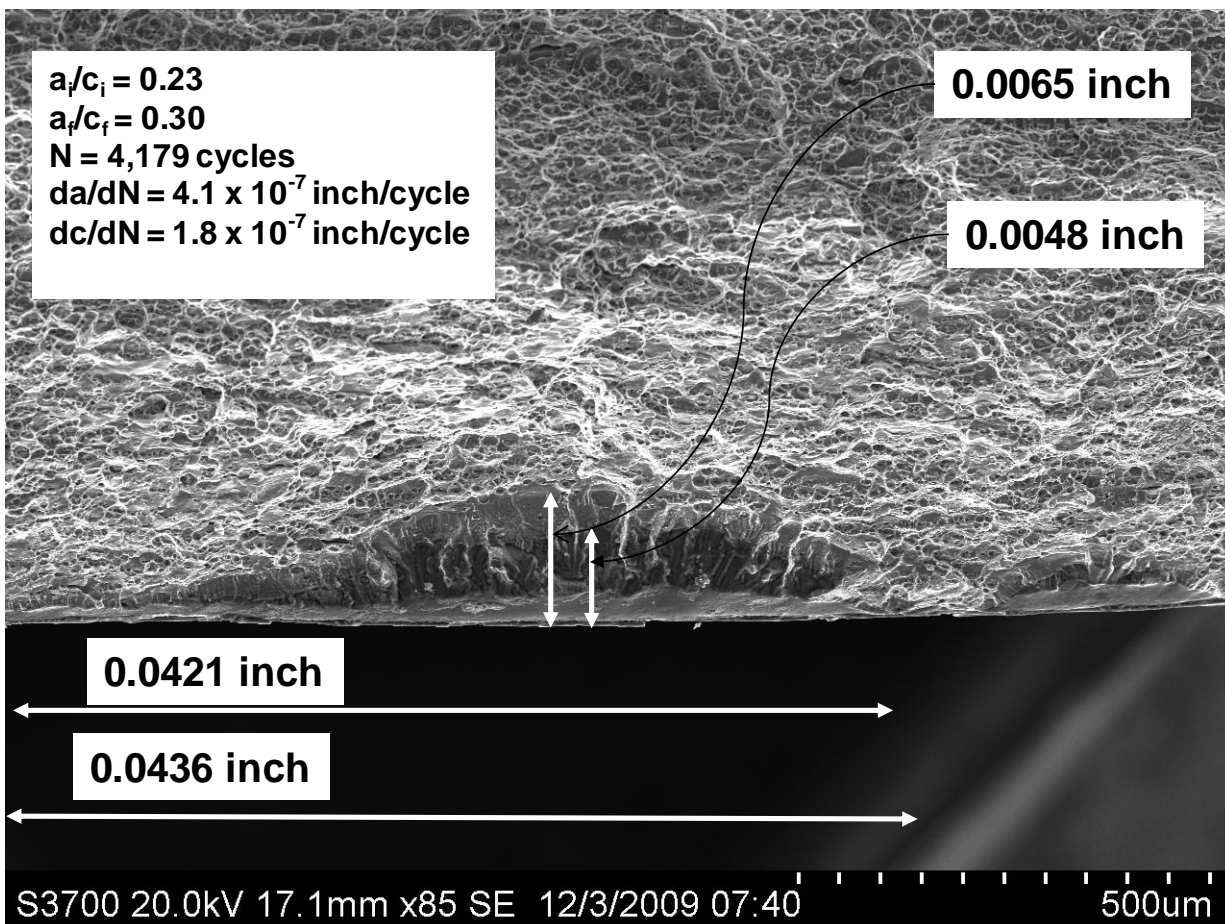


Figure C.38. SEM photograph (85x) of the interior crack ID9 found on the liner of COPV test 18119.



**NASA Engineering and Safety Center
Technical Assessment Report**

Document #:
**NESC-RP-
06-065**

Version:
1.0

Title:

**Fracture Mechanics Based Methods Development for
COPVs with Metallic Liners**

Page #:
154 of 164

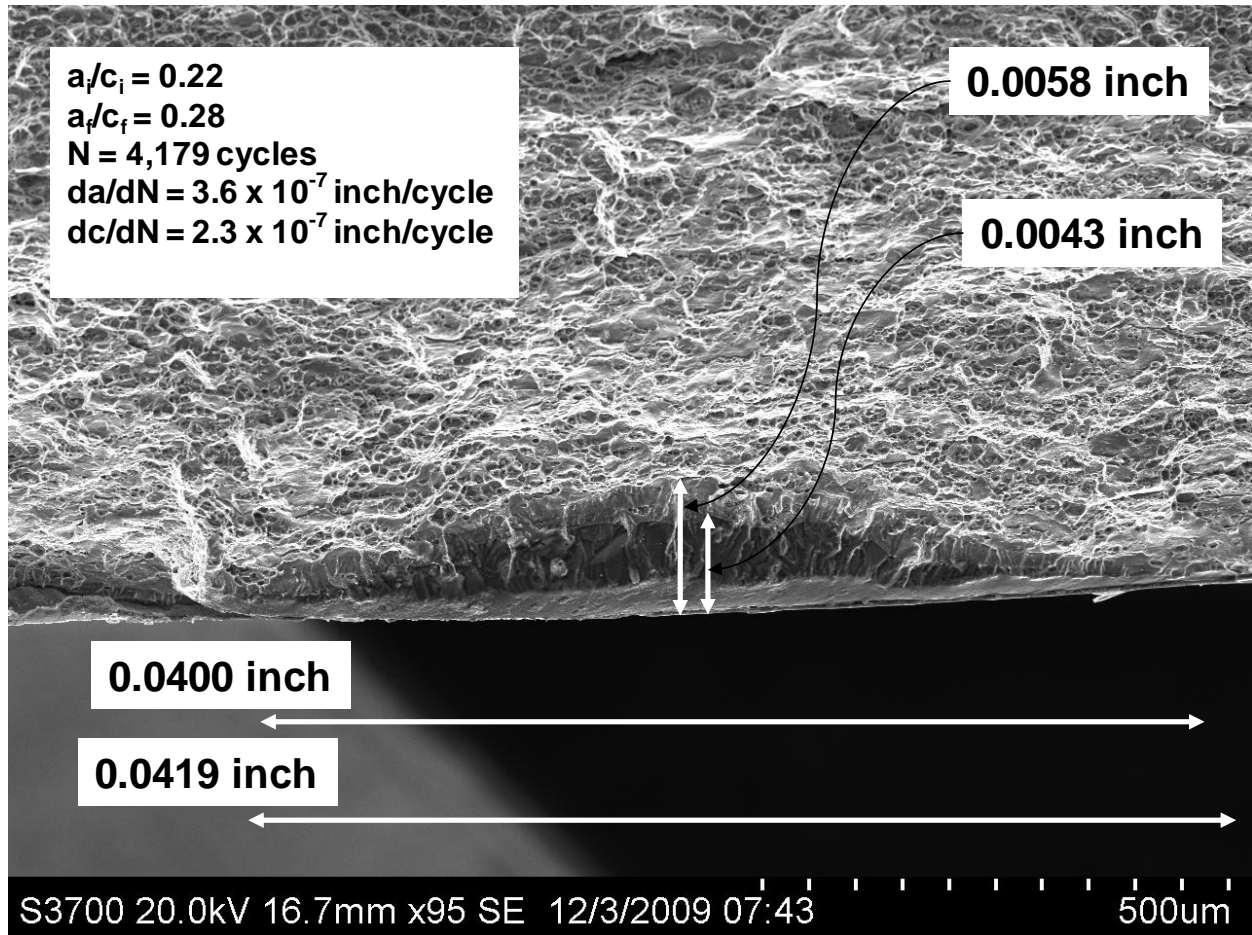


Figure C.39. SEM photograph (95x) of the interior crack ID10 found on the liner of COPV test 18119.



**NASA Engineering and Safety Center
Technical Assessment Report**

Document #:
**NESC-RP-
06-065**

Version:
1.0

Title:

**Fracture Mechanics Based Methods Development for
COPVs with Metallic Liners**

Page #:
155 of 164

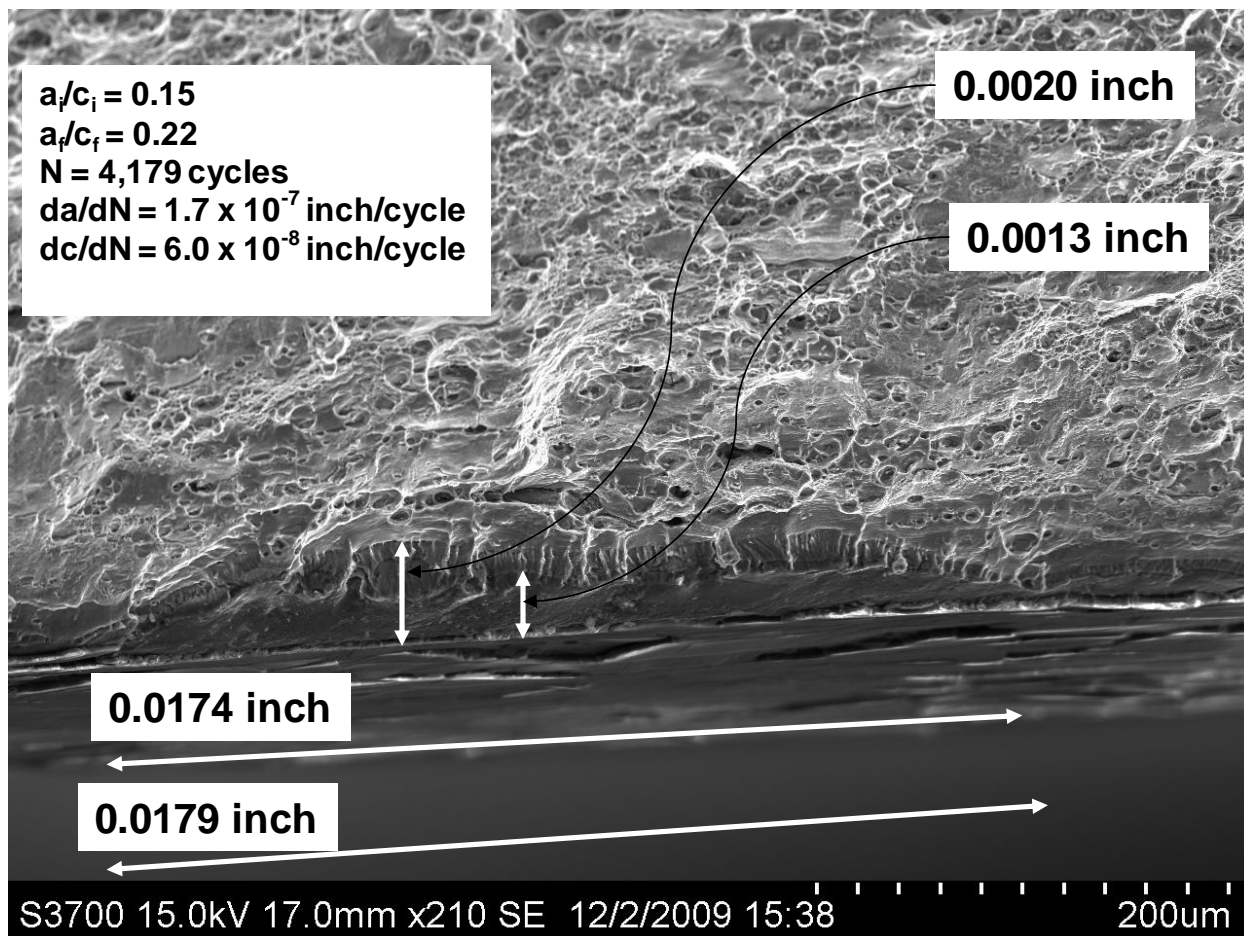


Figure C.40. SEM photograph (210x) of the interior crack ID11 found on the liner of COPV test 18119.



**NASA Engineering and Safety Center
Technical Assessment Report**

Document #:
**NESC-RP-
06-065**

Version:
1.0

Title:

**Fracture Mechanics Based Methods Development for
COPVs with Metallic Liners**

Page #:
156 of 164

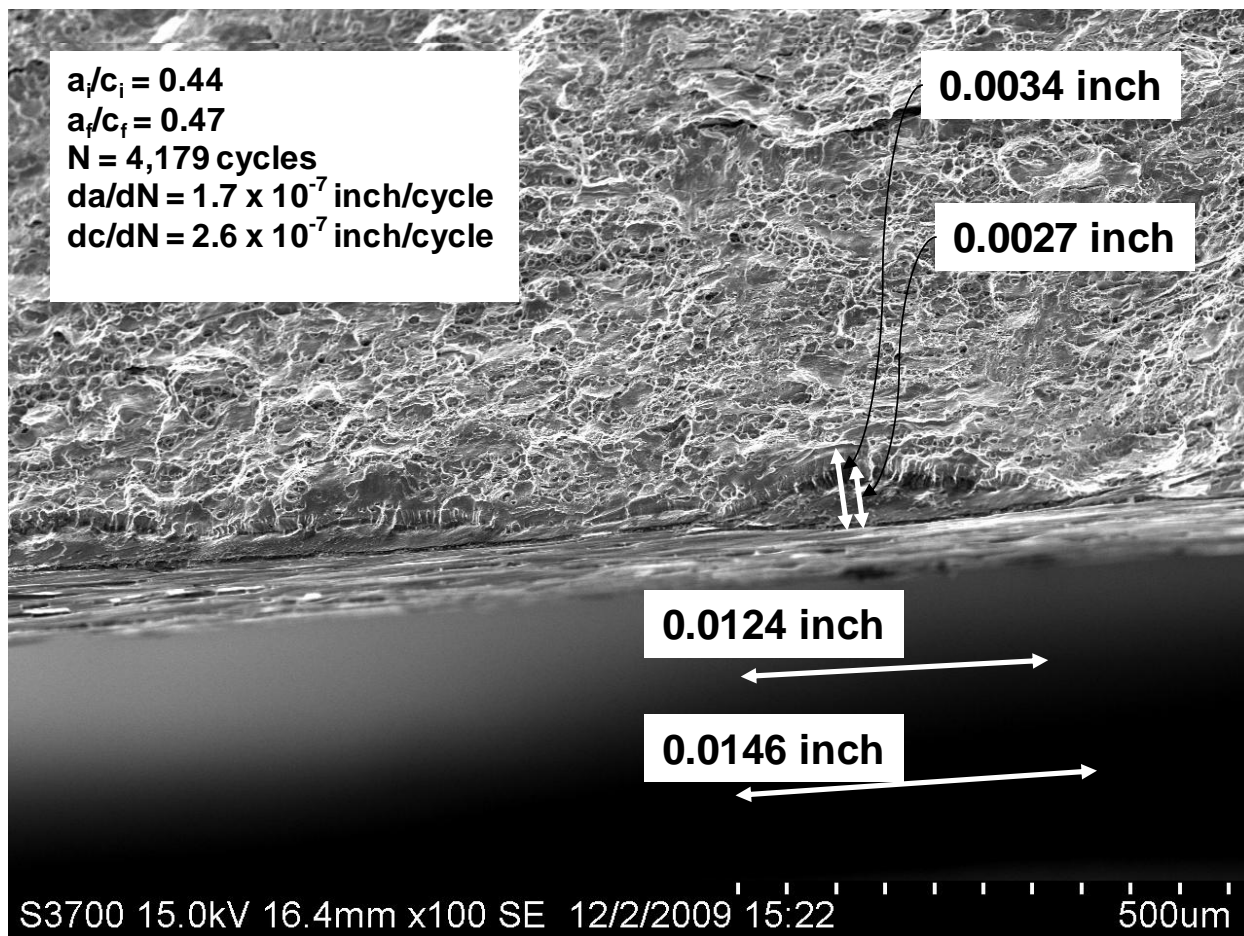


Figure C.41. SEM photograph (100x) of the interior crack ID12 found on the liner of COPV test 18119.



**NASA Engineering and Safety Center
Technical Assessment Report**

Document #:
**NESC-RP-
06-065**

Version:
1.0

Title:

**Fracture Mechanics Based Methods Development for
COPVs with Metallic Liners**

Page #:
157 of 164

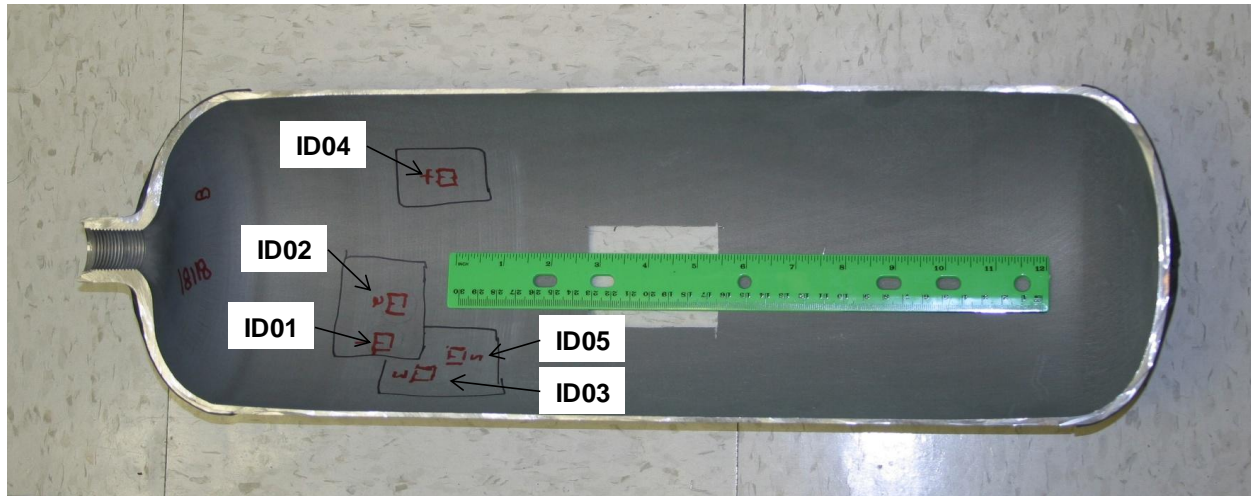


Figure C.42. Locations of the interior cracks found in the liner of COPV 18118.



**NASA Engineering and Safety Center
Technical Assessment Report**

Document #:
**NESC-RP-
06-065**

Version:
1.0

Title:

**Fracture Mechanics Based Methods Development for
COPVs with Metallic Liners**

Page #:
158 of 164

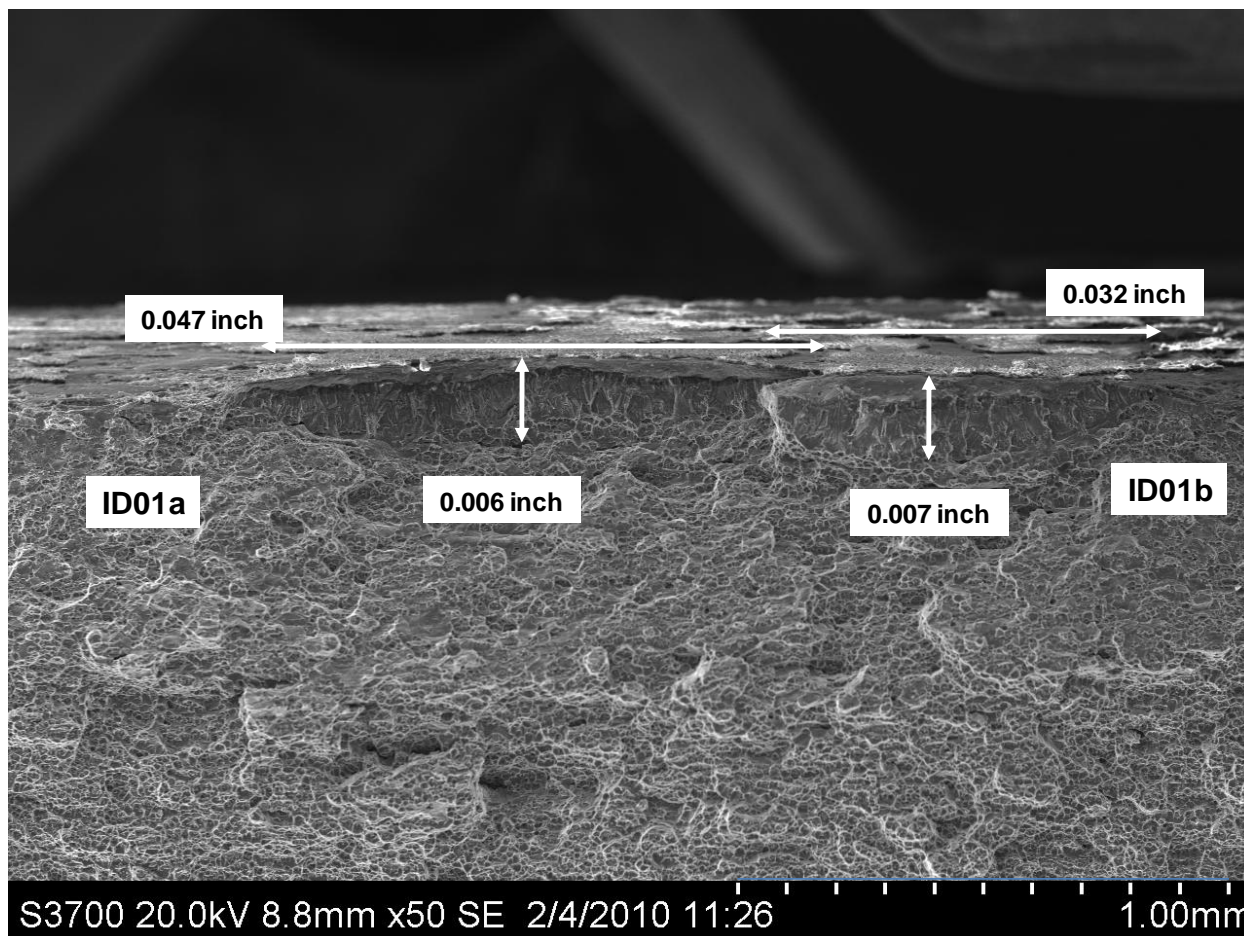


Figure C.43. SEM photograph (50x) of the interior cracks ID01a and ID01b found on the liner of COPV test 18118.



**NASA Engineering and Safety Center
Technical Assessment Report**

Document #:
**NESC-RP-
06-065**

Version:
1.0

Title:

**Fracture Mechanics Based Methods Development for
COPVs with Metallic Liners**

Page #:
159 of 164

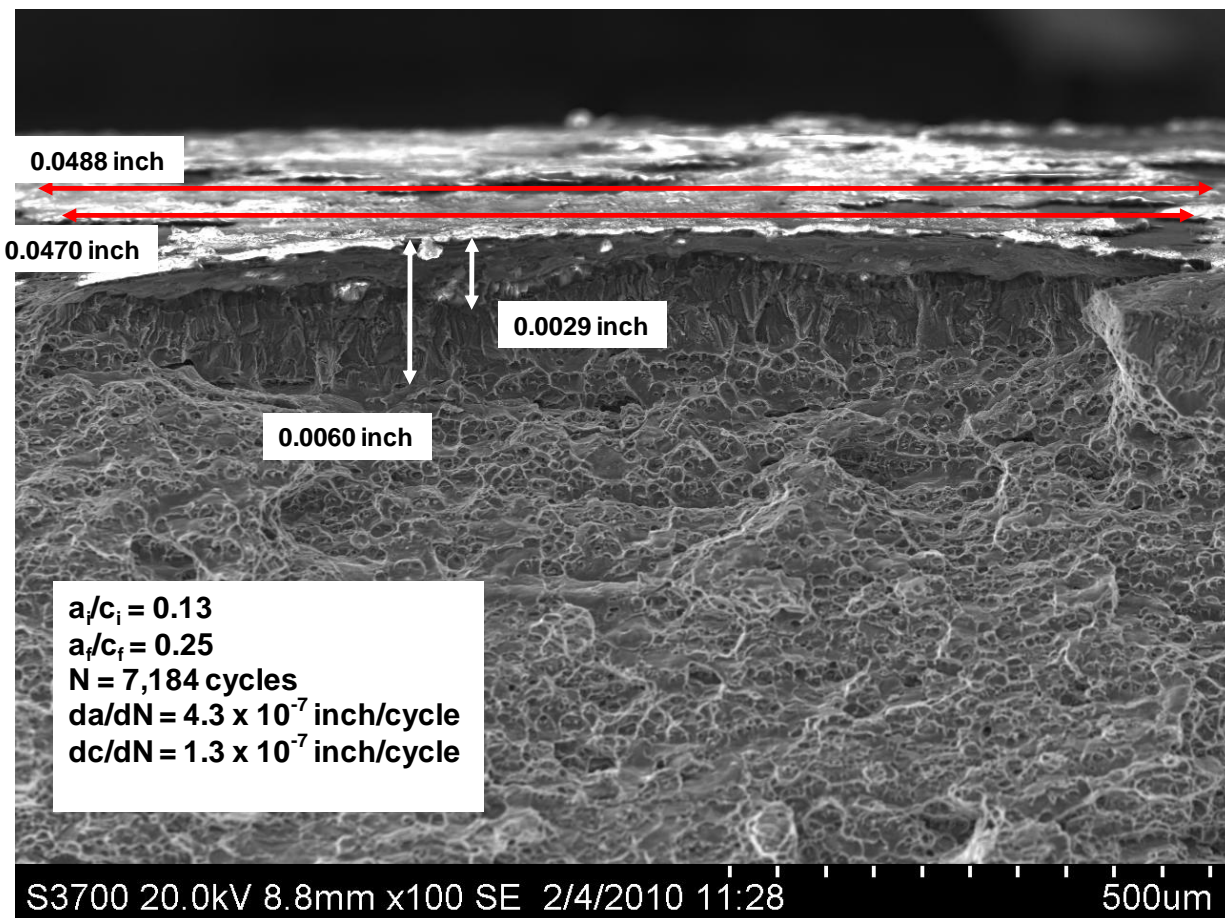


Figure C.44. SEM photograph (100x) of the interior crack ID01a found on the liner of COPV test 18118.



**NASA Engineering and Safety Center
Technical Assessment Report**

Document #:
**NESC-RP-
06-065**

Version:
1.0

Title:

**Fracture Mechanics Based Methods Development for
COPVs with Metallic Liners**

Page #:
160 of 164

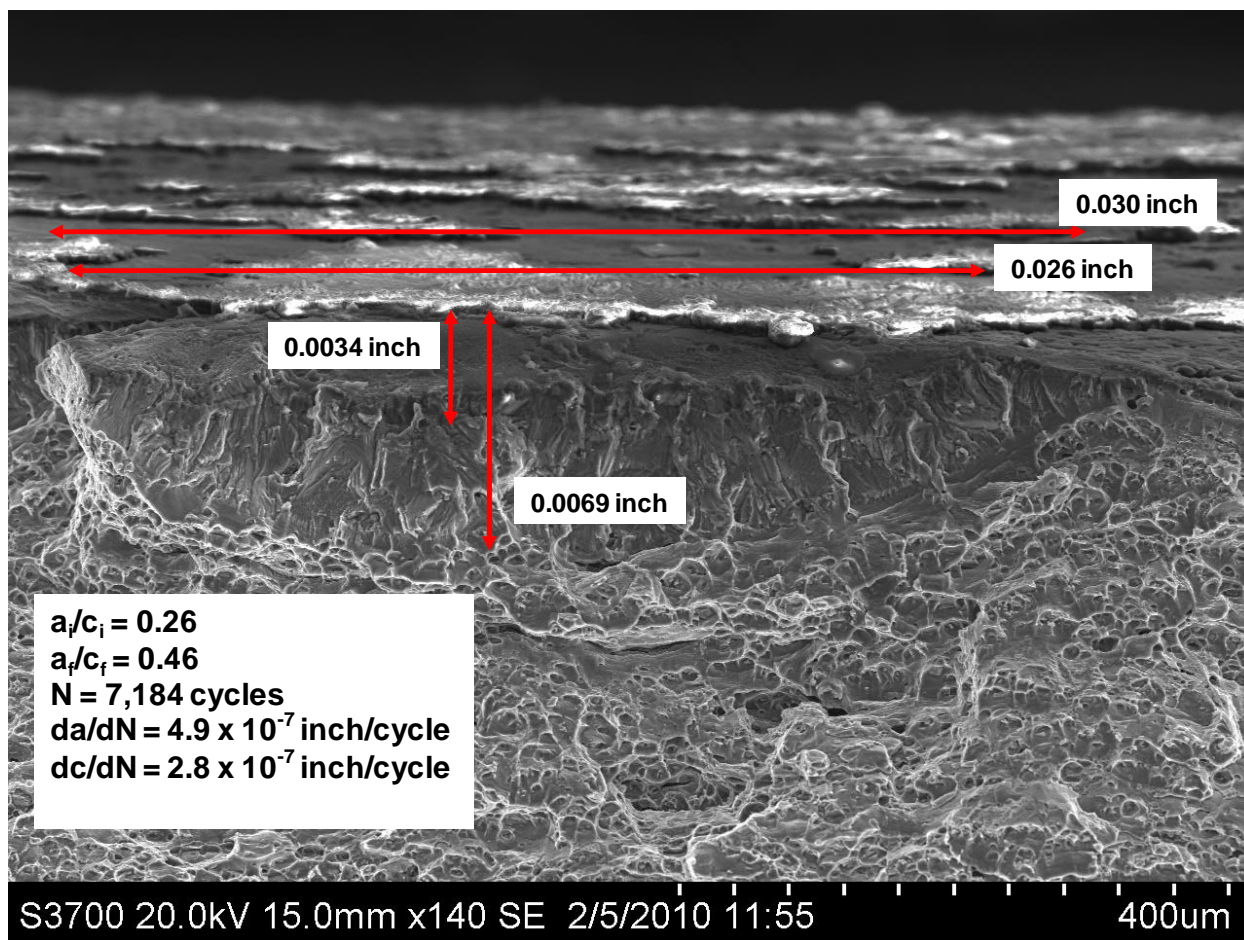


Figure C.45. SEM photograph (140x) of the interior crack ID01b found on the liner of COPV test 18118.



**NASA Engineering and Safety Center
Technical Assessment Report**

Document #:
**NESC-RP-
06-065**

Version:
1.0

Title:

**Fracture Mechanics Based Methods Development for
COPVs with Metallic Liners**

Page #:
161 of 164

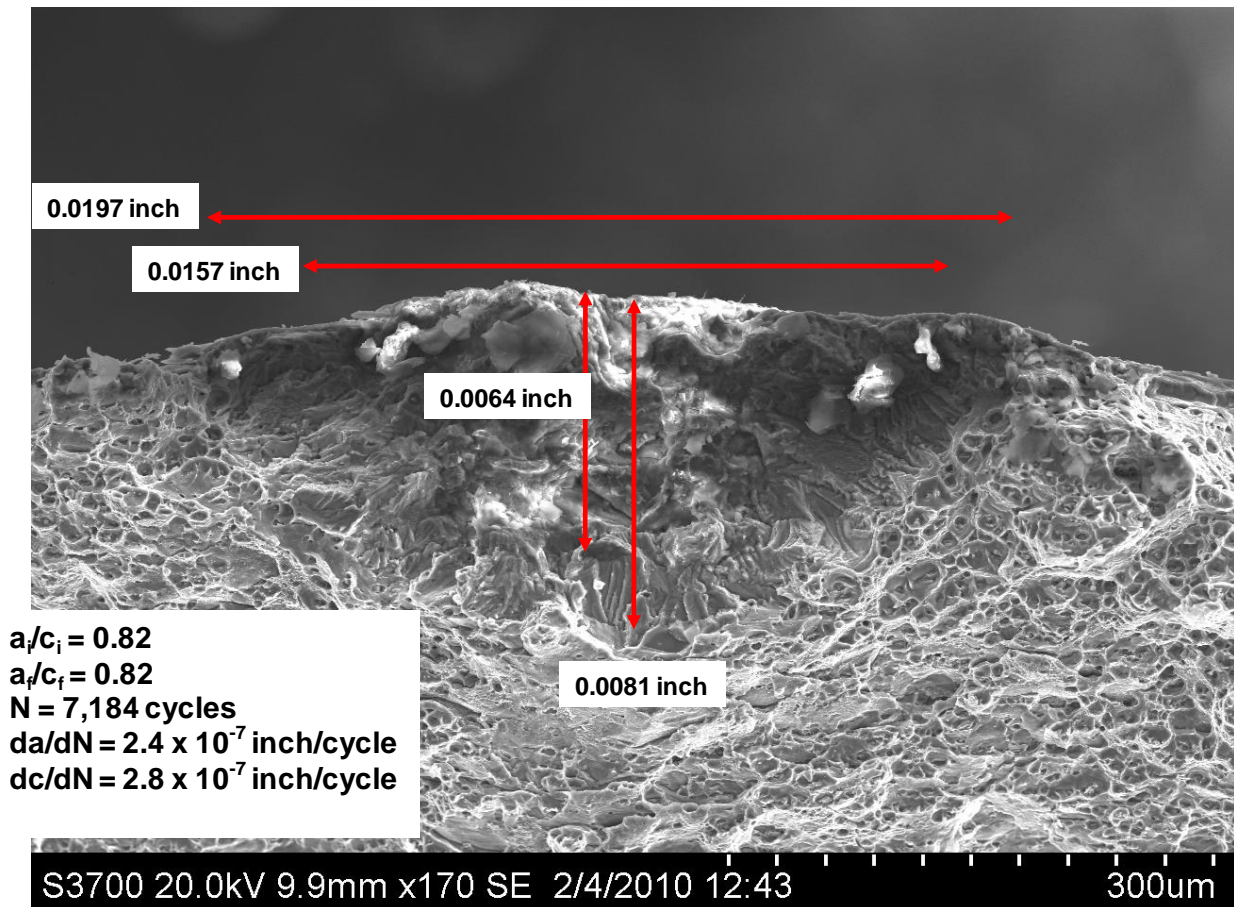


Figure C.46. SEM photograph (170x) of the interior crack ID02 found on the liner of COPV test 18118.



Title:

Fracture Mechanics Based Methods Development for
COPVs with Metallic Liners

Page #:
162 of 164

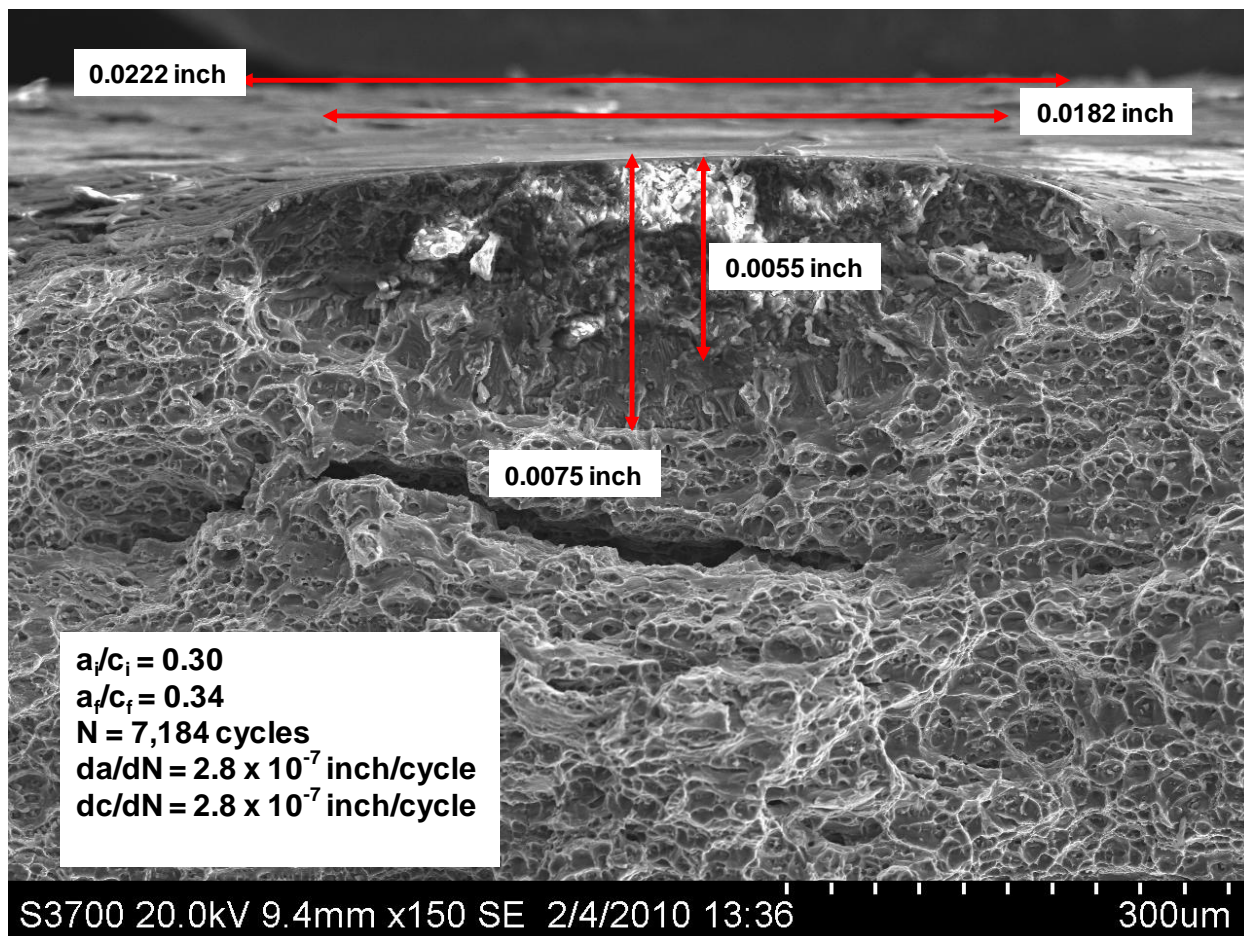


Figure C.47. SEM photograph (150x) of the interior crack ID04 found on the liner of COPV test 18118.



**NASA Engineering and Safety Center
Technical Assessment Report**

Document #:
**NESC-RP-
06-065**

Version:
1.0

Title:

**Fracture Mechanics Based Methods Development for
COPVs with Metallic Liners**

Page #:
163 of 164

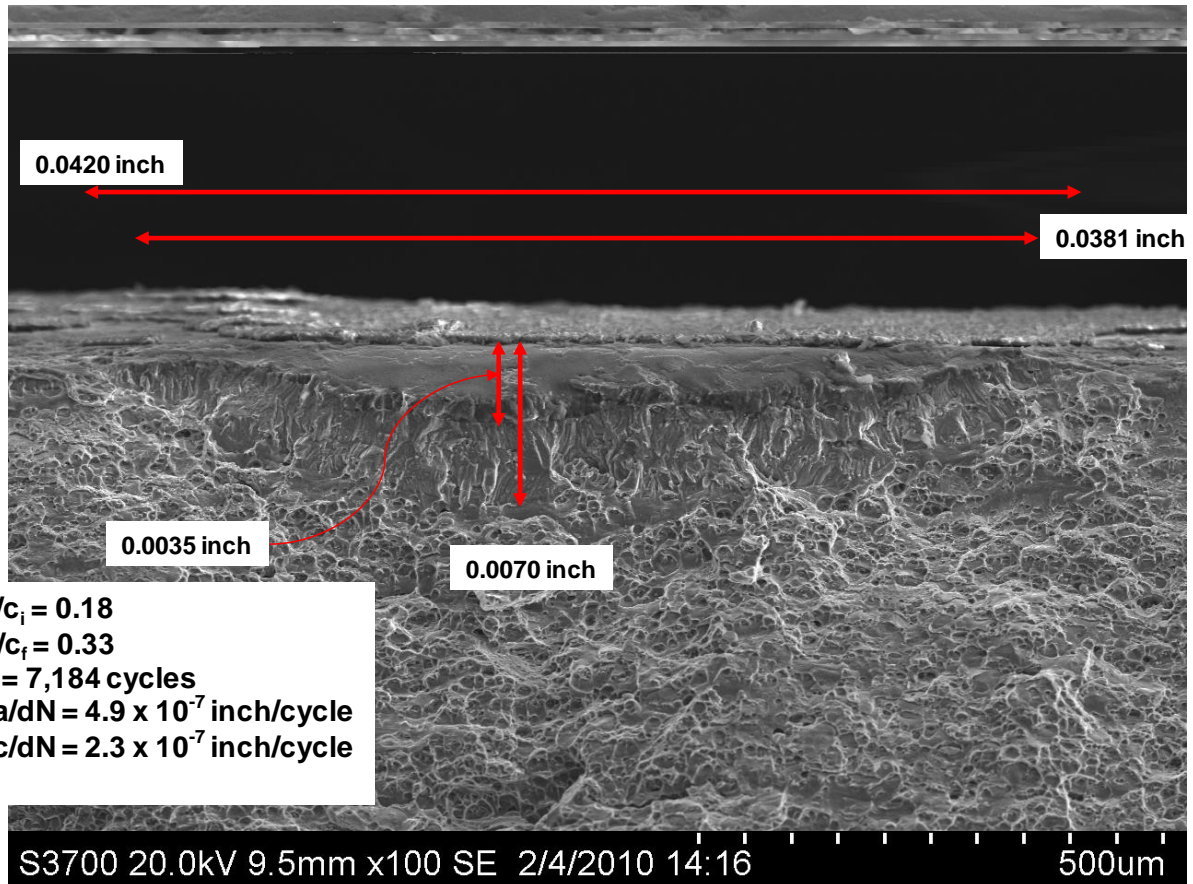


Figure C.48. SEM photograph (100x) of the interior crack ID05 found on the liner of COPV test 18118.



**NASA Engineering and Safety Center
Technical Assessment Report**

Document #:
**NESC-RP-
06-065**

Version:
1.0

Title:

**Fracture Mechanics Based Methods Development for
COPVs with Metallic Liners**

Page #:
164 of 164

**Appendix D. Calculated Stress Intensity Factor Values for the
Elastic Uniaxial and COPV Tests**

Table D.1. Stress Intensity Factors and Crack Growth Rates for the COPV Tests

| Test ID | Crack ID | a_{avg} (inch) | a_{avg}/c_{avg} | K_{SC04} Depth (ksi inch ^{1/2}) | K_{op} Depth (ksi inch ^{1/2}) | K Depth (ksi inch ^{1/2}) | da/dN (inch/cycle) | K_{SC04} Surface (ksi inch ^{1/2}) | K_{op} Surface (ksi inch ^{1/2}) | K Surface (ksi inch ^{1/2}) | dc/dN (inch/cycle) |
|---------|----------|---------------------|-------------------|---|---|--|-------------------------|---|---|--|-------------------------|
| 18118 | 1 | 0.057 | 0.624 | 9.12 | 0.00 | 9.12 | 5.85E-06 | 9.00 | 0.00 | 9.00 | 7.93E-06 |
| 18118 | 3 | 0.051 | 0.579 | 8.98 | 0.00 | 8.98 | 4.44E-06 | 8.35 | 0.00 | 8.35 | 7.73E-06 |
| 18117 | 1 | 0.039 | 0.586 | 7.49 | 0.00 | 7.49 | 6.18E-06 | 6.70 | 0.00 | 6.70 | 5.70E-06 |
| 18117 | 2 | 0.036 | 0.548 | 7.44 | 0.00 | 7.44 | 5.62E-06 | 6.38 | 0.00 | 6.38 | 5.60E-06 |
| 18117 | 3 | 0.029 | 0.455 | 6.91 | 0.00 | 6.91 | 2.84E-06 | 5.35 | 0.00 | 5.35 | 2.90E-06 |
| 18107 | 1 | 0.044 | 0.575 | 8.18 | 0.00 | 8.18 | 4.40E-06 | 7.39 | 0.00 | 7.39 | 6.00E-06 |
| 18107 | 2 | 0.052 | 0.602 | 8.78 | 0.00 | 8.78 | 4.60E-06 | 8.35 | 0.00 | 8.35 | 8.80E-06 |
| 18107 | 3 | 0.050 | 0.596 | 8.64 | 0.00 | 8.64 | 4.60E-06 | 8.09 | 0.00 | 8.09 | 8.00E-06 |
| 18105 | 1 | 0.018 | 0.324 | 5.69 | 0.00 | 5.69 | 2.26E-06 | 3.70 | 0.00 | 3.70 | 1.50E-06 |
| 18105 | 2 | 0.022 | 0.379 | 6.14 | 0.00 | 6.14 | 2.60E-06 | 4.30 | 0.00 | 4.30 | 1.90E-06 |
| 18105 | 3 | 0.018 | 0.324 | 5.71 | 0.00 | 5.71 | 1.92E-06 | 3.72 | 0.00 | 3.72 | 1.20E-06 |
| 18103 | 1 | 0.014 | 0.906 | 3.46 | 0.00 | 3.46 | 8.17E-07 | 3.67 | 0.00 | 3.67 | 1.13E-06 |
| 18103 | 2 | 0.023 | 0.903 | 4.56 | 0.00 | 4.56 | 9.00E-07 | 4.85 | 0.00 | 4.85 | 1.72E-06 |
| 18103 | 3 | 0.014 | 0.901 | 3.48 | 0.00 | 3.48 | 4.50E-07 | 3.67 | 0.00 | 3.67 | 9.17E-07 |
| 18103 | 1a | 0.016 | 0.221 | 5.66 | 0.00 | 5.66 | 2.22E-06 | 3.17 | 0.00 | 3.17 | 2.58E-06 |
| 18119 | 1 | 0.015 | 0.963 | 3.48 | 0.00 | 3.48 | 7.42E-07 | 3.82 | 0.00 | 3.82 | 1.30E-06 |
| 18119 | 2 | 0.020 | 0.873 | 4.18 | 0.00 | 4.18 | 1.15E-06 | 4.39 | 0.00 | 4.39 | 2.07E-06 |
| 18119 | 3 | 0.015 | 0.910 | 3.55 | 0.00 | 3.55 | 9.33E-07 | 3.77 | 0.00 | 3.77 | 1.29E-06 |
| 18118 | ID6 | 0.007 | 0.298 | 3.31 | 0.36 | 3.67 | 5.29E-07 | 2.14 | 0.66 | 2.80 | 3.13E-07 |
| 18119 | ID1 | 0.007 | 0.281 | 3.43 | 0.37 | 3.80 | 8.14E-07 | 2.18 | 0.70 | 2.89 | 9.93E-07 |
| 18119 | ID2 | 0.005 | 0.336 | 2.66 | 0.30 | 2.97 | 4.79E-07 | 1.82 | 0.52 | 2.35 | 4.31E-07 |
| 18119 | ID3 | 0.012 | 0.546 | 3.94 | 0.48 | 4.41 | 1.29E-06 | 3.22 | 0.64 | 3.86 | 7.06E-07 |
| 18119 | ID4 | 0.007 | 0.291 | 3.22 | 0.35 | 3.57 | 8.14E-07 | 2.06 | 0.65 | 2.72 | 2.75E-07 |
| 18119 | ID5 | 0.008 | 0.387 | 3.41 | 0.39 | 3.80 | 8.61E-07 | 2.42 | 0.62 | 3.05 | 2.63E-07 |
| 18119 | ID6 | 0.008 | 0.500 | 3.17 | 0.38 | 3.55 | 6.94E-07 | 2.47 | 0.54 | 3.01 | 7.42E-07 |
| 18119 | ID7 | 0.004 | 0.291 | 2.33 | 0.26 | 2.59 | 2.63E-07 | 1.51 | 0.48 | 1.99 | 2.63E-07 |
| 18119 | ID8 | 0.005 | 0.130 | 2.76 | 0.30 | 3.06 | 4.79E-07 | 1.49 | 0.83 | 2.32 | 2.99E-07 |
| 18119 | ID9 | 0.006 | 0.264 | 3.00 | 0.33 | 3.33 | 4.07E-07 | 1.90 | 0.64 | 2.53 | 1.79E-07 |
| 18119 | ID10 | 0.005 | 0.247 | 2.86 | 0.31 | 3.17 | 3.59E-07 | 1.75 | 0.62 | 2.38 | 2.27E-07 |
| 18119 | ID11 | 0.002 | 0.187 | 1.61 | 0.18 | 1.79 | 1.68E-07 | 0.96 | 0.41 | 1.37 | 5.98E-08 |
| 18119 | ID12 | 0.003 | 0.452 | 2.02 | 0.24 | 2.26 | 1.68E-07 | 1.54 | 0.36 | 1.89 | 2.63E-07 |
| 18118 | ID1a | 0.004 | 0.186 | 2.69 | 0.29 | 2.98 | 4.32E-07 | 1.56 | 0.67 | 2.23 | 1.25E-07 |
| 18118 | ID2 | 0.007 | 0.819 | 2.59 | 0.37 | 2.96 | 2.37E-07 | 2.59 | 0.41 | 3.00 | 2.78E-07 |
| 18118 | ID4 | 0.007 | 0.644 | 2.71 | 0.35 | 3.06 | 2.78E-07 | 2.38 | 0.44 | 2.81 | 2.78E-07 |
| 18118 | ID5 | 0.005 | 0.262 | 2.90 | 0.32 | 3.22 | 4.87E-07 | 1.82 | 0.62 | 2.44 | 2.71E-07 |
| 18118 | ID1b | 0.005 | 0.368 | 2.74 | 0.31 | 3.05 | 4.87E-07 | 1.92 | 0.52 | 2.44 | 2.78E-07 |